N° Enregistrement
au C.N.R.S.

1518

THESE

présentée à

l'Université de Paris-Sud
centre d'Orsay

pour obtenir

Le Grade de Docteur ès-Sciences Physiques

par

Serge OTMEZGUINE

SUJET de la THESE : Propriétés de transport des alliages de tellurures de mercure et de cadmium au voisinage de la transition semimétal – semiconducteur.

Soutenue le 27 Juin 1975 devant la Commission d'examen

MM J. FRIEDEL ---------- Président

C. BENOIT à la Guillaume ----- }
D. JEROME ---------- } Examinateurs
M. AVEROUS ---------- }
C. VÉRIÉ ---------- }

N° Enregistrement
au C.N.R.S.

THESE

présentée à

l'Université de Paris-Sud
centre d'Orsay

pour obtenir

Le Grade de Docteur ès-Sciences Physiques

par

Serge OTMEZGUINE

SUJET de la THESE : Propriétés de transport des alliages de tellurures de mercure et de cadmium au voisinage de la transition semimétal – semiconducteur.

Soutenue le 27 Juin 1975 devant la Commission d'examen

MM J. FRIEDEL ---------- Président

C. BENOIT à la Guillaume ----- }
D. JEROME ---------- } Examinateurs
M. AVEROUS ---------- }
C. VÉRIÉ ---------- }

UNIV.
LEIDEN
BIBL.

SOMMAIRE

pages

INTRODUCTION 1

CHAPITRE I. CONSIDERATIONS GENERALES SUR LES ALLIAGES HgTe-CdTe. 7

I.1. Configurations semimétallique (SM) et semiconductrice (SC) 7

I.1.A. Méthode $\vec{k}.\vec{p}$ 7

I.1.B. Etats propres à k = 0 11

I.1.C. Relations de dispersion : configurations normale (SC) et inversée (SM) 13

I.1.D. Fonctions d'onde 17

I.1.E. Incidence de la symétrie des fonctions d'onde sur le calcul de la mobilité 18

I.2. Transition SM-SC dans les alliages HgTe-CdTe 21

I.2.A. Effets relativistes 21

I.2.B. Transition SM-SC induite par la composition 22

I.2.C. Transition SM-SC induite par la température 23

I.2.D. Transition SM-SC induite par la pression hydrostatique 24

I.3. Spéculations sur la transition SM-SC 25

I.3.A. Configuration SC à petit gap direct Γ_6-Γ_8 26

I.3.B. Configuration SM type α-Sn ou HgTe 27

I.4. Singularité de la constante diélectrique dans la configuration SM 27

I.5. Etats d'impuretés dans les semiconducteurs à gap nul 31

CHAPITRE II. PRINCIPAUX RESULTATS DE CETTE ETUDE 34

II.1. Bandes de valence, de conduction, transition SM-SC 35

II.1.A. Bande de valence 36

II.1.B. Bande de conduction 37

II.1.C. Transition SM-SC 38

II.2. Porteurs extrinsèques. Etats accepteurs.....40
II.2.A. Etat accepteur dû à un potentiel très localisé.....40
II.2.B. Etat accepteur dû à un potentiel coulombien.43
II.3. Etude de la mobilité : constante diélectrique ; effets résonnants.....44
II.3.A. Etude de la mobilité à 292°K.....44
II.3.B. Etude de la mobilité à très basse température.....46
II.3.C. Mise en évidence d'une diffusion résonnante sur le niveau accepteur.....49

CHAPITRE III. CONCLUSIONS.....50

BIBLIOGRAPHIE SUCCINCTE*.....53

SOMMAIRE DE L'ANNEXE I.....56

RESUME DE L'ANNEXE I.....57

SOMMAIRE DE L'ANNEXE II.....59

RESUME DE L'ANNEXE II.....60

o o
o

* Des bibliographies détaillées sont données à la fin de chacune des deux Annexes.

INTRODUCTION

Le tellurure de mercure HgTe et le tellurure de cadmium CdTe sont deux composés appartenant à la famille des semiconducteurs dits "intermétalliques", de type $A^N B^{8-N}$, N et 8-N numérotant les colonnes du tableau périodique. Ces deux composés cristallisent dans le système de la blende de zinc. Dans le cadre d'un modèle de bandes à un électron, au centre de la zone de Brillouin (point Γ), les fonctions d'onde appartiennent à l'une des représentations irréductibles Γ_6, Γ_7 ou Γ_8 du double groupe du point Γ. Elles sont construites à partir des représentations du groupe d'espace T_d de la blende de zinc qui a 5 représentations irréductibles. Les figures 1a et 1b ci-dessous représentent schématiquement les structures de bande respectives de HgTe et CdTe au voisinage de k = 0.

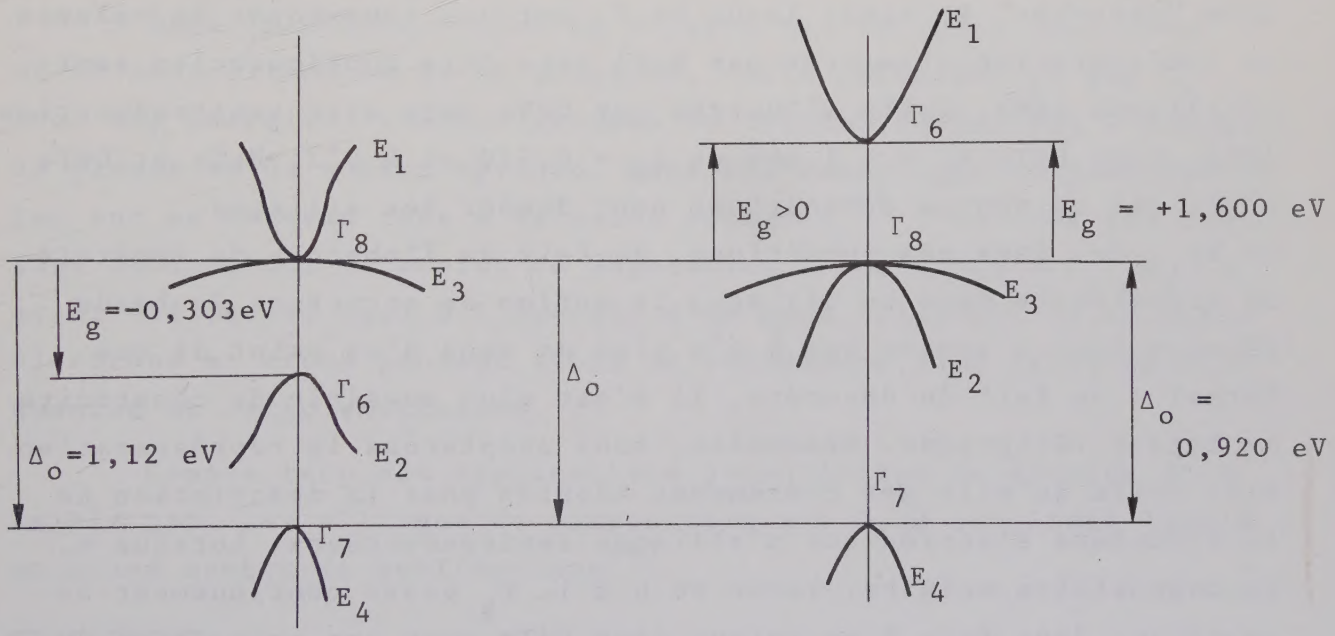

a) HgTe b) CdTe

Figure 1

Configuration semimétallique (SM) et semiconductrice (SC) au point Γ correspondant respectivement aux composés HgTe et CdTe à 0°K.

Posons $E_g \equiv E(\Gamma_6) - E(\Gamma_8)$.
HgTe (Fig.1a), pour lequel $E_g(0°K) = - 0,303$ eV, apparaît comme un semimétal à recouvrement nul ou encore un semiconducteur à gap nul. La symétrie impose la dégénérescence en Γ_8 de la bande de conduction et de la bande de valence de trous lourds. Le sommet de la bande de valence des trous légers est en Γ_6. Dans la configuration SM, il est à noter que cette bande est une sous-bande. La bande provenant de Γ_7 est une sous-bande de valence classique. En l'absence de couplage spin-orbite les niveaux Γ_7 et Γ_8 sont dégénérés.

Posons $\Delta_o = E(\Gamma_8) - E(\Gamma_7)$: $\Delta_o = 1,12$ eV dans HgTe
Cette structure de bande ressemble à celle de l'étain-gris α-Sn dite "inversée", en ce sens que l'ordre des niveaux Γ_6, Γ_8 a été inversé par rapport à leurs positions respectives habituelles dans les semiconducteurs de la famille diamant-blende de zinc.

CdTe (Fig.1b), pour lequel $E_g > 0$, est un semiconducteur à gap direct de structure de bande classique. La bande de conduction issue de Γ_6 est séparée des bandes de valence de trous lourds et légers dégénérées en Γ_8 par l'intervalle E_g. Comme dans la structure "inversée" la bande issue de Γ_7 est une sous-bande de valence. La configuration illustrée par HgTe sera dite configuration semimétallique (SM). Celle illustrée par CdTe sera dite semiconductrice (SC). Dans CdTe $E_g = + 1,606$ et $\Delta_o = 0,920$ eV à 0°K. HgTe et CdTe s'allient en toutes proportions pour donner des alliages $Cd_xHg_{1-x}Te$. Dans ces conditions, du fait de l'absence de symétrie de translation dans un alliage, la notion de structure de bande décrite dans l'espace des $\vec{k}$ n'a plus de sens d'un point de vue formel : du fait du désordre, il n'est plus possible de construire un espace réciproque. Néanmoins, nous adopterons la représentation E(k) telle qu'elle est couramment adoptée pour la description de la structure électronique d'alliages semiconducteurs. Lorsque x, la composition molaire, varie de 0 à 1, E_g passe continuement de sa valeur dans HgTe à sa valeur dans CdTe avec une transition du type semimétal-semiconducteur autour de la composition x = 0,16 au voisinage de 0°K. Cette transition SM-SC qui correspond à la

dégénérescence accidentelle des niveaux Γ_6-Γ_8 peut aussi être obtenue par la pression hydrostatique et la température. Dans les trois cas, composition, température, pression, la symétrie du cristal est conservée.

Les études entreprises sur ces matériaux ont, en général, été motivées par les possibilités d'application dans le domaine de la détection infra-rouge. En effet par alliage on peut obtenir des semiconducteurs à faible bande interdite et accorder cette bande interdite (ce gap) à la longueur d'onde à détecter. Du fait de la symétrie s, p respectivement des niveaux Γ_6, Γ_8 les deux bandes issues de ces deux niveaux sont couplées par le terme $\vec{k}.\vec{p}$. Ce couplage conduit à une masse effective des électrons de la bande de conduction proportionnelle à $|E_g|$ et donc de très faibles valeurs possibles de cette masse. En conséquence du fait de la forte valeur du couplage spin-orbite Δ_o dans ces matériaux, on peut avoir accès à de forts facteurs gyromagnétiques de l'électron et de ce fait donc, des propriétés et perspectives d'applications intéressantes dans le domaine de l'émission stimulée par renversement du spin : "Spin-flip Raman Lasers" dans l'infrarouge, accordables par le champ magnétique[2].

Dans la configuration SC on peut par un choix judicieux de la composition ou de la pression, faire coïncider le gap E_g avec des énergies caractéristiques du cristal telles que l'énergie de plasma ou de phonon optique. Dans ces conditions on peut spéculer sur un nouveau type d'émission stimulée[3] : on crée par pompage optique une inversion de population à une énergie E_g. E_g ayant été choisi égal à l'énergie d'un mode collectif du cristal, électrons et trous peuvent alors se recombiner avec émission d'un quantum de cette excitation.

Compte tenu des applications potentielles du domaine SC à faible gap, les alliages de composition $x \gtrsim 0{,}20$ ont donné lieu à un grand nombre de publications[*].

(*) Cf. étude bibliographique reportée dans la Section I de l'Annexe I.

Les compositions $x < 0,20$ correspondent à la transition "gap-zéro" et à la configuration SM. La transition SM-SC a fait l'objet d'un nombre d'études beaucoup plus restreint. Dans un travail antérieur effectué au Laboratoire[4], cette transition a été étudiée en fonction de la composition à l'aide d'une analyse de la dépendance en température du régime intrinsèque pour différentes compositions $0 \leq x \leq 0,18$ et d'une caractérisation par extrapolation de mesures optiques (transmission, électroluminescence et effets photovoltaïques) effectuées dans le domaine SC $x \geq 0,175$. Enfin une observation préliminaire de la transition SM-SC induite par la pression à 77°K a été publiée, mettant en évidence un effet de redressement dans la caractéristique courant-tension, observé à partir de 6 Kbar sur des jonctions p-n pour $x = 0,11$[5]. Plus récemment, un certain nombre d'études théoriques ont souligné les caractéristiques particulières d'une transition gap-zéro et de la configuration inversée dans le système diamant-blende de zinc (α-Sn ; $Cd_xHg_{1-x}Te$) : spéculations sur la possibilité d'une phase excitonique, singularité de la constante diélectrique, existence de niveaux d'impureté du type accepteur pouvant interférer avec le continuum des états de la bande de conduction. L'ensemble des résultats obtenus dans ce travail sera analysé dans le contexte de ces propriétés originales et fondamentales.

Le thème central de la présente étude a trait à l'analyse des effets associés au croisement de Γ_6 et Γ_8 et à la configuration SM. Comme nous le verrons dans la suite, un modèle d'états électroniques décrits essentiellement à l'aide d'une relation de dispersion E(k) à un électron, de fonctions d'onde présentant la particularité d'un changement de symétrie type s-type p associé au croisement Γ_6-Γ_8 et de niveaux virtuels liés quasi-discrets associés à des états accepteurs résonnants, permet de rendre compte de l'ensemble des propriétés de transport observées au voisinage de la transition SM-SC dans les régimes intrinsèque et extrinsèque. Les résultats expérimentaux utilisés concernent des mesures galvanomagnétiques que nous avons effectuées de façon systématique dans le domaine de compositions $0 \leq x \leq 0,14$, utilisant comme paramètres la température ($1,5 \leq T \leq 300$ K), le champ magnétique ($0 \leq B \leq 10$KG) et la pression hydrostatique ($0 < P \leq 12$ Kbar).

Le chapitre I est essentiellement consacré à une revue du contexte théorique dans lequel a été entreprise cette étude de la transition SM-SC dans les alliages $Cd_xHg_{1-x}Te$. Dans un modèle de bandes à un électron, la méthode $\vec{k}\vec{p}$ appliquée aux niveaux Γ_6, Γ_7, Γ_8 montre que l'inversion des niveaux Γ_6, Γ_8 s'accompagne lorsque $|E_g| \to 0$ de deux effets

1) forte non parabolicité de la bande de conduction

2) changement de symétrie des fonctions d'onde de l'électron en k = 0. En Γ_8 fonction d'onde de symétrie p, en Γ_6 fonction d'onde de symétrie s. Dans les deux situations SM et SC, mélange s-p lorsque $k \neq 0$.

Ces deux effets doivent être pris en considération dans une analyse de la mobilité.

Dans le paragraphe I.2 nous décrivons les différentes actions susceptibles d'induire une transition SM-SC dans ces alliages :

- Variation de E_g avec la composition et interprétation de l'inversion des niveaux $\Gamma_6 - \Gamma_8$ en termes de corrections relativistes.

- Variation de E_g avec la température et anomalie du signe du coefficient dE_g/dT dans HgTe.

- Variation de E_g avec la pression hydrostatique.

Des possibilités d'anomalies de structure électronique sont discutées dans le paragraphe I.3 en termes de phase excitonique et nous amènent dans le paragraphe I.4 à parler du comportement singulier de la constante diélectrique statique $\varepsilon(q \to 0)$ dans la configuration SM. Cette singularité a pour origine la contribution des transitions $\Gamma_8 - \Gamma_8$ à la constante diélectrique.

Enfin dans le paragraphe I.5 nous rappelons dans ses grandes lignes le problème des impuretés dans la configuration gap nul (SM) et en particulier l'existence d'états accepteurs quasi-discrets interférant avec le continuum des états de la bande de conduction. En particulier une contribution théorique[6] récente, rappelée brièvement ici, nous permet de rendre compte d'une partie des résultats expérimentaux rapportés dans ce mémoire.

Le chapitre II reprend l'essentiel des résultats et de leur analyse qui sont décrits par ailleurs dans les études détaillées(*) jointes en Annexes (I et II) et qui ont fait l'objet de communications à des congrés(7-12).

La conclusion de ce travail souligne en particulier d'une part la compréhension maintenant établie de l'ensemble des propriétés intrinsèques à la transition SM-SC dans CdHgTe, du moins telles qu'elles apparaissent à travers l'analyse d'effets de transport, et d'autre part indiquent les perspectives d'études nouvelles susceptibles de conduire à une analyse plus quantitative de nos mises en évidence d'effets nouveaux associés aux niveaux accepteurs résonnants.

o o
o

(*) Les deux documents joints en Annexe ont été rédigés en vue d'en faire des publications. En fait, une description détaillée des résultats a conduit à des longueurs de texte incompatibles avec les règles courantes de l'édition. Ces deux annexes sont donc en fait des "pré-publications" et des versions condensées ont été soumises à différentes revues.

CHAPITRE I

CONSIDERATIONS GENERALES SUR LES ALLIAGES HgTe-CdTe

I.1. CONFIGURATIONS SEMIMETALLIQUE (SM) ET SEMICONDUCTRICE (SC)

I.1.A. Méthode k.p

L'origine de l'inversion des niveaux Γ_6 et Γ_8 dans la configuration SM et l'incidence de cette inversion sur la structure des bandes issues de ces deux niveaux sont deux aspects fondamentaux du couple HgTe-CdTe.

Pour éclaircir cette notion de structure de bande "inversée" revenons à l'équation de Schroedinger à un électron :

$$\left[\frac{p^2}{2m_o} + V(\vec{r}) + \frac{\hbar^2}{4m_o^2c^2}(\nabla\vec{V}_\Lambda\vec{p}).\vec{\sigma}\right]\psi_{nk} = E_{nk}\psi_{nk} \qquad (1)$$

ψ_{nk} est la fonction d'onde décrivant un électron de vecteur d'onde $\vec{k}$ dans la bande n. La partie périodique $u_{nk}(\vec{r})$ d'un état de Bloch $\psi_{nk}(r) = u_{nk}e^{ikr}$ satisfait l'équation :

$$\left[H_o + H_1 + H_2 + H_3\right]u_{nk}(r) = E'_{nk}u_{nk}(r) \qquad (2)$$

Dans cette équation

$$E'_{nk} = E_{nk} - \frac{\hbar^2k^2}{2m_o}$$

$$H_o = \frac{p^2}{2m_o} + V(\vec{r})$$

$$H_1 = \frac{\hbar}{m_o}\vec{k}.\vec{p} \quad \text{est appelé terme d'interaction } \vec{k}.\vec{p}$$

$H_2 = \frac{\hbar}{4m_o c^2}(\vec{\nabla} V_\Lambda \vec{p}).\vec{\sigma}$ est le terme d'intéraction spin-orbite indépendant de k

$H_3 = \frac{\hbar^2}{4m_o c^2}(\vec{\nabla} V_\Lambda \vec{k}).\vec{\sigma}$ est le terme d'intéraction spin-orbite dépendant de k.

Ce terme H_3 est vraisemblablement très faible car le terme $\hbar\vec{k}$ est très faible comparativement au moment atomique $\vec{p}$ à l'intérieur de l'atome où a lieu la majeure partie de l'interaction spin-orbite.

E_{nk} est l'énergie d'un électron de vecteur d'onde k dans la bande n. m_o est la masse de l'électron libre. V est un potentiel qui a la périodicité du réseau ; $\vec{p}$ est l'opérateur impulsion, σ est l'opérateur de spin.
Pour un vecteur d'onde $\vec{k}$ les fonctions propres de l'équation (1) pour toutes les bandes forment un ensemble complet.
Dans la représentation $\vec{k} = 0$ l'opérateur H_o est diagonal, ses valeurs propres correspondent aux représentations du groupe simple du point Γ. (Γ_1, Γ_2, Γ_{12}, Γ_{15}, Γ_{25})[13].

La méthode k.p, appliquée par Kane à InSb[14], consiste à diagonaliser $H_o + H_1 + H_2$ sur une base tronquée formée par les fonctions propres n'appartenant qu'à deux états propres de H_o :

- un niveau E_s appartenant à la représentation Γ_1 qui est la représentation identique d'ordre 1. La fonction propre appartenant à cette représentation est un scalaire dénoté S. $|S\uparrow\rangle$ et $|S\downarrow\rangle$ sont les fonctions propres dégénérées de l'état E_s quand on tient compte du spin.

- un niveau E_p appartenant à la repésentation Γ_{15}, qui est une représentation d'ordre 3. Les fonctions propres de cette représentation se transforment comme x, y, z sous les opérations du groupe du tétraèdre et seront notées X, Y, Z.
Dans un problème à symétrie sphérique X, Y, Z sont les états propres de moment cinétique orbital $\ell = 1$ c'est-à-dire de symétrie p. $|X\uparrow\rangle$, $|X\downarrow\rangle$, $|Y\uparrow\rangle$, $|Y\downarrow\rangle$, $|Z\uparrow\rangle$, $|Z\downarrow\rangle$ sont alors les fonctions propres dégénérées de l'état E_p quand on tient compte du spin.

Pour tenir compte du spin il est nécessaire de construire le double groupe associé au groupe simple du point Γ[13] : parmi les représentations du double groupe apparaissent non seulement celles du groupe simple mais aussi de nouvelles représentations qui dans le cas du point Γ sont appelées Γ_6, Γ_7 et Γ_8. Ces représentations sont respectivement 2,2 et 4 fois dégénérées.

Quand on tient compte du spin de l'électron la fonction d'onde devient le produit d'une fonction d'espace par une fonction de spin notée $\uparrow$ ou $\downarrow$ dans le cas de l'électron. Ces fonctions de spin 1/2 se transforment comme les fonctions de base de la représentation $D_{1/2}$ du groupe des rotations. La fonction d'onde totale se transformera alors comme les fonctions de base de $\Gamma \times D_{1/2}$. Dans les représentations de $\Gamma \times D_{1/2}$ on montre que seules apparaissent Γ_6, Γ_7, Γ_8 introduites lors de la construction du double groupe[13].

Dans un premier temps du calcul le terme H_3 de couplage spin orbite dépendant de k est négligé. Du fait de la troncature de la base aux seules fonctions propres de E_s et E_p, la diagonalisation de $H_o + H_1 + H_2$ est simplifiée par le choix d'une base formée des 8 fonctions suivantes :

$$|is\downarrow\rangle, \quad \left|\frac{X-iY}{\sqrt{2}}\uparrow\right\rangle, \quad |Z\downarrow\rangle, \quad \left|\frac{X+iY}{\sqrt{2}}\uparrow\right\rangle, \quad |is\uparrow\rangle, \quad \left|-\frac{X+iY}{\sqrt{2}}\downarrow\right\rangle,$$

$$|Z\uparrow\rangle \text{ et } \left|\frac{X-iY}{\sqrt{2}}\downarrow\right\rangle.$$

Les quatre dernières fonctions sont déduites des quatre premières par renversement du temps (opération de conjugaison complexe + retournement du spin). Par ailleurs du fait du couplage spin-orbite le spin n'est plus un bon nombre quantique. En revanche j_z, projection du moment orbital total commute avec l'hamiltonien de l'équation 1.

Les 8 fonctions ci-dessus apparaissent comme fonctions propres de j_z : $j_z = -\frac{1}{2}$ et $+\frac{3}{2}$ pour les 4 premières, $j_z = +\frac{1}{2}$ et $-\frac{3}{2}$ pour les 4 dernières. L'hamiltonien (Eq.1) ne couplera pas ces deux sous-ensembles.

Comme cela a été dit, la méthode de Kane consiste à négliger dans un premier temps le terme H_3. La recherche des solutions de l'équation 2 sous forme de combinaison linéaire des 8 fonctions ci-dessus conduit alors à une matrice d'intéraction 8 × 8 qui s'écrit :

$$\mathcal{H} = \begin{bmatrix} \mathcal{H}' & 0 \\ 0 & \mathcal{H}' \end{bmatrix}$$

avec

$$\mathcal{H}' = \begin{bmatrix} E_s & 0 & kP_K & 0 \\ 0 & E_p - \Delta_o/3 & \sqrt{2}\Delta_o/3 & 0 \\ kP & \sqrt{2}\Delta_o/3 & E_p & 0 \\ 0 & 0 & 0 & E_p + \Delta/3 \end{bmatrix}$$

Des considérations de symétrie montrent que les seuls éléments de matrice à considérer sont P_K et Δ_o définis par

$$\left.\begin{aligned} P_K &= -i(\hbar/m_o)\langle S|p_z|Z\rangle \\ \Delta_o &= \frac{3\hbar i}{3m_o^2c^2}\langle X|\frac{\partial V}{\partial x}p_y - \frac{\partial V}{\partial y}p_x|Y\rangle \end{aligned}\right\} \qquad (3)$$

La matrice d'intéraction a pris cette forme particulière par le fait que k a été choisi parallèle à la direction z : cela ne restreint en aucune manière la généralité des résultats car la troncature de l'espace complet des u_{no} aux seules fonctions appartenant aux niveaux E_s et E_p fait que le milieu de symétrie T_d est formellement identique à un milieu de symétrie sphérique[6] : cela entraine nécessairement des bandes d'énergie de symétrie sphérique.

I.1.B. Etats propres à k = 0

La recherche des états propres à k = 0, s'obtient par résolution du déterminant $\mathcal{H} - E'.\mathcal{I} = 0$, $\mathcal{I}$ étant la matrice unité. On obtient l'équation

$$(E_s-E')^2(E_p+\frac{\Delta_o}{3}-E')^2\left[\{(E_p-\frac{\Delta_o}{3})-E'\}\{E_p-E'\} - (\frac{\sqrt{2}\Delta_o}{3})^2\right]^2 = 0 \qquad (4)$$

Cette équation admet 3 solutions :

$$E' = E_s \qquad \text{d'ordre 2}$$

$$E' = E_p + \frac{\Delta_o}{3} \qquad \text{d'ordre 4}$$

$$E' = E_p - 2\frac{\Delta_o}{3} \qquad \text{d'ordre 2}$$

Compte tenu de la multiplicité des racines on peut déjà dire que E_s sera le niveau Γ_6 2 fois dégénéré ; $E_p+(\Delta_o/3)$ le niveau Γ_8 4 fois dégénéré et $E_p-(2\Delta_o/3)$ le niveau Γ_7 2 fois dégénéré.

La similitude avec un problème atomique de symétrie sphérique est ici illustrée par le fait que le couplage spin-orbite lève une partie de la dégénérescence d'ordre 6 du niveau E_p, en donnant un niveau $E_p+(\Delta_o/3)$ dont les quatre fonctions correspondent à $j = 3/2$ ($\vec{j} = \vec{\ell} + \vec{s}$) et un niveau $E_p-(2\Delta_o/3)$ dont les deux fonctions correspondent à $j = 1/2$.

Posons $\qquad E_g = E(\Gamma_6) - E(\Gamma_8) = E_s - (E_p + \frac{\Delta_o}{3})$

On voit apparaître deux configurations possibles des niveaux Γ_6, Γ_7, Γ_8, selon que $E_s - E_p$ est > ou < à $\Delta_o/3$.

1°) Configuration semimétallique

$(E_s - E_p) < \Delta_o/3$ ou $E_g < 0$

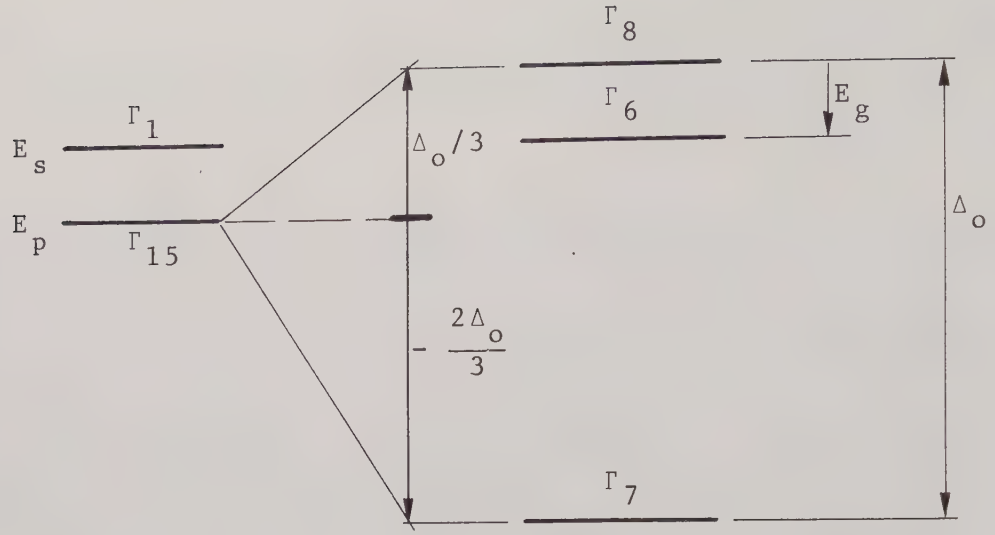

2°) Configuration semiconductrice $E_s - E_p > \Delta_o/3$, $E_g > 0$

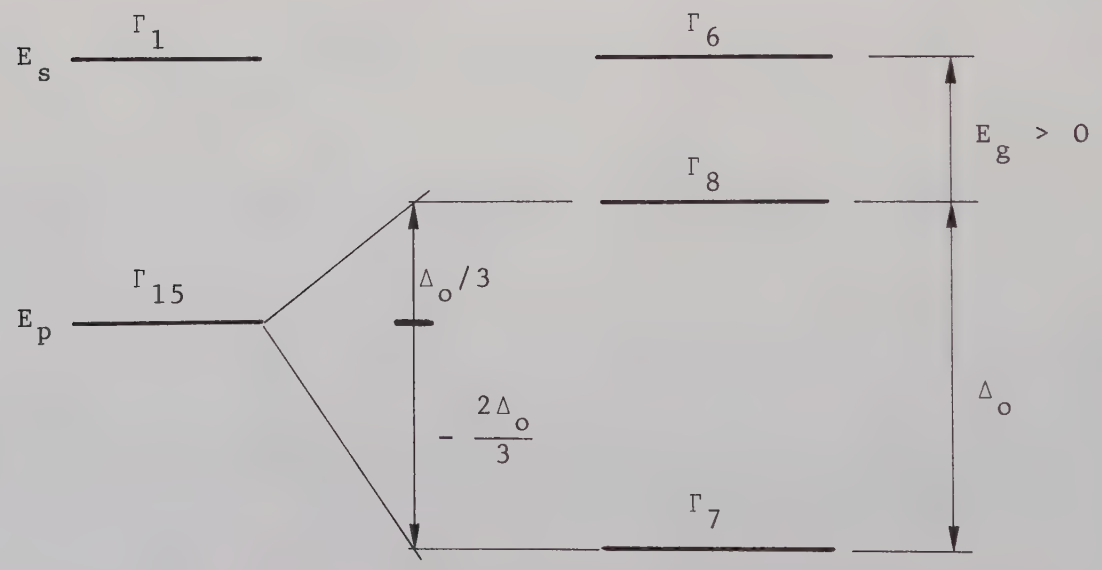

Ces résultats montrent que le formalisme $\vec{k}.\vec{p}$ développé par Kane dans le cas de InSb est général quel que soit l'ordre respectif des niveaux Γ_6 et Γ_8.

I.1.C. Relations de dispersions : configurations normale (SC) et inversée (SM)

Elles s'obtiennent en résolvant l'équation séculaire $\mathcal{H} - E(k).\mathcal{J} = 0$, $\mathcal{J}$ étant la matrice unité. Si on fixe l'origine des énergies sur le niveau $E(\Gamma_8) = E_p + (\Delta_o/3)$ les 4 racines doubles de l'équation séculaire s'écrivent :

$$\left.\begin{aligned} E' &= 0 \\ E'(E'-E_g)(E'+\Delta_o) - k^2P_K^2\left(E'+\frac{2\Delta_o}{3}\right) &= 0 \end{aligned}\right\} \qquad (5)$$

à k = 0 on retrouve E' = 0 racine d'ordre 4, E' = E_g racine d'ordre 2, E' = $-\Delta_o$ racine d'ordre 2.

Dans l'hypothèse $\Delta_o \gg kP_K, |E_g|$, et en négligeant le terme $\hbar^2k^2/2m_o$ on trouve :

$$\left.\begin{aligned} E_1(k) &= +\frac{1}{2}\left[E_g + \left(E_g^2 + \frac{8}{3}k^2P_K^2\right)^{1/2}\right] \\ E_2(k) &= +\frac{1}{2}\left[E_g - \left(E_g^2 + \frac{8}{3}k^2P_K^2\right)^{1/2}\right] \\ E_3(k) &= 0 \\ E_4(k) &= -\Delta_o - \frac{P_K^2k^2}{3(\Delta_o + E_g)} \end{aligned}\right\} \qquad (6)$$

Chacune des bandes décrites par ces relations est doublement dégénérée.

a) $E_g < 0$. Configuration semimétallique (SM), structure de bande dite inversée (Fig.1a)

Les bandes E_1 et E_3 sont dégénérées à k = 0. ELles sont donc issues du point Γ_8. E_1 est de par sa courbure une bande de conduction. Γ_8 étant le bas de la bande de conduction, devient le sommet de la bande de valence E_3 qui est la bande de trous lourds, qui apparait ici comme infiniment plate.

Dans cette approximation, où les niveaux éloignés de E_s et E_p ont été négligés, la méthode $\vec{k}.\vec{p}$ ne rend pas compte de la courbure de cette bande de trous lourds. La courbure de la bande de trous lourds apparaît, selon la méthode de Kane[14], dans un traitement en perturbation au second ordre qui prend en considération l'ensemble des bandes supérieures et inférieures. La bande de trous lourds n'apparaît plus alors comme isotrope. De plus ce traitement au second ordre, de même que l'effet au premier ordre du terme H_3 de couplage spin-orbite dépendant de k peuvent faire apparaitre des termes linéaires en k dans la relation de dispersion des trous lourds, conduisant à un extremum de cette bande éloigné de k = 0 avec une énergie supérieure à $E(\Gamma_8)$[14]. Ces termes linéaires existent du fait de la perte de symétrie d'inversion par rapport à la structure diamant. Ils n'existent pas dans les éléments simples de la colonne IV. Ces termes estimés par Kane dans InSb donneraient un très faible déplacement ΔE du maximum de la bande des trous lourds par rapport à $E(\Gamma_8)$. Dans CdTe, à notre connaissance il n'y a pas d'information publiée à ce jour. Nous verrons que dans HgTe des estimations théoriques et expérimentales donnent $\Delta E \lesssim 1$ meV.

Dans la suite de ce travail on décrira la bande de valence $E_3(k)$ par une relation du type

$$E_3(k) = E(\Gamma_8) + \Delta E - \hbar^2 k^2 / 2m_p \qquad (7)$$

Celà revient à supposer qu'en première approximation la bande de trous lourds peut être considérée comme parabolique, m_p jouant alors le rôle d'une masse effective de densité d'états, le maximum de cette bande pouvant alors être décalé de ΔE au-dessus du point Γ_8.

En termes de densité d'états on a alors les schémas à deux bandes suivants dans les configurations SM et SC.

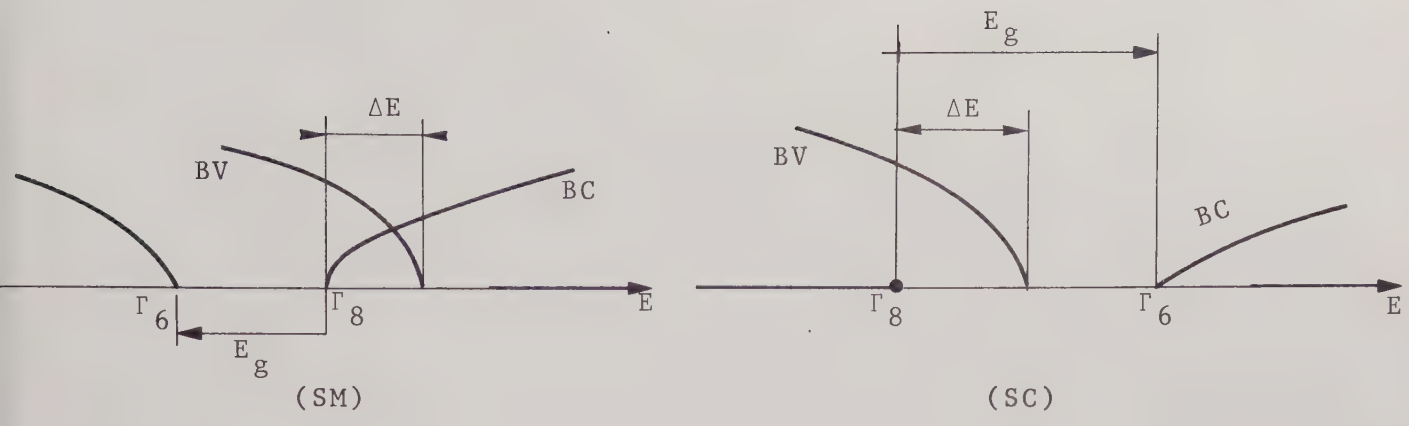

HgTe apparaît alors comme un semimétal à recouvrement ΔE. On obtient un semiconducteur à gap nul (ou un semimétal à recouvrement nul) en négligeant ΔE. α-Sn pour lequel ΔE = 0 par raison de symétrie est effectivement le prototype du semiconducteur à gap nul.

La bande $E_2(k)$ issue de Γ_6 apparaît comme une bande de valence de courbure identique en valeur absolue à celle de la bande de conduction : c'est la bande de trous légers. La bande $E_4(k)$ issue de Γ_7 apparaît elle aussi comme une bande de valence.

Les bandes E_1 et E_4, par la présence du terme kP_K ont des courbures qui dépendent de E_g. On dit qu'elles intéragissent par l'interaction $\vec{k}\vec{p}$. Cette configuration est illustrée par l'étain gris α-Sn[1]. Des études antérieures ont montré que cette configuration inversée s'appliquait à HgTe, HgSe et β-HgS.

b) $E_g \geq 0$. Configuration semiconductrice (SC) (Fig.1b)

Dans ce cas la bande E_1 est issue de Γ_6 et est une bande de conduction. A k = 0 ce sont les bandes E_2 et E_3 qui sont dégénérées en Γ_8. $E_2(k)$ décrit la bande de trous légers. E_4 décrit une bande de valence issue de Γ_7. Cette configuration est celle illustrée par InSb et correspond dans notre cas à CdTe et aux alliages CdHgTe semiconducteurs.

c) Formulation générale

La relation $E_1(k)$ montre que pour des électrons d'énergie telle que $kP_K \simeq |E_g|$ la relation de dispersion devient fortement non parabolique. C'est un trait caractéristique des matériaux à faible largeur de bande interdite $|E_g|$ en configuration SM ou SC.

Lorsque l'origine des énergies est prise au bas de la bande de conduction, la bande de conduction dans les situations SM et SC, c'est-à-dire quelque soit le signe de E_g, est décrite par la relation

$$E_c(k) = \frac{1}{2}\left[-|E_g| + \sqrt{E_g^2 + \frac{8}{3}k^2P_K^2}\right] \qquad (8)$$

La non parabolicité de la bande de conduction a pour conséquences

- une masse effective de l'électron $m(E) = \hbar^2 k(dk/dE)$ dépendant de l'énergie et qui en bas de bande à $k = 0$ dépend du gap $|E_g|$. La masse effective en bas de bande m_n est liée à E_g et P_K par

$$m_n = 3\hbar^2|E_g|/4P_K^2 \qquad (9)$$

- une densité d'états $N(E)$ de la bande de conduction dépendant de E_g et n'ayant plus la dépendance classique $E^{1/2}$ caractéristique d'une relation de dispersion parabolique

$$N(E) = \frac{\sqrt{2}}{\pi^2}\frac{1}{\hbar^3}m_n^{3/2}E^{1/2}(1+2E/|E_g|)(1+E/|E_g|)^{1/2} \qquad (10)$$

Dans la configuration SC quand on ne peut plus considérer que $E_g << \Delta_o$, la courbure de la bande issue de Γ_6 dépend aussi de Δ_o par la relation

$$m_n = \frac{3\hbar^2E_g}{4P_K^2}\frac{2\Delta_o + 2E_g}{2\Delta_o + 3E_g}$$

En revanche dans la configuration SM la courbure de la bande de conduction issue de Γ_8 est toujours donnée à k = 0 par la relation (9).

I.1.D. Fonctions d'onde

Pour chacune des bandes $E_i(k)$ (i = 1 à 4) on obtient la fonctions $u_{i,k}$ par un développement sur la base des 8 fonctions données plus haut. Cependant, compte-tenu de la structure de la matrice d'interaction, on obtient pour chaque bande et chaque valeur de k deux fonctions d'onde $u_{i,\vec{k},\alpha}$ et $u_{i,\vec{k},\beta}$ décrivant ainsi la dégénérescence d'ordre deux de chacune de ces bandes. Les indices α et β correspondent à la composante j_z du moment cinétique total qui, comme cela a été dit, est un bon nombre quantique quand l'interaction spin-orbite est prise en considération.

La structure de la matrice $\mathcal{H}'$ fait que les fonctions $|\sqrt{2}(X+iY)\uparrow>$ et $|\sqrt{2}(X-iY)\downarrow>$ ne se couplent pas aux autres fonctions. Ces deux fonctions décrivent les états de la bande des trous lourds $E_3(k)$.

Prenant par exemple k//Oz, pour les trois bandes E_1, E_2, E_4, on a toujours $j_z = \pm 1/2$ et les fonctions s'écrivent :

$$\left.\begin{aligned} u_{i,k_z,1/2} &= a_i|iS\uparrow> - b_i\left|\frac{X+iY}{\sqrt{2}}\downarrow\right> + c_i|Z\uparrow> \\ u_{i,k_j,-1/2} &= a_i|is\downarrow> + b_i\left|\frac{X-iY}{\sqrt{2}}\downarrow\right> + c_i|Z\downarrow> \end{aligned}\right\} \quad (11)$$

Les coefficients a_i, b_i, c_i sont déterminés pour les bandes E_1, E_2, E_4 par le système :

$$\begin{pmatrix} E_g - E_i & 0 & kP_K \\ 0 & -E_i - 2\frac{\Delta_o}{3} & \frac{\sqrt{2}}{3}\Delta_o \\ kP_K & \frac{\sqrt{2}}{3}\Delta_o & -E_i - \frac{\Delta_o}{3} \end{pmatrix} \begin{pmatrix} a_i \\ b_i \\ c_i \end{pmatrix} = 0$$

Il faut remarquer que dans de telles structures, la fonction d'onde d'un électron de la bande de conduction $E_1(k)$, n'est plus nécessairement une onde plane, c'est-à-dire que $u_{1\vec{k}}(r)$ n'est pas nécessairement un scalaire.

En k = 0 dans la situation SM, $a_1 = 0$ et la fonction d'onde de l'électron est purement de type p.
En k = 0 dans la situation SC, $b_1 = c_1 = 0$ et la fonction d'onde est purement de type s.
Ainsi, du fait des propriétés de dépendance angulaire des fonctions s et p, il apparait que si l'approximation de l'onde plane (utilisée par exemple dans la description des processus de diffusion élastique) est satisfaisante pour des états proches de Γ_6, il n'en est plus de même pour Γ_8. Ce point important sera analysé en détail dans le cadre de l'interprétation des mesures de mobilité électronique (cf. paragraphe suivant).

D'une manière très générale la fonction d'onde sera un mélange de fonctions de type s et de type p, d'autant plus prononcé que l'énergie de l'électron dans la bande de conduction sera comparable à $|E_g|$: en d'autres termes dès que le niveau de Fermi E_F sera comparable à $|E_g|$. Les expressions complètes des coefficients a, b, c pour la fonction d'onde d'un électron de la bande de conduction sont données dans la section II.C de l'annexe I en considérant explicitement les configurations SM et SC dans l'approximation $\Delta_o >> kP_K$, $|E_g|$.

I.1.E. Incidence de la symétrie des fonctions d'onde sur le calcul de la mobilité

D'une manière générale, dans le cadre d'un formalisme utlisant le concept du temps de relaxation, pour un gaz d'électrons dégénéré la mobilité s'écrit :

$$\mu = e\ \tau(E_F)/m(E_F) \qquad (12)$$

Dans le cas d'une bande non parabolique, la masse effective au niveau de Fermi s'écrit

$$m(E_F) = m_n(1 + 2E_F/|E_g|) \tag{13}$$

Compte-tenu de l'expression de la masse effective en bas de bande m_n, (cf. Eq.8) on peut écrire :

$$m(E_F) \propto (|E_g| + 2E_F) \tag{14}$$

Par ailleurs, pour une bande sphérique, le temps de relaxation a la forme générale

$$\tau^{-1}(E) \propto W(E)N(E)$$

N(E), la densité d'états par unité d'énergie tient compte de la non parabolicité de la bande de conduction (Eq.10). Le terme W(E) provient du calcul des probabilités de transition entre états ψ_k et $\psi_{k'}$ induites par le potentiel perturbateur U qui caractérise le mécanisme de diffusion. Dans le calcul de W(E) interviennent des termes du type $|\langle\psi_k|U|\psi_{k'}\rangle|^2$. Les intégrales étendues au volume du cristal du type

$$\int_V u^*_{k'}\, U\, u_k\, e^{i(\vec{k}-\vec{k}')\vec{r}}\, d^3r$$

conduisent à des intégrations sur le volume Ω de la cellule élémentaire du type

$$\int_\Omega u^*_{k'}\, u_k\, d^3r$$

par le fait des variations rapides des fonctions u_k sur le volume Ω.

Quand les états électroniques peuvent être décrits par des ondes planes, comme c'est le cas en Γ_6 où la fonction d'onde est purement de type s, le temps de relaxation prend la forme $\tau_s(E)$

$$\tau_s(E) \propto \frac{dE}{dk}(k^2)^r \tag{15}$$

k étant le vecteur d'onde, dE/dk et k(E) traduisant l'effet de non parabolicité de la relation de dispersion. r est un exposant qui vaut respectivement 1, 0, -1 pour les mécanismes de diffusion suivants : centres chargés (interaction coulombienne), phonons optiques (modes polaires), et phonons acoustiques.

Quand on tient compte de l'expression complète de la fonction d'onde telle qu'elle est obtenue par la méthode $\vec{k}.\vec{p}$, l'intégrale de recouvrement des fonctions u_k et $u_{k'}$ des électrons incident et diffusé introduisent dans l'expression du temps de relaxation un terme supplémentaire F qui traduit la prise en considération du mélange de composantes s et p dans la fonction d'onde. Le temps de relaxation $\tau_{sp}(E)$ prend la forme

$$\tau_{sp}(E) \propto \frac{1}{F_r} \frac{dE}{dk} (k^2)^r \qquad (16)$$

Pour l'exposant r la convention reste la même que dans le cas $\tau_s(E)$. Le facteur F_r dépend explicitement du mécanisme de diffusion considéré. Au paragraphe IV.B de l'Annexe I nous avons fait une bibliographie des différents travaux ayant traité du problème de la mobilité lorsque non parabolicité et vraies fonctions d'ondes sont prises en considération. Pour notre analyse nous avons retenu la formulation de Zawadzki et Szymanska[15] développée dans le cas d'une configuration SC et avons montré comment il était possible de l'étendre très simplement à la configuration SM. Très récemment Szymanska et al.[16] ont reconsidéré le problème de la configuration SM en insistant essentiellement sur le mécanisme de diffusion par phonons acoustiques qui pose un problème particulier du fait de la présence d'une composante de type p dans la fonction d'onde.

Du fait du mélange de fonctions d'onde de type s et p le modèle du potentiel de déformation est inadapté au traitement de la diffusion par phonons acoustiques et cela particulièrement dans la configuration SM où le poids de la composante p est plus important. Néanmoins cet effet important du point de vue du principe n'intervient au niveau calcul que par des termes correctifs qui ne modifient pas sensiblement le résultat final tel que nous l'avons obtenu et utilisé dans ce travail.

I.2. TRANSITION SEMIMETAL-SEMICONDUCTEUR DANS LES ALLIAGES HgTe-CdTe

I.2.A. Effets relativistes

Dans le paragraphe précédent nous avons vu quel était l'effet de l'inversion éventuelle des niveaux Γ_6 et Γ_8 sur la structure de bande au voisinage de k = 0 du point de vue des relations de dispersion et de l'importance de la symétrie des fonctions d'onde. Ces points sont à la base de nombreuses propriétés particulières à cette famille de matériaux. Ces considérations n'ont en rien élucidé le pourquoi de l'inversion des niveaux Γ_6 et Γ_8. On peut seulement remarquer que cette inversion a lieu dès que $E_s - E_p = \left[E(\Gamma_1) - E(\Gamma_{15})\right] < \Delta_o/3$.
Dans HgTe à 0°K on a $E_g = -0{,}303$ eV et $\Delta_o = 1{,}12$ eV.
Dans CdTe à 0°K on a $E_g = 1{,}606$ eV et $\Delta_o = -0{,}920$ eV.

La substitution d'atomes Cd par Hg entraîne une variation de E_g, $\Delta E_g \simeq 1{,}910$ eV. Il faut de plus remarquer que bien que Hg soit un atome beaucoup plus lourd que Cd pour lequel on s'attendrait à ce que le rayon covalent soit plus grand que celui de Cd, on observe pour HgTe un paramètre cristallin d'environ 0,3 % inférieur à celui de CdTe. C'est un fait caractéristique de tous les chalcogénures de Cd et de Hg, HgX et CdX (S = S, Se et Te), et c'est la seule irrégularité de ce type rencontrée dans les semiconducteurs du type $A^N B^{8-N}$ à coordination tétraèdrique [17].

Revenons aux composés HgTe et CdTe. Compte-tenu des valeurs de E_g et Δ_o on trouve pour $(E_s - E_p) \equiv E(\Gamma_1) - E(\Gamma_{15})$:

$$E(\Gamma_1) - E(\Gamma_{15}) = 0{,}070 \text{ eV dans HgTe}$$

$$E(\Gamma_1) - E(\Gamma_{15}) = 1{,}30 \text{ eV dans CdTe.}$$

Dans l'étain gris $E_g = -0{,}413$ eV et $\Delta_o = 0{,}800$ eV. On a alors $E_s - E_p = -0{,}147$ eV. Les niveaux Γ_1 et Γ_{15} sont déjà inversés avant introduction du couplage spin-orbite. Par un calcul de structure bande tenant compte des corrections relativistes autres que

le couplage spin-orbite, Herman et al.[18] ont donné l'interprétation la plus crédible de cette inversion des niveaux Γ_{8+}-Γ_{7-}*.

Lorsque le nombre atomique augmente, l'énergie des électrons s décroît plus vite que celle des électrons p dans l'atome libre. Cela est dû au fait que d'après la comparaison des parties radiales des fonctions d'onde lorsque $r \to 0$, la probabilité de présence d'un électron s au voisinage du noyau est plus forte que celle d'un électron p. Il y a alors augmentation relativiste de la masse de l'électron ($V(r)$ peut être comparable à $2m_o c^2$), diminution de l'énergie cinétique et augmentation de l'énergie de liaison.

Dans le langage des orbitales atomiques, les fonctions d'onde des électrons en Γ_{15} sont obtenues par construction d'orbitales liantes à partir de fonctions d'onde de type p localisées sur chaque atome. Ce langage bien que moins adapté à la description des bandes de conduction, peut encore qualitativement décrire le niveau Γ_1[19] : les fonctions d'onde en Γ_1 sont alors obtenues par combinaison antiliante de fonctions atomiques de type s centrée sur chaque atome. Cela explique la sensibilité de ce niveau aux effets relativistes lors de la substitution Cd → Hg dans le passage CdTe → HgTe. Il semble que de tels effets rendent compte d'une manière satisfaisante de la variation de E_g entre CdTe et HgTe : en utilisant les calculs de corrections relativistes atomiques de Herman et al.[18b] et en s'inspirant de leur analyse sur le couple Ge- Sn[18a], ces calculs donnent E_g = 2,2 eV (voir Section II de l'Annexe I).

I.2.B. Transition SM-SC induite par la composition

A partir de HgTe et CdTe des alliages $Hg_{1-x}Cd_xTe$ peuvent être obtenus pour toutes les valeurs de la composition molaire x ($0 < x < 1$).

---

* Dans la structure diamant $\Gamma_8 \to \Gamma_{8+}$, $\Gamma_7 \to \Gamma_{7-}$, $\Gamma_2 \to \Gamma_{2'}$ et $\Gamma_{15} \to \Gamma_{25'}$

Au voisinage de 0°K E_g varie d'une manière continue et presque linéaire entre les valeurs extrêmes de -0,303 eV et +1,606 eV caractéristiques de HgTe et CdTe. Pour une composition voisine de 0,16 les niveaux Γ_6 et Γ_8 sont accidentellement dégénérés donnant lieu à une transition SM → SC. Cette variation monotone quasi linéaire de l'intervalle Γ_6-Γ_8 avec la composition x peut se comprendre en termes de variation linéaire avec x de la différence des corrections relativistes appliquées aux niveaux Γ_6 et Γ_8.

I.2.C. Transition SM-SC induite par la température

HgTe se singularise également en ce qui concerne le coefficient de température dE_g/dT du gap $E(\Gamma_6) - E(\Gamma_8)$. A la différence de tous les semiconducteurs cristallisant dans le système diamant-blende de zinc, pour lesquels ce coefficient du gap en Γ est négatif, ce coefficient est positif dans HgTe.

Dans HgTe le signe anormal du dE_g/dT n'a pas encore reçu d'explication. Dans les alliages, ce coefficient de température dépend de la composition, s'annule pour $x \simeq 0{,}50$ et reprend un signe négatif pour $x < 0{,}50$. En ce sens HgTe (de même que β-HgS et HgSe) sont similaires aux sels de plomb pour lesquels l'expérience montre que le gap augmente avec la température. En général on impute les variations du gap avec la température à deux mécanismes[20] :

- (i) L'expansion thermique liée aux variations du gap avec le paramètre cristallin. Dans HgTe, $dE_g/dP > 0$ et ne peut être à l'origine d'un $dE_g/dT < 0$. Dans les sels de plomb la situation est moins étonnante en ce sens que le gap étant situé au point L de la zone de Brillouin, dE_g/dP est < 0.

- (ii) Le second mécanisme, dont la contribution est prépondérante, est dû à l'interaction électron-phonon. Cette interaction électron-phonon est traitée en perturbation. Un électron au bas de la bande de conduction interagit avec les vibrations thermiques

et peut être diffusé vers un état de plus haute énergie dans la bande de conduction. Cet effet dépend du nombre de phonons et augmente avec la température. La théorie des perturbations au second ordre montre que deux états qui interagissent de cette manière se repoussent mutuellement. L'énergie d'un électron au bas de la bande de conduction est "repoussée" vers le bas à cause de l'interaction avec les autres états de cette bande. Un électron au sommet de la bande de valence voit son énergie "poussée" vers le haut pour les mêmes raisons. Le résultat global est une diminution de E_g. Pour être plus précis tout se passe comme si le niveau Γ_6 "descend" dans les semiconducteurs du type $A^N B^{8-N}$ tandis que dans HgTe et CdHgTe SC avec $x < 0,5$ le niveau Γ_6 "monte" avec la température.
La transition SM-SC peut être obtenue par augmentation de la température à partir d'une configuration SM.

I.2.D. Transition SM-SC induite par la pression hydrostatique

La dégénérescence accidentelle des niveaux Γ_6 et Γ_8 peut enfin être obtenue par application d'une pression hydrostatique compte tenu d'un coefficient de pression du gap dE_g/dP positif. La pression ainsi que la composition et la température sont des effets qui conservent la symétrie du cristal. Les différents types de transition SM-SC sont schématiquement illustrés sur le schéma ci-après.

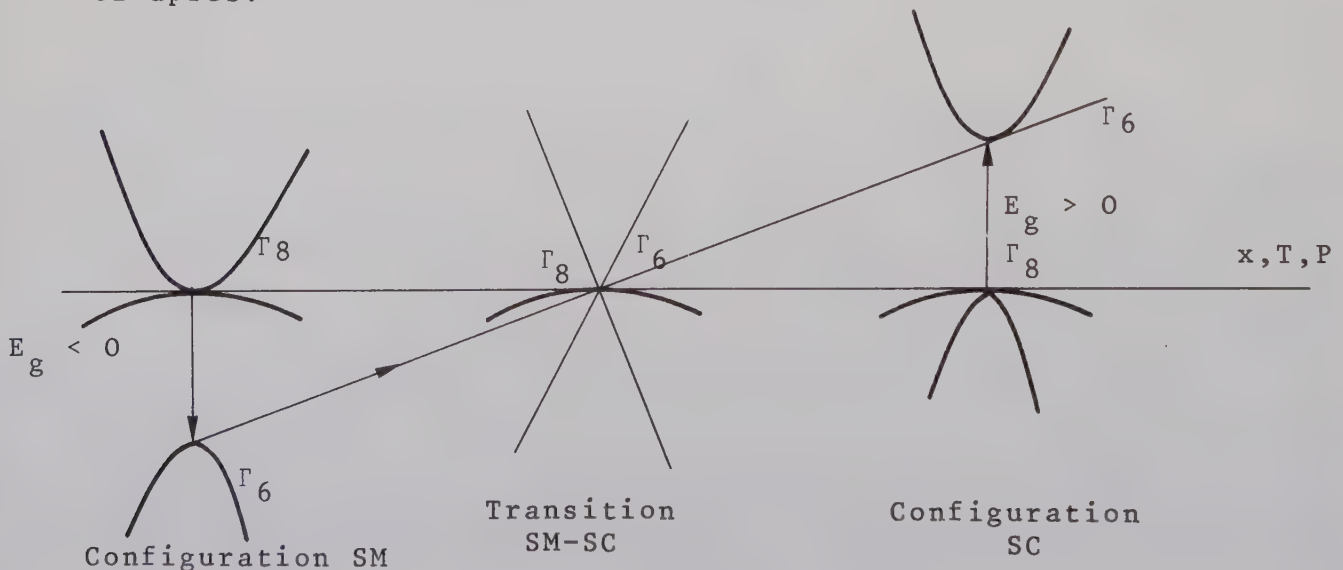

- Illustration de la transition SM-SC induite par variation de composition (x), de température (T) ou de pression (P) dans les alliages $Hg_{1-x}Cd_xTe$.

I.3. SPECULATIONS SUR LA TRANSITION SM-SC

Dans la description d'un solide par un modèle de bandes à un électron, le gap E_g est fonction de paramètres extérieurs tels que paramètre de réseau et température. Dans le cas d'une transition SM-SC obtenue par annulation de E_g il n'y a lieu de s'attendre à aucune discontinuité d'aucune propriété physique.

Quand on prend en considération les interactions électron-électron le passage SM → SC devrait se faire sans singularité à haute température. Néanmoins il semble qu'une température T_M devrait exister au dessous de laquelle le passage de la configuration SM à la configuration SC doive s'effectuer à travers une ou plusieurs transitions de phase[21].

Les arguments avancés en faveur de l'existence éventuelle d'anomalies sont liés à la notion d'état lié électron-trou.

Du côté SM, Mott[22] considère que dans un semimétal avec un petit nombre d'électrons et de trous le nombre de porteurs est assez faible pour limiter l'écrantage de l'interaction coulombienne entre électrons et trous. Dans ces conditions électrons et trous formeraient des états liés non conducteurs, le semimétal devenant alors un isolant. La température à laquelle cette transition aurait lieu serait alors inférieure à l'énergie de liaison électron-trou.

Du côté SC, dans le cas d'un semiconducteur à bande interdite indirecte E_g, l'énergie nécessaire à la création d'un exciton est $E_g - E_B$. L'énergie d'un exciton E_B est déterminée par la masse effective réduite de l'ensemble électron-trou m_r et par la constante diélectrique ε du matériau

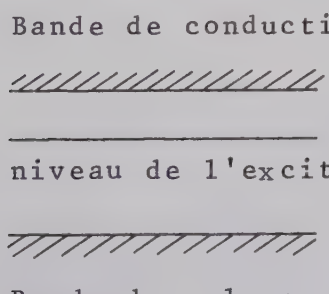

$$\left.\begin{aligned} E_B &= \frac{m_r e^4}{2\hbar^2 \varepsilon^2} \\ m_r^{-1} &= m_n^{-1} + m_p^{-1} \end{aligned}\right\} \quad (17)$$

m_p et m_n étant les masses effectives du trou et de l'électron. Dans le cas d'un gap indirect ε et m_r ne dépendent pas de E_g et on peut rendre E_g arbitrairement petit jusqu'à ce que $E_g < E_B$. L'énergie nécessaire pour créer un exciton est négative et l'état fondamental normal du cristal devient instable : il y a formation spontanée d'excitons. Cet argument a été développé par Knox[23].

D'un point de vue physique, la phase excitonique serait caractérisée par l'apparition d'un ordre antiferromagnétique, ou par une distorsion du réseau avec oscillations de densité de charge. Dans les deux cas il y aurait modification de la périodicité du réseau. La plupart des études spéculatives sur la transition SM-SC ont été faites pour des configurations de bande interdite indirecte[21].

Le cas du gap direct est beaucoup plus délicat à traiter car dans ce cas il peut y avoir de très fortes variations de la constante diélectrique avec le gap.

Les processus de polarisation les plus simples qui contribuent à la constante diélectrique sont les excitations d'un électron des bandes occupées vers les bandes vides. C'est l'approximation de la phase aléatoire (RPA, random phase approximation). Dans ce contexte les excitations qui envoient un électron de la bande de valence vers la bande de conduction à travers le petit gap contribuent d'une manière prédominante à la constante diélectrique. La dépendance de l'énergie et de la fonction d'onde de telles excitations par rapport au gap est directement liée à la symétrie des extrema de bandes.
Cependant l'élévation d'un électron de la bande de valence à la bande de conduction n'est pas l'excitation de plus basse énergie : pour de petits gaps l'exciton peut contribuer de manière significative à la polarisation.

I.3.A. Configuration SC à petit gap direct Γ_6-Γ_8

Sham et Ramakrishnan[24] ont montré que dans cette configuration la contribution des excitons à la constante diélectrique est

négligeable quand $E_g \to 0$. On a vu que dans une telle configuration lorsque $E_g \to 0$ la masse effective des électrons $m_n \to 0$ (Eq.9). Or comme $m_p >> m_n$ la masse réduite $m_r \to 0$. Sham et Ramakrishman rejoignent alors la conclusion de Halperin et Rice[21], à savoir que E_B (Eq.17) tend vers zéro plus vite que E_g. Dans ces conditions on n'attend aucune singularité.

I.3.B. Situation SM type α-Sn du HgTe

Les problèmes posés par cette configuration ont donné lieu à quelques réflexions d'Halperin et Rice[21] d'une part et de Sherrington et Kohn[25] d'autre part.

Il apparaît qu'une conclusion formelle quant à l'existence ou pas d'une transition de phase de type excitonique soit impossible à énoncer. En effet le problème de la détermination de l'énergie E_B de l'exciton est compliqué dans de telles structures par l'apparition, dans le calcul de la constante diélectrique dans le cadre de la RPA, d'une singularité en q^{-1} lorsque le matériau est pur. Ce comportement singulier de la constante diélectrique entrainerait une réduction de l'énergie de liaison de l'exciton de plusieurs ordres de grandeur.

I.4. CONSTANTE DIELECTRIQUE DANS LA CONFIGURATION SM

Dans l'approximation de la phase aléatoire, l'expression de la constante diélectrique à fréquence nulle $\varepsilon(q)$ dans un solide est donnée par

$$\varepsilon(\vec{q}) = 1 - \frac{4\pi e^2}{q^2} \sum_{n,n',k} \left| \langle k,n | e^{-i\vec{q}\vec{r}} | \vec{k}+\vec{q},n' \rangle \right|^2 \times \frac{N_{\vec{k}+\vec{q},n'} - N_{\vec{k},n}}{E_{\vec{k}+\vec{q},n'} - E_{\vec{k},n}}$$

Les bandes sont indicées par n,n'. $N_{\vec{k},n}$ sont les nombres d'occupation. L'élément de matrice représente le recouvrement entre la partie spatiale périodique des deux fonctions de Bloch. Dans la discussion de la constante diélectrique on peut diviser $\varepsilon(q)$ en trois parties.

$$\varepsilon(q) = \varepsilon_o + 4\pi\, \alpha^{inter}(q) + 4\pi\, \alpha^{intra}(q) \qquad (18)$$

Dans la configuration SM qui est celle de α-Sn, HgTe, β-HgS, HgSe les bandes de valence de trous lourds et de conducteur sont dégénérées à k = 0. Le couplage interbande entre ces deux bandes est isolé dans le terme $4\pi\, \alpha^{inter}$. Les transitions intrabandes dues aux excitations des porteurs libres sont prises en considération dans $4\pi\, \alpha^{intra}(q)$. Dans l'approximation de Thomas-Fermi $4\pi\, \alpha^{intra}(q) = k_{FT}^2/q^2$. k_{FT}^2 pour un gaz dégénéré est donné par

$$k_{FT}^2 = 4\pi e^2 \left(\frac{dN(E)}{dE}\right)_{E=E_F}$$

Dans cette expression N(E) est la densité d'états.
ε_o correspond à la contribution de toutes les transitions entre les autres bandes, et entre les autres bandes et celles de valence et de conduction. ε_o ne dépend pas de q. Dans une approximation à deux bandes $4\pi\, \alpha^{inter}(q)$ est donné par

$$4\pi\, \alpha^{inter} = 1 - \frac{8\pi e^2}{q^2} \sum_{\vec{k}} \frac{|\langle \vec{k},c|\, e^{-iqr}\, |\vec{k}+\vec{q},v\rangle|^2}{E_{\vec{k}+\vec{q},v} - E_{\vec{k},c}}$$

$$\times \left(N_{\vec{k}+q,v} - N_{\vec{k},c}\right)$$

L'état $|\vec{k},n\rangle$ a l'énergie $E_{\vec{k},n}$ et le nombre d'occupation $N_{\vec{k},n}$ avec n = v ou c pour les bandes de valence et de conduction respectivement.

Liu et Brust d'une part[26], Halperin et Rice[21] d'autre part, et enfin Sherrington et Kohn[25], ont fait ce calcul dans le cas de l'étain gris intrinsèque à 0°K, c'est-à-dire lorsque le niveau de Fermi est au point de contact des bandes de valence et

de conduction. La méthode kp permet, (cf. paragraphe I de ce même chapitre) de trouver les expressions des relations de dispersion et des fonctions d'onde de la bande de conduction et de la bande de valence.

Dans ces conditions, du fait que bande de valence et bande de conduction appartiennent à la même représentation irréductible en k = 0 on trouve que $4\pi\ \alpha^{inter}$ présente une singularité en q^{-1} pour $q \to 0$.

Cette singularité ne vient pas seulement du fait que l'on soit en situation de "zero-gap". Cette situation de gap nul peut être soit accidentelle, soit imposée par la symmétrie. L'élément de matrice de couplage $|M|^2 = |\langle\vec{k},c|e^{-iqr}|\vec{k}+\vec{q},v\rangle|^2$ dans l'expression de $4\pi\ \alpha^{inter}$ se comporte différemment dans les deux cas, selon la forme des fonctions de Bloch $|\vec{k},c\rangle$ et $|\vec{k},v\rangle$. Quand la dégénérescence est imposée par la symétrie la singularité en q^{-1} apparaît. Elle disparaît quand la dégénérescence est accidentelle.

Dans le cas d'un matériau de type n, c'est-à-dire lorsque l'énergie de Fermi E_F est $E_F > E(\Gamma_8)$, Liu et Tosatti[27] ont montré que bien que $4\pi\ \alpha^{inter}$ demeure fini pour $q \to 0$, cette contribution interbande due aux transitions $\Gamma_8 \to \Gamma_8$ dépend fortement de la concentration n et peut prendre de fortes valeurs quand n devient faible (quand E_F se rapproche de Γ_8).

Dans leurs calculs Liu et Tosatti supposent que le niveau de Fermi est tel que le remplissage de la bande de conduction ne nécessite pas la prise en considération de la non parabolicité. Dans ces conditions ils obtiennent

$$4\pi\ \alpha^{inter} \simeq \frac{3e^2}{\pi\hbar}\left(\frac{2m_n}{E_F}\right)^{1/2} f(q) + O(q) \qquad (19)$$

L'effet de la densité d'états de la bande de conduction Γ_8 sur $4\pi\ \alpha^{inter}$ apparaît à travers la masse effective m_n du bord de bande. f(q) ne dépend d'aucun paramètre de structure de bande. C'est une fonction monotone de q qui pour $q \to 0$ tend vers 4/3 avec

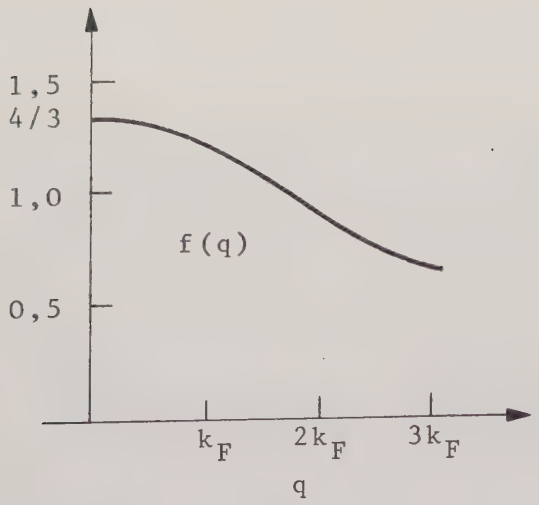

une pente nulle. Nous avons reporté sur la figure ci-contre les variations de la fonction $f(q)$ [27]. k_F est le vecteur d'onde d'un électron au niveau de Fermi.

Fonction f(q) d'après Réf.(27)

Si on appelle $\varepsilon_i(q) = \varepsilon_o + 4\pi\ \alpha^{inter}$ la partie interbande complète de la constante diélectrique et que l'on utilise une forme explicite de k_{FT}^2/q^2 pour $4\pi\ \alpha^{intra}$, la constante diélectrique totale devient

$$\varepsilon(q) = \varepsilon_i(q)\left[1 + \frac{k_{FT}^{eff\,2}}{q^2}\right] \qquad (20)$$

$k_{FT}^{eff} = k_{FT}/\varepsilon_i(q)^{1/2}$ est un paramètre d'écrantage effectif de Thomas-Fermi. k_{FT}^{eff} est l'inverse de la longueur d'écran R.

A basse température, la mobilité est limitée par la diffusion due aux impuretés ionisées. Le comportement singulier de la constante diélectrique dans la configuration SM a pour conséquences

- une réduction de la force du potentiel de l'impureté
- une augmentation de la longueur d'écran de Thomas-Fermi
- une modification de l'écrantage d'une impureté coulombienne : si on suppose un donneur on obtient le potentiel coulombien écranté en faisant la transformée de Fourier suivante :

$$V(r) = -\frac{e^2}{2\pi^2}\int d^3q\ e^{i\vec{q}\vec{r}}\ \frac{1}{\varepsilon(q)q^2}$$

quand $\varepsilon_i(q)$ ne dépend pas de q, $\varepsilon_i(q) = \varepsilon$ alors V(r) prend la forme $-e^2\ e^{-\lambda r}/\varepsilon r$ dite forme de Yukawa, utilisée en général pour les semiconducteurs classiques pour lesquels ε_i ne dépend pas de q.

L'inverse de la longueur d'écran $\lambda = R^{-1}$ est le paramètre de Thomas-Fermi effectif $k_{TF}^{eff} = k_{FT}/\varepsilon^{1/2}$. Quand on tient compte de la dépendance en q de $\varepsilon_i(q)$ le potentiel écranté d'une impureté coulombienne n'est plus du type potentiel de Yukawa.

- une dépendance éventuelle de $4\pi\ \alpha^{inter}$ en température due au fait de la variation du niveau de Fermi E_F lors du remplissage de la bande de conduction par les porteurs intrinsèques excités à partir de la bande de valence[28].

On remarque que la contribution des transitions $\Gamma_8 \rightarrow \Gamma_8$ à la constante diélectrique $\varepsilon(q)$ dépend de la masse effective en bas de bande de conduction m_n et de la hauteur du niveau de Fermi E_F. On s'attend donc à ce que cette contribution soit d'autant moins importante que m_n diminue ou E_F augmente. Ces deux effets sont obtenus par diminution de $|E_g|$ (Eq.9) et/ou augmentation de la température.

Bien que dans le cadre de ce travail nous n'ayons pas eu à considérer la fonction diélectrique dépendant de la fréquence, $\varepsilon(q,\omega)$, il faut noter que les transitions $\Gamma_8 \rightarrow \Gamma_8$ contribuent à un comportement singulier de $\varepsilon(q,\omega)$ pour des moments de transfert $q \rightarrow 0$[29,30].

I.5. ETATS D'IMPURETES DANS LES SEMICONDUCTEURS A GAP NUL

La prise en considération de la non parabolicité de la bande de conduction, le caractère prépondérant de type p de la fonction d'onde de l'électron dans la configuration SM de même que le comportement singulier de la constante diélectrique dans cette configuration sont des caractéristiques importantes des matériaux que nous étudions. Elles ne suffisent pas à expliquer les anomalies observées dans les variations de la mobilité électronique en fonction de la température dans HgTe et certains alliages $Cd_xHg_{1-x}Te$ SM à basse température lorsque c'est la diffusion par centres chargés qui limite la mobilité.

Des études de la mobilité de Hall μ_H, du coefficient de Hall R_H et de la résistivité en fonction de la température T sur des échantillons monocristallins d'alliages $Cd_xHg_{1-x}Te$, ont montré l'existence d'un minimum très marqué des variations de μ_H vs.T pour $T_1 \simeq 9°K$. Autour de T_1, un petit creux apparaît sur les variations de R_H. Aux environs de $T_2 \simeq 40°K$ nous avons observé des effets semblables, bien que moins bien résolus. Cette séquence d'anomalies (appelées dans la suite A_1 et A_2) a été publiée (Fig.2) dans le cas de deux échantillons x = 0,113 et x = 0,129[7]. Dans une publication antérieure Ivanov-Omski et al[31] mentionnent une anomalie dans les variations de la conductivité en fonction de T sur des échantillons de HgTe : observation d'un "plateau" dans le domaine 20-40°K.

Une étude plus systématique sur des échantillons de HgTe ayant subi différents traitements de recuit[9] a montré que ces effets anormaux sont liés à la présence de trous excédentaires c'est-à-dire au caractère p de la conduction. Ce caractère p a pour origine des états accepteurs provenant soit d'écarts à la stoechiométrie du type lacunes de mercure V_{Hg} (anomalies A_1 et A_2) soit à la présence d'atomes appartenant à la 1° colonne du tableau périodique. Le cuivre en particulier semble être à l'origine d'anomalies similaires observées à $T < 1,5°K$[9].

Le caractère plus ou moins prononcé des anomalies A_1 et A_2 est lié au choix de la température du recuit sous pression saturante de vapeur de mercure. Ce traitement de recuit a pour but de corriger la forte concentration de lacunes de mercure donnant aux échantillons bruts de cristallisation un caractère p très marqué ($N_A \simeq 5 \times 10^{18}$ à 10^{19} cm^{-3}).

Plus récemment ces états accepteurs ont été mis en évidence dans HgTe par des expériences de magnéto-optique[32,33].

Le problème des états d'impuretés dans la configuration "gap nul" a été abordé par Liu et Brust d'une part[34] et Gel'Mont et Dyakonov d'autre part[35]. De ces études il résulte que les états d'impuretés intéragissent nécessairement avec le continuum des états étendus de la bande de conduction pour les états accepteurs, ou de la bande de valence pour les états donneurs. Les états

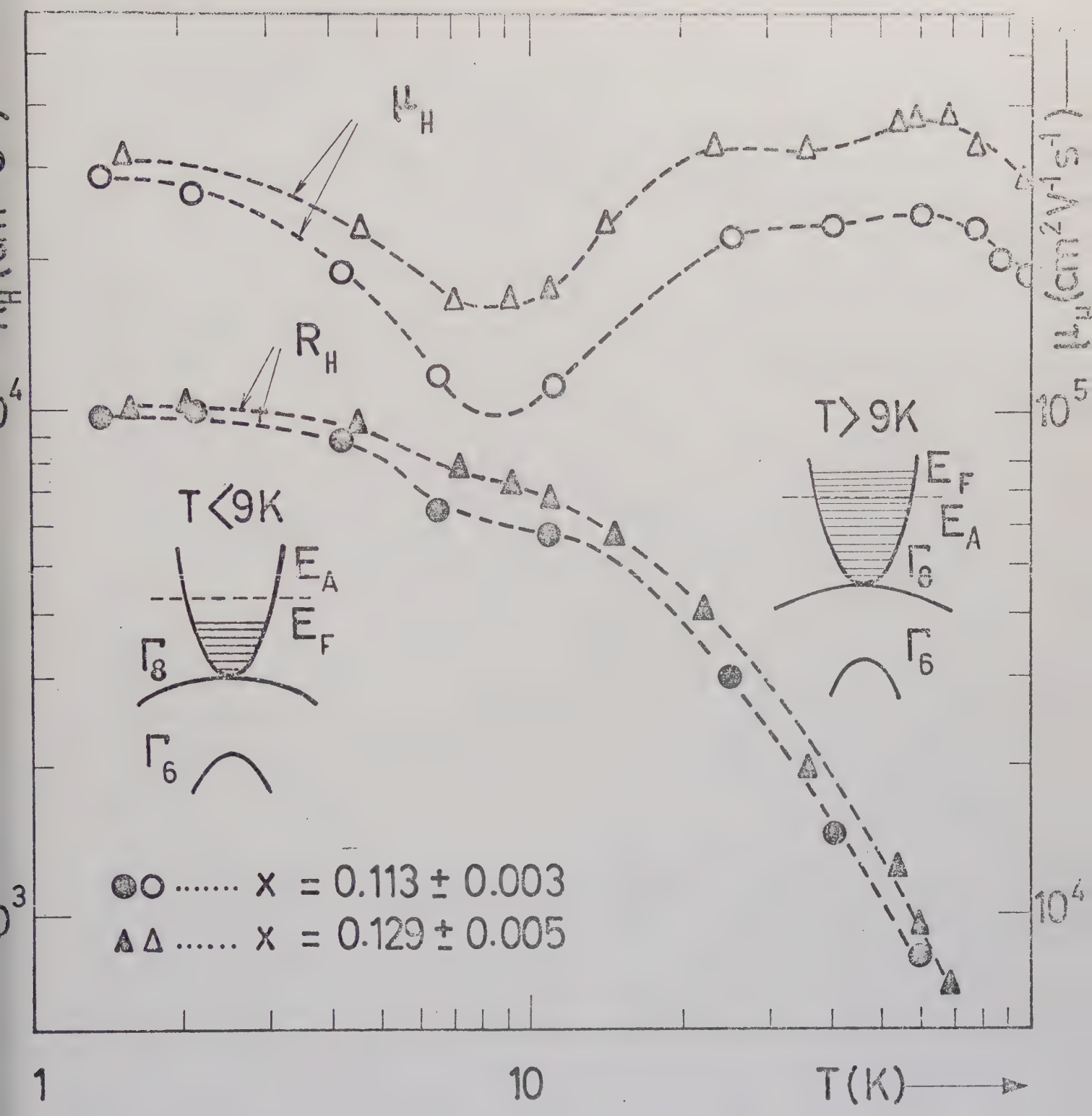

Fig.2 Variations de la mobilité de Hall μ_H et du coefficient de Hall R_H à faible champ en fonction de la température pour deux échantillons $Hg_{1-x}Cd_xTe$ de compositions x = 0.113 et 0.129. Au voisinage de la température de 9°K on observe une anomalie dans le comportement de μ_H et de R_H attribuée au passage du niveau de Fermi E_F devant un niveau accepteur E_A interfèrant avec les états étendus de la bande de conduction.

d'impuretés deviennent alors des états liés virtuels. La forte dissymétrie des densités d'états de la bande de valence et de la bande de conduction ($m_p >> m_n$) fait qu'il ne peut y avoir d'état lié d'un électron sur un donneur : les donneurs sont ionisés à toutes températures.

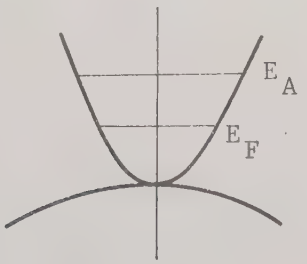

Quant aux états accepteurs E_A qui interfèrent avec la bande de conduction, ils sont neutres à basse température ($E_F < E_A$), ionisés à haute température ($E_F > E_A$).
(cf. figure ci-contre).

Du fait de leur interférence avec les états étendus de la bande de conduction, ces niveaux présentent une certaine largeur ΔE_A. Les anomalies observées sur les effets de transport sont alors explicables en termes de diffusion résonnante des électrons sur ces niveaux lorsque $E_F \simeq E_A \pm \Delta E_A$.

Le calcul du niveau de Fermi à la température de l'anomalie T_1 ou T_2 a montré[9] que l'énergie des niveaux accepteurs A_1 et A_2 variait avec la composition x. A.Mauger a pu rendre compte de la dépendance de E_A en fonction de la densité d'états de la bande de conduction, c'est-à-dire de E_g, donc de x dans une étude théorique[6].

Cette variation de l'énergie E_A de l'état accepteur avec la densité d'états est caractéristique des états accepteurs créés par de forts potentiels localisés tels que ceux résultant de lacunes. L'étude de Gel'Mont et Dyakonov ne permet pas de rendre compte de ce phénomène dans le cas d'un niveau accepteur dû à un potentiel coulombien tel que celui créé par une impureté substitutionnelle.

o o
o

CHAPITRE II

PRINCIPAUX RESULTATS DE CETTE ETUDE

Nous nous proposons de faire ressortir dans ce chapitre les résultats essentiels obtenus au cours de cette étude de la transition SM-SC dans les alliages $Cd_xHg_{1-x}Te$. Dans cette synthèse nous reprendrons les résultats des Annexes I et II sans respecter la chronologie de ces deux études afin d'éclairer dans toute la mesure du possible la lecture de ces annexes auxquelles nous renverrons pour le détail des analyses. Il ne faut pas perdre de vue que les études faites à 292 et 77°K (Annexe I) correspondent au régime intrinsèque ou quasi-intrinsèque, c'est-à-dire dans les deux cas à une situation où compte tenu de leur forte mobilité ce sont les électrons qui jouent un rôle prédominant dans les effets de transport. Dans ces conditions des analyses quantitatives ont pu être faites à ces deux températures où effet Hall et conductivité conduisent sans ambiguité à la concentration et à la mobilité des électrons. L'effet de la pression à 292 et 77 K pour chaque échantillon ($0 \leq x \leq 0,14$) a permis d'analyser de façon précise les caractéristiques essentielles de la bande de conduction et d'étudier avec une bonne résolution la transition SM-SC induite par la pression sur des alliages de composition appropriée. Cette analyse des effets de bandes est décrite en détail dans l'Annexe I.

L'installation expérimentale utilisée pour les études faites à très basse température (Annexe II) a permis par étude de l'effet Hall en fonction du champ magnétique de déterminer séparément concentration et mobilité des porteurs majoritaires d'une part et minoritaires d'autre part et par conséquent une étude complète des paramètres de conductivité des différents types de porteurs participant au régime extrinsèque : électrons minoritaires appartenant aux états étendus de la bande de conduction, électrons "lents" presque piégés sur des niveaux accepteurs résonnants ionisés, trous majoritaires appartenant à la bande de valence (cf. Annexe II).

II.1. BANDES DE VALENCE, DE CONDUCTION, TRANSITION SM-SC

Dans le contexte d'un modèle de bandes négligeant aussi bien les interactions électron-électron que les effets dus dans un alliage à la perte de la symétrie de translation, la bande de conduction, dans les situations SM et SC est décrite par la relation (Eq.8). Dans ces conditions, masse effective et densité d'états en bas de bande varient proportionnellement à $|E_g|$ (Eqs. I,10). Lorsque l'énergie de Fermi E_F est grande devant l'énergie thermique k_oT, c'est-à-dire quand $\eta \equiv E_F/k_oT > 1$, la concentration électronique n peut s'écrire en première approximation (les termes en $1/\eta^2$ sont négligés)

$$n \propto m_n^{3/2} E_F^{3/2} (1 + E_F/|E_g|)^{3/2} \qquad (21)$$

Le terme $(1 + E_F/|E_g|)^{3/2}$ traduit l'effet de la non-parabolicité de la bande de conduction dès que $E_F \simeq |E_g|$, et devient prépondérant lorsque $|E_g| \to 0$, au voisinage de la transition SM-SC. La relation 21 est valable en première approximation pour un gaz d'électrons dégénéré : c'est la situation effectivement rencontrée dans le domaine SM ($E_g < 0$) à toutes les températures. En régime intrinsèque, à 292 et 77°K on trouve $\eta \simeq 3$ à $4\ k_oT$, c'est-à-dire de l'ordre de 70-100 meV à 292°K et 20-30 meV à 77°K (Fig.3). Dans l'approximation d'une bande de valence de trous lourds parabolique, isotrope décrite par les paramètres ΔE et m_p (Eq.7), la concentration de trous p est donnée, lorsque $\eta' >> 1$, par

$$p \propto m_p^{3/2} \exp(-\eta') \qquad (22)$$

avec

$$\eta' = -(E_F + \Delta E)/k_oT \quad \text{dans la configuration SM}$$

$$\eta' = -(E_F + \Delta E)/k_oT - (E_g/k_oT) \quad \text{dans la configuration SC.}$$

L'analyse quantitative des résultats expérimentaux nécessite la connaissance des paramètres E_g, P_K, ΔE, m_p, ainsi que les variations éventuelles de ces paramètres avec la composition ou la pression.

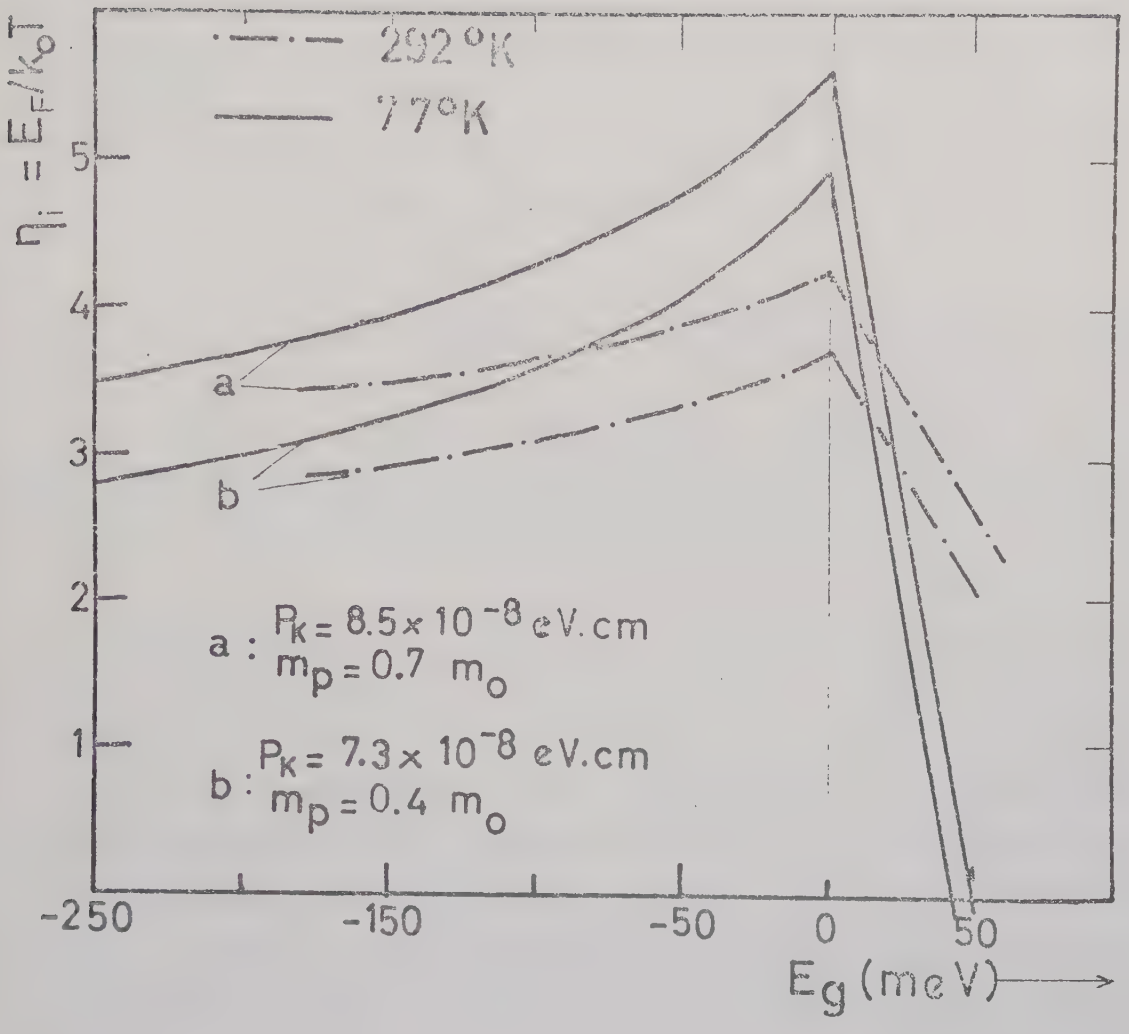

Fig.3 Variations calculées du niveau de Fermi réduit en régime intrinsique en fonction du gap $E_g = E(\Gamma_6) - E(\Gamma_8)$. Les courbes a et b correspondent aux valeurs extrêmes publiées pour P_k et m_p.

Cette analyse a été menée à 292 et 77°K dans le cadre d'un modèle à deux bandes (Eqs.7 et 8) qui néglige la contribution des trous légers aux effets de transport ; approximation raisonnable du fait de la densité d'états de cette bande comparée à celle des trous lourds et de l'éloignement de ces deux bandes de trous dans la configuration SM. Les calculs menés à 77°K et 292°K ont nécessité le recours à un ordinateur afin de ne faire aucune approximation sur l'état de dégénérescence des populations des bandes de valence et de conduction.

II.1.A. Bande de valence de trous lourds issue de Γ_8

L'ensemble des études faites à 292 et 77°K (Annexe I) a montré que sous l'effet de la pression cette bande est indéformable, en ce sens que l'on rend compte des résultats expérimentaux avec une masse effective de densité d'états

$$m_p/m_o = 0,55 \pm 0,1$$

qui ne varie pas avec la pression.

Les trous appartenant à cette bande Γ_8 ont une mobilité de 500-600 $cm^2\ V^{-1}\ sec^{-1}$ qui ne dépend pas de la pression. Des études faites au Laboratoire sur des échantillons de HgTe de type p (dopés à l'argent)[6] sont en accord sur ce point avec les résultats publiés par ailleurs (voir Annexe I).

Dans le cadre de l'analyse $\vec{k}.\vec{p}$, ce résultat est en accord avec le fait que la courbure de la bande de trous lourds est déterminée par l'interaction avec des bandes inférieures et supérieures dont le déplacement sous l'effet de la pression est négligeable compte-tenu de leur distance par rapport au niveau Γ_8.

A basse température l'analyse des résultats obtenus sur HgTe (Annexe II) a permis une estimation du recouvrement ΔE dû à la disparition de la symétrie d'inversion. Nous avons trouvé

$$\Delta E \lesssim 1 \text{ meV}$$

en accord avec d'autres déterminations expérimentales et théoriques citées dans l'Annexe II.

Compte-tenu des énergies de Fermi à 292 et 77°K il est évident que l'on a pu négliger dans ces analyses ce recouvrement.

II.1.B. Bande de conduction

Dans les configurations SM et SC on rend compte des variations de la concentration des électrons de la bande de conduction sous l'effet d'une variation de E_g en se référant à la relation (8) dans laquelle l'élément de matrice P_K vaut :

$$\boxed{P_K = (7,6 \pm 0,3) \times 10^{-8} \text{ eV cm}}$$

Le coefficient de pression de E_g a été déterminé à 292,77 et 1,7 K {Cf. Annexe I, § IV.A.a. et Annexe II, § II.B.2)}. A 292,77°K d'une part et 1,7°K d'autre part les résultats expérimentaux ont montré que, dans le domaine SM pour $|E_g| >> E_F$, $n^{2/3}$ varie linéairement avec la pression. Ce résultat est en accord avec l'expression (Eq.21) qui montre que l'on a alors $n^{2/3} \propto m_n$ c'est-à-dire $n^{2/3} \propto |E_g|$. En effet, conformément à l'analyse k.p, la masse effective m_n en bas de bande varie proportionnellement à $|E_g|$ (Eq.9), donc à la pression dans l'hypothèse d'une variation linéaire de E_g avec la pression. Les valeurs que nous obtenons sont les suivantes :

$$\boxed{\begin{array}{lll} dE_g/dP = (10 \pm 0,5) \times 10^{-6} \text{ eV bar}^{-1} & \text{à} & 292 \text{ K} \\ dE_g/dP = (9 \pm 0,5) \times 10^{-6} \text{ eV bar}^{-1} & \text{à} & 77 \text{ K} \\ dE_g/dP = (8,5 \pm 0,5) \times 10^{-6} \text{ eV bar}^{-1} & \text{à} & 1,7 \text{ K} \end{array}}$$

On observe une dépendance en température du coefficient dE_g/dP pour les alliages riches en Hg. Ceci peut être attribué aux variations

de la compressibilité (c'est-à-dire des constantes élastiques) induites par la température dans HgTe.

Dans CdTe ce coefficient vaut $(8,2 \pm 0,1) \times 10^{-6}$ eV bar^{-1} à 77°K et $(8,3 \pm 0,5) \times 10^{-6}$ eV bar^{-1} à 297 K. La similitude entre les valeurs du dE_g/dP à basse température dans HgTe et CdTe est en désaccord avec des calculs théoriques basés sur le modèle de la liaison chimique de Philipps qui donnent pour HgTe une valeur de 12×10^{-6} eV bar^{-1}. Ces différents points concernant le coefficient dE_g/dP sont plus longuement discutés à la Section V de l'Annexe I.

II.1.C. Transition semimétal-semiconducteur

Dans le cadre d'un modèle de bandes à un électron, la transition SM-SC, due à l'inversion des niveaux Γ_6 et Γ_8, entraîne une modification de la masse effective en bas de bande m_n qui décroît avec $|E_g|$ dans le domaine SM ($E_g < 0$), s'annule à la transition SM-SC ($E_g = 0$) et croît avec E_g dans le domaine SC ($E_g > 0$). La variation de masse effective est un effet observable sur la mobilité alors que, plus indirectement, c'est la variation de densité d'états qui gouverne le comportement de la concentration électronique au voisinage de la transition SM-SC.

Nous ne discuterons dans un premier temps, que de l'analyse de la transition SM-SC à travers l'étude du comportement de la concentration électronique ou, ce qui revient qualitativement au même, de la constante de Hall.

Nous avons reporté sur les figures 4-7 les variations de la concentration électronique n en fonction de la pression aux températures respectives de 292, 77 et 4;2 et 1,7 K pour des échantillons de différentes compositions. Sur ces courbes apparaissent deux domaines de pression où les variations sont quasi linéaires, séparés par une discontinuité de la pente à une certaine pression critique. Des calculs complets basés sur le modèle de bandes décrit par la méthode $\vec{k}.\vec{p}$ montrent que cette cassure de pente correspond

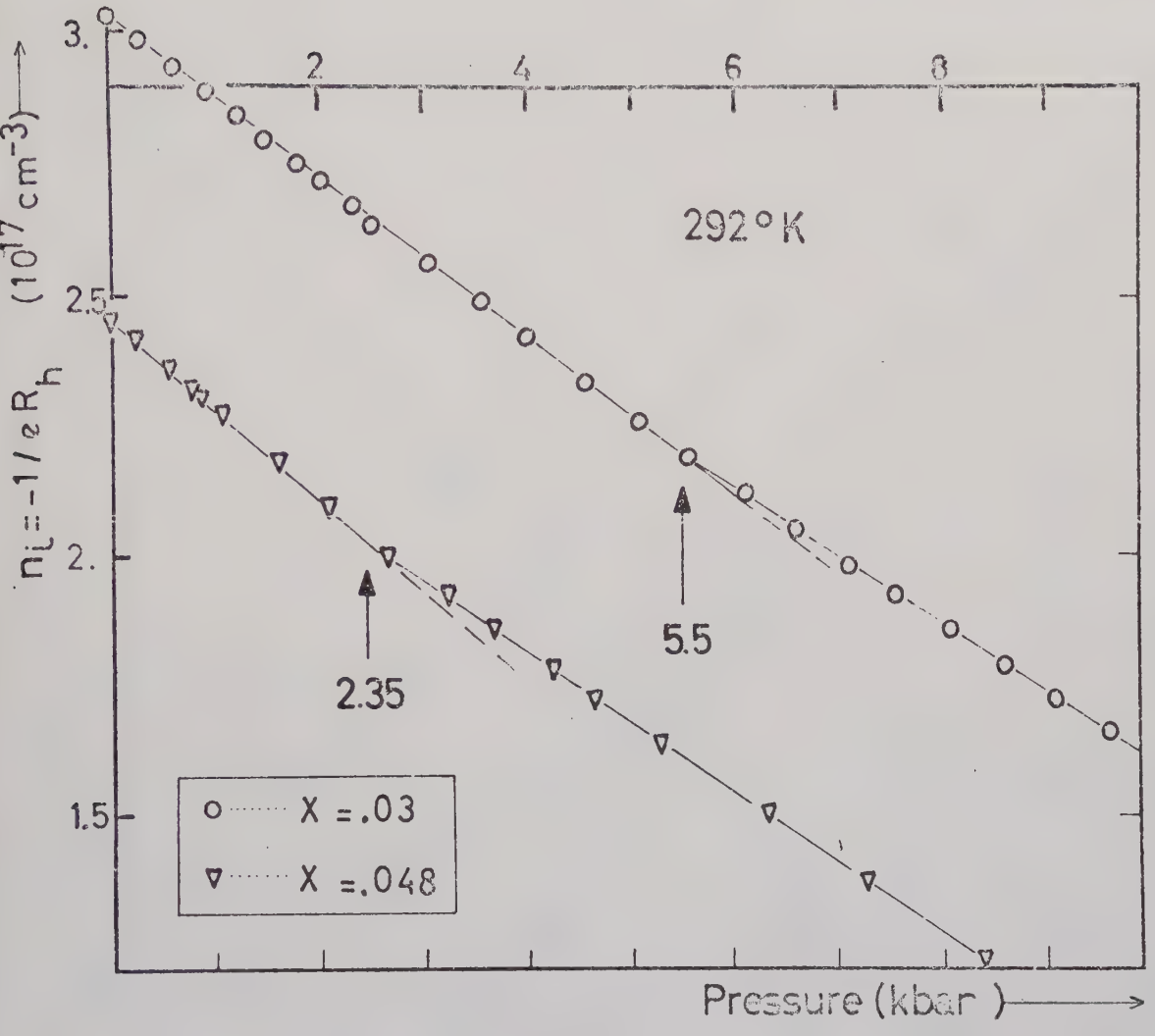

Fig.4 Variations expérimentales de la concentration électronique en fonction de la pression illustrant un changement de pente correspondant à la transition SM-SC pour deux échantillons $Cd_xHg_{1-x}Te$ de composition x = 0.03 et x = 0.048. Les flèches indiquent la pression de la transition.

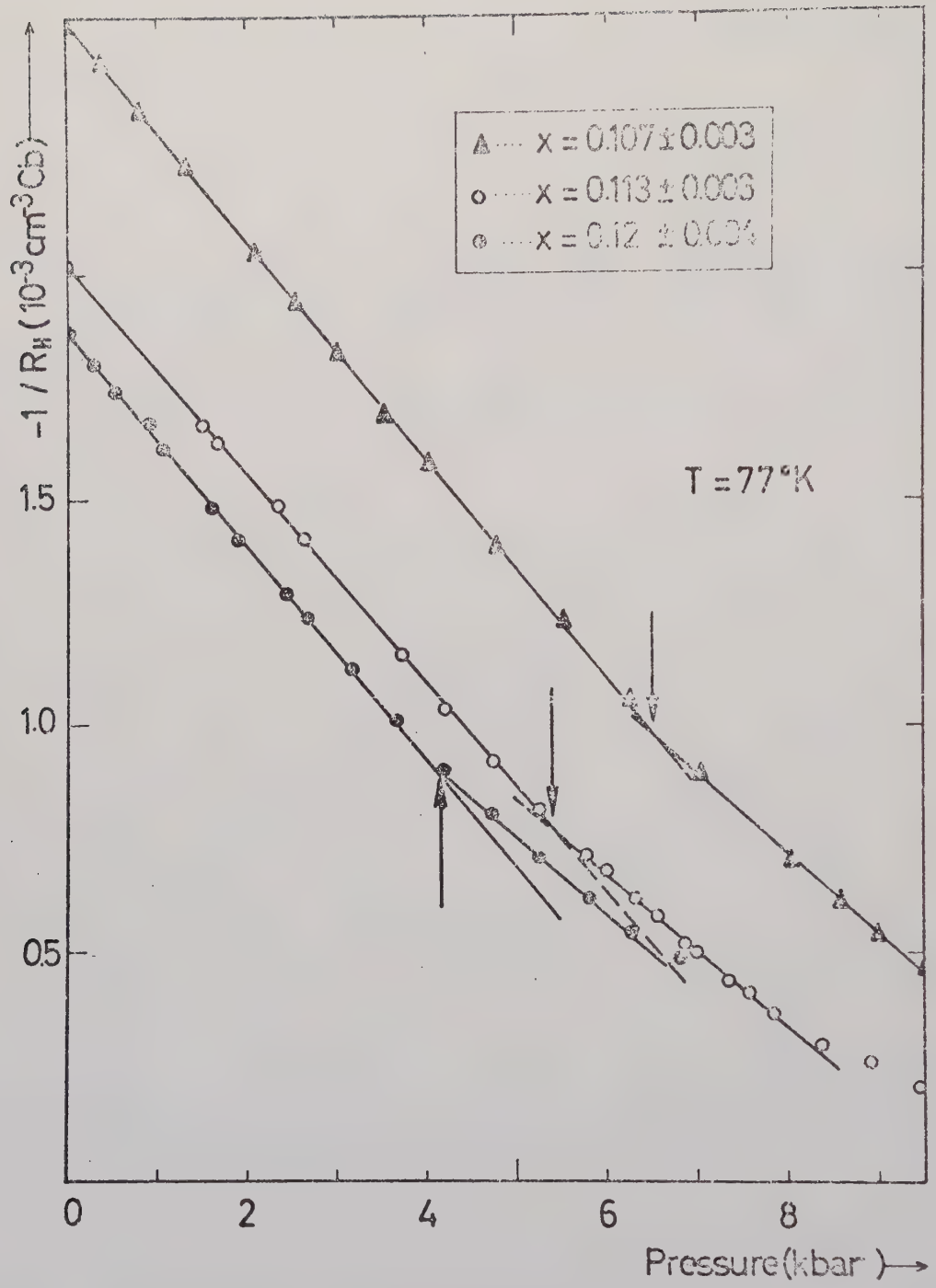

Fig.5 Illustration de la transition SM-SC induite par la pression à 77°K dans $Cd_xHg_{1-x}Te$ pour différents x. En reportant l'inverse de la constante de Hall mesurée à bas champ en fonction de la pression, on observe une cassure de pente attribuée au croisement des niveaux Γ_6, Γ_8.

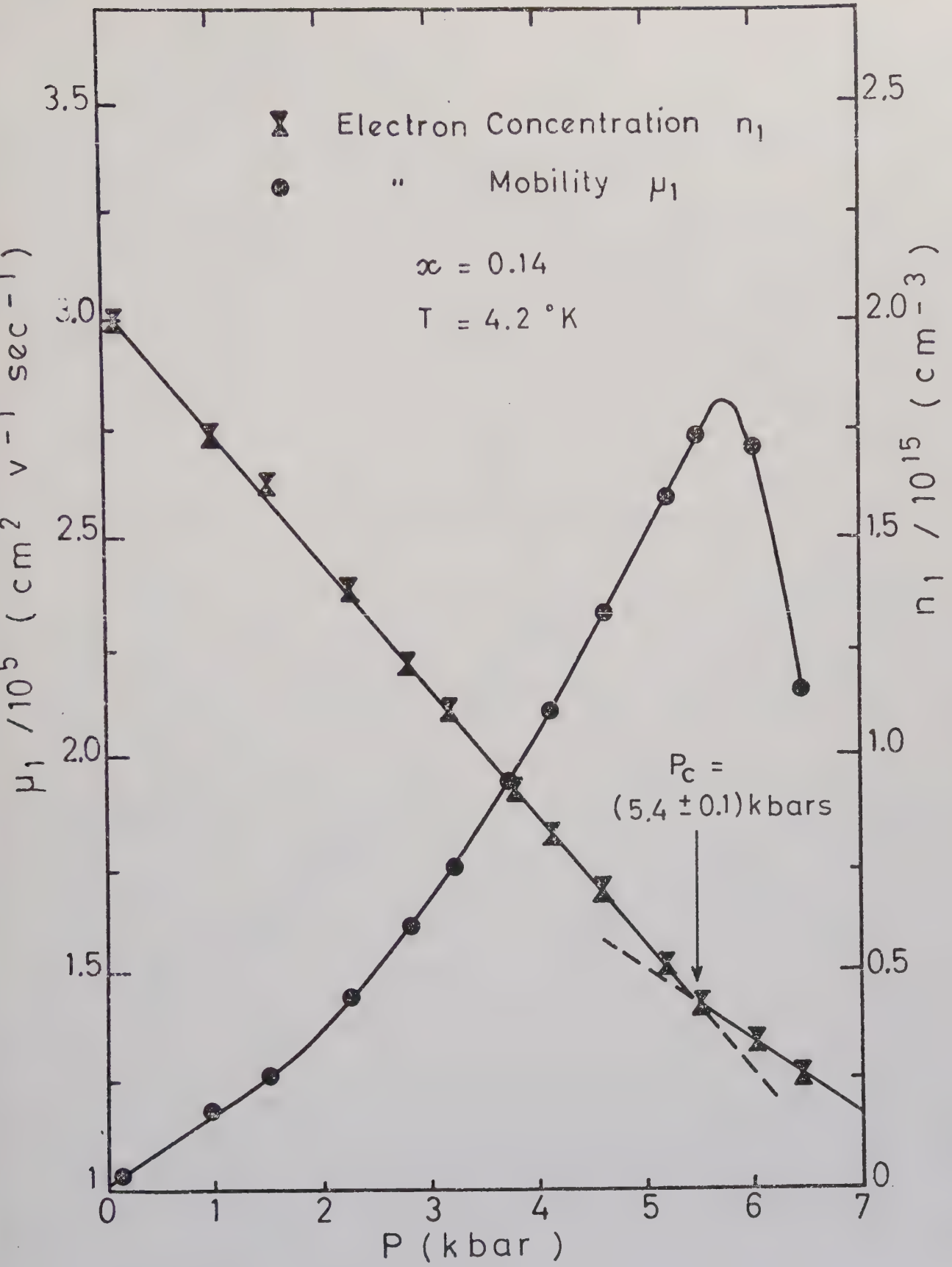

Fig.6 Variations expérimentales de la concentration électronique n_1 et de la mobilité électronique μ_1 en fonction de la pression à 4.2°K sur un alliage $Hg_{1-x}Cd_xTe$ pour $x = 0.14$. La cassure de pente observée à 5.4 kbar sur les variations de n_1 illustre la transition SM-SC induite par la pression.

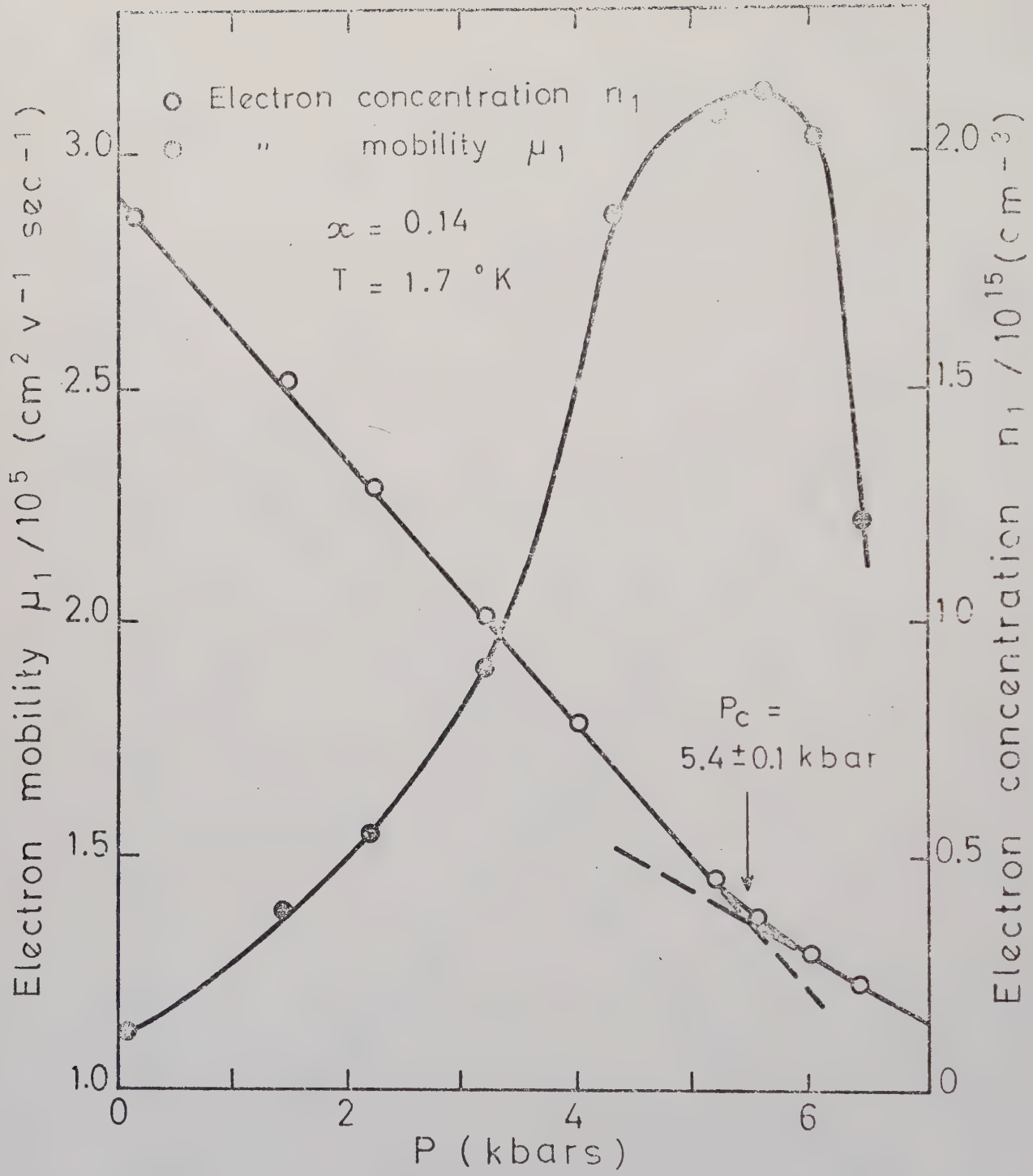

Fig.7 Variations expérimentales de la concentration électronique n_1 et de la mobilité électronique μ_1 en fonction de la pression à 1.7°K sur un échantillon $Hg_{1-x}Cd_xTe$ pour x = 0.14. La cassure de pente observée à 5.4kbar sur les variations de n_1 illustre la transition SM-SC induite par la pression.

au passage par la situation $E_g = 0$ (Annexe I Section IV.B.C) et est due à deux effets compétitifs qui entrent en jeu dans la configuration SC : l'ouverture du gap d'une part et l'augmentation de la densité d'états avec E_g d'autre part.

On peut déjà constater que la transition SM-SC ne s'accompagne d'aucun comportement singulier quant aux variations de la concentration électronique et ce même à très basse température. Par ailleurs le nombre de points expérimentaux utilisé pour caractériser cette transition SM-SC permet d'affirmer, compte-tenu des valeurs du dE_g/dP, que l'on a mis en évidence des valeurs de E_g de l'ordre de 4 à 5 meV. Des valeurs aussi faibles représentent un résultat qu'il est intéressant de situer dans le contexte de spéculations liées à l'existence même de petits gaps, voire du gap nul (Cf. § I.3).

Sur les figures 6 et 7 les variations de la mobilité des électrons de conduction en fonction de la pression à 4°K et 1,7°K sont également reportées. La transition SM-SC se manifeste alors par un maximum de la mobilité au voisinage immédiat de cette pression critique.

Nous avons reporté sur la figure 8 les variations relatives de la mobilité en fonction de la pression pour différentes compositions à 292°K. Partant de la configuration SM ($x = 0$) quand x varie un maximum de mobilité apparaît à des pressions d'autant plus basses que $|E_g|$ décroît. Ce maximum de mobilité apparaît toujours au voisinage immédiat de la pression critique déduite de la cassure de pente observée sur les variations de la concentration électronique.

Le même résultat apparaît quand la transition SM-SC est induite par la composition. Les variations de la mobilité des électrons à 292°K en fonction de la composition (Fig.9) montrent un maximum au voisinage de la composition $x = 0,06$. Or les analyses reportées à la section IV.A.b de l'annexe I ont permis de déterminer les lois $E_g(x)$ à 292 et 77°K (Figs. 5 et 6 de l'Annexe I). A 292°K la composition x_o pour laquelle a lieu la transition SM-SC à pression ambiante est $x_o = 0,07 \pm 0,01$ en accord avec celle pour laquelle

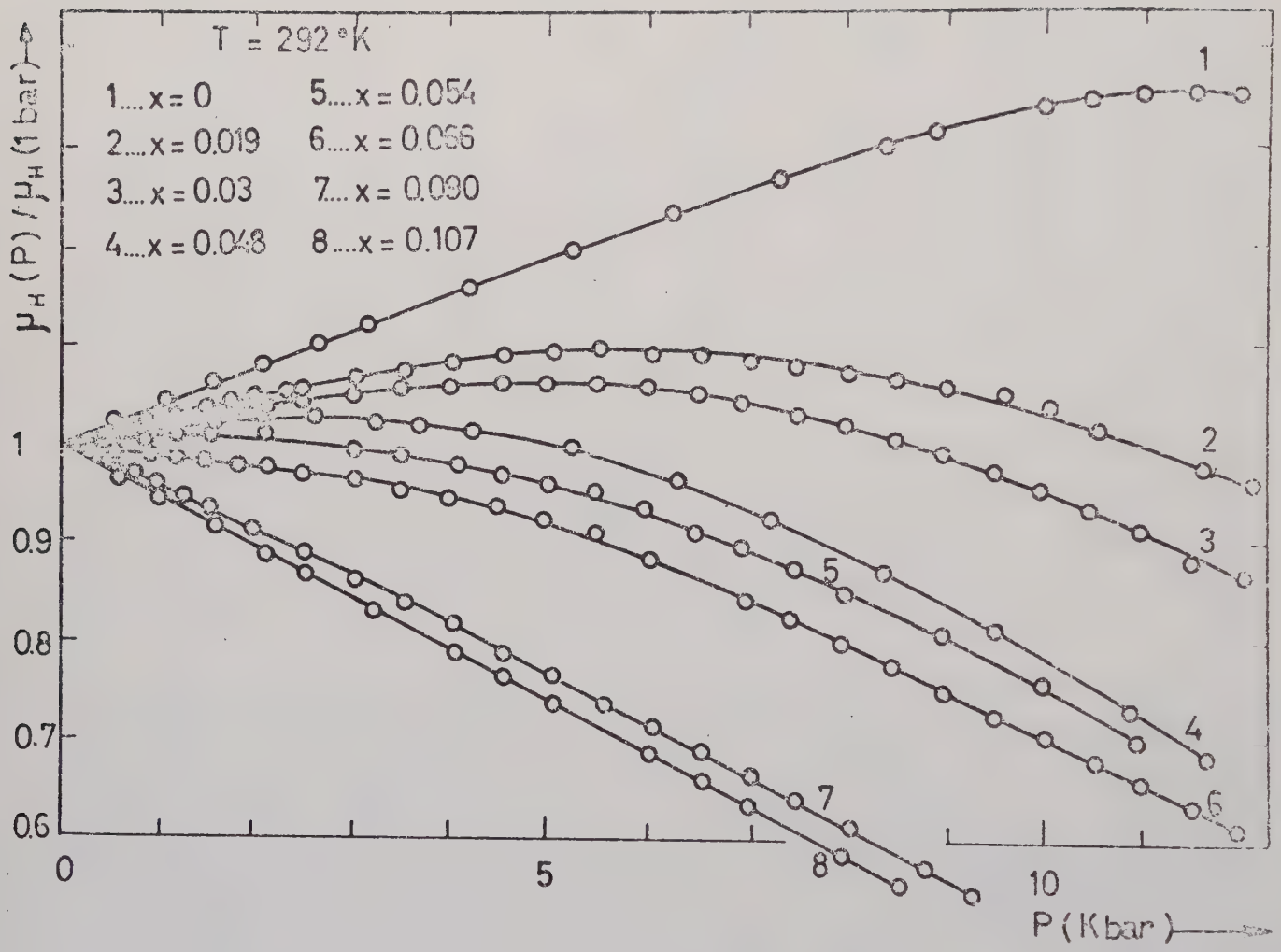

Fig.8 Variations relatives de la mobilité de Hall à 292°K en fonction de la pression dans $Cd_xHg_{1-x}Te$ pour différentes valeurs de la composition. Le maximum de mobilité (échantillons 1 à 5) correspond à la transition SM-SC et se déplace vers les basses pressions quand x croît.

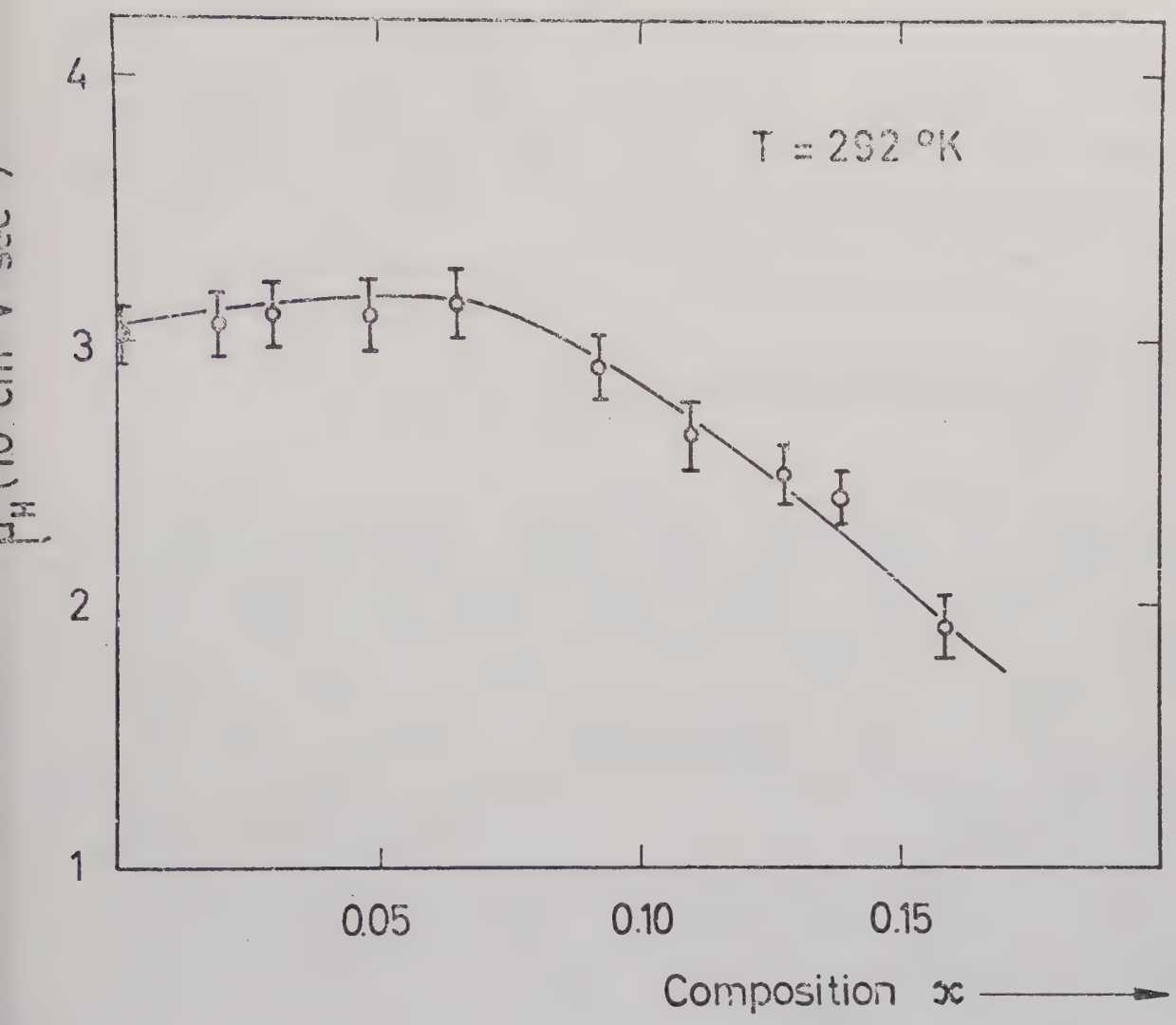

Fig.9 Valeurs expérimentales de la mobilité de Hall à la pression ambiante à 292°K en fonction de la composition dans $Cd_xHg_{1-x}Te$. Le maximum observé au voisinage de la composition x = 0.06 correspond à la transition SM-SC induite par l'effet d'alliage.

la mobilité des électrons présente un maximum. L'existence d'un maximum de mobilité au voisinage de $E_g = 0$ n'est pas un fait surprenant : conformément à l'analyse $\vec{k}.\vec{p}$, m_n décroît dans la configuration SM, s'annule à la transition SM-SC pour croître dans la configuration SC. Néanmoins, nous le verrons plus loin, l'analyse de la mobilité au voisinage de la situation SM-SC ne se satisfait pas de raisonnements aussi qualitatifs.

II.2. PORTEURS EXTRINSEQUES, ETATS ACCEPTEURS

L'étude des propriétés extrinsèques constitue le corps de l'annexe II. Cette étude a mis en jeu des mesures électriques à très basse température en ajoutant à l'ensemble des paramètres déjà utilisés tels que composition, température, pression, le paramètre champ magnétique. Des mesures d'effet Hall ou de résistivité en fonction du champ magnétique permettent, quand 2 types de porteurs participent aux effets de transport, d'accéder aux concentrations et mobilité de chaque type. Parmi les échantillons sélectionnés par un ensemble de mesures préalables pour cette étude, nous avons tout particulièrement étudié un alliage de composition $x = 0,14$ et un échantillon de HgTe.

L'analyse de l'ensemble des mesures a permis de mettre en évidence les résultats suivants.

II.2.A. Etat accepteur dû à un potentiel très localisé

Sur l'échantillon de composition $x = 0,14$ les mesures à bas champ magnétique ont permis d'illustrer la transition SM-SC (Figs 6,7). Les mesures faites en fonction du champ magnétique ont montré que l'effet Shubnikov-de Haas et notamment l'oscillation 0^+ apparaissait non seulement sur la magnétorésistance, mais aussi sur les variations de l'effet Hall en fonction du champ magnétique. Ces varia-

tions de l'effet Hall en fonction du champ magnétique ont mis en évidence l'existence d'électrons minoritaires dont concentration et mobilité en fonction de la pression ont été reportées à 4,2°K sur la figure 6. Sur la figure 10 sont reportées les variations de la concentration et de la mobilité des trous en fonction de la pression à 4,2°K, déduits de l'analyse de l'effet Hall en fonction du champ magnétique (cf. Annexe II, Section II.C).

Nous avons reporté sur la figure 11 les variations de la concentration d'impuretés $N_{A^-}-N_D = p - n$ en fonction de la pression (les valeurs de p et n sont déduites d'après les mesures illustrées sur les figures 6 et 10).

Compte-tenu du fait que dans la configuration SM les donneurs sont toujours ionisés[6,35], nous sommes conduits à attribuer les variations de $p - n = N_{A^-}-N_D$ à l'ionisation d'un état accepteur dont la distance E_{A_1} au point Γ_8 varie avec la pression, c'est-à-dire avec E_g (Fig.12). Un tel effet a déjà été mentionné dans une étude faite en fonction de la composition[9]. D'après l'étude théorique de Mauger[6], il apparaît que dans le cas de forts potentiels localisés, tels que ceux induits par des lacunes V_{Hg}, la position du niveau accepteur dépend de la densité d'états de la bande de conduction dégénérée en Γ_8 avec la bande de valence. Dans la configuration SM quand $|E_g|$ décroît, la densité d'état de la bande de conduction décroît et E_{A_1} croît. Dans la configuration SC l'ouverture du gap correspond à une variation brutale de la densité d'états de la bande de conduction au voisinage de Γ_8 et E_{A_1} continue de croitre. Cependant l'ouverture du gap a un effet compensateur du fait que la bande de valence issue de Γ_8 intervient alors de façon déterminante dans la hauteur de E_{A_1}. Il ne devrait plus se déplacer par rapport à Γ_8 pour apparaître enfin comme un niveau discret situé dans la bande interdite. Notre installation expérimentale ne nous a pas permis d'atteindre cette configuration SC où le niveau accepteur entre dans la bande interdite.

La détermination expérimentale de $(E_{A_1} - E_F)$ a montré qu'aux basses pressions $E_{A_1} < E_F$. E_{A_1} et E_F se croisent à 3,7 kbar (cf. Annexe II, Section II.C.2, Fig.19 de l'Annexe).

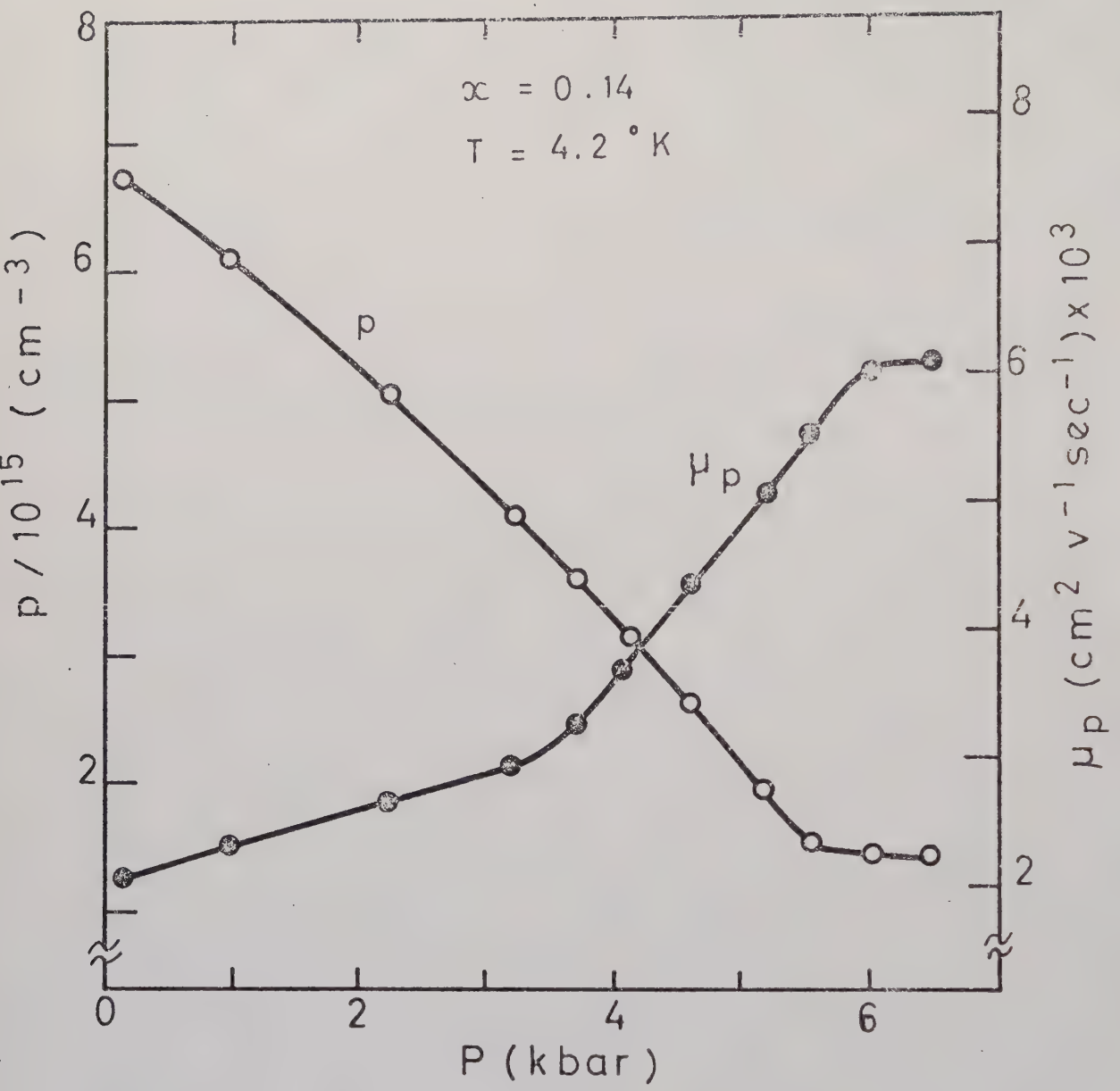

Fig.10 Variations de la concentration en trous p et de leur mobilité μ_p en fonction de la pression à 4.2 °K sur un échantillon de $Hg_{1-x}Cd_xTe$ pour x = 0.14.

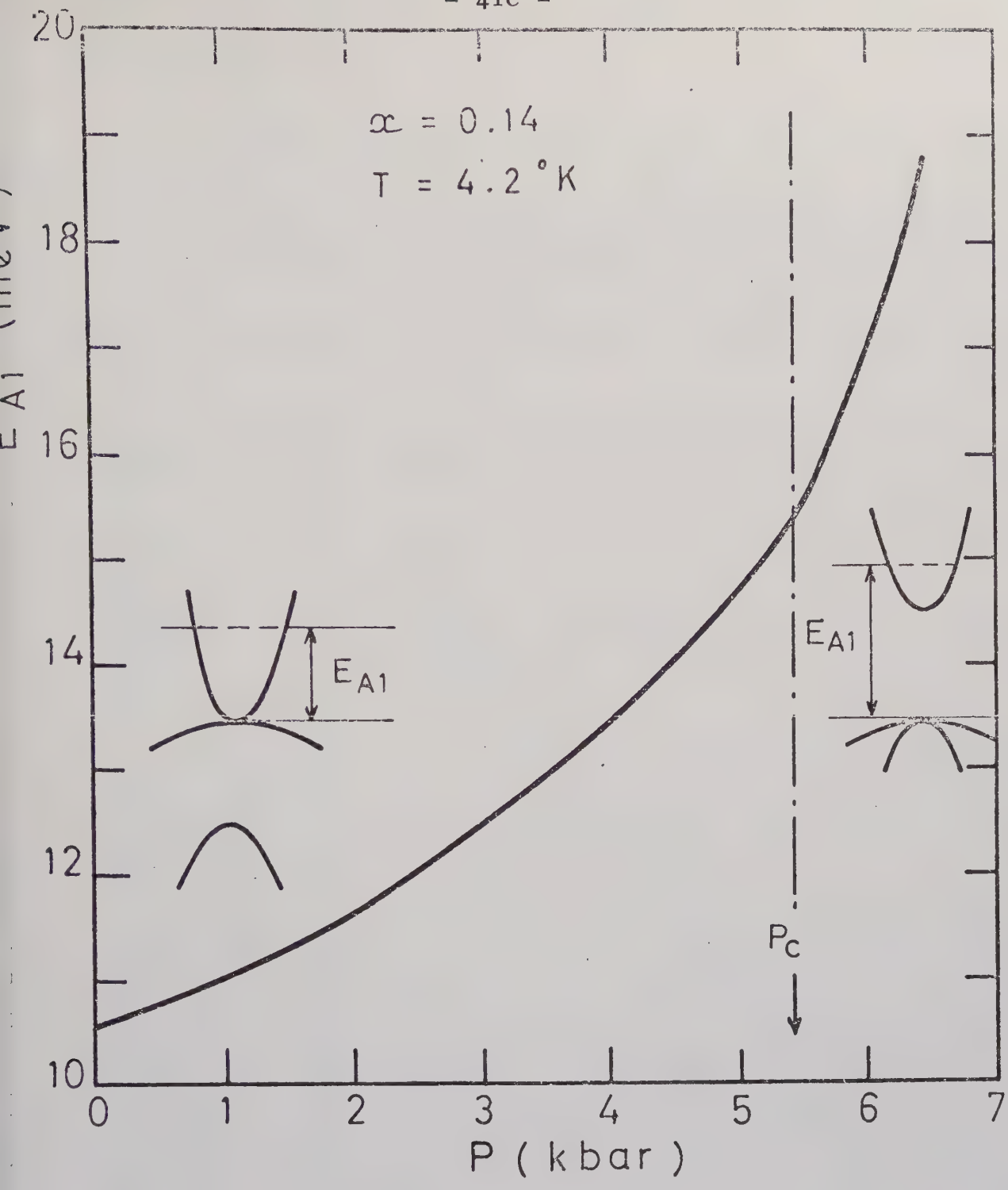

Fig.12 Variations de l'énergie E_{A1} du niveau accepteur observé dans l'échantillon de $Hg_{1-x}Cd_xTe$ (x=0.14) en fonction de la pression à 4.2°K. L'origine des énergies est prise en Γ_8. P_c est la pression critique de transition.

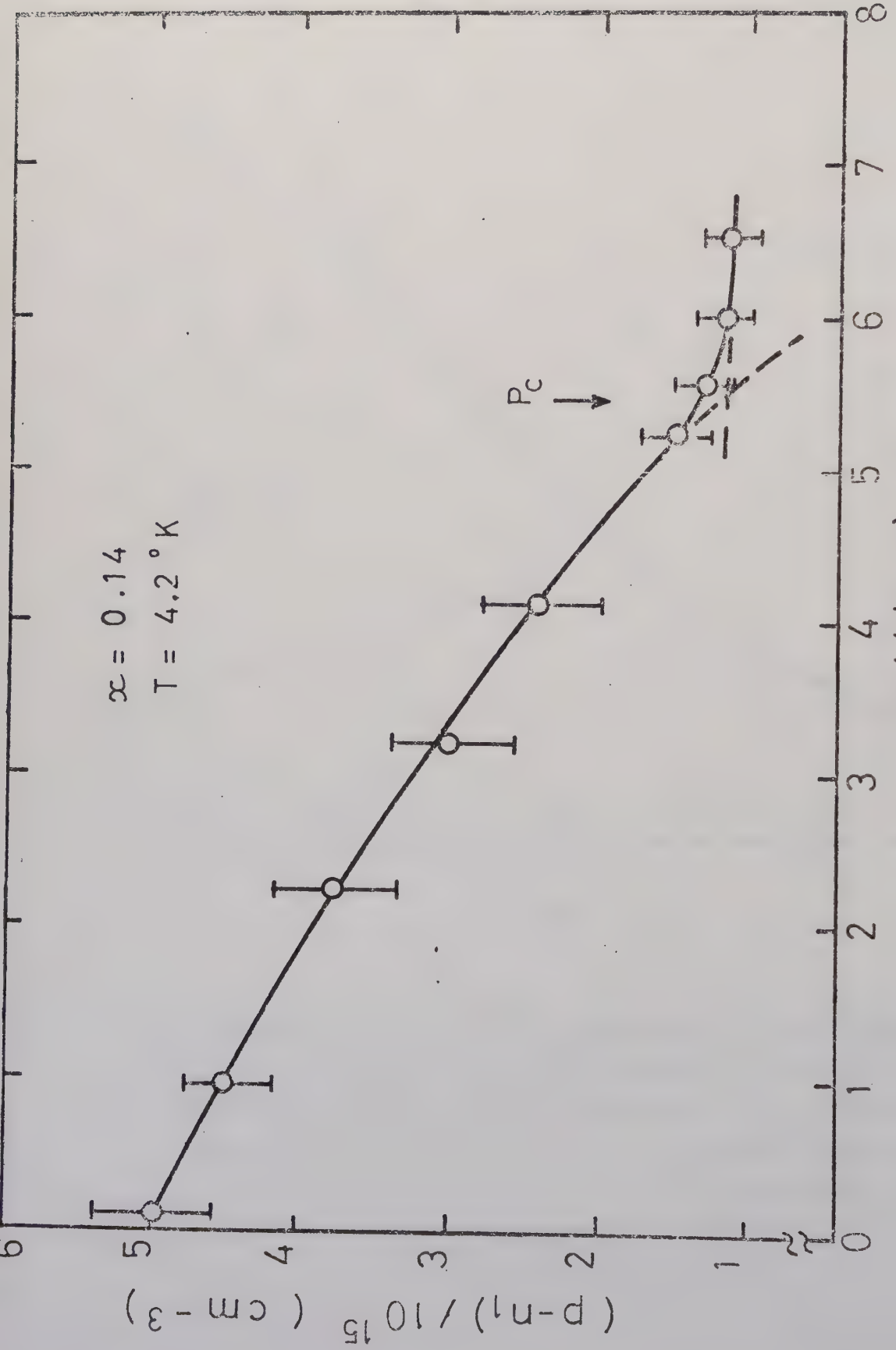

Fig.11 Différence entre les concentrations de trous et d'électrons en fonction de la pression dans l'échantillon $Hg_{1-x}Cd_xTe$ pour $x = 0.14$ à 4.2°K. P_c est la pression critique de transition.

Cette pression de 3,7 kbar apparaît comme jouant un rôle déterminant sur les variations de la mobilité des trous reportée sur la figure 10. Nous reviendrons plus loin sur les effets liés au passage du niveau de Fermi devant le niveau accepteur.

Il nous faut revenir à cette population de trous dont la figure 10 décrit les variations de la concentration et de la mobilité.

Ces trous sont, dans l'état actuel de nos études, une énigme du fait des valeurs de leur mobilité et de leur concentration. Compte-tenu de l'ensemble des résultats expérimentaux concernant la bande Γ_8, une mobilité variant de 2000 à 6000 $cm^2\ V^{-1}\ sec^{-1}$ est incompatible avec les mobilités de trous lourds de 500 $cm^2\ V^{-1}\ sec^{-1}$ ne variant ni avec la composition, ni avec la pression conformément aux résultats de l'analyse $\vec{k}.\vec{p}$. (Cf. plus haut paragraphe II.1.A).

La concentration de ces trous est également incompatible avec un peuplement de la bande de valence du fait de la distance du niveau de Fermi E_F au point Γ_8 (E_F est obtenu d'après la détermination de la concentration d'électrons).

Dans les Sections II.C.2. et la IV.A. de l'Annexe II, nous avons été amenés à introduire une densité d'états supplémentaires à la bande de trous lourds pour des énergies $E > E(\Gamma_8)$. Afin de rendre compte des variations du nombre de trous avec la pression, nous avons été amenés à décrire d'une manière très abrupte ces états supplémentaires par une loi de densité en $E^{1/2}$. L'objet principal de ce modèle très simple était d'estimer l'étendue en énergie de cette "queue de densité d'état" au delà du point Γ_8. A l'aide d'un tel modèle, on trouve alors que la densité d'états dans cette "queue" est très faible. D'une manière tout à fait spéculative et en dehors de toute information complémentaire nous avons évoqué à ce sujet la possibilité d'un phénomène de queue de densité d'état dû au fait que l'échantillon étudié est un alliage. Le problème étant de savoir si on est alors en présence d'un "accident" dû à des défauts locaux de recristallisation ou à un effet spécifique lié à la notion même d 'alliage.

Ce problème de l'incompatibilité entre les concentrations de trous et leur appartenance à la bande Γ_8 a été évoqué par d'autres auteurs qui compte-tenu de mobilités de trous inférieures à 100 $cm^2\ V^{-1}\ sec^{-1}$ attribuent ces trous à des bandes d'impuretés. (Réf.9 de l'Annexe II).

II.2.B. Etat accepteur dû à un potentiel coulombien

Sur l'échantillon de HgTe des oscillations Shubnikov-de-Haas sont observées sur les variations de l'effet Hall en fonction du champ magnétique. Le coefficient dE_g/dP à 1,7°K a été déduit de la mesure du déplacement de l'oscillation 0^+ avec la pression sur cet échantillon (Section II.B.2 de l'annexe II). Cette valeur de dE_g/dP, déterminée selon cette méthode est en bon accord avec les autres déterminations obtenues à 77 et 292 K si l'on tient compte de l'effet de température sur ce coefficient de pression (cf. § II.1.B). L'analyse de la variation de la partie monotone de la constante de Hall en fonction du champ magnétique dans cet échantillon a mis en évidence la présence de deux types d'électrons. Une première catégorie dont les concentration et mobilité à pression ambiante sont $8 \times 10^{14}\ cm^{-3}$ et $3,3 \times 10^5\ cm^2\ V^{-1}\ sec^{-1}$, a été attribuée aux porteurs peuplant les états étendus de la bande de conduction. Le second type d'électrons, de concentration et mobilité $7 \times 10^{14}\ cm^{-3}$ et $9 \times 10^3\ cm^2\ V^{-1}\ sec^{-1}$ à pression ambiante a été attribué aux électrons "presque localisés" sur un niveau accepteur A_o complètement ionisé d'énergie $E_{A_o} = 0,7$ meV attribué à des traces de cuivre. (Cf. références sur ce point dans l'Annexe II).

Du fait de leur interférence avec les états étendus la bande de conduction, les niveaux accepteurs ne sont pas des niveaux discrets et la délocalisation possible des électrons occupant ces niveaux permet à ceux-ci de participer aux effets de transports(*).

(*) L'existence d'électrons "lents" dans HgTe est un fait expérimental déjà cité dans la littérature, qui avait été attribué alors à la forme particulière de la bande de valence de HgTe (Cf. Section II.C.1 de l'Annexe II).

Dans le cadre de cette étude il n'a pas été possible de déceler un éventuel déplacement de la position de cet état accepteur avec la pression. Dans le cas d'un accepteur hydrogénoïde, Gel'Mont et Dyakonov, dans leur analyse théorique, ne prévoient pas de dépendance de l'énergie de l'accepteur avec la densité d'état de la bande de conduction compte-tenu de la forte masse effective de la bande de valence[35].

II.3. ETUDE DE LA MOBILITE. EFFETS RESONNANTS

Ce paragraphe résume l'essentiel des Sections IV.B de l'Annexe I et III de l'Annexe II. Nous n'avons tenté une analyse détaillée de la mobilité électronique qu'à 292°K et 4,2°K.

- à 292°K, on peut faire une analyse qui ne tient pas compte des effets extrinsèques : les seuls mécanismes de diffusion possibles sont les processus électron-trou, par phonons optiques (modes polaires) et par phonons acoustiques.

- à 4,2°K, les effets extrinsèques sont prédominants mais on peut les prendre en compte explicitement grâce à l'analyse en fonction du champ magnétique qui donne accès aux concentrations d'impuretés ionisées. A 77°K ces effets extrinsèques interviennent également dans l'analyse des mécanismes de diffusion. Le dispositif expérimental utilisé pour les expériences faites à 77 et 292°K ne permettant pas l'analyse en fonction du champ magnétique, nous avons renoncé à une étude quantitative des résultats obtenus à 77°K.

II.3.A. Etude de la mobilité à 292°K

Dans le paragraphe II.A.C. traitant de la transition SM-SC nous avons souligné que la transition SM-SC, induite par la composition ou par la pression, s'accompagne d'un maximum de mobilité

au voisinage de $E_g = 0$. En ce qui concerne la pression par exemple, maximum de mobilité et cassure de pente sur les variations de la concentration électronique sont distants de moins de 500 bars.

A titre de comparaison, il est intéressant d'effectuer les calculs de la mobilité en régime intrinsèque en fonction de E_g pour les trois mécanismes de diffusions suivants : diffusion électron-trou par interaction coulombienne écrantée, diffusion par phonons optiques par interaction polaire en tenant compte de l'écrantage par les porteurs libres, diffusion par phonons acoustiques. Pour chaque mécanisme de diffusion les calculs, peuvent être faits dans deux cas :

i) en supposant que la fonction d'onde de l'électron est une onde plane.

ii) en prenant en considération l'expression complète de la fonction d'onde, c'est-à-dire en tenant compte du mélange de composantes s et p.

Une telle étude indique alors les résultats suivants :

1. Seuls les mécanismes de diffusion par phonons optiques et phonons acoustiques donnent lieu à un maximum de mobilité. La diffusion électrons-trous donne une variation monotone croissante bien au delà de $E_g = 0$.

2. Pour rendre compte d'un maximum de mobilité au voisinage de $E_g = 0$, il faut tenir compte de la fonction d'onde complète de l'électron. L'utilisation d'ondes planes conduit à un décalage de pression entre le croisement des niveaux Γ_6 et Γ_8 et le maximum de mobilité, de 3 à 7 kbar.

Ceci est incompatible avec les résultats expérimentaux qui, compte-tenu des incertitudes expérimentales, indiquent un écart au plus de 500 bars.

Il est difficile de procéder à une comparaison quantitative des valeurs absolues des mobilités expérimentales et calculées du fait des incertitudes sur les valeurs d'un certain nombre de paramètres du cristal tels que, par exemple, les constantes diélectri-

que, statique et optique. Une évaluation qualitative permet toutefois de rendre compte du bon ordre de grandeur de μ_n dans HgTe à 292°K avec un processus de diffusion par phonons optiques (Cf. tableau ci-dessous)

HgTe (292°K) μ_n	Phonons optiques écrantés	Phonons optiques non écrantés	Phonons acoustiques	Electron-trous	Expérience
en 10^4 cm^2/Vs	5,6	4,0	$\geq$ 600	7,0	3 ± 0,3

En revanche, l'utilisation de la combinaison pression-composition de l'alliage apparaît être un bon moyen de discrimination et permet ainsi de tester nos conclusions relatives à l'analyse du maximum de la mobilité au voisinage de $E_g = 0$. En effet, la grandeur expérimentale $\mu^{-1} (d\mu/dP)_{P\to 0}$ reportée en fonction de x sur la figure 13 est liée à $\mu^{-1}(d\mu/dE_g)$ et dE_g/dP. Or les calculs de mobilité montrent que $\mu^{-1}d\mu/dE_g$ est une grandeur très sensible au mécanisme de diffusion (Fig.14). Sur la figure 13 on constate un très bon accord entre les valeurs expérimentales et la courbe calculée dans le cas d'une diffusion par phonons optiques. Cette étude nous conduit aux conclusions suivantes :

1. Il est indispensable, dans les configurations SM et SC de prendre en considération la fonction d'onde complète donnée par la méthode $\vec{k}.\vec{p}$.

2. A la température ambiante le mécanisme de diffusion par phonons optiques est prédominant.

II.3.B. Etude de la mobilité à très basse température

Compte tenu de l'ensemble des informations tant expérimentales que théoriques, l'abord d'une analyse de la mobilité à très basse température doit se faire en gardant présents à l'esprit les points suivants :

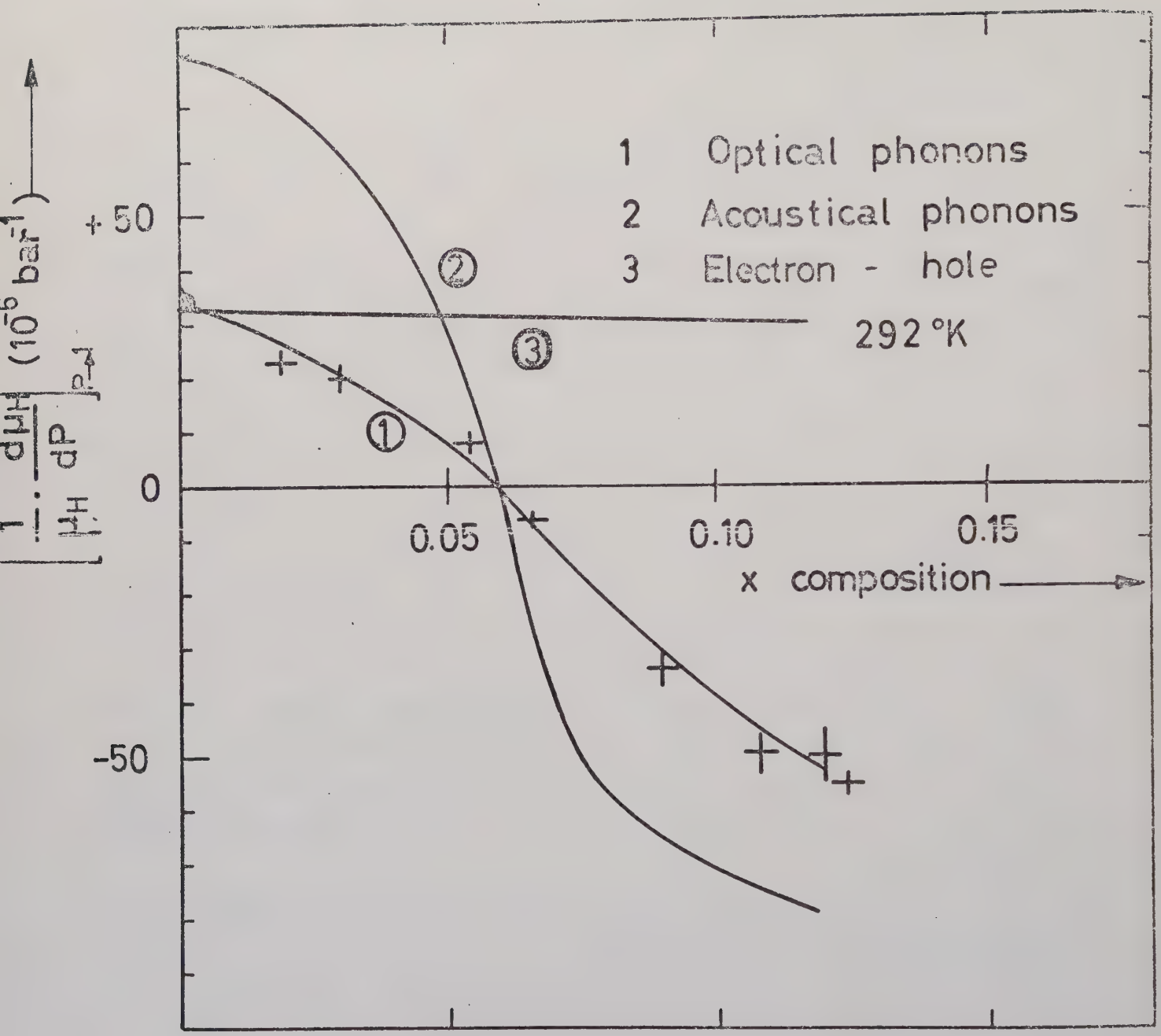

Fig.13 Dérivée logarithmique de la mobilité de Hall par rapport à la pression, au voisinage de la pression ambiante, à 292°K en fonction de la composition. Les croix correspondent aux valeurs expérimentales. Les courbes calculées 1, 2,3 correspondent aux mécanismes de diffusion par phonons optiques, phonons acoustiques, électron-trou.

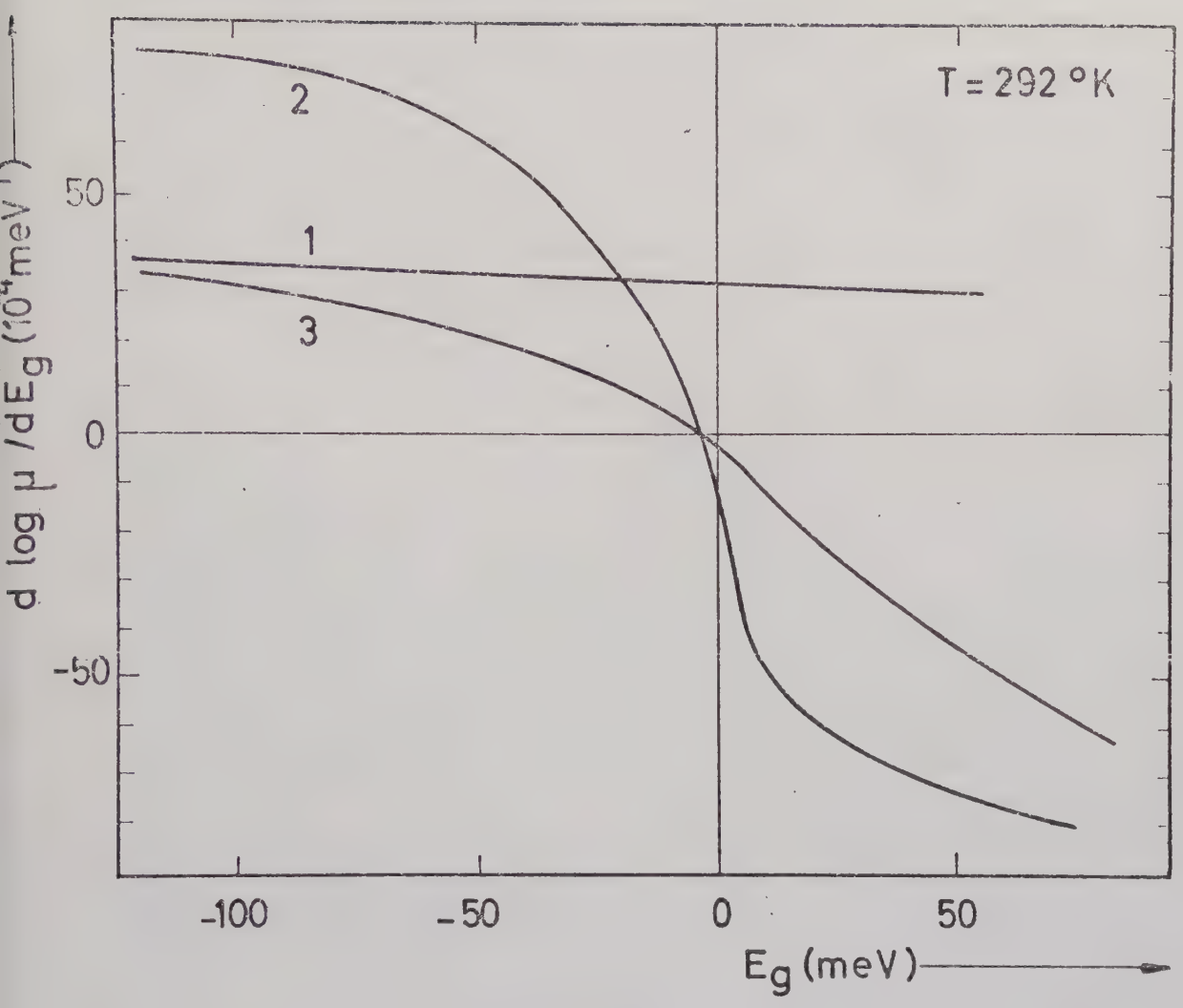

Fig.14 Dérivée logarithmique calculée de la mobilité électronique par rapport à E_g à 292°K pour différents mécanismes de diffusion en fonction de E_g. Les courbes 1,2,3 correspondent respectivement aux processus de diffusion : électron-trou, phonons acoustiques, phonons optiques.

1. Problème du mélange de composantes s et p dans la fonction d'onde, avec comme cas extrême celui d'une fonction d'onde de type p dans la configuration SM au voisinage de Γ_8 (cette dernière situation se rencontrant quand $E_F << |E_g|$).

2. Problème de la constante diélectrique et de sa singularité éventuelle dans la configuration inversée.

3. Problème posé par l'existence d'états accepteurs interférant avec le continuum des états de la bande de conduction. Ce problème a lui-même deux incidences :

a. A basse température la diffusion est gouvernée par interaction coulombienne avec les centres chargés. Nous avons vu que sous l'effet de la pression le déplacement relatif de E_F et E_A entraine une variation de la concentration en centres chargés du fait de la modification du taux d'ionisation des états accepteurs. C'est un phénomène qui intervient explicitement dans l'expression du temps de relaxation puisqu'il est inversement proportionnel à la concentration en centres chargés.

b. Lorsque $E_F \simeq E_A$ on s'attend à une diffusion résonnante des électrons de la bande de conduction sur ces niveaux accepteurs.

Dans le cas de l'échantillon de HgTe, E_F (1 meV) > E_A (0,7 meV) à 1,7°K. Sous l'effet de la pression ni E_F ni E_A ne sont sensiblement modifiés. Cette propriété (analysée en détail dans l'Annexe II, Section IV.B) s'établit à partir d'une détermination de la concentration d'impuretés ionisées (essentiellement des accepteurs résonnants dans le cas présent) déduite de mesures de la variation du coefficient de Hall en fonction du champ magnétique qui donnent la concentration d'électrons lents. L'accord entre la valeur expérimentale de la mobilité et une valeur calculée (cf. Annexe II, Section IV et références citées) permet, compte tenu de la concentration en impuretés ionisées, de montrer que la singularité de la constante diélectrique a une incidence certaine dans le cas de HgTe.

Dans le cas de l'alliage de composition x = 0,14 les variations expérimentales de la mobilité des électrons sont en parfait accord avec une courbe calculée (courbe n° 2 sur la figure 15), sauf au voisinage de la pression de 3,7 kbar. Cette courbe calculée correspond aux variations du produit de la mobilité μ par la concentration en centres diffuseurs N_{cc}. Cette concentration de centres diffuseurs tient compte des variations du nombre d'accepteurs ionisés déterminées expérimentalement (Fig.11).

Le calcul tient compte explicitement de l'expression complète de la fonction d'onde et ne prend pas en considération la singularité de la constante diélectrique observée dans HgTe. En effet pour rendre compte quantitativement de la valeur absolue de la mobilité dans cet échantillon, on doit avoir recours à une valeur de la constante diélectrique statique $\varepsilon_o = 11$ beaucoup plus faible que celle déduite par interpolation linéaire entre $\varepsilon_o = 9,2$ dans CdTe et les valeurs publiées dans HgTe se situant autour de 20. Une comparaison avec CdTe implique que cette valeur de 20 dans HgTe correspond à $\varepsilon_o + 4\pi\alpha^{inter}$ où $4\pi\alpha^{inter}$ représente la partie singulière. On peut estimer cette dernière contribution en remarquant que la valeur de 20 a été déterminée à 77°K en régime intrinsèque, c'est-à-dire pour un peuplement des états de la bande de conduction défini par $E_F = 30$ meV. Un calcul donne alors $4\pi\alpha^{inter} \simeq 8$ d'où $\varepsilon_o \simeq 12$ dans HgTe. Dans ces conditions la valeur $\varepsilon_o = 11$ pour l'alliage de composition x = 0,14 apparaît plausible. Par ailleurs, en ce qui concerne la contribution $4\pi\alpha^{inter}$ dans cet alliage, comme cela a été dit au paragraphe I.4, et bien que l'expression (Eq.19) ne tienne pas compte de la non parabolicité de la bande de conduction on peut dire, qualitativement, que la contribution des transitions Γ_8-Γ_8 à la constante diélectrique dépend de la densité d'états de la bande de conduction et qu'il est concevable que cette contribution disparaisse quand $E_g \to 0$ au voisinage de la transition SM-SC.

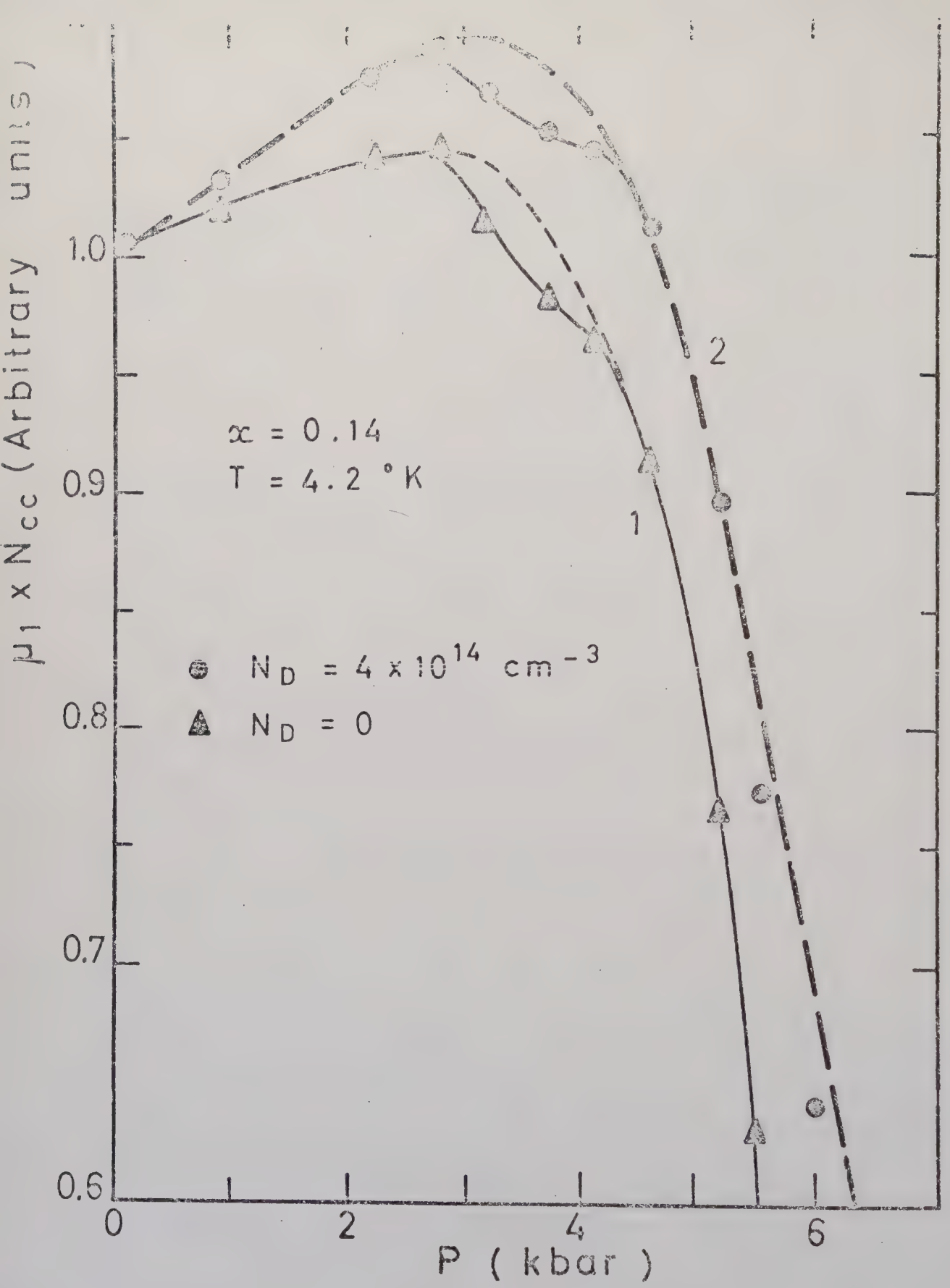

Fig.15 Variations de la grandeur $\mu_1 \times N_{cc}$ en fonction de la pression dans l'échantillon de $Hg_{1-x}Cd_xTe$ (x=0.14) à 4.2°K. μ_1 est la mobilité électronique, N_{cc} est la concentration en centres chargés. La courbe 1 et les triangles sont obtenus pour une concentration de donneurs $N_D = 0$. En prenant $N_D = 4 \times 10^{14}$ cm^{-3} les points expérimentaux (cercles pleins) sont sur la courbe théorique (courbe 2) exception faite du domaine $2.7 < P < 4.7$ kbars où une dépression est observée.

II.3.C. Mise en évidence d'une diffusion résonnante sur le niveau accepteur

Nous avons remarqué dans le paragraphe précédent qu'au voisinage de la pression de 3,7 kbar les variations expérimentales et calculées de la grandeur $\mu \times N_{cc}$ n'étaient plus en accord. Il nous faut rappeler que l'analyse expérimentale des variations relatives du niveau de Fermi et du niveau accepteur a montré que l'on avait $E_F \simeq E_A$ autour de cette pression critique. Dans ces conditions la singularité sur les courbes reportées sur la figure 15 apparaît comme une diffusion résonnante des électrons appartenant aux états étendus de la bande de conduction, pour le niveau accepteur. Un accident du même type apparaît quand on reporte la quantité $\mu_p \times N_{cc}$ en fonction de la pression (Fig.16) ; μ_p étant la mobilité des trous déterminée par l'analyse à deux types de porteurs (Fig. 10).

Une autre mise en évidence de diffusion résonnante, mais beaucoup plus spéculative, résulte de l'analyse de la dépendance en champ magnétique de l'effet Hall dans la configuration SC ($P > 5,4$ kbar) pour laquelle on a E_A proche du bas de la bande de conduction. En effet, cette étude nous amène à considérer que dans la limite ultra quantique (lorsque le gaz d'électron se condense sur la niveau O^-) nous pouvons alors observer le passage du niveau O^- devant le niveau accepteur qui entraîne une diminution brutale de la mobilité des électrons occupant ce niveau O^-. Nous pensons que les phénomènes expérimentaux décrits dans l'Annexe II peuvent être interprétés selon ce modèle qualitatif.

Il faut enfin noter au sujet de cet état accepteur qu'une estimation de la limite supérieure de la largeur de ce niveau donne $\Delta E_A < 0,3$ meV.

L'analyse expérimentale et la discussion de cette étude préliminaire de l'aspect "résonance" du niveau accepteur sont détaillées dans les Sections III et IV.B de l'Annexe II.

o o
o

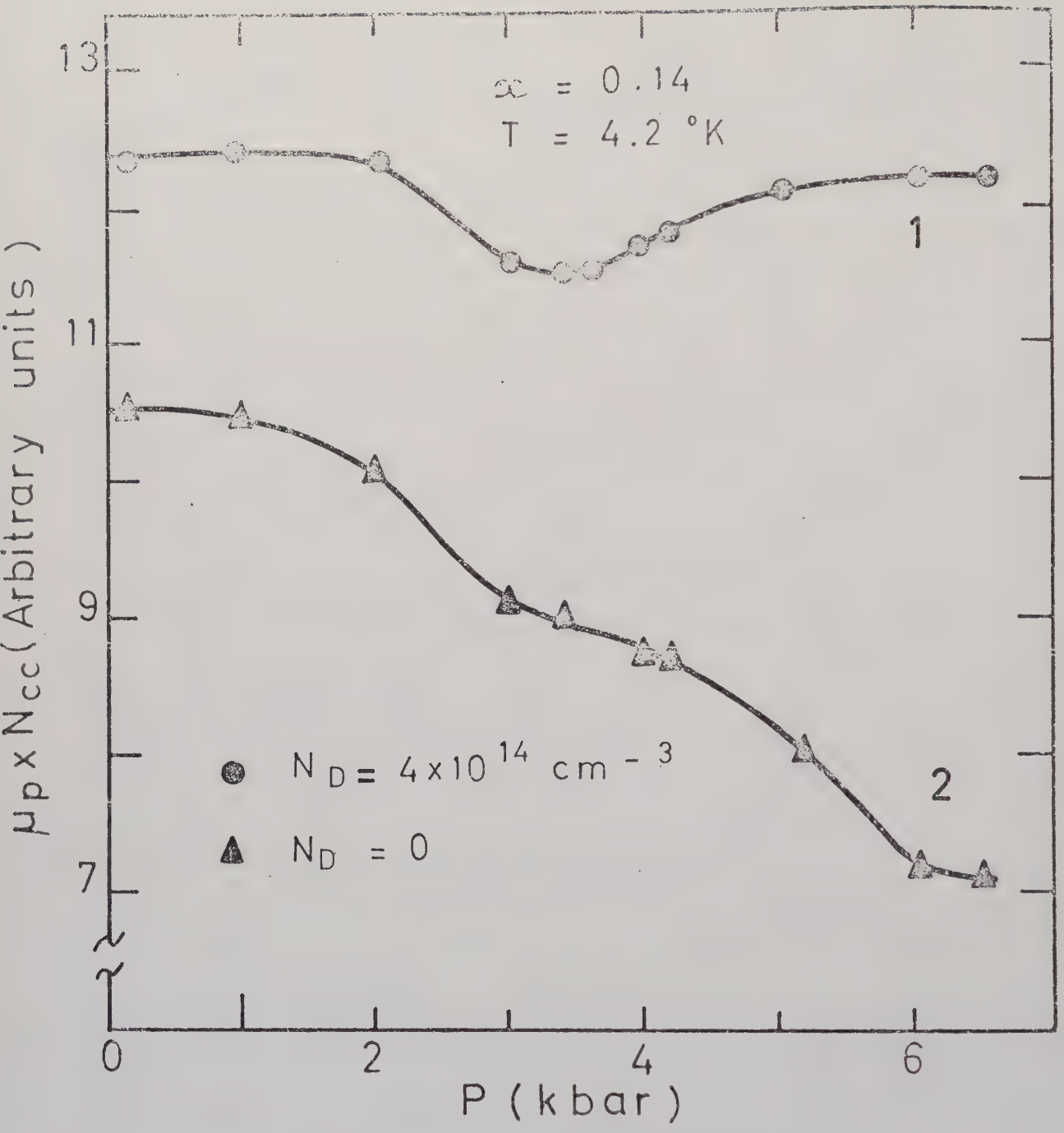

Fig.16 Variations de $\mu_p \times N_{cc}$ en fonction de la pression dans l'échantillon $Hg_{1-x}Cd_xTe$ (x=0.14) à 4.2°K. μ_p est la mobilité de trous, N_{cc} la concentration de centres chargés diffuseurs. La courbe 1 (cercles pleins) correspond à une concentration de donneurs $N_D = 4 \times 10^{14}$ cm^{-3}. La courbe 2 (triangles) correspond à $N_D = 0$.

CHAPITRE III

CONCLUSIONS

De l'ensemble de cette étude de phénomènes de transport au voisinage de la transition semimétal - semiconducteur et de leur dépendance en pression, il ressort deux types de conclusions, ayant trait respectivement aux effets de bandes et aux caractéristiques particulières des niveaux d'impuretés, au voisinage du croisement des niveaux Γ_6 et Γ_8 dans les alliages CdHgTe. En particulier, nous soulignons ici les traits marquants de la transition gap-zéro qui apparaissent comme inhabituels dans le contexte des lois conventionnelles gouvernant la dynamique des électrons dans les semiconducteurs classiques.

Dans le cadre de notre étude de structure électronique de ces alliages, l'ensemble des résultats expérimentaux indiquent l'absence d'anomalies du type excitonique aussi bien au voisinage de la transition gap-zéro que dans la configuration semimétallique. Il est à noter que dans ces deux cas le modèle de bandes à un électron utilisé, construit à partir de la théorie $\vec{k}.\vec{p}$, permet de rendre compte dans l'ensemble quantitativement des propriétés de transport en régime intrinsèque sous pression tant du point de vue de la relation de dispersion décrivant la bande de conduction (non-parabolicité) que de celui de l'incidence notable de la nature des fonctions d'onde des électrons de conduction et de leur dépendance angulaire dans la diffusion élastique de ces porteurs. Il faut toutefois remarquer qu'en aucun cas nous n'avons eu accès, à la transition SM-SC, aux états très proches des niveaux $\Gamma_6 - \Gamma_8$. En effet même à très basse température, la bande de conduction est, dans notre cas, peuplée jusqu'à des énergies de Fermi $E_F \geq 10$ meV. Il serait donc intéressant de reprendre ce type d'étude sur des échantillons beaucoup plus purs.

La très bonne définition de la pression de croisement obtenue par la méthode de la cassure de pente sur les variations de la concentration électronique a permis de mettre en évidence des valeurs de E_g de l'ordre de + 5 meV.

Il est à noter que le même résultat, recherché par des méthodes optiques nécessiterait une infrastructure expérimentale beaucoup plus complexe du fait de la nécessité d'opérer dans le domaine de l'infrarouge lointain ou le domaine submillimétrique[31]. La finesse des méthodes optiques (magnétooptique, thermoréflectance) justifierait néanmoins leur extension au domaine des hautes pressions. De telles expériences devraient permettre d'obtenir des informations décisives et sans doute confirmer les valeurs du coefficient dE_g/dP à différentes températures dans les alliages à forte teneur en Hg. En effet la valeur $dE_g/dP = 8,5 \times 10^{-6}$ eV bar^{-1} obtenue pour HgTe à 1,7°K est très proche de celle de CdTe ($8,2 \times 10^{-6}$ eV bar^{-1} à 77°K).

Alors que des méthodes de calcul de structure de bande du type "pseudopotentiels" permettent de comprendre qualitativement cette similitude des valeurs de dE_g/dP dans HgTe et CdTe (p.48 Annexe I), la théorie de la liaison chimique de Phillips[17] appliquée par D.L.Camphausen et al. (p. 49 Annexe I) donne pour CdTe un bon accord avec l'expérience (8×10^{-6} eV bar^{-1}) tandis que pour HgTe, HgSe et β-HgS, elle conduit à une valeur de 12×10^{-6} eV bar^{-1}. Ce désaccord flagrant n'intervient que pour HgTe alors que la théorie rend parfaitement compte du dE_g/dP d'un ensemble de composés A^3B^5 et A^2B^6. Il n'existe pas actuellement de valeurs expérimentales de dE_g/dP dans les autres chalcogénures de mercure HgSe et β-HgS. Ces matériaux ne s'obtiennent que fortement dopés de type n alors que des alliages $HgTe_y\ Se_{1-y}$, $HgTe_zS_{1-z}$ peuvent être obtenus intrinsèques jusqu'à des compositions de l'ordre de 50 %. Il serait intéressant de déterminer expérimentalement le coefficient de dE_g/dP dans de tels alliages par effets de transport en régime intrinsèque. Ceci devrait permettre d'analyser de façon plus fondamentale le désaccord théorie - expérience dans le cas des chalcogénures de mercure. En particulier, il est possible que la difficulté rencontrée

par Philipps et Van Vechten dans l'application de leur théorie de l'ionicité aux chalcogénures de mercure[36] soit liée au problème de la constante diélectrique statique et de sa singularité dans ces composés à structure de bande inversée.

Nous avons pu noter dans cette étude que si la singularité de constante diélectrique doit être prise en considération dans le cas de HgTe, il n'en est plus de même au voisinage de la transition SM-SC, du fait que la densité d'états de la bande de conduction décroît fortement lorsque $|E_g| \to 0$. Les mesures sous pression à basse température ont permis une analyse détaillée d'effets anormaux dus à des états accepteurs interférant avec les états étendus de la bande de conduction. Nous avons mis en évidence l'ionisation de ces états ainsi qu'une variation de leur position en fonction de la densité d'états de la bande de conduction quand ces états accepteurs sont dus à des potentiels très localisés (lacune de mercure).

Nous avons mis en évidence certains effets résonnants dus à la diffusion anormale des électrons de la bande de conduction quand l'énergie de Fermi E_F est voisine de l'énergie de l'accepteur E_A. Les électrons quasi-liés à ces états accepteurs participent à la conduction en tant qu'électrons à faible mobilité.

Ces études sur les niveaux accepteurs résonnants de type hydrogénoïde ou induits par un potentiel très localisé mériteraient un ensemble d'études plus systématiques. On pourrait en particulier s'intéresser à la transition niveau résonnant → niveau discret induite par la pression dans la configuration SC au voisinage de la transition SM-SC.

o o
o

BIBLIOGRAPHIE SUCCINCTE

(1) S.GROVES, W.PAUL, Phys.Rev.Lett., 11, 194 (1963).

(2) P.KACMAN et W.ZAWADZKI, Phys.Status Solidi (b) 47, 629 (1971). Cet article théorique traite plus particulièrement du moment magnétique de spin et de la résonance de spin des électrons de conduction dans la structure de bande de type α-Sn. Il contient cependant une bibliographie très complète de ce problème non seulement sur le plan théorique mais aussi sur le plan expérimental.

(3) P.A.WOLFF, Phys.Rev.Letters, 24, 266 (1970).

(4) C.VERIE, Thèse d'Etat, Orsay (1967) ; Proceedings of the Int. Conf. on the II-VI Compounds, Providence, 1967, D.G.Thomas Ed. (Benjamin New-York, 1967) p.1124.

(5) C.VERIE, G.MARTINEZ, Comptes-Rendus, 266, 720 (1968).

(6) A.MAUGER, Thèse de Doctorat de 3e Cycle, spécialité "Physique du Solide", Orsay (1974).

(7) S.OTMEZGUINE, F.RAYMOND, G.WEILL, C.VERIE, Proc.Xth Int.Conf. Phys.Semicond., Cambridge 1970, Edited by S.P.Keller, J.C.Hensel, F.Stern (USAEC, Conf.700801), 1970, p.536.

(8) G.WEILL, S.OTMEZGUINE, C.VERIE, Communication présentée à la réunion de "European High Pressure Research Group" UMEA, Sweden, 1971 (non publié).

(9) C.FINCK, S.OTMEZGUINE, G.WEILL, C.VERIE, Proceedings of the 11th International Conference on the Physics of Semiconductors, edited by PWN.Polish Scientific Publishers (Warsaw, Poland, 1972), Vol.2, p.944.

(10) S. OTMEZGUINE, G.WEILL, C.VERIE, Colloque International du CNRS n° 228 sur la "Transition Semiconducteur - Semimétal", Nice (1973).

(11) A.MAUGER, S.OTMEZGUINE, G.WEILL, C.VERIE, dans la Ref.10.

(12) A.MAUGER, S.OTMEZGUINE, C.VERIE, J.FRIEDEL, Proceedings of the 12th International Conference on the Phys.of Semiconductors, Stuttgart (Jully 1974), p.1166.

(13) R.H.PARMENTER, Phys.Rev., 100, 573 (1955) ; G.DRESSELHAUS, Phys.Rev., 100, 580 (1955).

(14) E.O.KANE, J.Phys.Chem.Sol., 1, 249 (1957).

(15) W.ZAWADZKI, W.SZYMANSKA, Phys.Status Solidi (b), 45, 415 (1971).

(16) W.SZYMANSKA, P.BOGUSLAWSKI, W.ZAWADSKI, Phys.Status Solidi (b) 65, 641 (1974).

(17) BONDS and BANDS in SEMICONDUCTORS by J.C.PHILLIPS, (Academic Press New-York and London 1973), p.197.

(18) a) F.HERMAN, Proc.Int.Conf.Phys.Semicond., Paris 1964 (Dunod, Paris) p.3 ;
b) F.HERMAN, C.D.KUGLIN, K.F.CUFF, R.L.CORTUM, Phys.Rev.Lett., 11, 541 (1963).

(19) Référence 17 page 147.

(20) H.Y.FAN, Phys.Rev., 82, 900 (1951).

(21) Voir par exemple B.I.HALPERIN, T.M.RICE, Review of Modern Physics, 40, 755 (1968) et la bibliographie citée dans cet article.

(22) N.F.MOTT, Phil.Mag., 6, 287 (1961).

(23) R.S.KNOX, Solid State Phys., Suppl.5, 100 (1763).

(24) L.J.SHAM et T.V.RAMAKRISHNAN, Proceedings of the Conf. on the Phys. of Semimetals and narrow-gap semiconductors, Dallas 1970, Carter and Bate ed. (Pergamon Press, New-York, 1971) p.219.

(25) D.SHERRINGTON, W.KOHN, Review of Modern Physics, 40, 767 (1968).

(26) L.LIU, D.BRUST, Phys.Rev., 173, 777 (1968).

(27) L.LIU, E.TOSATTI, Phys.Rev. B 2, 1926 (1970).

(28) J.G.BROERMAN, Phys.Rev.Letters, 25, 1658 (1970).

(29) D.SHERRINGTON, W.KOHN, Phys.Rev.Letters, 21, 153 (1968).

(30) J.G.BROERMAN, Phys.Rev. B 5, 397 (1972).

(31) V.I.IVANOV-OMSKII, B.T.KOLOMIETZ, V.K.OGORODNIKOV, K.P.SMEKALOVA, Fiz.Teckh.Poluprov., 1, 289 (1967) (Sov.Phys.Semiconductors 1, 232, 1967).

(32) J.TUCHENDLER, M.GRYNBERG, Y.COUDER, H.THOME, R. LE TOULLEC, Phys.Rev.B 8, 3884 (1973).

(33) G.BASTARD, Y.GULDNER, C.RIGAUX, NGUYEN HY'HAU, A.MYCIELSKI, in Ref. 10.

(34) L.LIU, D.BRUST, Phys.Rev., 157, 627 (1967)

(35) B.L.GEL'MONT, M.I.DYAKONOV, Zh.Eksp.Teor.Fiz., 62, 713 (1972) (Soviet Physics JETP, 35, 377 (1972).

(36) J.C.PHILLIPS, J.A.VAN VECHTEN, Phys.Rev. B 2, 2147 (1970).

o o
o

SOMMAIRE DE L'ANNEXE I

Annexe I. On the pressure. Induced semimetal to semiconductor transition in HgCdTe alloys :

I. Intrinsic effects

by

S.OTMEZGUINE, G.WEILL, C.VERIE

pages

Abstract..... 1

I. INTRODUCTION..... 2

II. THEORETICAL BACKGROUND

II.A. Band structure model within the Γ_6, Γ_8 cross over... 5

II.B. Dispersion law expressions..... 8

II.C. Wave function representations.....12

III. EXPERIMENTAL STUDIES

III.A. Experimental procedures.....13

III.B. Experimental results.....15

IV. INTERPRETATION

IV.A. Hall coefficient measurements analysis.....18

a. Determination of dE_g/dP.....22

b. $E_g(x)$ law at 77 and 292°K.....23

c. Evidence of the pressure induced Γ_6-Γ_8 cross-over.....25

IV.B. Electron mobility analysis

a. Theoretical considerations.....27

b. Experimental results analysis.....35

V. DISCUSSION AND CONCLUSIONS.....40

REFERENCES.....51

LEGENDE DES FIGURES.....59

RESUME DE L'ANNEXE I

Cette annexe est consacrée à l'analyse de la transition SM-SC dans $Cd_xHg_{1-x}Te$ à l'aide de mesures galvanomagnétiques (effet Hall, résistivité) en fonction de la pression ($P \leq 12$ kbar) à température constante (292 et 77°K) sur une douzaine d'échantillons de compositon $0 \leq x \leq 0{,}14$. L'effet Hall n'est analysé qu'à faible champ magnétique pour des raisons d'ordre expérimental (Section III).

L'introduction comporte une revue bibliographique des principales études antérieures faites sur ces alliages, dans le cadre de la transition SM-SC induite soit par la composition, la température ou la pression.

Dans la Section II sont chiffrées les corrections relativistes dans le cas de la substitution Hg → Cd. Dans cette même Section les résultats de la méthode $\vec{k}.\vec{p}$ sont très brièvement rappelés et l'accent est particulièrement mis sur l'expression de la fonction d'onde d'un électron de la bande de conduction dans les deux configurations SM et SC.

La Section III décrit rapidement les aspects expérimentaux de l'étude et donne certains résultats sans analyse.

Dans la Section IV on analyse les variations de l'effet Hall en fonction de la pression. L'objectif essentiel de cette analyse est d'illustrer avec la meilleure résolution possible la transition SM-SC et d'autre part de préciser un certain nombre de paramètres de bande dans ce domaine de compositions, qui par ailleurs n'avait fait l'objet que d'un nombre très restreint d'études :

- Coefficient de pression du gap dE_g/dP
- Lois $E_g(x)$ à 77 et 292°K
- Elément de matrice P_K et masse effective de densité d'états de la bande de trous lourds m_p.

La Section V est consacrée à l'analyse de la mobilité à 292°K en tenant compte de la symétrie de l'extremum de la bande de conduction, c'est-à-dire de l'expression complète de la fonction d'onde.

La Section VI contient une discussion détaillée de l'ensemble des résultats.

o o
o

SOMMAIRE DE L'ANNEXE II

Annexe II. On the pressure. Induced semimetal to semiconductor transition in HgCdTe alloys :

II. Extrinsic effects

by

S.OTMEZGUINE, A.MAUGER, M.MONCHANIN, C.VERIE

pages

Abstract..... 1

I. INTRODUCTION..... 1

II. EXPERIMENTAL RESULTS..... 6

II.A. SM-SC transition..... 7

II.B. Quantum domain analysis..... 8

II.C. Two carrier type Hall effect.....13

1. HgTe at 1.7°K.....14

2. $Cd_{0.14}Hg_{0.86}Te$ at 4.2°K.....17

III. MOBILITY AND RESONANCES.....21

IV. DISCUSSION

IV.A. Electronic structure.....27

IV.B. Location of the acceptor levels.....29

CONCLUSIONS.....34

APPENDIX A.....37

APPENDIX B.....41

REFERENCES.....45

LEGENDES DES FIGURES.....49

RESUME DE L'ANNEXE II

Nous abordons ici l'analyse des effets extrinsèques. En effet par une technique de miniaturisation de l'enceinte haute pression, nous avons eu accès au domaine des basses températures (de l'hélium pompé c'est-à-dire 1°5 jusqu'à 77°K) et nous avons pu élargir le domaine de champ magnétique jusqu'à 10 kG. La contrepartie de l'extension des intervalles températures et champ magnétique a été une diminution de l'intervalle pression du fait de l'utilisation de chambre haute pression en Cu-Be (bronze au beryllium) de faible encombrement. Cette technique a imposé un système d'étanchéité rudimentaire limitant le domaine de pressions à 8 kbar.

Dans cette étude sont rapportés les résultats concernant deux échantillons : HgTe et un alliage CdHgTe de composition $x = 0,14$.

Dans la Section II sont exposés les résultats expérimentaux classés selon trois domaines de champ magnétique : faibles champs magnétiques ($\mu_n B << 1$), le domaine quantique dans lequel apparaissent les oscillations Shubnikov-de-Haas, le domaine ultra-quantique correspondant au passage du niveau de Fermi devant le niveau de Landau 0^+.

Les variations de l'effet Hall sont attribuées à un effet à deux types de porteurs. Les études faisant l'objet de cette Section II ont permis

- d'illustrer la transition SM-SC à 4,2 et 1,7°K,
- de déterminer le coefficient dE_g/dP à 1,7°K,
- d'analyser en fonction de la pression le comportement de deux types d'accepteurs interférant avec les états étendus de la bande de conduction, c'est-à-dire :

(i) un accepteur engendré par substitution d'un atome de cuivre à un atome de mercure

(ii) un accepteur engendré par des défauts de stoechiométrie dus à des lacunes de mercure.

La Section III est consacrée à une analyse de la mobilité dans les deux échantillons, compte-tenu des problèmes spécifiques à ces matériaux :

(i) mélange de composantes s et p dans la fonction d'onde,

(ii) éventualité de la singularité de constante diélectrique dans la configuration SM,

(iii) modification de la concentration en accepteurs ionisés due à une modification de l'état d'ionisation de l'accepteur induite par un déplacement du niveau de l'accepteur avec E_g. Cet effet a été mis en évidence dans la Section II dans le cas de l'état accepteur induit par une lacune de mercure.

Dans cette Section III nous avons mis en évidence un ensemble de manifestations de l'interaction résonnante du point de vue de la diffusion des électrons de la bande de conduction par ce niveau accepteur interférant avec les états étendus de la bande de conduction.

La Section IV est consacrée à une discussion de l'ensemble des résultats de cette étude.

o o
o

ANNEXE I

ON THE PRESSURE-INDUCED SEMIMETAL-TO-SEMICONDUCTOR TRANSITION IN HgCdTe ALLOYS : I. INTRINSIC EFFECTS.[+(*)]

by

S.OTMEZGUINE, G.WEILL and C.VÉRIÉ

Laboratoire de Physique des Solides
CNRS-Bellevue, 1, place A.Briand, 92190,Meudon(France)

+ This paper is based on the first part of a thesis to be submitted by S.Otmezguine for the degree : Doctorat d'Etat at the Université d'Orsay.

(*) Supported by the D.R.M.E.

ANNEXE I

ON THE PRESSURE-INDUCED SEMIMETAL-TO-SEMICONDUCTOR TRANSITION IN HgCdTe ALLOYS : I. INTRINSIC EFFECTS.+(*)

by

S.OTMEZGUINE, G.WEILL and C.VÉRIÉ

Laboratoire de Physique des Solides
CNRS-Bellevue, 1, place A.Briand, 92190,Meudon(France)

+ This paper is based on the first part of a thesis to be submitted by S.Otmezguine for the degree : Doctorat d'Etat at the Université d'Orsay.

(*) Supported by the D.R.M.E.

ABSTRACT

The zero bandgap transition is investigated in $Cd_xHg_{1-x}Te$ through transport measurements in intrinsic regime as a function of x, hydrostatic pressure up to 14Kbar, at temperatures of 292 and 77°K. The experimental results are interpreted in terms of a model essentially depicted by a continuous Γ_6 ,Γ_8 crossover following the α-Sn inverted band model and the $\vec{k}.\vec{p}$. theory. An overall fit of the experimental data yields a self-consistent set of band parameters, mainly $E_g(x,T,P)$. Whereas the observation of a small variation of dE_g/dP vs. T is attributed to the temperature dependence of elastic constants, the inverted bandgap deformation potential value of HgTe is observed very close to the CdTe one, leading to a substantial disagreement with calculations deduced from ionicity theory. The electron mobility behaviour is carefully studied showing a direct evidence of the p-like-to s-like transition of the k.p. wave functions of the lowest conduction states, occuring at the Γ_6, Γ_8 crossover. The logarithmic pressure coefficient of mobility vs. x at 292°K is well fitted with an optical phonon scattering mechanism of electrons. This analysis yields a good characterization of the alloying-induced semimetal-to-semiconductor transition at room temperature, consistently with the intrinsic regime carriers studies. This critical composition value appears substantially lower than previous published ones and the $E_g(x)$ law exhibits a significant departure from linearity at 292°K.

I - INTRODUCTION.

The electronic structure studies of narrow gap semiconductors or small overlap semimetals have revealed, during these past few years a strong interest for the zero gap transition problem. In the case of transitions with symmetry-conservation, some intermetallic couples such as Ge - α Sn, Sb - Bi, CdTe - HgTe, SnTe (Se) - PbTe (Se), have the appropriate electron state-ordering of the conduction and valence band edges for this kind of electronic phase transition induced by band shift effects. In the present work, the zero gap transition is studied in the framework of diamond - zincblende symmetry. Thus, at a first glance, the band structure in the vicinity of Γ points of narrow gap semiconductors or small overlap semimetals can be sketched by following basic models exemplified essentially by InSb[1] and by the "inverted scheme" of α - Sn[2]. It is now well established that these two characteristic models hold for CdTe and HgTe respectively. As a result, the combination of these two models is expected to give the salient features of any starting model describing the electronic structure of the Cadmium Telluride - Mercury Telluride alloy system. This point is discussed in the present paper with particular emphasis on the zero gap transition.

Since the discovery of miscibility properties of $Cd_xHg_{1-x}Te$ solid solutions[3], extensive experimental works on the semiconducting phase, more or less stimulated by infrared device investigations, made these crystals available with good purity and homogeneity. This suggests that CdHgTe alloys within a definite composition range, appear suitable for zero gap transition experimental studies in the diamond-zincblende symmetry family. Such a typical feature would be exhibited by the hypothetical narrow gap Ge_xSn_{1-x} alloy system.

In a first approximation the zero bandgap transition exhibited by the $Cd_xHg_{1-x}Te$ system, i.e. the semiconductor - to - semimetal transition (hereafter SC $\rightarrow$ SM), occurs at the Γ_6, Γ_8 crossover. This accidental degeneracy can be reached and removed by a band shift process as usual in classical semiconductors. For that purpose we may use effects conserving

the zincblende symmetry such as variations of the alloy composition, hydrostatic pressure and temperature. Several experimental results dealing with these features on $Cd_xHg_{1-x}Te$ have been published :

(i) Evidences of alloying-induced SM → SC transition where shown by a number of authors who performed various studies as a function of x, i.e., magneto-reflection effects [4], measurements of pressure coefficients [5] and temperature dependance [6,7] of galvanomagnetic effects in the intrinsic regime and electron effective mass determination [8-10]. In the low temperature range the main experimental results obtained in the vicinity of the SM-SC transition can be summarized as follows [7,9] : at T ~ 0°K, $dE_g/dx \simeq 19$meV/percent and x (SM→SC) ~0.16. Here E_g denotes the $\Gamma_6 - \Gamma_8$ energy separation. A recent theoretical study [11] is in good agreement with these values. At 77°K the corresponding values are respectively ~ 18meV/percent and : $x \simeq 0.14$. The compositional error, about $\Delta x = 0.005$, is essentially limited by the precision of electron microprobe techniques. The resulting uncertainty on $|E_g|$ appears strongly unconvenient for alloying-dependance studies of the Γ_8, Γ_6 crossover in an energy scale lying within a few meV.

(ii) Indications of temperature induced SM → SC transition were reported for HgTe at 10.5 kbar near room temperature [12] and for $Cd_{0.16}Hg_{0.84}Te$ at ambient pressure [13]. Considering the strong compositional dependence of $\alpha = dE_g/dT$ observed in $Cd_xHg_{1-x}Te$ (a typical feature of these materials), the published values of α in the vicinity of the SM → SC transition appear rather scattered. For x ~ 0.20, α is believed to be approximately equal to 0.35 ± 0.05 meV/deg [7,14,15] for $0 < T < 77$°K while it is substantially lower at higher temperatures.

The order of magnitude of α and the composition value uncertainties, limit the actual possibilities of quantitative experimental studies of the temperature induced SM → SC transition.

(iii) The pressure-induced SM → SC transition was investigated through room-temperature thermoelectric power measurements

on HgTe[12], pressure induced electrical rectification of $Cd_{0.11}Hg_{0.89}Te$ p-n junctions[16] and galvanomagnetic measurements on various SM alloys[17-19]. Subsequently transport studies of $Cd_xHg_{1-x}Te$ under hydrostatic pressure have been reported more recently[20-23]. From these measurements, the published values of dE_g/dP are between 7 and 14meV/kbar. This parameter is important because an accurate analysis of the SM→SC transition is strongly affected by its determination. This point will be discussed in details in section IV.

All these investigations, summarized here with a particular emphasis on the $\Gamma_6 - \Gamma_8$ crossover, have taken place within the framework of an impressive amount of studies on $Cd_xHg_{1-x}Te$. More details on the investigations on these materials can be found in various review papers[24-25].

Pressure induced SM→SC transition studies in alloys are of interest for various reasons. From an experimental point of view, the continous variable bandgap effet provided by application of hydrostatic pressure together with the fact that the starting values of E_g can be adjusted using the alloying properties enables one to obtain easily the bandgap value range where the classical semiconductor band structure studies may be readily used. This results in an unambiguous observation of an opening of the gap as the pressure increases. This has been clearly visualised by different experiments on $Cd_xHg_{1-x}Te$[17-23]. Secondly, such a technique offers also the possibility of exploring the extremely narrow bandgap range i.e. E_g lying in the meV range.

In this paper, we describe more extensively our work which has been briefly reported in a previous communication[17]. The transport properties in almost intrinsic regime (at least near ambient pressure) at 77°K represent an approach to this interesting question. The experimental results we found in $Cd_xHg_{1-x}Te$ fit the $\Gamma_6 - \Gamma_8$ continous crossover scheme, an expected simple model deduced from one-electron band theory considerations (Section IV A). Another point of interest is related to the symmetry of the wave functions associated to the Γ_6 and Γ_8 states. According to the $\Gamma_6 - \Gamma_8$ crossover

model, the SM → SC transition is expected to be characterized by a change from s-like to p-like character of the Γ-point electron states of the conduction band. Our analysis of pressure dependance of the electron mobility supports strongly this feature (Section IV B).

From a more quantitative point of view the interpretation of the results leads to the establishment of a self-consistent set of band parameters with a particular emphasis on dE_g/dP and the alloy composition for which the SM → SC transition at 1 bar occurs, hereafter denoted x (SM → SC).

Finally, from a discussion of our results of the pressure-induced SM → SC transition, it appears that such studies can either provide a test of the extrapolation to vanishing bandgaps of one electron band theories through the use of the full $\Gamma_8 - \Gamma_6$ $\vec{k}.\vec{p}$ interaction method, or on the contrary, evidence any electronic structure anomaly induced either by disorder or collective effects.

II - THEORETICAL BACKGROUND.

II.A. Band Structure model within the Γ_6, Γ_8 crossover.

As a qualitative model focussed on the zero-bandgap transition, a band scheme dealing with the main features of the electronic levels lying in the vicinity of the bandgap is sufficient. The existence of SM or SC characters in $Cd_xHg_{1-x}Te$ can be simply understood from some principles such as the usual band shifts induced by alloying, together with the cubic symmetry rules. Starting with the Γ_6-Γ_8-Γ_7 normal ordering corresponding to the situation in CdTe, a well known direct gap SC, $E_g = E(\Gamma_6) - (\Gamma_8)$ decreases continously upon addition of Hg (Fig.1). Neglecting alloying effects due to the lack of translation symmetry, the shift of the Γ_6 - conduction band state (Γ_{6c}) relative to the Γ_8 one appears to be mainly due to the relativistic corrections induced by the Hg-core introduction in the Cd-sublattice of the crystal[26-27]. In more explicit words, neglecting at first the small effect of the lattice parameter change,

the difference of the Darwin term and mass-velocity correction acting on the s-like Γ_6 level, leads to a downward shift of this state stronger than the downward shift of the p-like Γ_8 level produced by the net effect of mass-velocity and spin-orbit splitting corrections applied to this state. An extension of these considerations to other states suggests that the conduction band edge of the CdHgTe SC sequence will be *a fortiori* at Γ_6 - point since, in CdTe, the subsidiary minima are well above Γ_{6c} : these other levels have either p - like or s - p mixing characters by virtue of cubic symmetry rules. Using a first principle relativistic calculation of the band structure of the couple Ge - α Sn, Herman and co-workers[28,29] gave the more plausible theoretical explanation of the $\Gamma_{(8^+)}$ - $\Gamma_{(7^-)}$ inversion occuring in the band model of α- Sn proposed by Groves and Paul[2].

Qualitatively the CdTe-HgTe couple can be examined by following this procedure together with the published values of the atomic relativistic corrections inducing band shifts which were calculated for various elements corresponding to the compounds belonging to the zincblende symmetry group[29]. In that case a difficulty arises from the choice of an accurate weighting factor $x_{s,p}$ defined according to the well - known time sharing principle[29,30] as :

$$\Delta E_s = x_s \, \Delta E_s \, (M) + (1 - x_s) \, \Delta E_s \, (X) \qquad (1)$$

where ΔE_s is the net relativistic shift of a s - like level E_s in an intermetallic compound MX, M denoting the metal. Making a substitution s-p in the subscripts a similar expression describes the effect experienced by a p - like state E_p; x_s and x_p are related by $x_p = 1 - x_s$. A deviation from the 5/6 - 1/6 rule (usually admitted for II-VI compounds) produces significant differences in any calculation of the Darwin and mass - velocity shifts induced by the Cd $\rightarrow$ Hg substitution. As a fisrt approach to this problem, an empirical adjustement of $x_{s,p}$ can be obtained through the experimental value of Δ_o, the Γ point spin - orbit splitting[27]. This is a reasonnable

way since this well known relativistic splitting is also essentially an atomic - core effect. From (1) and the appropriate factor for p like states, the adjusted parameters is defined by :

$$x_s = \frac{\Delta_o - \Delta_p(M)}{\Delta_p(X) - \Delta_p(M)} \qquad (2)$$

where Δ_p is the adjusted spin - orbit correction of the isolated atom in the crystal MX. Using the published values[29] of Δ_p(Cd), Δ_p(Te), Δ_p (Hg) and the low temperature experimental data Δ_o (CdTe) = - 0.920 eV[31], Δ_o(HgTe) = - 1.12eV[32], (2) gives :

$$x_s \text{ (CdTe)} = 0.67 \qquad (3)$$

$$x_s \text{ (HgTe)} = 0.66 \qquad (4)$$

Using the parameters (3), (4) the net relativistic shift difference applied to Γ_6 and Γ_8 in the CdTe → HgTe substitution produces a total variation ΔE_g =•2.2eV. Comparing with ΔE_g (experimental) = - 1.91 eV, these rough estimations indicate surprisingly a fair agreement and support strongly the relativistic nature of the origin of the $\Gamma_8 - \Gamma_6$ inversion occuring in the band structure of HgTe. Following this oversimplified model, the continuous decrease of E_g resulting from the addition of HgTe to CdTe is understandable since, within the (Hg,Cd) - core regions an electron shares its time statistically in proportion to x. This would indicate a linear dependance of E_g upon x over the whole sequence $Cd_xHg_{1-x}Te$. A recent theoretical study[11] and various experimental data obtained at low temperature[7,9,24] support fairly this picture. For definite values of the composition x, temperature T and pressure P, we can have E (Γ_6) = E (Γ_8) corresponding to an accidental degeneracy of the Γ_6 and Γ_8 levels. The experimental analysis of this particular feature is one of the main purposes of the present study.

II.B. Dispersion law expressions.

The E(k) relations of the bands stemming from the Γ_6, Γ_7, Γ_8 levels and the wave-functions associated with each wave-vector in these bands are expected to be obtained through the $\vec{k}.\vec{p}$ method[1] as widely observed in small gap semiconductors. In these materials, the energy intervals between these three levels are supposed to be small as compared to their distance from lower or higher bands. Within this assumption, the Hilbert space may be truncated by taking as a basis 8 eigenfunctions of the Hamiltonian $H_o = p^2/2m_o + V$ (V is the crystalline field and m_o the free electron mass). The choosen eigenfunctions describe the eigenvalues E_s and E_p which have respectively s-like and p-like symmetry. These wavefunctions are :

$$|iS\downarrow\rangle \quad ; \quad |iS\uparrow\rangle \tag{5}$$

for the level E_s and :

$$\left.\begin{array}{l} |2^{-\frac{1}{2}}(X-iY)\uparrow\rangle \; ; \; |Z\downarrow\rangle \; ; \; |2^{-\frac{1}{2}}(X+iY)\uparrow\rangle \\ |2^{-\frac{1}{2}}(X+iY)\downarrow\rangle \; ; \; |Z\uparrow\rangle \; ; \; |2^{-\frac{1}{2}}(X-iY)\downarrow\rangle \end{array}\right\} \tag{6}$$

for the level E_p. As usual $\uparrow$ and $\downarrow$ denote spin wave-functions. The functions denoted S and X,Y,Z are transformed as the s-like and p-like atomic wave functions under T_d^2 point group operations. When taking into account the $\vec{k}.\vec{p}$ and the spin orbit interactions, two matrix elements are to be considered, namely

$$P_k = -i\frac{\hbar}{m_o}\langle S|p_z|Z\rangle \tag{7}$$

$$\Delta_o = \frac{3\hbar i}{4m_o c^2}\langle X|\frac{\partial V}{\partial x}p_y - \frac{\partial V}{\partial y}p_x|Y\rangle \tag{8}$$

P_K is the momentum matrix element and $\Delta_o = E(\Gamma_8)-E(\Gamma_7)$ is the spin-orbit splitting energy. In the present study the condition $\Delta_o >> k P_K$, $|E_g|$ is always fulfilled. In this case the dispersion laws become the well known Kane's expressions, describing the four bands stemming from the three levels Γ_6, Γ_8 and Γ_7:

$$\left.\begin{aligned} E_1(k) &= \frac{\hbar^2 k^2}{2m_o} + \frac{1}{2}\left[E_g + \left(E_g^2 + \frac{8}{3} k^2 P_k^2\right)^{\frac{1}{2}}\right] \\ E_2(k) &= \frac{\hbar^2 k^2}{2m_o} + \frac{1}{2}\left[E_g - \left(E_g^2 + \frac{8}{3} k^2 P_k^2\right)^{\frac{1}{2}}\right] \\ E_3(k) &= \frac{\hbar^2 k^2}{2m_o} \\ E_4(k) &= -\Delta_o + \frac{\hbar^2 k^2}{2m_o} - \frac{P_k^2 k^2}{3(\Delta_o + E_g)} \end{aligned}\right\} \qquad (9)$$

These four eigenvalues are twofold degenerate with respect to the j_z component of the total angular momentum which is now a good quantum number because of the spin-orbit interaction[1].

In a second step of the calculations the interaction with other far lying bands is introduced. The twofold degeneracy of E_1, E_2, E_4 is slightly removed by terms proportionnal to k^3. $E_3(k)$ becomes the heavy hole band. Since the curvature of this band is determined by such interactions with far lying bands, its shape is expected to be independent of the $\Gamma_6 - \Gamma_8$ ordering in a first approximation. In other words it may be postulated that no important change of the shape of this band will occur through the whole sequence $Cd_xHg_{1-x}Te$. Owing to the terms k^3, strictly speaking this band is not parabolic. The detailed structure of this band in various directions is correlated to the lack of inversion symmetry of the zinc blende lattice. This problem has been widely discussed by Parmenter [33] and

Dresselhauss[34] from a group-theory point of view. The lack of inversion symmetry of the zinc blende lattice would lead to change somewhat the degeneracy of the bands : the Λ_6 and Λ_5 bands remain two-fold degenerate whereas the Σ_3, Σ_4 and Λ_5 bands become non degenerate. Further-more, the presence of linear k terms would lead to a small bump ΔE of the heavy hole band near the Γ point along the Λ and Σ axis.

The order of magnitude of ΔE suggests the possibility of some simplification of the valence band structure corresponding to the present study of $Cd_xHg_{1-x}Te$ alloys. In effect, Kane showed theoretically that $\Delta E << 1meV$ in InSb[1], which has been confirmed experimentally. To our knowledge no information was published for CdTe whereas estimates such as $\Delta E < 1meV$[6,7,24] or $\Delta E = 1meV$[35] were obtained in HgTe from intrinsic regime studies. A recent theoretical study gave $\Delta E = 0.3$ meV[36]. These considerations indicate that within the experimental uncertainty of the present study the overlap may be neglected. In this first approximation, taking the origin of energies at Γ_8, the dispersion law of the heavy hole valence band will be assumed to be depicted by the parabolic relation :

$$E_v(k) \equiv E_3(k) = -\frac{\hbar^2 k^2}{2m_p} \qquad (10)$$

We have neglected the term $\hbar^2 k^2/2m_o$. In the SM configuration, the band structure is then similar to that of gray tin sometimes called a "symmetry induced zero gap semiconductor", or a "zero overlap semimetal". In this simplified situation, the $\Gamma_6 - \Gamma_8$ crossover corresponds to the SM-SC transition , and has been schematically illustrated in Fig.1.

According to the high value of Δ_o encountered in CdHgTe (see sect.II.A.), the split-off band $E_4(k)$ is a far lying subvalence band and thus may be neglected in transport studies. In the expressions of $E_1(k)$ and $E_2(k)$, we take into account the normal or inverted ordering of levels by giving E_g a positive or a negative value respectively.

For both signs of E_g the Eqs.9 show that for $k \to 0$, $E_1(k)$ and $E_2(k)$ depict respectively a conduction band and a valence band.

(i) SM case. With E_g negative, $E_1(k)$ and $E_v(k)$ are degenerate at k = 0 (Fig.1.a) inducing a fourfold degeneracy at this point. This state is the Γ_8 one and represents both the extrema of the conduction band $E_1(k)$ and of the heavy hole valence band $E_3(k)$. In this situation the light hole band $E_2(k)$ becomes a subvalence band, the maximum of which is Γ_{6v}. Here $E_g = E(\Gamma_{6v}) - E(\Gamma_8) < 0$.

(ii) SC case. E_g being positive, $E_2(k)$ and E_v are degenerate at k=0 giving the Γ_8 level (Fig.1.c.). This corresponds to the well known situation exemplified by InSb, i.e. the normal ordering with the Γ_{6c} level lying higher than the Γ_8 one. Here $E_g = E(\Gamma_{6c}) - E(\Gamma_{8v}) > 0$.

A more tractable expression of the conduction band dispersion law : E(k) can describe both cases by taking the zero energy at the bottom of this band (Γ_6 and Γ_8 in the SC and SM configurations respectively) i.e. :

$$E_c(k) = \frac{1}{2}\left[-|E_g| + \left(E_g^2 + \frac{8}{3} k^2 P_K^2\right)^{\frac{1}{2}}\right] \qquad (11)$$

Besides the neglect of the overlap ΔE in all what follows we shall use a simplified two band model in order to analyze our results. In either SM or SC configuration we shall consider a single parabolic heavy valence band depicted by Eq. 10 and a single isotropic conduction band, dispersion relation of which is given by Eq.11. The neglect of the light hole valence band in intrinsic regime studies is supported by the large band edge effective mass ratio m_p/m_n where m_n, the electron effective mass at the bottom of the conduction band is also equal to the band edge light hole mass. This property is obtained for both SC and SM cases by expanding $E_1(k)$ and $E_2(k)$ of Eqs.9 for $k \to 0$, leading to :

$$m_n = \frac{3\hbar^2 |E_g|}{4 P_K^2} \qquad (12)$$

Note that in the SM configuration, this approximation is valid a fortiori since the light hole band stemming from Γ_{6v} is lower then the heavy hole band.

II.C. Wave function representations.

In Kane's work[1] the periodic part $u_{\vec{k}}(\vec{r})$ of the Bloch wave function $\psi_{\vec{k}}$ is expanded on the basis provided by (5) and (6).

For each eigen-value E_i (i running from 1 to 4) given by (9) two wave functions $u_{i,\,k,\,\alpha}$ and $u_{i,\,k,\,\beta}$ are obtained. α and β are the two values of the j_z component of the total angular momentum. For the three bands E_1, E_2, E_4 we have always $j_z = \pm \frac{1}{2}$ and taking for example k parallel to k_z we may write explicitely.

$$u_{i,k_z,\frac{1}{2}} = a_i |iS\uparrow\rangle + b_i \frac{-1}{\sqrt{2}} |(X+iY)\downarrow\rangle + c_i |Z\uparrow\rangle$$
$$u_{i,k_z,-\frac{1}{2}} = a_i |iS\downarrow\rangle + b_i \frac{1}{\sqrt{2}} |(X-iY)\uparrow\rangle + c_i |Z\downarrow\rangle \qquad (13)$$

A general expression for a_i, b_i, c_i can be readily obtained for the conduction band states in the SM or SC configurations, i.e. for the band stemming from Γ_8 or Γ_{6c} respectively. Provided that E_g is taken algebrically, when $\Delta_o \gg |E_g|$ and kP_k, denoting $A = (E_g^2 + 8k^2P_K^2/3)^{\frac{1}{2}}$ this general formulation is :

$$a = \left[(A+E_g)/2A\right]^{\frac{1}{2}} \quad , \quad b = \left[(A-E_g)/6A\right]^{\frac{1}{2}} \quad c = \left[(A-E_g)/3A\right]^{\frac{1}{2}} \qquad (14)$$

Under these assumtions we may notice that $c^2 = 2b^2$, moreover $a^2 + b^2 + c^2 = 1$, so that the usual normalization condition of $u_{\vec{k}}$ in the unit cell is fulfilled.

In all what follows, the zero of energy is taken at the bottom of the conduction band. With $\gamma = k_o T/|E_g|$ and $z = E/k_o T$, k_o being the Boltzman constant, the coefficients a, b, are expressed as :

$$a^2_{SM} = \gamma z/(1+2\gamma z) \; ; \; b^2_{SM} = (1+\gamma z)/(3+6\gamma z)$$
$$a^2_{SC} = (1+\gamma z)/(1+2\gamma z) \quad b^2_{SC} = \gamma z/(3+6\gamma z) \qquad (15)$$

At the center of the Brillouin zone, i.e. for $z = 0$, it appears from the above expressions, that the wave function characters are, as expected, either p - like in the SM configuration or s - like, as usual in the SC one. On the other hand, off - $k = 0$, the s - p mixing is indicated by (15) and must be taken into account as soon as $2\gamma\zeta$ becomes comparable to 1. Its impact on the electron density of states appears through the non - parabolicity of the dispersion law (see Eq.11). In our case, the reduced intrinsic Fermi level $\eta = E_F/k_oT$, is such that $\eta > 3$ in HgTe and SM alloys and also in narrow gap SC alloys with E_g of the order of k_oT. Thus the s - p mixing is expected to be an important effect for $|E_g|$ values smaller than at least $6k_oT$. In the particular case of the SM $\rightarrow$ SC transition corresponding to the accidental degeneracy of the Γ_6 and Γ_8 points, by making $\gamma\eta \gg 1$ in Eqs.15 we observe the s - p mixing to occur for any wave vector in the Brillouin zone. Denoting by a_+, b_+ and c_+ the above coefficients in the vicinity of the Γ_6, Γ_8 crossover, we have $a_+^2 = \frac{1}{2}$, $b_+^2 = 1/6$ and $c_+^2 = 1/3$.

III - EXPERIMENTAL STUDIES.

III.A. Experimental procedures.

In this work, we studied $Cd_xHg_{1-x}Te$ alloys within a composition range extending from $x = 0$. (HgTe) up to $x \simeq 0.15$. Each sample has to be specified from the point of view of :

i) atomic Cd composition : x

ii) compositional homogeneity, throughout sample.

iii) concentration of electrically active centers or impurities.

That specification is achieved in the following way : x is measured by electron microprobe analysis as well as Hall constant measurements at different temperatures in the range $4.2 < T < 373°K$. Deviations from homogeneity in a given sample are detected and evaluated by measuring at 273°K and 373°K the intrinsic Hall constant across various set of probes located along the sample. Small size monocrystalline samples, cut out along lowest compositional gradient directions of ingots have been selected for the present work. Composition deviation within each of them does not exceed 0.003 (we shall therefore label these samples by the value x).

Concentration of extrinsic carriers has been checked using Hall measurements as a function of temperature and magnetic field, at normal pressure and low T. For all samples studied in this work, the net concentration of electrically active centers appeared to be lower than $2 \times 10^{16} cm^{-3}$ acceptors. At 77°K, this concentration of acceptor impurities does not lead to any noticeable deviation from the intrinsic conduction regime for samples with $x < 0.15$, provided that pressure will not exceed 3 kbar. We shall denote such a situation as "pseudo - intrinsic" regime.

For the characterization procedure as well as Hall constant conductivity measurements under pressure, we use an A.C. null - bridge technique described previously [37], allowing a sensitivity better than 10^{-4} and accuracy within 10^{-3}. Galvanomagnetic measurements at normal pressure are performed with a classical electromagnet giving a field up to 10 kG, with an accuracy better than 10^{-3}. Measurements under pressure are performed at two fixed temperatures 292°K and 77°K. Helium is used as a pressure transmitting medium, insuring purely hydrostatic conditions in the whole investigated pressure range, 1 bar $< P <$ 13 Kbar. With such an equipement it was not possible to perform experiments at temperature lower than liquid N_2. The pressure generating system is a commercially available apparatus built by

BASSET - BRETAGNE - LOIRE*. P is measured with a manganine wire gauge, having 10 bars sensitivity. In the course of measurements we did not observe any hysteresis effect, within the limits of experimental errors. The magnetic field for Hall measurements under pressure is provided by a coaxial-shaped electromagnet mounted inside the pressure vessel. Induction in this magnet is < 600 gauss.

III.B. Experimental results.

In $Cd_xHg_{1-x}Te$ crystals which have not been doped intentionally the low temperature transport properties exhibit a p-type character because of stoichiometric defects, Hg vacancies. For materials in the SM or zero gap configuration Gelmont and Dyakonov[38] have shown that the acceptor states are located within the conduction band and interfere with it. When the Fermi energy E_F is comparable to the activation energy E_A[27], an abnormal behaviour in the temperature dependence of the conductivity is observed in HgTe in the range 20-40°K[39-41] together with strong anomalies of the Hall coefficient R_H and Hall mobility μ_H at 9°K and 40°K in the case of CdHgTe SM alloys[17]. An analysis of transport phenomena dealing with extrinsic effects needs measurements versus magnetic field in order to separate the contributions of the different types of carriers[42]. As already pointed out our experimental set-up did not allow us to use magnetic fields higher than the 600 G available inside the experimental vessel, so-that in the present work the choice of 77°K as the lowest temperature appeared to be the best compromise between minimizing the extrinsic effects and lowering k_oT in order to deal with electrons in the vicinity of the Γ_6 or Γ_8 levels.

In the SM configuration, when decreasing $|E_g|$ the density of states in the conduction band decreases so that extrinsic effects due to p-type conduction are more pronounced

---

* 92 Sèvres - FRANCE.

The electron concentration : n, and hole concentration : p are less and less balanced ($n < p$) so that the low field Hall coefficient R_H no longer reflects the electron concentration. The p type conduction appears clearly in the SC configuration through a maximum of the variations of $R_H(P)/R_H(1\ bar)$ vs. P as shown at 77°K for samples 0.113, 0.12, 0.14 (Fig.2).

This behaviour is typical of a material with $n < p$ and $\mu_n \gg \mu_p$ (Sect.IV A). All the alloys used in the present study are SM at zero pressure and 77°K and the curves in Fig.2 are typical of samples for which the available range of pressures allowed the SC configuration to be reached : namely $x > 0.09$. In the SC configuration the opening of a thermal gap makes this configuration very sensitive to the presence of impurities.

Nevertheless for compositions $x < 0.09$ as far as $(N_A - N_D) < 2 \times 10^{16} cm^{-3}$, electronic concentration : n, does not deviate from the intrinsic value n_i by more than 10% . For all other samples, this deviation does not exceed 20%. Considering that the hole mobility is known to be around 550 $cm^2\ V^{-1} sec^{-1}$ and that electron mobility ranges from $8 \times 10^4 cm^2\ V^{-1}\ sec^{-1}$ (for HgTe) to $3 \times 10^5 cm^2\ V^{-1} sec^{-1}$ (for the x = 0.14 sample), we may take for granted (Sect.IV A) that the electron concentration n is given by the low field Hall coefficient R_H through $n = -1/e\ R_H$, at least over the first 2 or 3 kbars.

The next section is devoted, in its first part (IV A), to the analysis of these low field Hall measurements at 77°K and 292°K. For this latter temperature the intrinsic regime is prevailing for all the samples. It will be shown that pressure measurements can provide an additional means of studying the compositional behaviour of the band model in the SM and narrow gap SC configurations.

The quantity $(d\text{Log}\ R_H/dP)_{P \to 1bar}$ will be shown to be mainly sensitive to E_g (1bar) and $d E_g/dP$. This logarithmic derivative has been plotted vs.x at 77°K and 292°K in Figs. 3 and 4 respectively. The pressure coefficient dE_g/dP

may be deduced from independent experiments such as current-voltage characteristics on p-n junctions[16,17]. In section IV.A.a. this parameter will be deduced from an appropriate plot of R_H versus pressure. A determination of the $E_g(x)$ law will thus be deduced from the fits obtained in Figs.3 and 4, leading to useful informations in the whole SM range at 77°K and 292°K (Fig.5 and 6 respectively).

On another hand systematic measurements vs. P on samples with different x values have led to the observation of the pressure induced SM → SC transition. An illustration of this transition is provided by the relative variations of the Hall mobility $\mu_H(P) / \mu_H$ (1bar) against pressure reported in Figs.7 and 8 at 77°K and 292°K respectively. The observed maxima can be qualitatively understood according to a k.p. approach of the band structure scheme (Sect.II) leading to an expected minimum of the electron effective mass at the pressure induced $\Gamma_6 - \Gamma_8$ crossover (Eq.12).

While the Hall mobility provides a good illustration of the pressure induced $\Gamma_6 - \Gamma_8$ crossover, no evidence of this feature is observed on a direct plot of R_H vs. P (Figs.2 and 9), which shows an apparent monotonic behaviour of the intrinsic regime (Fig.9). However following a procedure deduced from the intrinsic regime calculations, the crossover of the Γ_6 and Γ_8 levels appears in an appropriate plot of R_H vs. P (Sect.IV.A.c).

In Sect.IV.B an analysis of the electron mobility results obtained at room temperature will be attempted taking into account the exact symmetry of the conduction band extremum through the use of the true electron wave functions as given in Sect.II. The same analysis was not possible at 77°K because one should have taken into account

(i) The influence ionized impurities which are present in variableconcentrations from sample to sample.

(ii) The mixed conductivity which becomes important in the vicinity of the crossover pressure and makes the Hall mobility very different from the electron mobility. The lack of variable magnetic field did not allow us to overcome these two difficulties.

IV - INTERPRETATION.

IV.A. Hall coefficient measurements analysis.

In this section we shall analyse the measurements of low field Hall coefficient versus pressure at 77°K and 292°K : the analysis will be carried out within the framework of the simplified two band model described in Sect.II.B.

The electron and hole concentrations are given by

$$n = \frac{4}{3\sqrt{\pi}} N_n \, {}^{0}L_{0}^{\frac{3}{2}}(\eta, \gamma) \tag{16}$$

$$p = N_p \, \mathcal{F}_{\frac{1}{2}}(\eta') \tag{17}$$

where $N_{n,p} = 2\,(2\pi m_{n,p}\, k_o\, T/h^2)^{3/2}$, $\eta' = -\eta$ in the SM configuration and $\eta' = -\eta - E_g/k_oT$ in the SC configuration $\mathcal{F}_{\frac{1}{2}}(\eta)$ is the classical Fermi-Dirac integral whereas, according to Kolodziejczak [44] ${}^{n}L_{j}^{m}(\eta, \gamma)$ is a similar integral which takes into account the non parabolicity of the conduction band as depicted by Eq.11. ${}^{n}L_{j}^{m}(\eta, \gamma)$ is given by

$${}^{n}L_{j}^{m}(\eta, \gamma) = \int_{0}^{\infty} -\frac{\partial f_o}{\partial z}\, z^n \left(z + \gamma z^2\right)^m (1 + 2\gamma z)^j \, dz \tag{18}$$

In the limiting case when $\gamma = k_oT/|E_g| = 0$ (negligible non-parabolicity) the integral in (16) becomes

$${}^{0}L_{0}^{\frac{3}{2}}(\eta, 0) = \frac{3\sqrt{\pi}}{4}\, \mathcal{F}_{\frac{1}{2}}(\eta) \tag{19}$$

The intrinsic regime reduced Fermi level η_i is obtained by solving the electrical neutrality equation

$$n = p \tag{20}$$

According to Eqs.10,11,12,16,17 the above equation include three parameters : E_g, P_K, m_p, with a dependence on P_K and m_p through $P_K^2\, m_p$.

When temperature and composition are fixed, hydrostatic pressure produces a decrease of the lattice parameter: a, and consequently a shift of the band extrema as illustrated for instance by a calculation of Herman et al.[45] for Germanium. According to Eq.7 the matrix element P_K is in a first approximation, pressure sensitive through the variation of the lattice parameter a (p_z varies as a^{-1}) and the renormalization of the wave functions S and Z, both effects leading to a total relative variation : $-4\,\Delta a/a$. According to the published values of the elastic constants of HgTe[46] this simple approach would lead to $\Delta P_K/P_K \simeq 3 \times 10^{-6}$ bar^{-1}. Such a low value of $\Delta P_K/P_K$ allows the pressure dependence of P_K to be neglected.

Since the curvature of the heavy hole valence band is determined by interaction with far lying bands (see Sect.IIB) we shall assume that m_p does not vary significantly over the investigated range of compositions and pressures : as a matter of fact any shift of the Γ_6 level is expected to be small as compared to the large energy separation of this level from the far lying bands to be considered. Regarding the pressure effect this hypothesis is supported by pressure experiments on p-type HgTe which show that the hole mobility does not vary with pressure[47].

In our analysis E_g will be the only pressure sensitive parameter. E_g will be assumed to depend linearly on pressure with a positive coefficient dE_g/dP which in both SM and SC configurations makes the Γ_6 level to shift upwards. Starting from a SM configuration ($E_g < 0$), the Γ_6 level comes closer to the Γ_8 one, then crosses over it at the SM-SC transition ($E_g = 0$) and eventually lies above the Γ_8 level in the SC configuration ($E_g > 0$). In this latter situation E_g becomes a thermal gap. Such will be the framework of our analysis of the band structure deformation experienced by the $Hg_{1-x}Cd_xTe$ alloys under pressure.

We have reported in Fig.10 calculated values of η_i versus E_g at 77°K and 292°K. The equation 20 was solved with the help of a computer, which allowed us to calculate the integral $\int_0^\infty$ and $\mathcal{F}_{\frac{1}{2}}$ without any approximation concerning

the degree of statistical degeneracy in the conduction and valence bands. The calculations have been carried out for two values of the product $P_K^2\, m_p$ corresponding to the rather widespread range of published values for these parameters : namely $0.3 \leqslant m_p/m_o \leqslant 0.7$ [9,13,48] and $7.3 \leqslant P_K \leqslant 8.5 \times 10^{-8}$ eVcm [49].

We can see in Fig.10 that η_i slowly increases in the SM side, reaches a maximum at $E_g = 0$ and then quickly decreases in the SC side. Within the SM and samll gap SC ranges , η_i remains positive so that the electron gas is degenerate. Furthermore the gap derivative : $(\partial \eta_i / \partial E_g)_T$ appears rather insensitive to the choice of $P_K^2\, m_p$ for a given value of E_g. This latter result may be approximatively accounted for, without the help of a computer, when $\eta \gg 1$ and $\gamma\eta \ll 1$ (i.e. when the non parabolicity of the conduction band is negligible). These conditions may be fulfilled in the SM configuration for large values of E_g : from Eqs.16 and 17 we may then write for a given temperature

$$n \sim (m_n\ \eta\ )^{3/2} \tag{21}$$

$$p \sim \exp\ (-\eta\ ) \tag{22}$$

So that

$$\frac{1}{n}\frac{dn}{dE_g} = \frac{3}{2}\frac{1}{|E_g|} + \frac{3}{2}\frac{1}{\eta}\frac{d\eta}{dE_g} \tag{23}$$

and

$$\frac{1}{p}\frac{dp}{dE_g} = -\frac{d\eta}{dE_g} \tag{24}$$

In the intrinsic regime and SM configuration we obtain

$$\left(\frac{d\eta_i}{dE_g}\right)_{SM} = \frac{3\eta_i}{2\eta_i + 3}\ \frac{1}{|E_g|} \tag{25}$$

when $\eta_i \gg 1$ this last equation shows that $(d\eta_i/dE_g)_{SM}$ essentially depends on $|E_g|$. This result is supported by exact calculations performed from Eqs.16 and 17 with a computer. From the knowledge of the variations of η_i and

$d\eta_i/dE_g$ versus E_g it was possible to calculate the intrinsic concentration $n_i(E_g)$ and its logarithmic derivative $d\,\mathrm{Log}\, n_i/dE_g$. On the experimental side, we measured the low-field Hall coefficient and the zero-field conductivity.

The low field Hall coefficient R_H may be written

$$R_H = \frac{1}{pe} \quad \frac{1 - b^2 c}{(1 + bc)^2} \tag{26}$$

where $c = n/p$ is the electron to hole concentration ratio, and $b = \mu_n/\mu_p$ the electron to hole mobility ratio. In intrinsic regime $c = 1$, and for $b \gg 1$ the low field Hall coefficient gives the electron concentration so that $n_i = -1/e\, R_H$ and $d\,\mathrm{Log}\, n_i/d\, E_g = -\, d\,\mathrm{Log}\, R_H/d\, E_g$.

The zero field conductivity may be written

$$\sigma = \sigma_n \quad \frac{1 + bc}{bc} \tag{27}$$

For $c = 1$ and $b \gg 1$ the zero field conductivity gives the electron conductivity $\sigma = \sigma_n$. In such conditions the Hall mobility $R_H\sigma$ gives the electron mobility μ_n.

When extrinsic carriers are present, n and p may be derived if one calculates the value of which is a solution of the neutrality equation $n - p = N_D - N_A^-$. N_D is the concentration of donors which in narrow SM or SC gap materials are completely ionized,[38] NA^- is the concentration of ionized acceptors. This equation was solved numerically for various values of E_g and $(N_A - N_D)$. For a given value of $N_A^- - N_D$, c is a decreasing function of E_g. In the SM range μ_n increases so that the increase of b compensates the decrease of c. However in the SC range μ_n and then b decrease so that the condition $b\,c \simeq 1$ is fulfilled leading to a maximum in $|R_H(E_g)|$ as given by Eqs.26. For $b^2c = 1$, R_H changes its sign and for $b^2c \ll 1$ it should be possible to reach $N_A^- - N_D$. However as illustrated in Fig.2 it was only possible to reach the maximum of $|R_H(E_g)|$ and according to the set of band parameters we shall determine below, the location and order of magnitude

of this maximum was accounted for with ionized impurities concentrations : $N_A^- - N_D \leq 2 \times 10^{16} cm^{-3}$. According to the order of magnitude of $N_A^- - N_D$, although most of our samples were strictly speaking p type, in the range of pressures up to 4 kbars, α was never less than 0.85 for compositions $x > 0.09$ at 77°K. This range of pressure was significantly wider for those samples of compositions $x < 0.09$.

Although $\alpha < 1$ the condition $bc >> 1$ was thus fulfilled over the above mentioned ranges of pressure so that the relation $n = -1/e\ R_H$ holds true with an error less than 15% at 77°K. We shall denote such a situation as : "pseudo-intrinsic regime". At room temperature such impurity concentrations do not affect the intrinsic regime.

a. Determination of dE_g/dP.

In Figs.11 and 12, we have plotted $(1/e\ |R_H|\ )^{2/3}$ versus pressure at 77°K and 292°K respectively, for some samples which are SM at zero pressure. According to the above discussion for these samples $n_i = 1/e\ |R_H|$. The Figs.11 and 12 thus show that $n_i^{2/3}$ is a linear function of pressure within a range of a few kbars. According to equation 12 and within the range of validity of Eq.21 we may write

$$n_i^{2/3} \sim |E_g|\ \eta_i$$

The above relation shows that within the framework of the k.p method and taking into account the smooth dependence of η_i versus E_g in the SM configuration, $n_i^{2/3}$ is expected to be an almost linear function of E_g and hence, of pressure. Detailed calculations confirmed such an approximate analysis and we have reported in Fig.13 computed values of $n_i^{2/3}$ for E_g values ranging from-270 meV to -130 meV at 77°K. It is clear from this figure that the variations of $n_i^{2/3}$ versus E_g are essentially linear. Actually the derivative $d(n_i^{2/3})/dE_g$ is not exactly a constant when considered over a wide range of E_g values. Nevertheless for E_g lying within the range -130 to -30meV at 292°K and - 270 to -130 meV at 77°K. The detailed

calculations give

$$(d(n_i^{2/3})/dE_g)_{292°K} = -(16 \pm 0.5) \times 10^8 cm^{-2}\ meV^{-1}$$

$$(d(n_i^{2/3})/dE_g)_{77°K} = -(42 \pm 2) \times 10^7 cm^{-2}\ meV^{-1}$$

In both cases the quoted uncertainties include linearity departure of the $n_i^{2/3} = f(E_g)$ function, and variations of the calculated values of this slope when values of P_K and m_p are varied within the range mentioned before.

At room temperature, the experimental value of $d(n_i^{2/3})/dP$ for the whole series of sample we studied was found to be $-(1.68 \pm 0.05) \times 10^{10} cm^{-2}\ bar^{-1}$ leading to

$$(dE_g/dP)_{292°K} = (10.5 \pm 1) \times 10^{-6} eV\ bar^{-1}$$

The same analysis carried out at 77°K for those samples of composition $x \leq 0.07$ for which the intrinsic regime prevails has given an experimental value $d(n_i^{2/3})/dP = -(38 \pm 0.5) \times 10^8 cm^{-2}\ bar^{-1}$ so that

$$(dE_g/dP)_{77°K} = (9 \pm 0.5) \times 10^{-6} eV\ bar^{-1}$$

b. $E_g(x)$ law at 77°K and 292°K.

Within the SM range of compositions, the $E_g(x)$ law may be derived from the knowledge of dE_g/dP together with the determination of the crossover pressure. However the crossover pressure may not be reached for any composition. [50] The zero pressure E_g value may then be deduced from the study of the logarithmic derivative of the electron concentration versus pressure, i.e. from

$$n^{-1}(dn/dP)_{P \to o} = n^{-1}(dn/dEg)(dEg/dP) \qquad (28)$$

In the intrinsic regime and SM configuration using the Eq.12 together with the simplified relations 21 and 25 we obtain :

$$\frac{1}{n_i}\frac{dn_i}{dP} = \frac{3\eta_i}{2\eta_i + 3} \cdot \frac{1}{|E_g|}\frac{dE_g}{dP}$$

This simplified analysis lets us expect that $dLogn_i/dP$ only depends on E_g and dE_g/dP and is not significantly sensitive to P_K and m_p at least in the SM configuration. Detailed calculations of $dLog\ n_i/dE_g$ have shown that this property holds valid not only in the whole SM range, but also for the small gap SC range. When P_K and m_p are varied from 7.3 to 8.3 x 10^{-8} eV cm and from 0.4 to 0.7 m_o respectively, the calculated values of $dLog\ n_i/dE_g$ do not vary by more than five per cent for any value of E_g ranging from -130 to + 130 meV at 292°K and from -260 to + 20meV at 77°K. The range of E_g values explored at both temperatures corresponds to the range of compositions studied in this paper.

On the experimental side $d(Log\ n_i)/dE_g$ was deduced from $\left[d(Log\ |R_H|\ )/dP\right]_{P\to o}$ according to Eq.28 taking into account the values of dEg/dP determined in the previous section. This determination of $d\,Log\ n_i/dE_g$ yields the values of E_g for all the studied compositions : they have been reported in Figs.5 and 6 for 77°K and 292°K respectively.

Computed and experimental values of $(dLog|R_H|\ /dP)_{P\to o}$ as a function of the composition have been reported in Figs.3 and 4 at 77°K and 292°K respectively.

From this analysis we may draw the following conclusions :

- For SM or small gap SC materials, this method in principle, allows the determination of $E_g(P=o)$ with an uncertainty lower than 10meV and requires only a few kbars; $dLog|R_H|/dP$ was determined by measurements performed at 300 bar intervals up to 2 kbar.

- At 292°K, we obtained for HgTe (x = 0) Eg=-(115±10)meV in agreement with thermo-reflectivity measurements performed in our laboratory [17,51].

- At 292°K the $E_g(x)$ law is non linear and we find the crossover composition to be

$$x^{+}_{292°K} = 0.07 \pm 0.01$$

in significant discrepancy with other published values around 0.09-0.10 [9,10,21].

- At 77°K the $E_g(x)$ law is linear and our value $E_g\ (x=0) = -(255 \pm 10)$meV is in good agreement with the magnetoreflection measurement by Groves et al. who reported -266 meV at this temperature[52].

- At 77°K the crossover composition is found equal to $x^+_{77°K} = 0.145 \pm 0.005$.

All these results are consistent with E_g determinations obtained through characterization of the $\Gamma_6 - \Gamma_8$ crossover, which problem we are to examine now.

c. Evidence of the pressure induced $\Gamma_6 - \Gamma_8$ crossover.

As will be seen in the next section the pressure induced Γ_6-Γ_8 crossover may be evidenced by a maximum exhibited by a plot of μ_n versus pressure. However μ_n is deduced from R_H and σ by $\mu_n = R_H.\sigma$ only when intrinsic or pseudo-intrinsic regime prevails. According to Eqs.26 and 27 and to the discussion presented at the beginning of Sect.IV, at 77°K in the vicinity of the crossover, c decreases and in the limit of bc = 1, $R_H\sigma = \mu_n/2$: the Hall mobility no longer reflects the only variations of μ_n but rather the variations of R_H. We shall see in this section that it is possible to evidence the pressure induced crossover by an appropriate plot of the low field Hall coefficient variations.

As an example the measured quantity $n_i = 1/e\ |R_H|$ for two samples which are SM at zero pressure and room temperature has been reported in Fig.14 versus pressure. The $n_i(p)$ curves exhibit a change of slope which can be assigned to the Γ_6-Γ_8 crossover. In Fig.15 are reported calculated values of n_i versus E_g at 292°K for E_g values ranging from -40meV to + 40meV. It is clear from the figure that $n_i(E_g)$ is essentially a straight line on each side of E_g=0 but the slope of the graph displays a significant change when going from negative values of E_g to positive ones.

The same change of slope appears when one calculates $n_i(E_g)$ at 77°K on both sides of $E_g = 0$.

Such a discontinuity of the rate of variation of the intrinsic population from SM to SC configuration is not suprising according to the opening of a thermal gap in the SC configuration, but one would expect n_i to decrease faster with E_g in the SC range than in the SM one because of the opening of a thermal gap. But experimental results and calculations are in agreement to show that the rate of variation of n_i is lower in the SC range than in the SM one. It is difficult to illustrate this change of slope by such simple calculations as those based on the relation 21. This relation is no longer valid according to the fact that in the vicinity of the $\Gamma_6 - \Gamma_8$ crossover, $\gamma\eta >> 1$. Nevertheless this behaviour of n_i (E_g) may be qualitatively understood bearing in mind that, when the Γ_6 level crosses the Γ_8 one, not only a thermal gap appears, but also, according to Eqs.12 and 16 the density of states N_n at the bottom of the conduction band increases with E_g.

This last effect opposite to the first is predominant and gives rise to observed variations of $n_i(E_g)$ at the SM-SC transition.

This change of slope observed on a plot of $1/e\,|R_H|$ vs. pressure allowed us to locate the crossover pressure within better than 0.5 kbar uncertainty range at 292°K. The same result was obtained at 77°K by a plot of R_H^{-1} versus pressure despite of the fact that in the vicinity of the crossover pressure and for higher pressures $1/e.|R_H|$ no longer gives the electron concentration unambigously. It was actually shown by a computer calculation that as far as $(N_A^- - N_D) < 3 \times 10^{16} cm^{-3}$ the $\Gamma_6 - \Gamma_8$ crossover is still correlated with a change of slope of $1/R_H$ plotted against pressure. We have reported in Fig.16 the variations of $1/|R_H|$ versus pressure for the three samples at 77°K on all the curves the change of slope is clearly appearent and its location shifts towards decreasing pressures when increasing x, i.e. decreasing the $|E_g|$ value at zero pressure.

For both-temperatures of 77°K and 292°K the E_g (x) determinations from an analysis of $(d \text{ Log } n_i/dP)_{P \to 0}$ was in close agreement (better than 10meV) with the determinations obtained from the crossover pressure location, for all the samples for which our experimental set up allowed the crossover pressure to be reached.

IV.B. Electron mobility analysis.

IV.B.a. Theoretical considerations.

The variations of the electron mobility with pressure, illustrated in Figs.7 and 8, are qualitatively assigned to the decrease of $|E_g|$ with pressure in the SM configuration, and the increase of this same central parameter in the SC one. According to the Eq.12, the effective mass at the bottom of the conduction band goes through zero at the crossover pressure which could in principle lead to a very sharp maximum of the electron mobility for this pressure. In fact, according to the values of the electron concentration in our samples at 77°K and 292°K, the Fermi energy is high enough in order that the effective mass to be considered in analyzing the electron mobility is the effective mass $m_n(E_F)$ at the Fermi level. In small gap materials the effective mass, defined as $m_n(E) = \hbar^2 k \, (dE/dk)^{-1}$, depends on the energy because of the non parabolicity . m(E) is given by

$$m(E) = m_n \left(1 + \frac{2E}{E_g}\right) \tag{29}$$

or

$$m(\zeta) = m_n \left(1 + 2\gamma\zeta\right) \tag{30}$$

According to Eq.12 m(E) may be written

$$m(E) = \frac{3}{4} \frac{\hbar^2}{P_K^2} \left(|E_g| + 2E\right) \tag{31}$$

From Eq.31 we can see that $m(E_F)$ is not necessarily minimum when E_g goes through zero. The location of this minimum depends on the rate of variation of E_F with E_g : consequently a maximum of mobility is not correlated to the situation $E_g = 0$, in a straight-forward manner. Two features, specific to small or zero gap materials, are to be considered to perform any calculations of the mobility.

When $|E_g| \lesssim 2E_F$, we must take into account the exact electron wave function which is no longer a plane wave. As developped in Sect.II.C. the exact electron wave function (Eq.13) is a linear conbination of s and p like functions. After Ehrenreich[53], many workers[54] performed theoretical analyses of transport effects in InSb-like materials for which the bottom of the conduction band has the Γ_6 symmetry. These authors used the results of the k.p. method not only through the non parabolicity of the conduction band (Eq.11) but also through the complete wave function supplied by this method (Eq.13). BROERMAN[55] stressed the importance of the p-character of the electron wave-function when analyzing ionized impurity scattering at low temperature in HgSe which is a zero gap material with a conduction band degenerate with the heavy hole valence band at Γ_8.

For such SM or zero gap materials as HgSe, HgTe or α-Sn a second specific feature to be considered is the dielectric constant : $\varepsilon(q)$. At zero momentum transfer[56], $\varepsilon(q)$ exhibits a singularity. This effect, due to the symmetry induced degeneracy of the conduction and valence bands at Γ_8 should be observed at low temperatures when these materials are intrinsic, i.e. when E_F lies very close to Γ_8. The presence of carriers in the conduction band removes this singularity, leading to a dielectric constant depending on the electron concentration[57]. This particular feature, as well as the symmetry of the conduction band have been considered by Broerman[58], Gelmont et al[59], in order to analyse the electron mobility at low temperature

for such zero gap materials when electrons are scattered by ionized impurities.

In addition to the above features we have to consider other points specific to small and zero gap materials in general.

i) the first point is to know whether the relaxation time approximation is valid or not. This approximation may be used when the scattering mechanism is elastic. When such is not the case a variational method must be used [53]. Rode [60] has developped an interative solution of the Boltzman equation. For any elastic scattering mechanism, this method gives the same result as does the relaxation time approximation. This method allowed Rode and Wiley [61] to calculate the electron mobility for zinc blende semimetals HgTe, HgSe and α-Sn as a fonction of the electron concentration in the frame work of the Born approximation.

ii) The second point is to know whether the Born approximation is valid. Rode and Wiley [61] have discussed the effects of the corrections needed to go beyond this approximation.

These different considerations show that the analysis of the electron mobility is not straightforward. Neverthless, in our case some simplifications are possible. In effect, we shall only carry out the electron mobility analysis at room temperature for which the Fermi energy is high . ($E_F \simeq 3\ k_o T$, i.e. $E_F \geq 70$meV for the range of E_g values met in our samples at zero pressure as can be seen in Fig.10). On one hand this allows the singular behaviour of the static dielectric constant ε_o to be neglected. On another hand at this temperature all the scattering mechanisms will be considered as elastic so that we shall confine ourselves to the relaxation time approximation within the Born approximation, following the work by Zawadzki and Szymanska [62]

(hereafter Z.S.). These authors have obtained very tractable analytical expressions of the relaxation time in small gap semiconductors, which takes the general form

$$\tau(E) = \frac{A_r}{F_r} \frac{dE}{dk} \left(k^2\right)^r \qquad (32)$$

r, F_r and A_r depend on the scattering mechanism : $r = 1, 0,$ or -1 respectively for scattering by charged centers (Coulomb interaction), optical phonons (polar modes), and acoustic phonons. A_r contains parameters which do not depend upon the energy such as elastic constants, optical phonon energy, static and high frequency dielectric constants. More over these parameters will be assumed to be pressure independant.

When $\Delta_o \gg E_g$, F_r depends upon the parameter $L = 1-a^2$ which measures the amount of p component in the wave function. In their work (Z,S) use the expression of a, corresponding to a conduction band stemming from Γ_6 (a_{SC} in Eqs.15). When the conduction band stems from Γ_8 the calculation of $\tau(E)$ is formally the same, so that the work by (Z,S) can be extended to the SM configuration provided that the appropriate expression for the coefficient a, in this configuration, be used : a_{SM} in eqs.15. Consequently, for SM and SC configurations, we have :

$$L_{SM} \equiv 1 - a^2_{SM} = \frac{1+\gamma\zeta}{1+2\gamma\zeta}$$
$$L_{SC} \equiv 1 - a^2_{SC} = \frac{\gamma\zeta}{1+2\gamma\zeta} \qquad (33)$$

at Γ_8 : $a = 0$, $L = 1$; at Γ_6 : $a = 1$, $L = 0$;
for $E_g = 0$, $L = 1/2$

For an arbitrary function A (E) we can define :

$$\langle A \rangle = \int_0^\infty - \frac{\partial f_o}{\partial E} A(E) k^3(E) dE \qquad (34)$$

The electron mobility is then given by :

$$\mu = \left\langle \frac{e\,\tau(E)}{m(E)} \right\rangle \Big/ \langle 1 \rangle$$

with $z = E/k_oT$ and $\gamma = k_oT/|E_g|$, m(z) is given by Eq.30. From Eqs.11 and 12 we may write :

$$\left.\begin{aligned} k^3 &= \frac{2}{\hbar^2} m_n k_o T \,(z + \gamma z^2) \\ \text{and} \quad \frac{dE}{dk} &= \sqrt{2}\,\hbar \left(\frac{k_oT}{m_n}\right)^{\frac{1}{2}} \frac{(z+\gamma z^2)^{\frac{1}{2}}}{(1+2\gamma z)} \end{aligned}\right\} \qquad (35)$$

We are now to summarize the expressions giving the electron mobility for various scattering mechanism according to the formulation of the relaxation time given by Z.S.

Scattering by charged centers.

The charged centers may consist of fixed ionized impurities as well as heavy holes considered as fixed charges because of their heavy mass. Their concentration is then $N_{cc} = N_d + N_A^- + p$, or

$$N_{cc} = n + 2\,N_A^-$$

In the intrinsic regime $n \gg 2N_A^-$, so that only the electron hole scattering is efficient, and $N_{cc} \simeq n$, then depends on pressure according to Eq.16. The mobility, calculated for the screened Coulomb potential induced by these charged centers, is given by :

$$\mu_{cc} = A_{cc} \frac{(k_oT)^{\frac{3}{2}}}{N_{cc}} \left(\frac{m_n}{m_o}\right)^{\frac{1}{2}} \frac{1}{{}^oL_o^{\frac{3}{2}}} \int_o^\infty -\frac{\partial f_o}{\partial z} \frac{1}{F_{cc}} \frac{(z+\gamma z^2)^2}{(1+2\gamma z)^2}\, dz \qquad (36)$$

With

$$A_{cc} = \frac{\varepsilon_o^2 \sqrt{2}}{\pi e^3}\, m_o^{-\frac{1}{2}} \qquad (37)$$

ε_o is the static dielectric constant.

The screening of the Coulomb potential by electrons as well as the symmetry of the conduction band are taken into account in the derivation of F_{cc}, leading to :

$$F_{cc} = \left[\mathrm{Log}(1+\xi) - \frac{\xi}{(1+\xi)}\right] - (4L - L^2) \times \left[1 - \frac{2\,\mathrm{Log}(1+\xi)}{\xi} + \frac{1}{1+\xi}\right] + \frac{3}{2} L^2 \times \frac{\xi - 4}{\xi} \qquad (38)$$

where $\xi = 4k^2R^2$

R is the screening length calculated in the Thomas-Fermi approximation. Taking into account the non parabolicity of the conduction band this parameter is given by [44]

$$R^2 = \frac{\pi \varepsilon_o \hbar^3}{4\sqrt{2}\, e^2 (k_o T)^{\frac{1}{2}}} \frac{m_n^{-\frac{3}{2}}}{{}^{o}L^{\frac{1}{2}}_{1}(\eta, \gamma)}$$

${}^{o}L^{\frac{1}{2}}_{1}$ is defined by Eq.18.

The expression F_{cc} is deduced from that given in Ref.62 neglecting the terms $1/\xi^2$ and assuming $\Delta_0 \gg E_g$. In our case the Fermi energy is always so high that $\xi(E_F) \geqslant 15$. The L parameter is given by Eq.33 and changes its form according to the sign of E_g. In the SC configuration, at the bottom of the conduction band L=0 and $F_{cc} = \mathrm{Log}(1+\xi) - \xi/(1+\xi)$ which gives the classical Brooks-Herring formulation.

Scattering by optical phonons.

The electron mobility is now given by

$$\mu_{OP} = A_{OP} \frac{2(k_o T)^{\frac{1}{2}}}{\hbar \omega_L (2N_L + 1)} \frac{(m_n/m_o)^{-\frac{3}{2}}}{{}^{o}L^{3/2}_{o}} \int_0^{\infty} -\frac{\partial f_o}{\partial z} \frac{1}{F_{OP}} \left(\frac{z + \gamma z^2}{1 + 2\gamma z}\right)^2 dz \qquad (39)$$

with

$$A_{OP} = \frac{\hbar^2}{e\sqrt{2}} \frac{\varepsilon_o \varepsilon_\infty}{\varepsilon_o - \varepsilon_\infty} (m_o)^{-\frac{3}{2}} \qquad (40)$$

In the above expression $N_L = \left[\exp(\hbar\omega_L/k_oT)-1\right]^{-1}$ is the number of longitudinal phonons of energy $\hbar\omega_L$, ε_o and ε_∞ are respectively the static and high frequency dielectric constants which appear in the effective ionic charge according to the definition of Callen[63]. For temperatures such that $k_oT \gg \hbar\omega_L$ the factor $2(koT)^{\frac{1}{2}}/\hbar\omega_L(2N_L + 1)$ is reduced to : $(k_oT)^{-\frac{1}{2}}$. Once again the symmetry of the conduction band and the screening of the polar interaction are taken into account in the factor F_{op}.

$$F_{op} = \left(1 - \frac{2}{\xi}\mathrm{Log}(1+\xi) + \frac{1}{1+\xi}\right) - 2L\left(1 - \frac{4}{\xi}\right) + \frac{3}{2}L^2\left(1 - \frac{10}{3\xi}\right) \qquad (41)$$

The parameter ξ is the same as previously introduced for the screening of the Coulomb interaction. F_{op} is obtained from the expression given by Z.S., neglecting the terms ξ^{-2} and ξ^{-3} and assuming $\Delta_o \gg |E_g|$.

In the SC configuration at Γ_6, $L_{SC} = 0$, so that neglecting the screening, $F_{op} = 1$, and we come back to a classical expression obtained when the electron state is described by a plane wave[64]. In the SM configuration at Γ_8, $L = 1$ so that, neglecting the screening $F = 0.5$. The mobility of an electron at Γ_8, which is described by a plane wave may be half the one calculated with the true wave function.

It must be noticed that the above expression of the mobility, when used for CdHgTe alloys does not take into account a problem specific to these alloys : in pure HgTe and pure CdTe a single LO phonon mode is present with respective energies $\hbar\omega_L$ of 17meV and 21meV at the zone center. However in CdHgTe alloys two LO phonon modes characteristic of those for pure HgTe and pure CdTe are present as shown by infrared measurements[65] and Raman scattering[66]. To our knowledge this feature has not been taken into acccunt in any theoretical work up to now. We shall thus ignore the two mode behaviour in these

alloys. In any case, due to the value of E_F and to the spread out of the Fermi distribution of electrons around E_F, the kinetic energy of the conduction electrons, for the range of alloy compositions presented in this work, may be as high as 100meV at room temperature, which value may be considered large as compared to the energy of L O phonons. Scattering by L O phonons may therefore be considered as quasi elastic, legitimating the use of the relaxation time formulation as a first approximation.

Scattering by acoustic phonons.

Although the longitudinal modes give the main contribution, the transverse modes also contribute to the scattering because of the p component in the wave function. Moreover, since the electron states are not described in the framework of a single band effective mass approximation, the deformation potential approximation may not be used. (Z.S.) have used the deformable ion model. According to the expression of the relaxation time given by these authors the electron mobility is

$$\mu_{AP} = A_{AP}(k_o T)^{\frac{3}{2}} \left(\frac{m_n}{m_o}\right)^{-\frac{5}{2}} \frac{1}{{}^{o}L_{o}^{3/2}} \int_0^{\infty} -\frac{\partial f_o}{\partial \zeta} \frac{1}{F_{AP}} \frac{(\zeta+\gamma\zeta^2)}{(1+2\gamma\zeta)^2} d\zeta \qquad (42)$$

with:

$$A_{AP} = \frac{e\hbar^4\pi}{\sqrt{2}} \frac{C_L}{E_d^2} (m_o)^{-\frac{5}{2}} \qquad (43)$$

When $\Delta_o \gg |E_g|$ the F factor, which includes scattering by longitudinal as well as transverse modes, is given by

$$F_{AP} = (1-1.3L)^2 + 0.124 (C_L/C_T) L^2 \qquad (44)$$

For a Γ_6 conduction band at k=o, L=o and F_{Ap}=1 according to the usual formula [64].

The parameter E_d acts as a deformation potential constant, C_L and C_T are averaged elastic constants, which may be defined as [67]:

$$C_L = \frac{1}{5}\left(3C_{11} + 2C_{12} + 4C_{44}\right)$$
$$C_T = \frac{1}{5}\left(C_{11} - C_{12} + 3C_{44}\right) \qquad (45)$$

The C_{ij} are the elastic constants.

It must be noticed that for the scattering by acoustic phonons, the expression of the relaxation time needs the knowledge of the exact form of the functions labelled S,X,Y,Z, in Sect.II. For the integrals involving the functions we have used the estimated values given by (Z,S) for InSb assuming that the extreme atomic and empty lattice approximations do not lead to any drastic change when going from InSb to CdHgTe alloys.

IV.B.b. Experimental results analysis.

This section is devoted to the mobility analysis in our samples at room temperature in order to answer two questions :

(i) Do the mixing of s and p components in the electron wave function together with the change of symmetry of the conduction band extremum have a significant effect on the electron mobility when going from the SM to the SC configuration?

(ii) Does there exist features allowing the scattering mechanism to be characterized from mobility-pressure measurements, in a way analogous to what was done with power laws of the mobility-temperature variations for classical semiconductors?

Aiming to the first problem we have reported in Figs.17,18,19 the results of some calculations performed within the framework of the above theoretical analysis for E_g values ranging from -150meV to + 100 meV. These calculations have been performed using a computer in order to evaluate the integrals entering the expressions of the mobility.

In Fig.17 we have first considered the electron-hole scattering according to Eq.36. We have reported vs. E_g the quantities $\mu_{cc} \times A_{cc}^{-1} \times N_{cc}$ and $\mu_{cc} \times A_{cc}^{-1}$ with $N_{cc} = n_i$. For each value the Fermi energy in the intrinsic regime was determined by solving the equation 20 assuming that $P_K = 7.9 \times 10^{-8}$ eVcm and $m_p = 0.6 m_o$. In the calculation of the screening length, ε_o was taken equal to 18.5 [68]. The quantities $\mu_{cc} \times A_{cc}^{-1}$ and $\mu_{cc} \times A_{cc}^{-1} \cdot N_{cc}$ have been calculated in two ways : by using the complete expression of F_{cc} given by Eq.38 (curves a and a' respectively), and its simplified expression obtained by taking L = 0 (curves b and b' respectively).

In the same way the results of calculations performed for optical phonon scattering (Eq.39) have been reported in Fig.18. The quantity $\mu_{op} \cdot A_{op}^{-1}$ has been plotted vs. E_g : the curve (a) has been obtained by using the complete expression of F_{op} (Eq.41). The curve (b) corresponds to L = 0 in Eq.41. The curve (a') has been obtained by taking into account the true wave function, but neglecting the screening ($\xi \gg 1$).

The scattering by acoustical phonon has been considered in Fig.19. The quantity $\mu_{AP} \times A_{AP}^{-1}$ (Eq.41) has been plotted vs. E_g using the complete expression of F_{cc} given by Eq.44 (curve a) and its simplified expression with L = 0, F = 1 (curve b). C_L/C_T calculated from Ref.46 according to Eq.45 does not vary by more than three per cent from HgTe to CdTe and was taken equal to 2 at room temperature.

Considering the Figs.17,18,19 we can already draw the following remarks :

(i) using the complete expression of F, i.e. using the true wave function, one finds an electron mobility value higher than the one obtained by using plane waves (L = 0). The ratio of the mobilities calculated in the two ways is 2 for electron-hole scattering, 4 for optical phonons scattering and may reach a value of 5 for acoustical phonons scattering

around $E_g = 0$. This effect is due to the p component of the wave function which produces a reduction in large-angle scattering. This has been widely discussed by Broerman for zero gap materials [55] and by Zawadzki and Szymanska [69] in their analysis of transport phenomena in InSb.

(ii) For electron hole scattering the quantity $\mu_{cc} \times A_{cc}^{-1} \times N_{cc}$ (curves a' and b' in Fig.17) is a monotonically decreasing function of E_g. The decrease of $N_{cc} = n_i$ with E_g leads to a continuous increase of mobility ($\mu_{cc} \times A_{cc}^{-1}$) without any maximum in the vicinity of $E_g = 0$ (curves a and b in Fig.17).

On the contrary both lattice scattering mechanisms may give a maximum of mobility. However, when using the true wave function a maximum of mobility occurs in both cases with SM range for $|E_g| < 10$meV (curves a in Figs.18 and 19). On theother hand the use of plane wave gives a maximum of mobility lying on the SC side for E_g values around 35meV and 70meV for optical and acoustical phonon respectively (curves b in Fig. 18 and 19). According to the value of dE_g/dP obtained at 292°K (Sect .IV A) the maximum of mobility would have been located at a pressure, at least, by 3 kbar higher than the crossover pressure given by the change of slope of n_i (P) (Fig.14). This clearly disagrees with the experimental results which show a maximum of the electron mobility separated by less than 1 kbar from the crossover pressure deduced from the n_i(P) analysis (Fig.8).

We are led to think that the electron-hole scattering is not the dominant scattering process. Consequently in order to account for a maximum of mobility in the vicinity of $E_g = 0$ we must not only consider the effect of the lattice scattering processes, but also take into account the symmetry of the conduction band by using the exact electron wave function.

In order to answer the second question the best way is to calculate the absolute value of the electron mobility for each scattering mechanism. However such a calculation needs the reliable knowledge not only of the parameter P_K

which appears in the expression of m_n vs. E_g (Eq.12) but also of such parameters as ε_o, ε_∞ and E_d. For acoustic phonon scattering m_n appears to the power 5/2 so that P_K appears to the power 5. For optical phonons this power reduces to 3. In both cases a range of P_K values from 7.3 to 8 x 10^{-8}eVcm may lead to significant changes in the calculation. From hydrostatic pressure experiments one obtains the difference between the deformation potentials of the Γ_6 and Γ_8 levels so that E_d is a parameter rather difficult to reach. Within the framework of the random phase approximation ε_o and ε_∞ [70] may behave singularly in the zero gap configuration and the lack of experimental data on this parameters vs. composition makes any quantitative analysis questionable. Even for HgTe the experimental values of ε_o have been obtained at rather low temperatures and according to the analysis of Broerman [71] the component of ε_o due to Γ_8 bands may be temperature-dependent leading to a value of ε_o significantly different at room-temperature. The factor A_{op} would be very sensitive to these changes.

Assuming in a first approximation that E_d may be deduced from dE_g/dP by $E_d = -(dE_g/dP)\beta^{-1}$ in which the bulk modulus β is related to the C_{ij} by $\beta^{-1}=(C_{11}+2C_{12})/3$. we obtain $E_d \simeq 4$eV. The C_{ij} have been taken from Ref.46 and $dEg/dP = 10 \times 10^{-6}$eV bar^{-1}. C_L may be calculated from Ref.46 according to Eq.45 so that from Eq.43 we deduce $A_{cc} = 4 \times 10^4 cm^2\ V^{-1}\ sec^{-1}\ meV^{3/2}$. Such a value of A_{cc} leads to $\mu_{AP} \geqslant 6 \times 10^6\ cm^2V^{-1}\ sec^{-1}$ in the range of E_g values considered in Fig.19. We have reported in Fig.20 a plot of the Hall mobilities measured at room temperature for a set of samples, composition of which extend from 0 to 0.16, among which were selected the samples studied in this work. On the same figure have been reported values taken from other reference [21], [72] .

This plot shows mobilities clustering around 3 x $10^4 cm^2 V^{-1} sec^{-1}$ in complete discrepancy with the order of magnitude

obtained from AP scattering calculation.

With $\varepsilon_o = 18.5$, $\varepsilon_\infty = 13$ [68] we obtain $A_{op} = 230\ cm^2 V^{-1} sec^{-1} meV^{\frac{1}{2}}$ For HgTe ($E_g = -115meV$) from the curve (a) in Fig.18 (which takes into account the screening of the interaction) we can deduce $\mu_{op} = 5.6 \times 10^4 cm^2\ V^{-1} sec^{-1}$. This value reduced to $\mu_{op} = 4 \times 10^4 cm^2 V^{-1}\ sec^{-1}$ when the screening is neglected (Fig.18 cruve a').

For electron hole scattering with $\varepsilon_o = 18.5$ we obtain for HgTe $\mu_{cc} \simeq 7 \times 10^4\ cm^2\ V^{-1}\ sec^{-1}$. The experimental values published for the HgTe electron mobility at room temperature cluster around $3 \times 10^4 cm^2\ V^{-1}\ sec^{-1}$. This absolute value would be accounted for by mixing optical phonon and electron-hole scattering. The lack of reliable experimental values for these materials makes such a detailed quantitative analysis impossible and in order to get rid of the parameters mentioned above we shall only analyse the logarithmic derivative of the mobility vs. E_g through an analysis of $(d \text{ Log } \mu/dP)_{P \to 1bar}$ vs. composition. We have reported in Fig.21 the calculated variations of $\mu^{-1}(d\mu/dE_g)$ vs. E_g for all three scattering processes when the true wave function is taken into account. For both lattice scattering mechanisms this logarithmic derivative is very sensitive to E_g. Not only does it behave very differently according to whether the scattering process is a lattice one or not, but , its value for scattering by acoustic phonons is twice the value for optical phonons. In this latter case $(d \text{ Log } \mu/dE_g)_{1 \text{ bar}}$ appears to be quite insensitive to the screening effect by free carriers. We have reported in Fig.22 the experimental and calculated values of $\mu^{-1}(d\mu/dP)_{P \to 1bar}$ as a function of composition, using, for the calculation, the $E_g(x)$ law given in Fig.6 and $dE_g/dP = 10 \times 10^{-6} eV\ bar^{-1}$. It can be seen that the experimental values agree fairly well with the calculated ones for scattering by optical phonons.

Within the framework of the above analysis, we can conclude that the acoustical phonon scattering is of no major importance at room-temperature over the range of composition studied in this work. The electron scattering gives higher mobilities than the scattering by optical phonons. The first one (electron-hole) does not account for a maximum of μ around $E_g = 0$. The second one (0 P) accounts for the pressure logarithmic variations of the mobility versus composition and thus is apparently the dominant one.

Besides, the close agreement between the experimental and calculated values of $\mu^{-1} (d\mu/dP)_{P \rightarrow 1bar}$ leads to rely upon the law $E_g(x)$ at room-temperature, according to which $E_g = 0$ for $x \simeq 0.07$. The fact that $\mu^{-1} (d\mu/dP)_{P \rightarrow 1bar}$ goes through zero for $x = 0.06$ is in agreement with the maximum of mobility for $-10meV < E_g < 0$ and scattering by optical phonons (Fig.18 and 21). The averaged behaviour of the electron mobility versus composition reported in Fig.20 shows also a flat maximum in the range $0.06 < x < 0.07$.

At 77°K it has not been possible to perform such an analysis of the electron mobility because of the presence of holes for the values of E_g in the vicinity of the crossover. Due to the concentration of ionized acceptors, the maximum of the mobility is not located far from that of R_H so that the Hall mobility $R_H\sigma$ is not a reliable quantity for such an analysis (see Sect.IV A).

V - DISCUSSION AND CONCLUSION.

At 77°K and 292°K Hall effect and Hall mobility analysis, although they do not provide a direct information about the conduction band extremum due to the high value of the Fermi energy, are consistent with the picture of a continuous upwards shift of the Γ_6 level with respect to the Γ_8 one induced either by alloying or by pressure.

For both temperatures, in the SM and SC configurations, the deformation of the band structure due to the variation of the $\Gamma_6 - \Gamma_8$ gap by alloying or pressure is well described within the framework of a k.p. analysis of the Γ_6, Γ_7 and Γ_8 levels which ignores all higher or lower far lying bands.

The k.p. method provides the dispersion relation of the conduction band (Eq.11). This relation does not make any difference whichever be the symmetry of this band. On another hand the k.p method gives the wave function of an electron in the conduction band. This wave function takes into account the Γ_8 or Γ_6 symmetry of the conduction band in the SM and SC configuration respectively. These two results of the k.p method have been checked in this work. Evidence of the first one is illustrated by the analysis of the Hall effect (Sect.IVA) which allows the crossover of the Γ_6 and Γ_8 levels to be illustrated by a change of slope on the plot of the electron concentration versus pressure. This analysis also provided a determination of dE_g/dP by a plot of $n_i^{2/3}$ versus pressure. The second result of the k.p method is illustrated not only by the discussion of the calculated, location of the maximum on $\mu(P)$ which occurs at $E_g \simeq 0$ when the true wave function is used, but also by the analysis of $(d\text{Log}\,\mu/dP)_{P \to o}$ vs. composition (Fig.22) which agrees with scattering by optical phonons although a quantitative analysis of the absolute value of the electron mobility seems unsucessfull using only one kind of scattering. However, a clear evidence of any singular behaviour of the low and high frequency dielectric function remains to be obtained. This is also the case for any incidence of a two mode behaviour of this alloy system upon the electron-optical phonon interaction.

From the Hall effect analysis the composition or pressure induced SM-SC transition appears clearly as a band structure effect. At both temperatures, the pressure induced $\Gamma_6 - \Gamma_8$ crossover is defined within a 0.5 kbar uncertainty range.

It appears thus that E_g values as low as 5meV keep a physical significance, even at room temperature. At this temperature, the blurring effect of the band extrema due to thermal energy ($k_o T \simeq 25$meV) does not smear out the change of slope of the n(P) plot (Figs 14,16). The low pressure range needed for studiying $(d\ Lg/R_H/dP)_{P \to o}$ makes this analysis a valuable tool for determining experimentally the band structure in the SM range at ambient pressure, according to the band structure model used in this work although we are dealing with alloys for which in principle the concept of band structure fails due to disorder effects. To our knowledge there exists no rigorous treatment of the effect of disorder in semiconducting alloys. However, Van Vechten and Bergstresser have given a tentative analysis of this problem in a study of the electronic structure of semiconducting alloys [73]. The problem is treated by the use of an empirical (local) pseudopotential and by a dielectric method of tetrahedrally coordinated semiconductors based on the Phillips's theory of electronegativity. Both methods, based on the virtual crystal approximation together with the assumption of a linear dependance on alloy concentration of the lattice constant and of the involved parameters, give in general a non-linear dependance of the interband gaps on concentration. The non linear behaviour of the law $E_g(x)$ is characterized by a bowing parameter C involving two contributions $C = C_i + C_e$. The first one labelled the intrinsic one C_i comes from the above treatment and the second one C_e, from disorder i.e. from the effects of aperiodicity. Strictly speaking the aperiodic potential due to disorder should cause a tailing of the density-of-states spectrum [74]. However in the above work, according to a lot of experimentals results alloys from III-IV compounds, the effect of disorder is believed to narrow the band-gap without altering the slope of the density of state spectrum. From experiments performed at low temperature vs. pressure on the x = 0.14 sample

we report in Ref.75 (hereafter labelled as II) an abnormal behaviour of the heavy hole concentration in the Γ_8 band, which could speculatively appear as a tailing effect induced by the disorder.

Regarding the bowing of the $E_g(x)$ law at zero or very low temperature, Chadi and Cohen [11] have carried out a calculation of the electronic structure of $Hg_{1-x}Cd_xTe$ alloys near the Γ point using the empirical-pseudopotential method. They obtain a linear variation of E_g with composition with a SM-SC transition occuring at $x = 0.165$ taking for endpoint values of E_g, - 0.3eV and 1,6 eV for HgTe and CdTe respectively. On the experimental side D.Long [76] has made a critical review of the existing published data on E_g vs. x in these alloys . From Refs.4, 13-15, 52,77, he finds that the data between $x = 0$ and $x = 0.40$ define a straight line which extrapolates to $E_g = - 0.280$eV at $x = 0$ and then suggests the possibility of downward bowing when E_g is negative. From optical absorption measurements Scott [15a] on one hand, and from photoconductive and photovoltaic response measurements Schmit and Stelzer [15b] on another hand give empirical expressions relating E_g to x and T for compositions $0.17 < x < 0.60$ and temperatures $20 < T < 300$°K. These authors conclude that the compositional dependance of the energy gap is not linear over the entire range in x with a maximum deviation from the linear approximation never greater than 0.1 eV . Within the above range of compositions they report a linear temperature dependance of the energy-gap, above 77°K.

For compositions ranging from $x = 0$ to $x = 0.14$ very few data have been published concerning the E_g (x, T) law. In the present work from the low field Hall coefficient measurements the E_g (x) relation has been established for $x \leqslant 0.14$ at room and liquid nitrogen temperatures with a maximum uncertainty lower than $\pm$ 10meV. At 77°K all the experimental results fit a linear dependance corresponding to the empirical expression $E_g(meV) = -255 + 1760\ x$, where x is expressed in mole percent. We thus obtain for HgTe

$E_g = -(255 \pm 10)$ meV which agrees with the value : - 266 meV given in Ref.52 from magnetoreflection measurements. At 77°K the crossover composition obtained in the present work is $x_{SM.SC} = (0.145 \pm 0.05)$. Our empirical linear expression cannot account for the value $E_g = 1.60$eV for CdTe at 77°K [25]. On another hand the values extrapolated from the expression given by Scott are - 0.260eV and 0.158 for E_g in HgTe and $x_{SM.SC}$ at 77°K. One obtains —0.210eV and $x_{SM.Sc} = 0.14$ from the work by Schmit and Stelzer so that it appears rather difficult to fit the E_g (x) law by a straight line over the entire x range. At 292°K the E_g(x) relation obtained in this work is no longer linear and exhibits a downward bowing. The E_g value for HgTe is $E_g = -115 \pm 15$meV and the crossover composition $x_{SM-SC} = 0.07 \pm 0.01$.

Our values are significantly different from those given in previous works. Extrapolating the empirical relation given by Schmit and Stelzer yields, at room temperature :

$$x_{SM \rightarrow SC} = 0.08 \text{ and } E_g = 0.100 \text{ eV for HgTe}$$

The $\Gamma_6 - \Gamma_8$ gap for HgTe obtained in the present work is in very close agreement with a determination obtained from thermo reflection measurements in our laboratory [51]. Assuming a linear dependence of E_g on T in the range 77-300°K we have reported in Fig.25 the temperature coefficient of the gap dE_g/dT vs. composition. Such a linear dependance of E_g on T has been found in Refs.15a and 15b for $T > 77$°K and for HgTe in Refs.12 and 56. However our value for HgTe : $(6.5 \pm 0.5) \times 10^{-4}$eV/°K which is in agreement with a value determined by thermoreflection around room temperature [51] is in disagreement with the value 5×10^{-4}eV $(°K)^{-1}$ given in Ref.56. Moreover in the range $0 < x \leqslant 0.14$, the parameter dE_g/dT does not vary linearly vs. composition as observed in the range $0.17 < x < 0.60$ in Refs.15a and 15b. This positive coefficient dE_g/dT observed in $Cd_xHg_{1-x}Te$ alloys up to x = 0.50 is a particular feature of these alloys which can be explained neither by lattice dilatation, nor by the simple treatment proposed by Fan [78].

Recent calculations based on a direct calculation of the band edges using Debye-Waller factors determined either experimentally [79] or by a lattice dynamical calculation [80] have been unsuccessful in obtaining the correct sign for dE_g/dT in HgTe at Γ point so that this interesting question is still open.

An overall agreement between the experimental results and the calculated ones was obtained by fitting the $R_H(P)$ curves over the whole range of pressures, taking into account the laws $E_g(x)$ reported in Figs.5 and 6 together with the following set of band parameters.

$$P_K = (7.6 \pm 0.3) \times 10^{-8} \text{ eVcm}$$

$$m_p = (0.55 \pm 0.1)\, m_o$$

$$(dE_g/dP)_{292°K} = (10 \pm 0.5) \times 10^{-6} \text{ eV bar}^{-1}$$

$$(dE_g/dP)_{77°K} = (9 \pm 0.5) \times 10^{-6} \text{ eV bar}^{-1}$$

According to the discussion presented in Sect.IVA for all samples for which the intrinsic regime prevails, $R_H = -1/en$. At 77°K for the samples $x > 0.09$, R_H was defined according to Eq.26 in which c was obtained from the resolution of $p - n = N_A^- - N_D$. N_A^- was assumed pressure independant. According to the results presented in paper II from low temperature analysis of the Hall effect vs. magnetic field and pressure it appears that N_A^- is pressure dependent due to a variation of the position of the acceptor level with E_g. Furthermore from this same analysis it follows that the electrons which are almost bounded to the acceptor level may take part to the conduction as slow electrons so that the lack of a variable magnetic field did not allow a complete analysis of $R_H(P)$ to be performed at 77°K.

Nevertheless, the maximum of $R_H(P)$ (Fig.2) must be assigned to the contribution of holes to the Hall effect.

In this latter case, Eq.26 shows that the location of the maximum of R_H vs. pressure, and the absolute value of this maximum are by far, more sensitive to $c = n/p$ than to $b = \mu_n / \mu_p$, so long as $b > 80$. (According to the order of magnitude of $\mu_p \simeq 600$ cm^2 V^{-1} Sec^{-1} [43], this condition is always fulfilled at 77°K). The parameter c is obtained through the solution of $N_A^- - N_D = p - n$, leading to a possible estimation of $N_A^- - N_D$. For instance, in the case of the sample x = 0.14, this analysis led us to take $N_A^- - N_D = 10^{16}$cm^{-3}, in agreement with low temperature measurements reported in paper II.

Hall coefficient measured at ambient pressure

We have reported in Figs.23 and 24 the low-field as a function of composition, at 292°K and 77°K respectively. Along with these experimental values, we have reported calculated curves depicting the intrinsic electron concentration : $R_H = - 1/n_i e$. For room temperature, this calculation was carried out on the basis of the $E_g(x)$ relation reported in Fig.6, and the best fit was obtained for the band parameters $P_K = 7.6 \times 10^{-8}$eV cm and $m_p = 0.6 m_o$. For liquid nitrogen temperature, the calculated value of intrinsic concentration n_i appears to be very sensitive to the $E_g(x)$ law. Thus we have reported on Fig.24 two curves corresponding to the following set of parameters : $P_K = 7.9 \times 10^{-8}$eV.cm, $m_p = 0,6\ m_o$ and a linear variation of E_g versus x between the values : $E_g = - 255$meV at x = 0 and $E_g = 0$ at x = 0.145 for the first curve; $PK = 7.9\ 10^{-8}$eV.cm, $m_p = 0.5\ m_o$ and on linear variation of E_g between $E_g = -255$ meV at x = 0 and $E_g = 0$ at x = 0.140 , for the second curve. According to the possible incidence of extrinsic effects on the measured values of R_H, the agreement of these calculations with experimental results is quite satisfactory.

Instead of P_K often appears in the litterature the quantity $E_p = (2m_o/\hbar^2)\ P_K^2$. The value $P_K = (7.6 \pm 0.3) \times 10^{-8}$eV.cm corresponds to $E_p = (15 \pm 1)$ eV. This value may be compared with other experimental values ranging from

13eV to 19eV [49] . It seems difficult to give this parameter an unique value characterizing not only $Cd_xHg_{1-x}Te$ alloys but also the II-VI compounds. Cardona [49e] reported a value of 21eV calculated by taking into account the k.p. interaction with the Γ_{15c} band. This value should characterize the II-VI compounds. However recent HgSe data [81] give $P_K = 7.2 \times 10^{-8}$ eVcm, i.e $E_p = 13.6$eV.

Recent magnetoabsorption measurements performed on HgTe have given $m_n/m_o = 0.031 \pm 0.001$ and $E_g = 302.5 \pm 0.5$meV [81] With $\Delta_o = 1.12$eV [31] , one obtains from the above relation $P_K = 7.6 \times 10^{-8}$ eVcm.

Thus, it does not seem possible to quote a value of E_p characteristic of the II-VI compounds. Regarding the value of $(0.55 \pm 0.1)\ m_o$ obtained in this work for the density of state effective mass of the heavy hole band, this value is located within the range of commonly published values [9, 22, 48, 83] . However from interband magnetoreflection on $Hg_{0.84}Cd_{0.16}Te$, Groves et al. [13] assign to m_p a value within the limits $(0.28 \pm 0.1)m_o$.

The previous published values of dEg/dP for $Cd_xHg_{1-x}Te$ range from 7 to 14 x 10^{-6} eV bar $^{-1}$ [5, 12, 16, 23] and were obtained at $T > 77°K$ from electrical measurements on homogeneous samples or p-n junctions. This wide range was reduced to (9-11) x 10^{-6} eV bar^{-1} by analysing measurements of Hall effect for various compositions in the temperature range $77 < T < 300°K$ [17, 22] . The analysis given in the present work supports a dependance of dE_g/dP on temperature for the range of compositions $0 < x \leqslant 0.14$ studied here. dE_g/dP is (10 ± 0.5) and $(9 \pm 0.5) \times 10^{-6}$ eV bar^{-1} respectively at 292 and 77°K. From the analysis of the shift of the 0^+ quantum oscillation induced by pressure on a HgTe samples a pressure coefficient $dE_g/dP = (8.5 \pm 0.5) \times 10^{-6}$ eV bar^{-1}

was determined at 4.2°K and 1.7°K.

According to the value $(8.2 \pm 0.1) \times 10^{-6}$ eV bar^{-1} given for CdTe [84] at 77°K it may be thought that this parameter does not significantly depend on composition at least at low-temperature. For CdTe, a value of $(8.3 \pm 0.5) \times 10^{-6}$ eV bar^{-1} at 297°K is reported in ref. 84.

This parameter has been theoretically calculated for various materials using band structure calculation methods. Taking advantage of the similarity in the general shape of the pseudopotential form factors for different materials Melz [85] has demonstrated a rule followed to within ± 20 per cent by the experimental data examined. This rule states that the pressure variation of the energy difference between two energy levels may be written :

$$\frac{dE_g}{dP} = -\frac{1}{a^2} D\beta$$

In this expression, $\beta = 3/(C_{11} + 2C_{12})$ is the bulk modulus, a is the lattice constant, and D is a constant depending on the symmetry of the two levels involved (D is related to the band gap deformation potential E_d through : $D = a^2 Ed$).

From HgTe to CdTe, a varies by less than 1 percent [25]. β may be calculated from Ref.46 and at 77°K is higher in CdTe by 5 percent. According to the rule stated above dE_g/dP is not expected to vary by more than 5 percent from HgTe to CdTe.

The above remark suggests an examination of the core effect on the bandgap due to the Cd → Hg substitution. One may write in a crude manner

$$\Delta E_g^{total}(Cd \rightarrow Hg) = \Delta E_g^{core}(Cd \rightarrow Hg) + \Delta E_g^{volume}$$

According to the experimental values reported above :

$\Delta E_g^{volume} = Ed \cdot \Delta V/V = 40$ meV and

$\Delta E_g^{total} = -1,91$ eV

leading to $\Delta E_g^{core} = -1,95$eV, which is in good agreement with the relativitic shifts calculated in section II A.

The 10 percent variation of dE_g/dP from 292°K to 77°K found in this Hg rich range of composition could be accounted for by the variations of the elastic constants with temperature reported in Ref.46 which lead to a decrease of β by 10 percent from 292°K to 77°K, for HgTe.

For CdTe the decrease of β with temperature is only 5 percent . The same amount of variation does not appear clearly on the dE_g/dP values reported in Ref.84 at 77°K and 292°K. However this above discussion neglects the possible temperature variations of the constant D and should be only considered as tentative.

Using the theory of the chemical bond, D.L.Camphausen et al. [86] have calculated the pressure coefficient of interband energy differences for nineteen group IV, group III-V and group II-VI semiconductors. For the $\Gamma_6 - \Gamma_8$ interband energy, they obtained a pressure coefficient $dE_g/dP = 8 \times 10^{-6}$ eV/bar in CdTe in good agreement with the experimental value. For HgTe, they obtained 12×10^{-6} eV/bar, which disagrees not only with the value determined in this paper but also with recently reported experimental results [5] determined at higher temperatures. The calculations reported in Ref. 86 corroborate a value around 12×10^{-6} eV bar^{-1} which was empirically considered as a characteristic feature of the $\Gamma_6 - \Gamma_8$ pair of states for the members of the Germanium family. However, the calculated values of this parameter, as well as the available experimental ones cluster around 8×10^{-6} eV bar^{-1} for the following II-VI zinc-blende coumpounds : ZnTe, ZnS, ZnSe, CdTe. For the mercury chalcogenides, (HgTe, HgSe, HgS) the calculated values cluster around 12×10^{-6} eV bar^{-1}. No experimental data are reported in Ref.85 for HgSe and HgS, so that any further discussion is difficult. However, we must notice that a value of 8.5×10^{-6} eV bar^{-1} for HgTe is in agreement with the values obtained for the other zinc-blende II-VI compounds.

Acknowledgements :

The constant interest of Dr.M.Rodot for this work has been gratefully appreciated. We are indebted to H.Rodot and C.Finck for the crystals used in the present study. We wish to thank our colleagues at CNRS Bellevue for many discussions.

REFERENCES

1 - E.O.KANE, J.Phys.Chem.Sol.,1,249(I957) ; E.O.KANE, "The k.p Method", in Semiconductors and Semi-metals," Vol.1, Willardson and Beer ed., (Academic Press, New York, I966) pp.75-100.

2 - S.H.GROVES, W.PAUL, Phys.Rev.Lett.,11,505(I963) ; S.H.GROVES, W.PAUL, Proceedings of the Int.Conf.on the Phys.of Semicond.,Paris, I964 (Dunod, Paris I964)p.41.

3 - W.D.LAWSON, S.NIELSEN, E.H.PUTLEY, A.S.YOUNG, J.Phys. Chem.Solids 9, 325 (I959).

4 - A.J. STRAUSS, T.C.HARMAN, J.G.MAVROIDES, D.H.DICKEY, M.S.DRESSELHAUS, Proceedings of the Int.Conf.on the Phys. of Semicond., Exeter, I962, (The Institute of Physics and the Physical Society, London 1962)p.703.

5 - M.LALLEMAND, G.WEILL, A.LACAM, M.RODOT, Comptes Rendus 260,4469 (I965); G.WEILL, C.VERIE, Comptes Rendus 263, 463(I966).

6 - C.VERIE, .Phys.Stat.Sol.17,889(I966).

7 - C.VERIE, Proceedings of the Int.Conf.on the II-VI compounds, Providence, 1967, D.G.Thomas ed.(Benjamin New York 1967) p.1124.

8 - a) L.SOSNOWSKI, R.R.GALAZKA, Proceedings of the Int. Conf. on the II-VI Semicond.Compounds, Providence, 1967, D.G.Thomas ed. (Benjamin, New York 1967) p.888;
b) C.VERIE, ibid., p.1461.

9 - J.D.WILEY, R.N.DEXTER, Phys.Rev.181,1181(I969).

10 - E.M.ALIEV, S.A.ALIEV, T.G.GADZHIEV, M.I.ALIEV, Phys. Status Solidi 40,K41(I970).

11 - D.J.CHADI, M.L.COHEN, Phys.Rev. B 7,692(I973).

12 - R.PIOTRZKOWZKI, S.POROWSKI, Proceedings of the Int.Conf. on the II-VI Semicond.Compounds, Providence, 1967, D.G.Thomas ed.(Benjamin, New York 1967)p.1090.

13 - S.H.GROVES, T.C.HARMAN, C.R.PIDGEON, Solid State Commun. 9, 451 (I971).

14 - W.D.SAUR, Infrared Phys. 8, 255(I968).

15 - a) M.W.SCOTT, J.Appl.Phys.40,4077(I969).
b) J.L.SCHMIDT, E.L.STELZER, J.Appl.Phys.40,4865(I969).
c) G.A.ANTCLIFFE, Phys.Rev.B2,345(I970).
d) R.A.REYNOLDS, M.J.BRAU, H.KRAUS, R.T.BATE, Proceedings of the Conf.on the Phys.of Semimetals and narrow-gap semiconductors, Dallas 1970, Carter and Bote ed. (Pergamon Press, New York, 1971)p.511.

16 - C.VERIE, G.MARTINEZ, Comptes Rendus, 266,720 (I968).

17 - S.OTMEZGUINE, F.RAYMOND, G.WEILL, C.VERIE, Proceedings of the Tenth International Conf.on the Phys. of Semicond., Cambridge 1970, Keller Hensel, Stern ed. (I.S.A.E.C.1970)p536

18 - G.WEILL, S.OTMEZGUINE, C.VERIE, Communication presented at the meeting of the European High pressure research group UMEA, Sweden 1971 (unpublished).

19 - C.T.ELLIOTT, J.MELNGAILIS, T.C.HARMAN, J.A.KAFALAS, W.R.KERNAN, Sol.Stat.Research Report, Lincoln Lab., M.I.T.(1971 : 1), p.31 and Bull.Amer.Phys.Soc.,16,401

(1971). We are indebted to these authors for sending us the next of their speech delivered at the A.P.S. meeting.

20 - J.STANKIEWICZ, W.GIRIAT, A.BIENENSTOCK, Phys.Rev. B 4, 4465 (I971).

21 - J.STANKIEWICZ, W.GIRIAT, Phys.Status Solidi(b) 48, 467 (I971).

22 - J.STANKIEWICZ, W.GIRIAT, Phys.Status Solidi(b) 49, 387 (I972).

23 - C.T.ELLIOTT, J.MELNGAILIS, T.C.HARMAN, J.A.KAFALAS, W.C.KERNAN, Phys.Rev.B 5,2985 (I972).

24 - See for instance review appers of :
a) M.RODOT, Proceedings of the Int.Conf.on the Phys. of Semicond., Moscow 1968, Acad. of Sc. of USSR ed. (Moscow 1968) p.639.
b) L.SOSNOWSKI, ibid.,p.700.

25 - D.LONG, J.L.SCHMIDT, in Semiconductors and Semimetals, Vol.5, Willardson and Beer ed.(Academic Press New York I970), p.175.

26 - C.VERIE, Festkorper probleme X Advances in Solid State Physics, edited by O.Madelung, (Pergamon Vieweg, Braunshweig 1970) p.1 and references therein.

27 - C.VERIE, New Developments in Semiconductors, Edited by P.R.Wallace, R.Harris, M.J.Zuckermann, (Noordhoff International, Leyden, 1973)p.511 and references therein.

28 - F.HERMAN, Proc.Int.Conf.Phys.Semicond., Paris I964(Dunod, Paris) p.3.

29 - F.HERMAN, C.D.KUGLIN, K.F.CUFF, R.L.CORTUM, Phys.Rev. Lett. 11,541 (I963).

30 - R.BRAUNSTEIN, E.O.KANE, J.Phys.Chem.Solids 23, 1432 (1962).

31 - M.CARDONA, Modulation Spectroscopy, Solid State Phys. Suppl.11, (Academic Press, New York, 1969).

32 - W.J.SCOULER, G.B.WRIGHT, Phys.Rev.133, A.736(I964).

33 - R.H.PARMENTER, Phys.Rev.100,573 (I955).

34 - G.DRESSELHAUS, Phys.Rev.100,580 (I955).

35 - R.R.GALAZKA, Phys.Rev.Lett. 32A,101 (1970).

36 - H.OVERHOF, Phys.Status Solidi(b) 43,221 (1971).

37 - G.WEILL,Revue Phys.Appl. 2,197 (1967).

38 - B.L.GEIMONT, M.I.DYAKONOV, Zh.Eksp.Teor.Fiz.62, 713 (1972) [Sov.Phys.JETP 35, 377 (1972)].

39 - V.I.IVANOV-OMSKII, B.T.KOLOMIETS, V.K.OGORODNIKOV, K.P.SMEKALOVA, Fiz.Tekh.Poluprov.1,289(I967). [Sov.Phys.Semicond. 1,232 (1967)].

40 - B.L.GEIMONT, M.I.DYAKONOV, V.I.IVANOV-OMSKII, B.T.KOLOMIETS, V.K.OGORODNIKOV, K.P.SMEKALOVA, Proceddeings of the 11th International Conference on the Physics of Semiconductors, edited by PWN-Polish Scientific Publishers (Warsaw, Poland, 1972), Vol.2 p.938.

41 - C.FINCK, S.OTMEZGUINE, G.WEILL, C.VERIE, in Ref.40, p.944.

42 - See for instance C.C.Y.KWAN, J.BASINSKI, J.C.WOLLEY, Phys.Status Solidi(b) 48,699-1971).

43 - See for instance Ref.15 d above and in the same Proceedings.
G.A.ANTCLIFFE, R.T.BATE, R.A.REYNOLDS, p.499.
B.ANCKER-JOHNSON, C.L.DICK, p.523.

44 - J.KOLODZIEJCZAK, Acta Phys.Pol.,20,289(1961).

45 - F.HERMAN, C.D.KUGLIN, K.F.KUFF, R.L.KORTUM, in Quantum Theory of Atoms, Molecular and the Solid State, edited by P.O.Löwdin (Academic Press New-York, 1966) p.381.

46 - Yu.Kh.VEKILOV, A.P.RUSAKOV, Fiz.Teverd.Tela 13, 1157 (1971) [Sov.Phys.Solid State 13, 956 (1971)] ; A.P.RUSAKOV, Fiz.Tverd.Tela 13,623 (1971) [Sov.Phys. Solid State 13, 510 (1971)] .

47 - M.I.DAUNOV, E.L.BROYDA, Phys.Status Solidi(b), 55, K155 (I973).

48 - a) V.I.IVANOV-OMSKII, F.P.KESAMANLY, B.T.KOLOMIETS, A.Sh.MEKHTIEV, V.A.SKRIPKIN, Phys.Status Solidi, 27, K169 (1968).
b) V.I.IVANOV-OMSKII, B.T.KOLOMIETS, A.A.MAL'KOVA, YU.F.MARKOV, A.Sh.MEKHTIEV, Fiz.Tekh.Poluprov., 2, 1340 (1968) [Sov.Phys.Semicond.2, 1122 (1969)] .
c) R.R.GALAZKA, T.ZAKRZEWSKI, Phys.Status Solidi 23, K39 (1967).

49 - a) C.VERIE, E.DECAMPS, Phys.Status Solidi 9, 797 (1965).
b) R.A.STRADLING, Proc.Phys.Soc. London 90, 175(1967) and references therein.
c) G.A.ANTCLIFFE, Phys.Rev. B2, 345 (1970) and references therein.
d) B.D.Mc COMBE, R.J.WAGNER, G.A.PRINZ, Solid State Comm.8, 1687 (1970) and references therein.
e) M.CARDONA, J.Phys.Chem.Solids 24,1543 (1963).

50 - S.NARITA, M.EGAWA, K.SUIZU, M.KATAYAMA, S.MIZUKAMI, Appl.Phys. 2, 151 (1973).

51 - F.RAYMOND, C.VERIE, Surface Sci.37,515(1973).

52 - S.H.GROVES, R.N.BROWN, C.R.PIDGEON, Phys.Rev.161, 779, (1967).

53 - H.EHRENREICH, J.Phys.Chem.Solids 2,131 (1957); J.Phys.Chem.Solids, 9, 129 (1959).

54 - D.MATZ, Phys.Rev.168, 843 (1968); L.L.KORENBLIT, V.E.SHERSTOBITOV, Fiz.Tekh.Puloprov.2, 675 (1968), [Sov.Phys.Semicond.2, 564 (1968)].

55 - J.G.BROERMAN, Phys.Rev.183, 754 (1969).

56 - L.LIU, D.BRUST, Phys.Rev.Lett. 20, 651 (1968); Phys.Rev.173, 777 (1968).

57 - L.LIU, E.TOSATTI, Phys.Rev.Lett. 23, 772(1969); Phys.Rev. B2, 1926 (1970).

58 - J.G.BROERMAN, Phys.Rev.B 2,1818 (1970).

59 - B.L.GELMONT , V.I.IVAŃOV-OMSKII, B.T.KOLOMIETS, V.K.OGORODNIKOV, K.P.SMEKALOVA, Fiz.Tekh.Poluprov. 5, 228 (1971) [Sov.Phys.Semicond.5, 266 (1971)].

60 - D.L.RODE, Phys.Rev.B 2, 1012 (1970); Phys.Rev. B 2, 4036 (1970); Phys.Rev. B 3, 3287 (1971).

61 - D.L.RODE, J.D.WILEY, Phys.Status Solidi (b) 56, 699 (1973).

62 - W.ZAWADZKI, W.SZYMANSKA, Phys.Status Solidi (b), 45, 415 (1971).

63 - H.B.CALLEN, Phys.Rev.76, 1394 (1949).

64 - J.KOLODZIEJCZAK, Phys.Status Solidi 19, 231 (1967).

65 - D.L.CARTER, M.A.KINCH, D.D.BUSS, in Ref.15d, p.273.

66 - A.MOORADIAN, T.C.HARMAN, in Ref.15d, p.297.

67 - J.ZOOK, Phys.Rev.136, A.869 (1964).

68 - See for instance :
a) V.I.IVANOV-OMSKII, B.T.KOLOMIETS, A.A.MAL'KOVA, YU.F.MARKOV, A.Sh.MEKHTIEV, Fiz.Tekh.Poluprov.4, 417 (1970) [Sov.Phys.Semicond.4, 352 (1970)].
b) L.SNIADOWER, Phys.Status Solidi 25, 233 (1968).
c) D.H.DICKEY, J.G.MAVROIDES, Solid State Comm. 2, 213 (1964).

69 - W.ZAWADZKI, W.SZYMANSKA, J.Phys.Chem.Solids, 32, 1151 (1971).

70 - D.SHERRINGTON, W.KOHN, Phys.Rev.Lett.21, 153 (1963).

71 - J.G.BROERMAN, Phys.Rev.Lett. 25,1658 (1970).

72 - W.SCOTT, J.Appl.Phys.43, 1055 (1972).

73 - J.A.VAN VECHTEN, T.K.BERGSTRESSER, Phys.Rev. B1,3351(1970).

74 - R.H.PARMENTER, Phys.Rev.97,587(1955).

75 - S.OTMEZGUINE, A.MAUGER, C.VERIE. (Submitted for publication)

76 - D.LONG, private communication.

77 - a) M.A.KINCH, D.D.BUSS, in Ref.15d , p.46 .
b) B.D.Mc COMBE, R.J.WAGNER, G.A.PRINZ, Phys.Rev.Lett. 25, 87 (1970).

78 - H.Y.FAN, Phys.Rev.82, 908 (1951).

79 - C.S.GUENZER, A.BIENENSTOCK, Phys.Rev.Lett. , 34A, 172 (1971).

80 - Y.F.TSAY, S.S.MITRA, J.F.VETELINO, J.Phys.Chem.Solids, 34, 2167 (1973).

81 - D.G.SEILER, R.R.GALAZKA, W.M.BECKER, Phys.Rev.B 3, 4274 (1971).

82 - Y.GULDNER, C.RIGAUX,A.MYCIELSKI, M.GRYNBERG, Phys.Rev., B 8, 3875 (1973) and references therein.

83 - A.MAUGER, Thèse 3e cycle, Paris 1974.

84 - P.J.MELZ, I.B.ORTENBERGER, Phys.Rev.B 3, 3257(1971).

85 - P.J.MELZ, J.Phys.Chem.Solids 28, 1441 (1967).

86 - D.L.CAMPHAUSEN, G.A.NEVILLE CONNELL, W.PAUL, Phys.Rev.Lett.26, 184 (1971).

FIGURE CAPTIONS

Figure 1 : Simplified band scheme of CdHgTe alloys vs. composition or pressure near the Γ point, when going from SM (a) to SC (c) configuration; (b) : SM-SC transition.

Figure 2 : Relative variations of the low field Hall coefficient measured as a function of pressure for samples of various compositions, illustrating the extrinsic p-type behaviour at 77°K.

Figure 3 : Logarithmic pressure derivative of the low field Hall coefficient as a function of composition at 77°K. The rectangles are the experimental values. The solid line curve has been calculated with $P_K = 7.9 \times 10^{-8}$ eV.cm, $m_p = 0.6 m_o$, $dE_g/dP = 9 \times 10^{-6}$ eV bar^{-1} and the law $E_g(x)$ reported in Fig.5.

Figure 4 : Logarithmic pressure derivative of the low field Hall coefficient as a function of composition at 292°K. Rectangles correspond to the experimental values. The solid line curve has been calculated with $P_K = 7.9 \times 10^{-8}$ eV cm, $m_p = 0.6\ m_o$, $dE_g/dP = 10 \times 10^{-6}$ eV bar^{-1}, and the law $E_g(x)$ reported in Fig.6.

Figure 5 : Dependance of E_g on composition in $Cd_xHg_{1-x}Te$ at 77°K. The experimental values have been deduced from the fit obtained in Fig.3 and from the determination of the crossover pressure. (see text : Sect.IV A).

Figure 6 : Dependance of E_g on composition in $Cd_xHg_{1-x}Te$ at 292°K. The experimental values have been deduced from the fit obtained in Fig.4 and from the determination of the crossover pressure. (see text : Sect.IVA).

Figure 7 : Relative variations of the low field Hall mobility as a function of pressure at 77°K for various values of composition.

Figure 8 : Relative variations of the low field Hall mobility as a function of pressure at 292°K for various values of composition.

Figure 9 : Relative variations of the low field Hall coefficient measured at room temperature as a function of pressure for various values of compositions.

Figure 10 : Calculated values of the intrinsic reduced Fermi level as a function of the $\Gamma_6 - \Gamma_8$ energy difference for two sets of parameters P_K and m_p, at 77°K and 292°K.

Figure 11 : Plot of the 2/3 power of the measured electron concentration : $n = -1/eR_H$ vs. pressure at 77°K for some samples, illustrating the linear behaviour of this quantity. (arrows refer to the scale to be read).

Figure 12 : Plot of the 2/3 power of the measured electron concentration $n = -1/e\ R_H$ vs. pressure at 292°K illustrating the linear behaviour of this quantity.

Figure 13 : Computed values of the 2/3 power of the intrinsic electron concentration as a function of the $\Gamma_6 - \Gamma_8$ energy difference in the SM configuration. Computation is carried out from the k.p. theory, using the parameters reported in the insert. The slope of this curve has to be compared to the slope of the experimental curves reported in Fig.11, in order to determine dE_g/dP.

Figure 14 : Plot of the measured electron concentration vs. pressure showing a slope change corresponding to the SM.SC transition for two samples at room temperature. (Arrows indicate the transition pressure which occurs at 2.35 and 5.5 kbar respectively).

Figure 15 : Computed variations of the intrinsic concentration n_i vs. E_g at 292°K, assuming $P_K = 7.9 \times 10^{-8}$ eV cm and $m_p = 0.6\ m_o$.

Figure 16 : Illustration of the SM-SC transition by a slope change of the experimental plot of the reciprocal low field coefficient, at 77°K. Arrows indicate the transition.

Figure 17 : Computed variations of the electron mobility for electron-hole scattering , at room temperature, on both sides of the SM-SC transition according to Eq.36, in Sect.IVB. Curves a' and b' (right scale) correspond to the quantity $\mu_{cc} \times N_{cc} \times A_{cc}^{-1}$ when respectively true wave-functions and plane waves are used. Curves a and b (left scale) correspond to the quantity $\mu_{cc} \times A_{cc}^{-1}$ when respectively true wavefunctions and plane waves are used.

Figure 18 : Computed variations of the electron mobility for optical phonon scattering (polar modes) at room temperature, on both sides of the SM-SC transition, according to Eq.39 in Sect.IVB. The quantity $\mu_{OP} \times A_{OP}^{-1}$ has been plotted as a function of E_g using plane waves (curve b) and true wavefunctions (a and a') taking into account or not the screening by free carriers (curves a and a' respectively). Arrows locate the maximum of mobility.

Figure 19 : Computed variations of the electron mobility for acoustic phonon scattering at room temperature on both sides of the SM-SC transition, according to Eq. 41 in Sect.IV B. The quantity $\mu_{AP} \times A_{AP}^{-1}$ has been plotted as a function of E_g using plane waves (b) and true wavefunctions (a). Arrows indicate the location of the maximum of mobility.

Figure 20 : Experimental values of the low field Hall mobility vs. composition at room temperature. Circles correspond to our measurements. Rectangles are taken from Ref.21, the triangle is taken from Ref.72.

Figure 21 : Computed variations of the logarithmic E_g - derivative of the electron mobility as a function of E_g at room temperature on both sides of the SM-SC transition : 1 - electron-hole scattering; 2 - Acoustic phonon scattering; 3 - Optical phonon scattering (polar modes). In all three cases the true electron wavefunction has been used in the calculation.

Figure 22 : Logarithmic pressure derivative of the electron mobility as a function of composition at room temperature. The crosses and the full circle correspond to the experimental determination. Curves 1 and 2 are calculated for optical and acoustic phonon scattering respectively with $dE_g/dP = 10 \times 10^{-6}$ eV bar^{-1} and the law $E_g(x)$ reported in Fig.6.

Figure 23 : Room temperature low field Hall coefficient as a function of x. Rectangles correspond to experimental data. The solid line curve has been calculated for intrinsic conduction with $P_K = 7.6 \times 10^{-8}$ eV cm, $m_p = 0.6\ m_o$ and the law $E_g(x)$ reported in Fig.6.

Figure 24 : Liquid nitrogen temperature low field Hall coefficient as a function of x. Rectangles and the full circle correspond to experimental data. Curve labelled 1 has been calculated with $P_K = 7.9 \times 10^{-8}$ eV cm, $m_p = 0.6 m_o$ and a law $E_g(x)$ linear between $E_g\ (x = 0) = -255$ meV and $E_g\ (x = 0.145) = 0$. Curve labelled 2 has been calculated with $P_K = 7.9 \times 10^{-8}$ eV cm, $m_p = 0.5\ m_o$ and a law $E_g(x)$ linear between $E_g\ (x = 0) = -255$ meV and $E_g(x = 0.140) = 0$.

Figure 25 : Temperature coefficient of the $\Gamma_6 - \Gamma_8$ energy difference in $Cd_xHg_{1-x}Te$ as a function of composition : x, between 292 and 77°K, assuming a linear dependance of E_g on temperature.

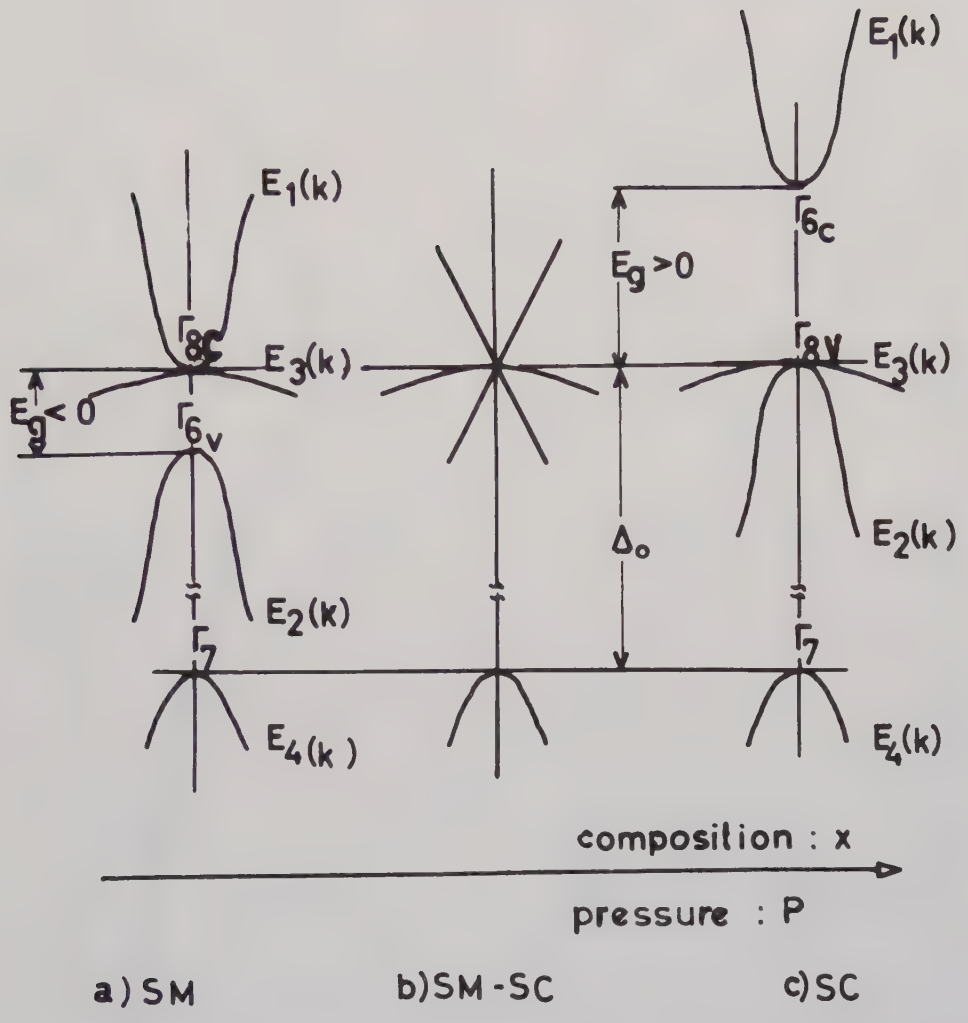
E1(k)
Γ6c
Eg>0
Γ8c
E3(k)
Γ8v
E3(k)
Eg<0
Γ6v
E2(k)
Δo
E2(k)
Γ7
Γ7
E4(k)
E4(k)
composition : x
pressure : P
a) SM
b) SM-SC
c) SC

Fig. 1

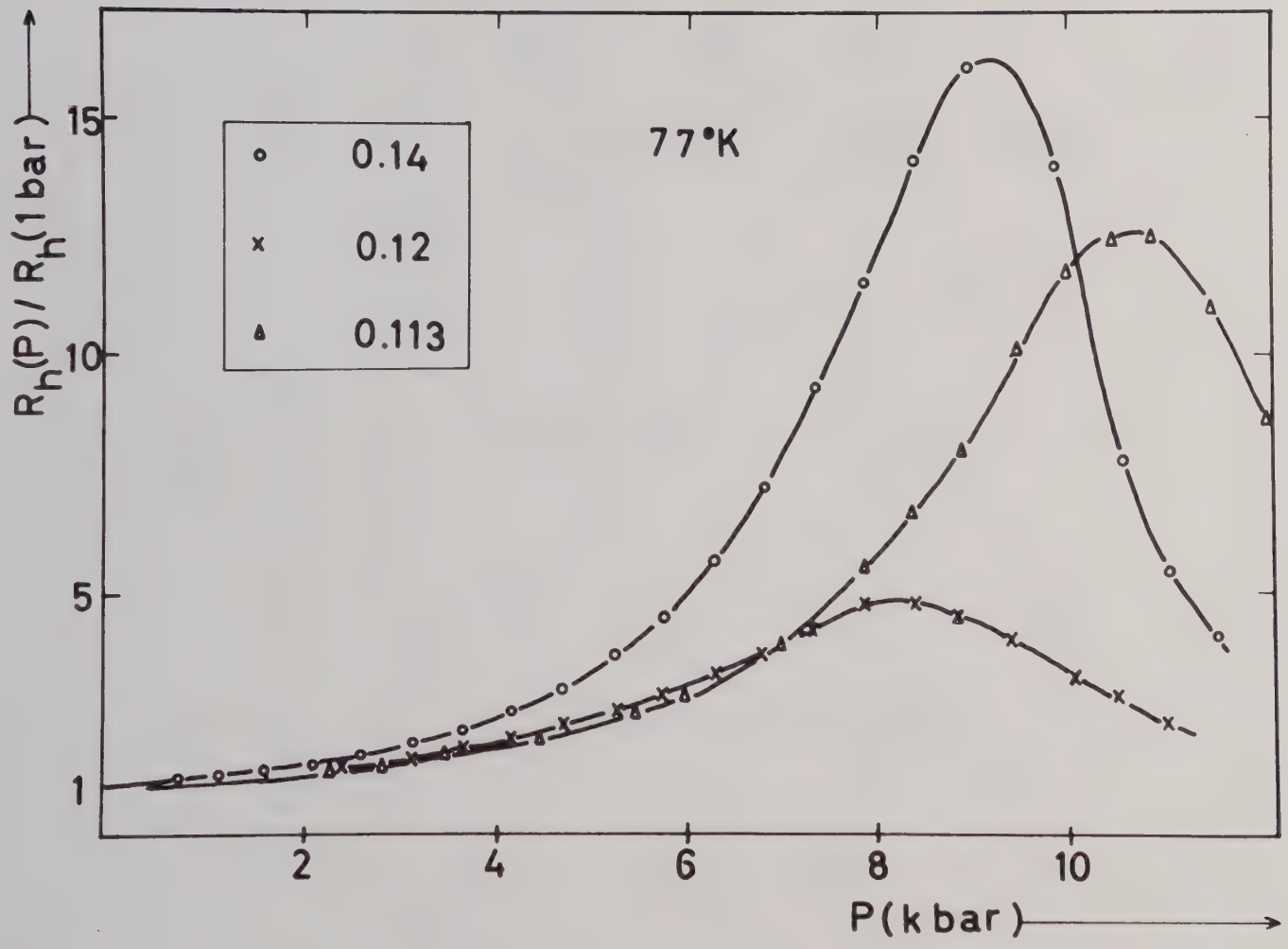

Fig. 2

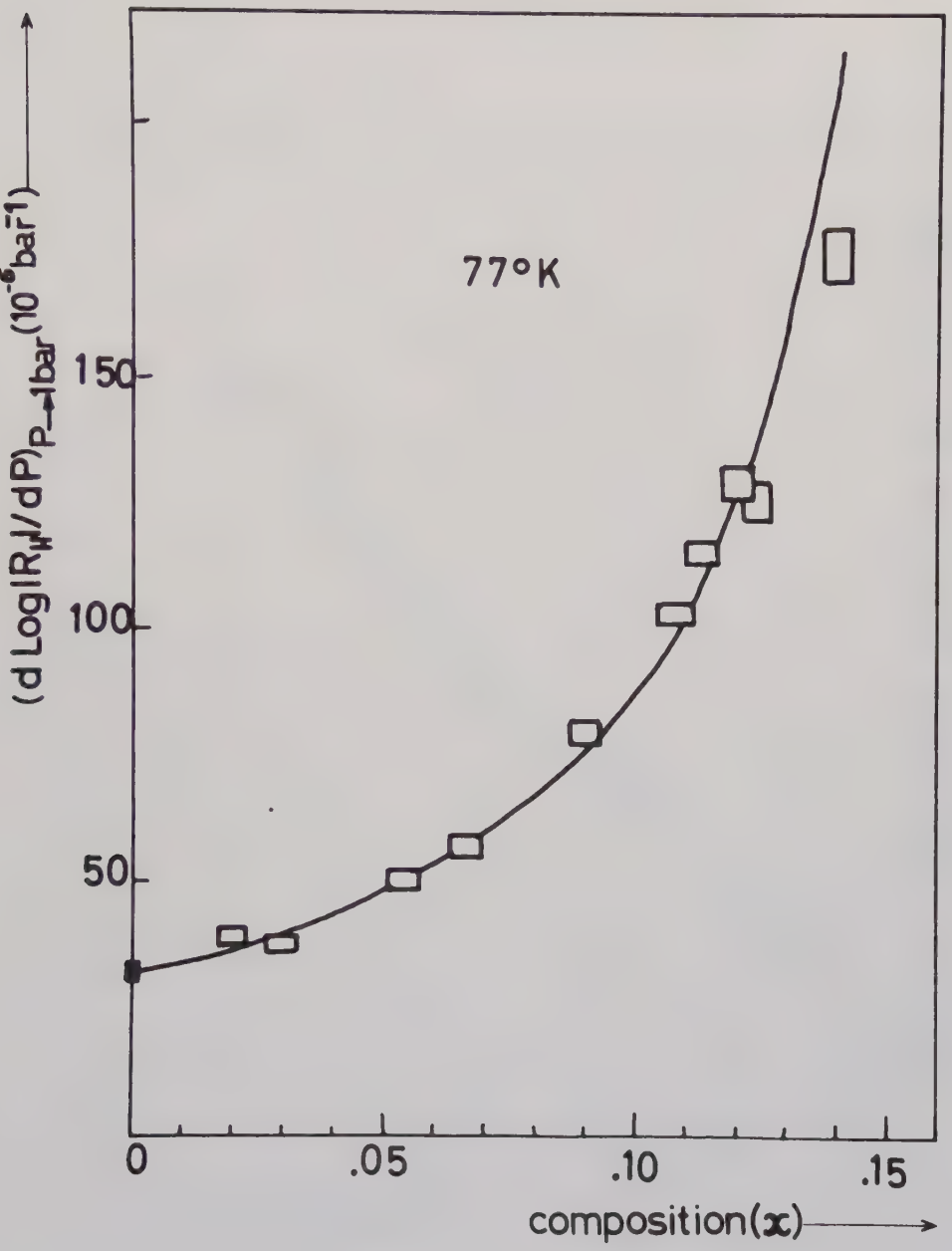
77°K
150
100
50
0
.05
.10
.15
composition(x)
(d Log|R_H|/dP)_{P→1bar}(10^-6 bar^-1)

Fig. 3

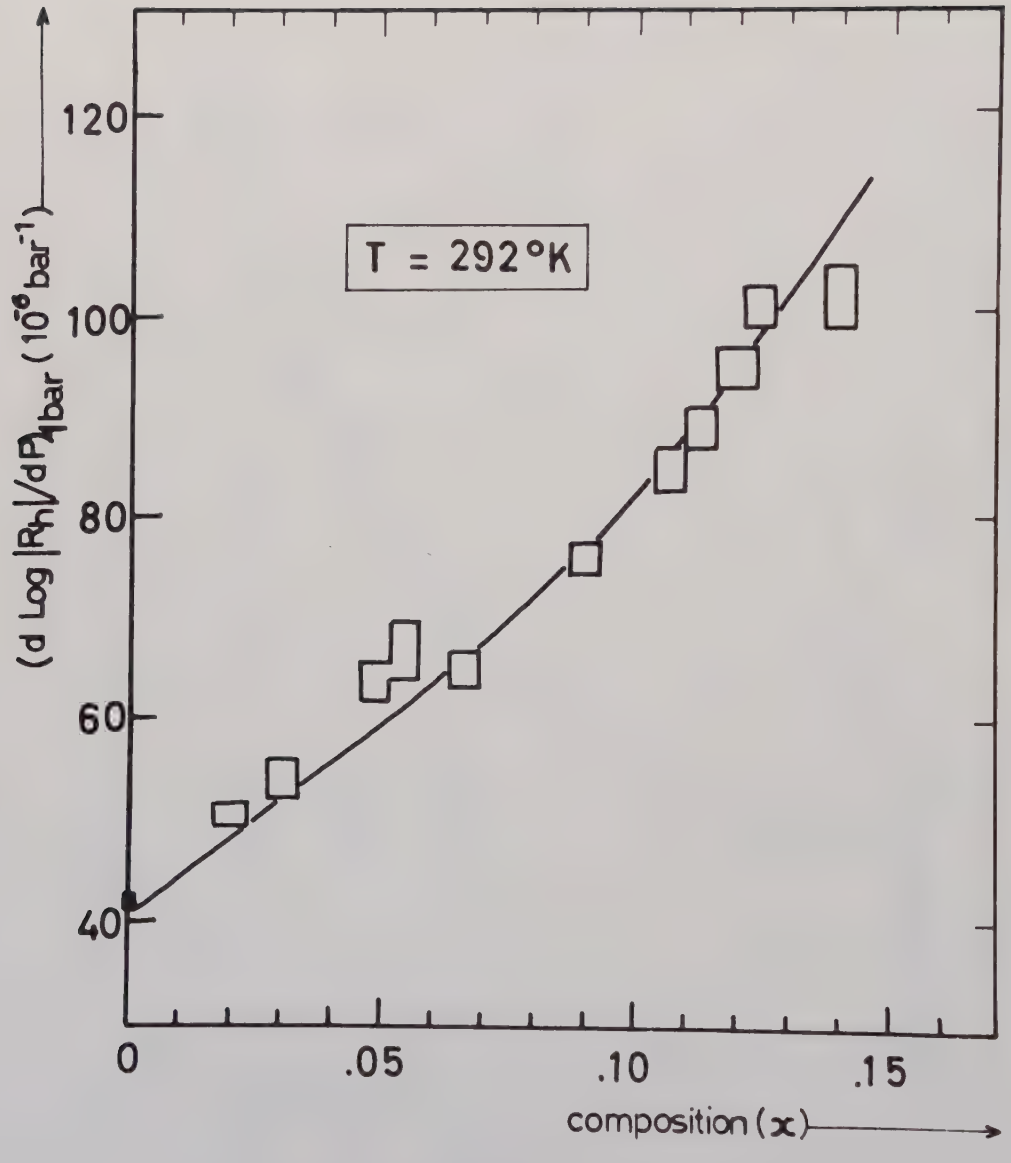
T = 292°K
120
100
80
60
40
0
.05
.10
.15
composition (x)
(d Log |Rh|/dP)1bar (10⁻⁶ bar⁻¹)

Fig. 4

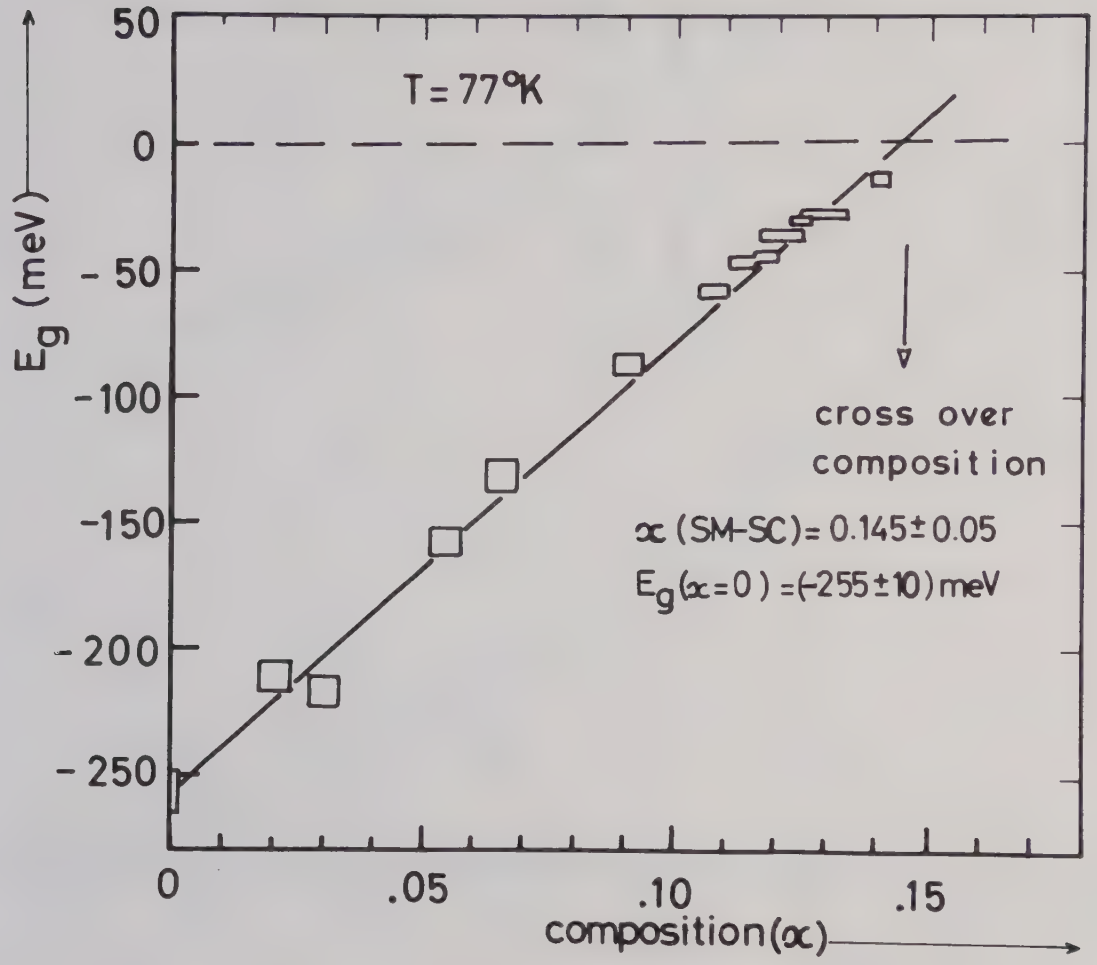
T = 77°K
50
0
- 50
-100
-150
- 200
- 250
E_g (meV)
0
.05
.10
.15
composition (x)
cross over
composition
x (SM-SC) = 0.145 ± 0.05
E_g(x=0) = (-255 ± 10) meV

Fig. 5

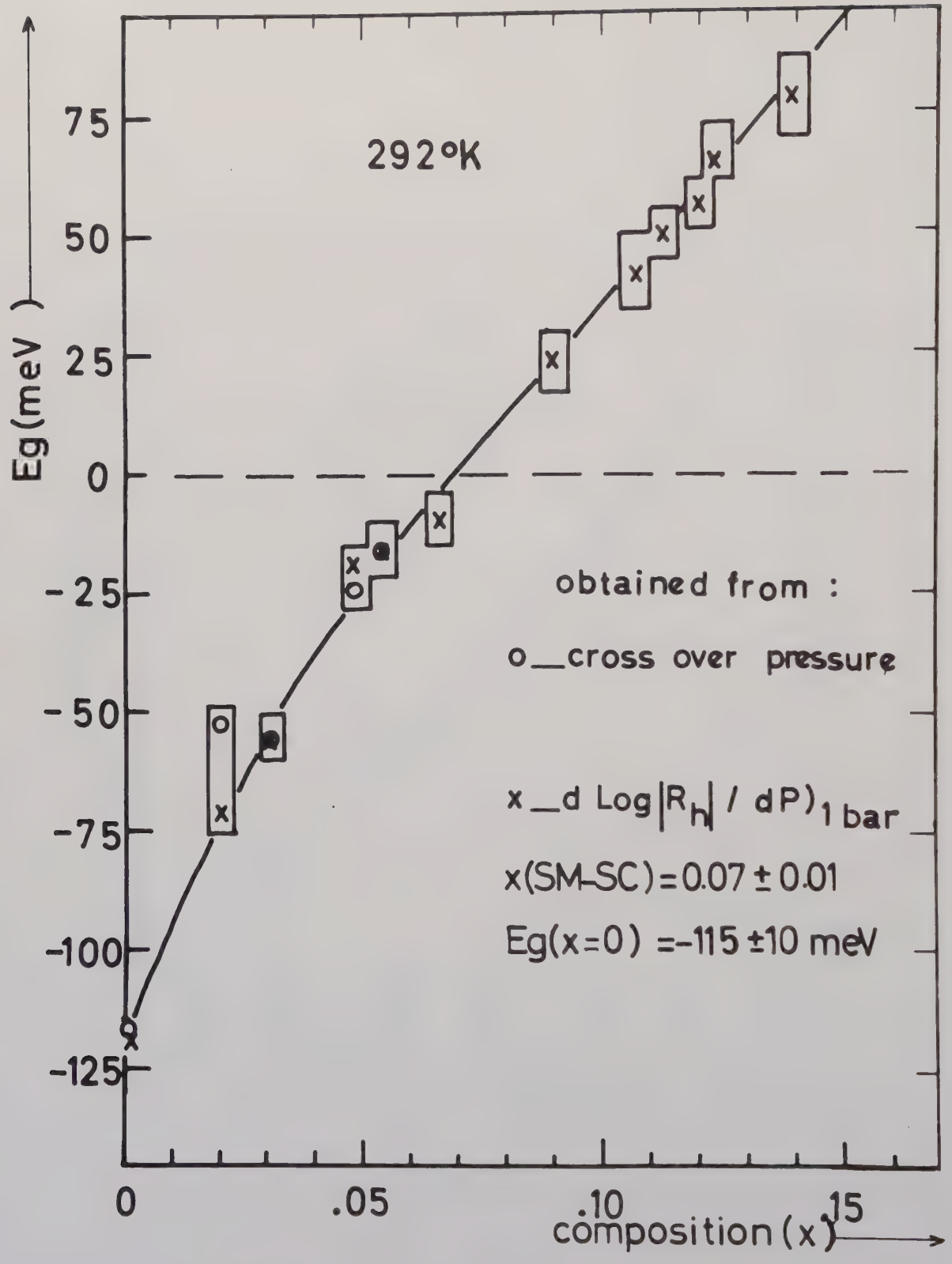
292°K
Eg(meV)
75
50
25
0
-25
-50
-75
-100
-125
0
.05
.10
.15
composition (x)
obtained from :
o__cross over pressure
x__d Log|R_h| / dP)_1 bar
x(SM-SC) = 0.07 ± 0.01
Eg(x=0) = -115 ±10 meV

Fig. 6

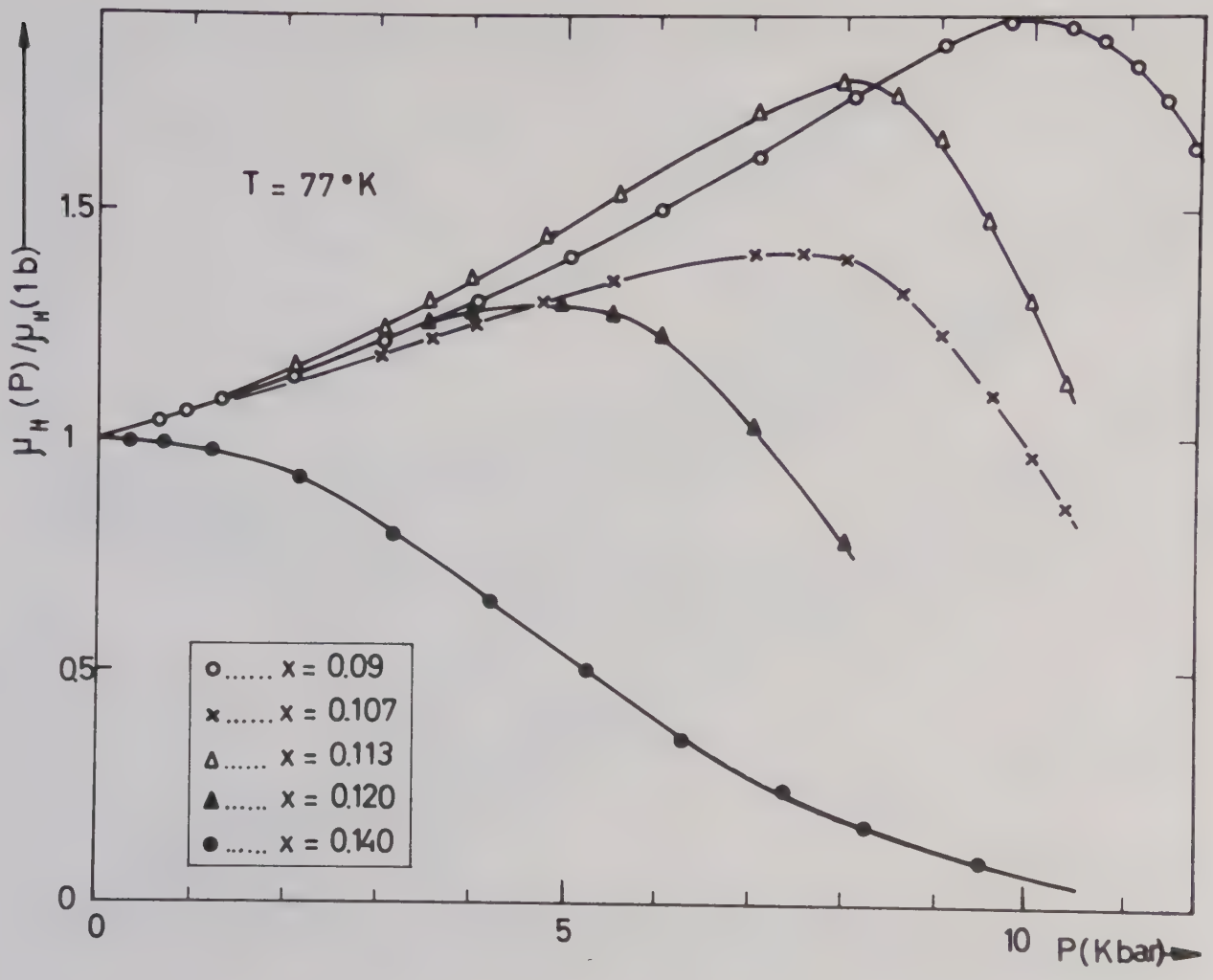
T = 77°K
$\mu_H(P)/\mu_H(1b)$
1.5
1
0.5
0
0
5
10
P(Kbar)
o..... x = 0.09
x..... x = 0.107
Δ..... x = 0.113
▲..... x = 0.120
● ..... x = 0.140

Fig. 7

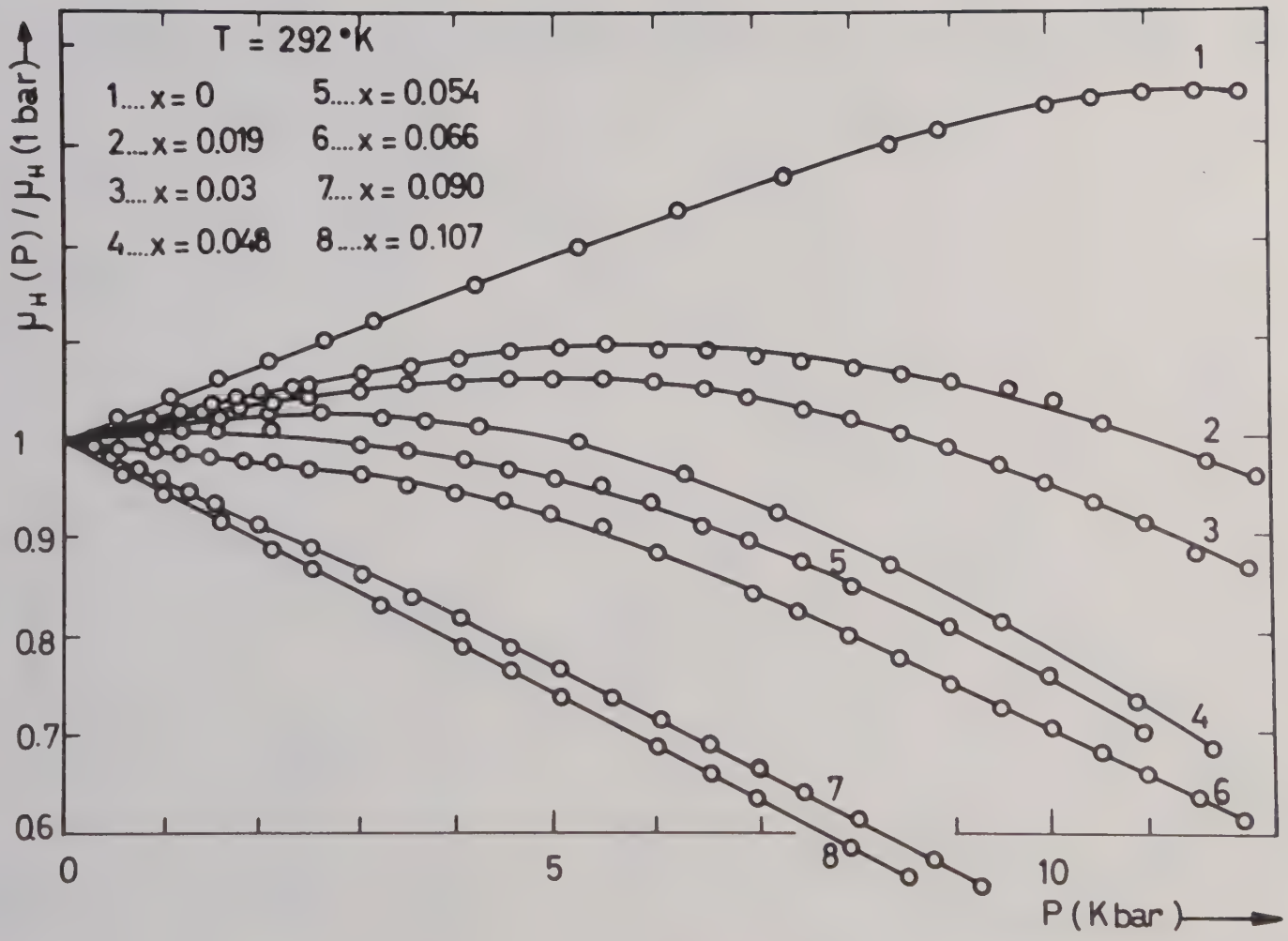
T = 292 °K
1.... x = 0
2.... x = 0.019
3.... x = 0.03
4.... x = 0.048
5.... x = 0.054
6.... x = 0.066
7.... x = 0.090
8.... x = 0.107
μH (P) / μH (1 bar)
1
0.9
0.8
0.7
0.6
0
5
10
P (K bar)
1
2
3
4
5
6
7
8

Fig. 8

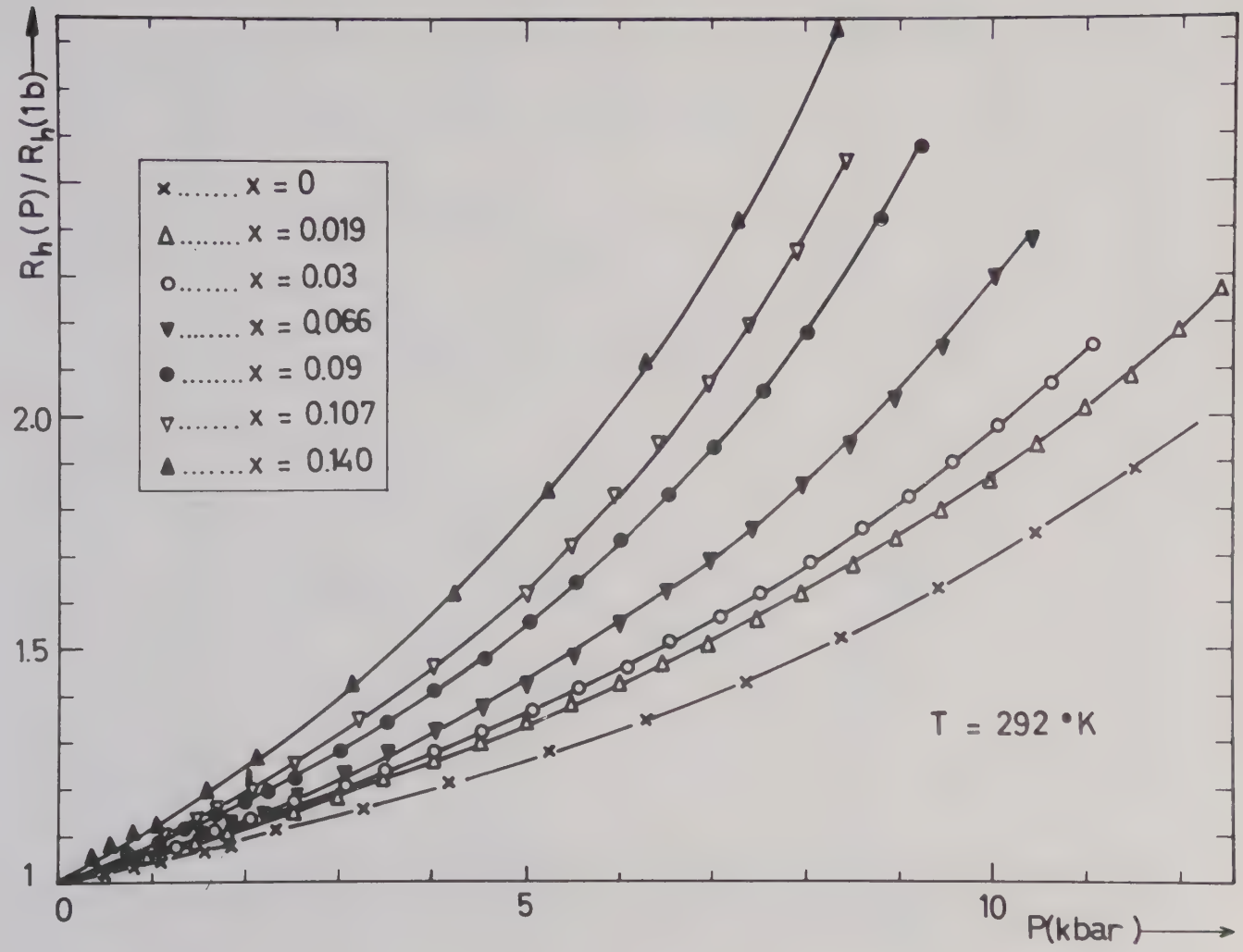
$R_h(P) / R_h(1b)$
x = 0
x = 0.019
x = 0.03
x = 0.066
x = 0.09
x = 0.107
x = 0.140
T = 292 °K
2.0
1.5
1
0
5
10
P(kbar)

Fig. 9

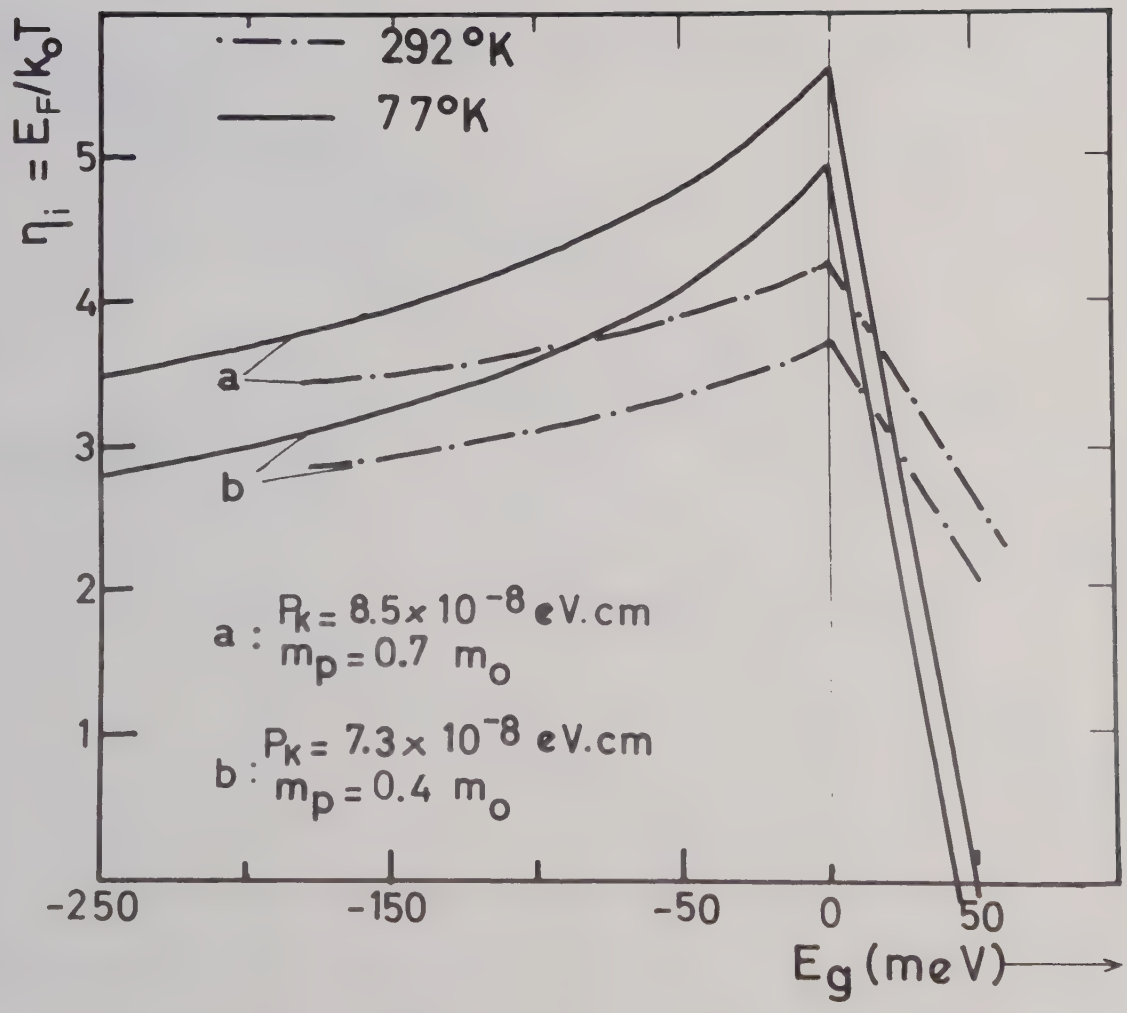
292 °K
77°K
$\eta_i = E_F/k_oT$
5
4
3
2
1
a
b
a : $P_k = 8.5 \times 10^{-8}$ eV.cm
$m_p = 0.7\ m_o$
b : $P_k = 7.3 \times 10^{-8}$ eV.cm
$m_p = 0.4\ m_o$
-250
-150
-50
0
50
E_g (meV)

Fig. 10

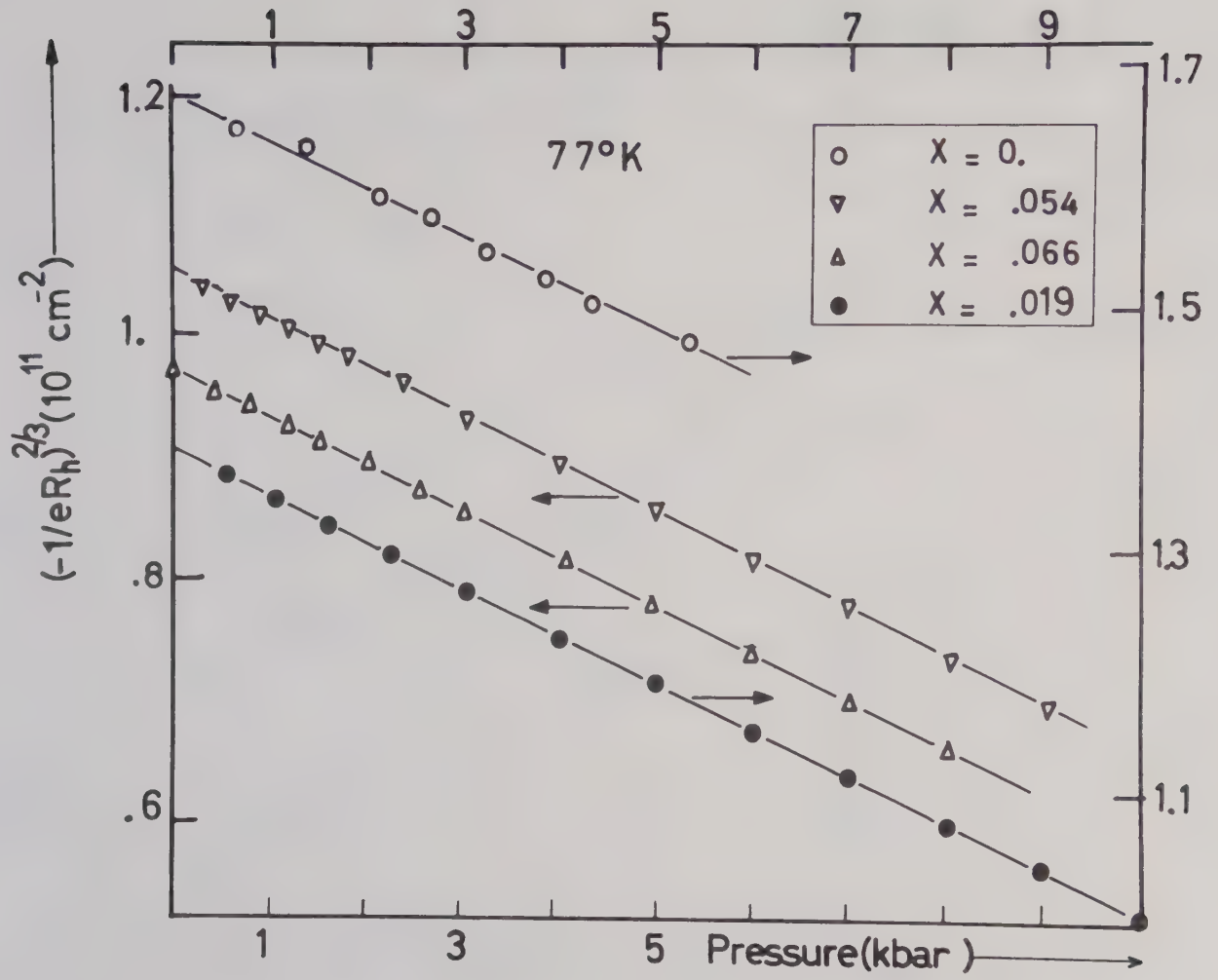
1
3
5
7
9
1.2
1.
.8
.6
1.7
1.5
1.3
1.1
77°K
X = 0.
X = .054
X = .066
X = .019
$(-1/eR_h)^{2/3}(10^{11}\ cm^{-2})$
1
3
5
Pressure(kbar)

Fig. 11

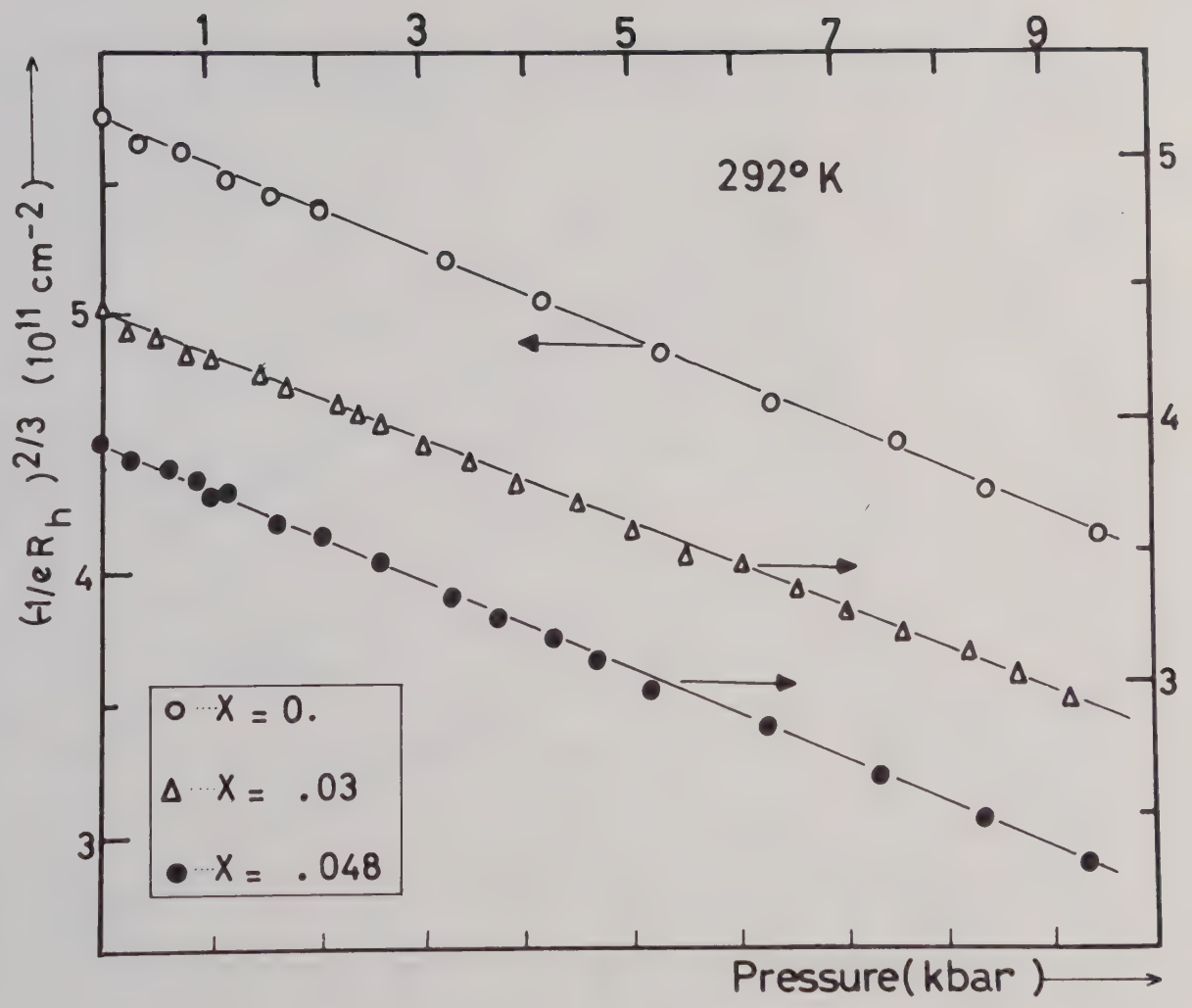

Fig. 12

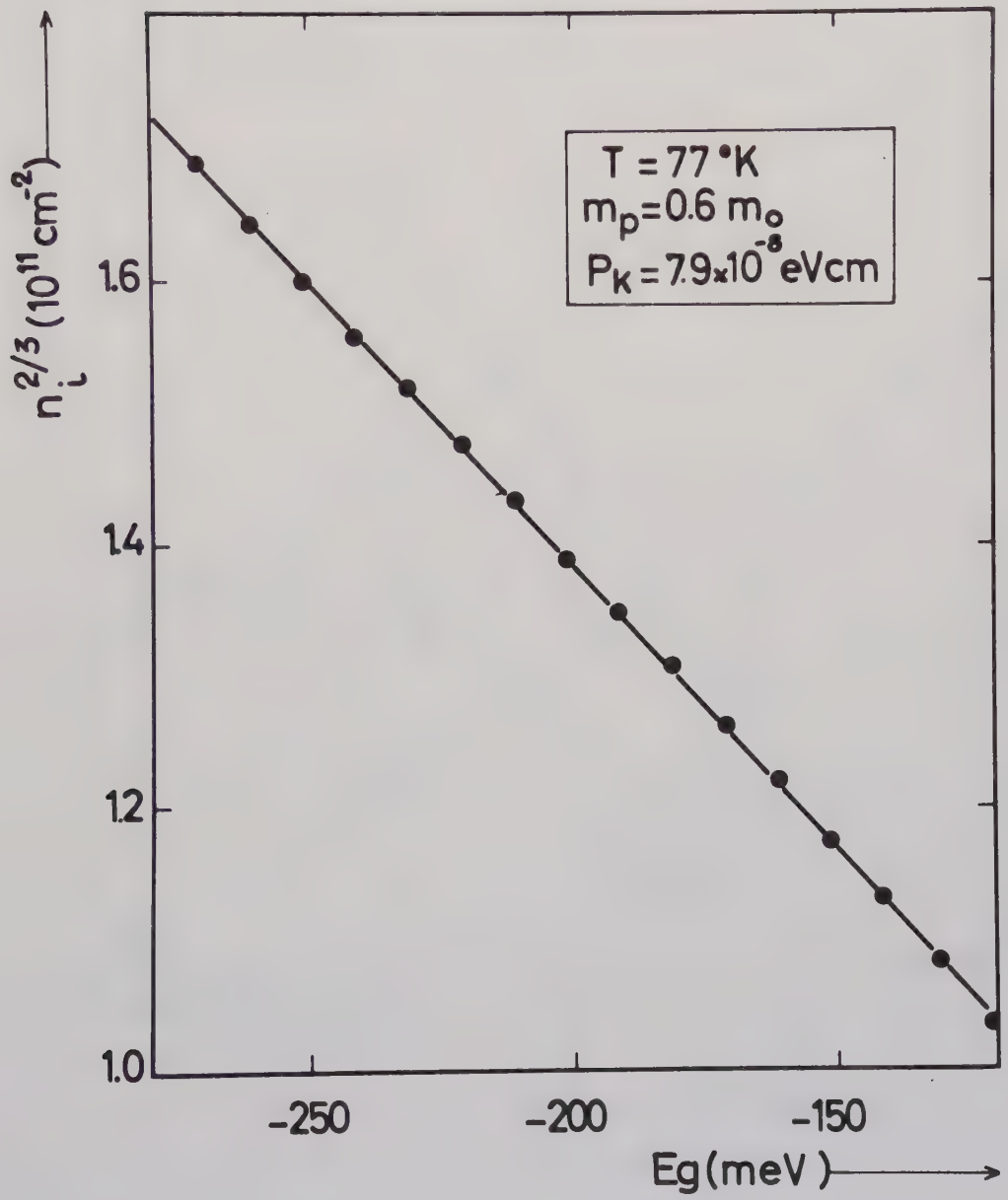
T = 77 °K
m_p=0.6 m_o
P_K = 7.9x10^{-8} eVcm
$n_i^{2/3}$ (10^{11} cm^{-2})
1.6
1.4
1.2
1.0
-250
-200
-150
Eg (meV)

Fig. 13

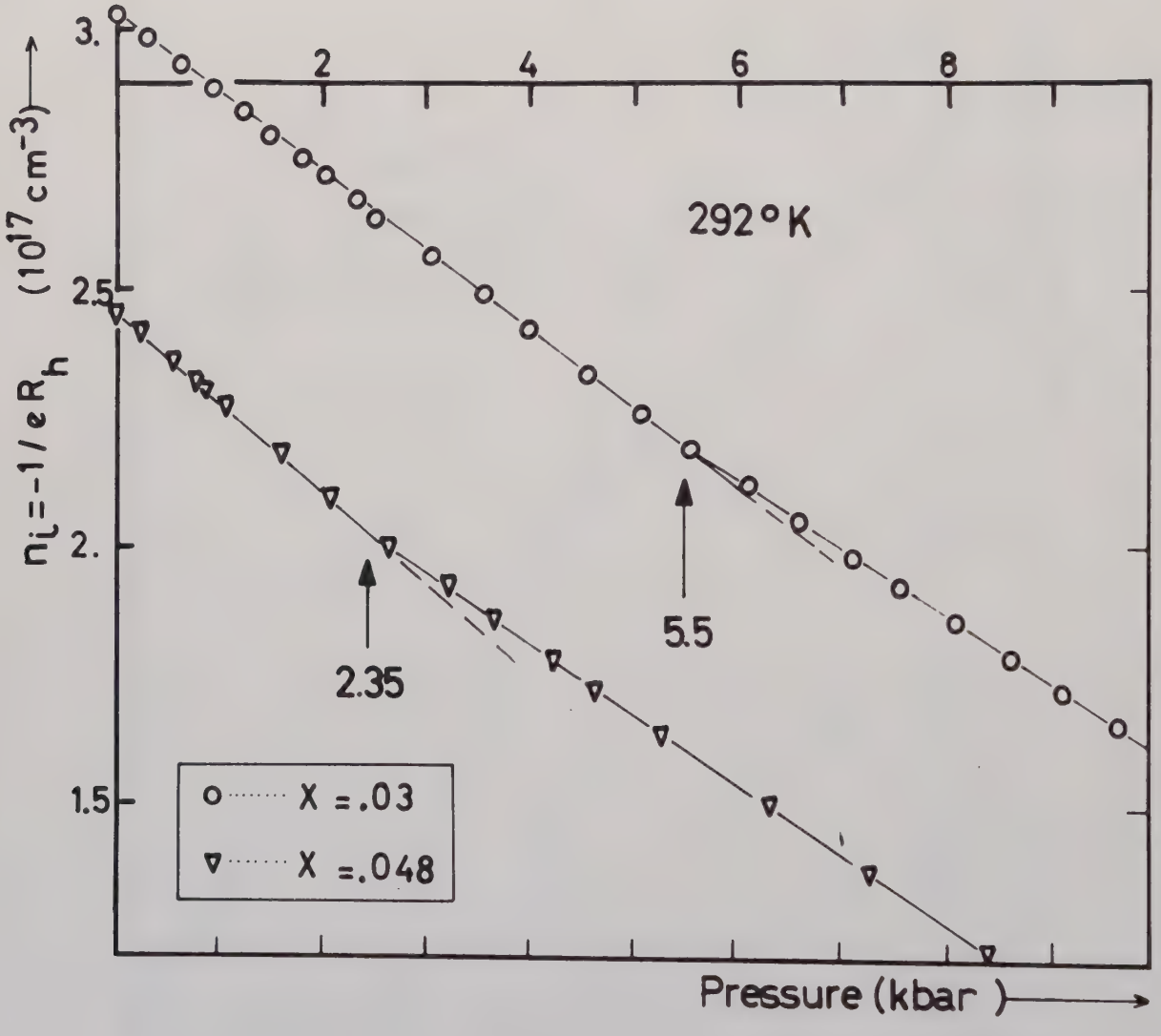
3.
2.5
2.
1.5
2
4
6
8
292° K
5.5
2.35
X = .03
X = .048
$n_i = -1/eR_h$ $(10^{17} cm^{-3})$
Pressure (kbar)

Fig. 14

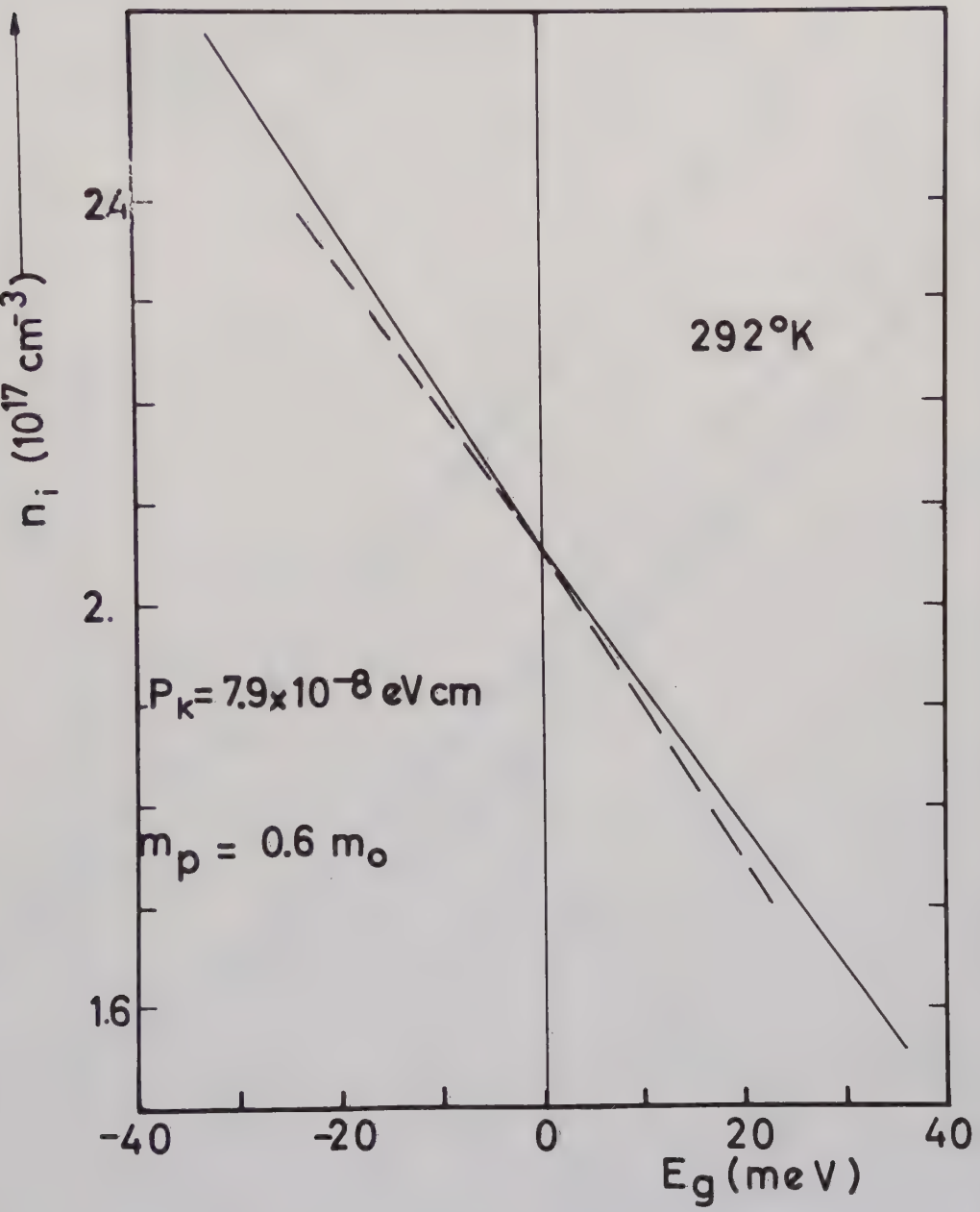
n_i (10^{17} cm^{-3})
2.4
2.
1.6
292°K
P_k= 7.9x10^{-8} eV cm
m_p = 0.6 m_o
-40
-20
0
20
40
E_g (meV)

Fig. 15

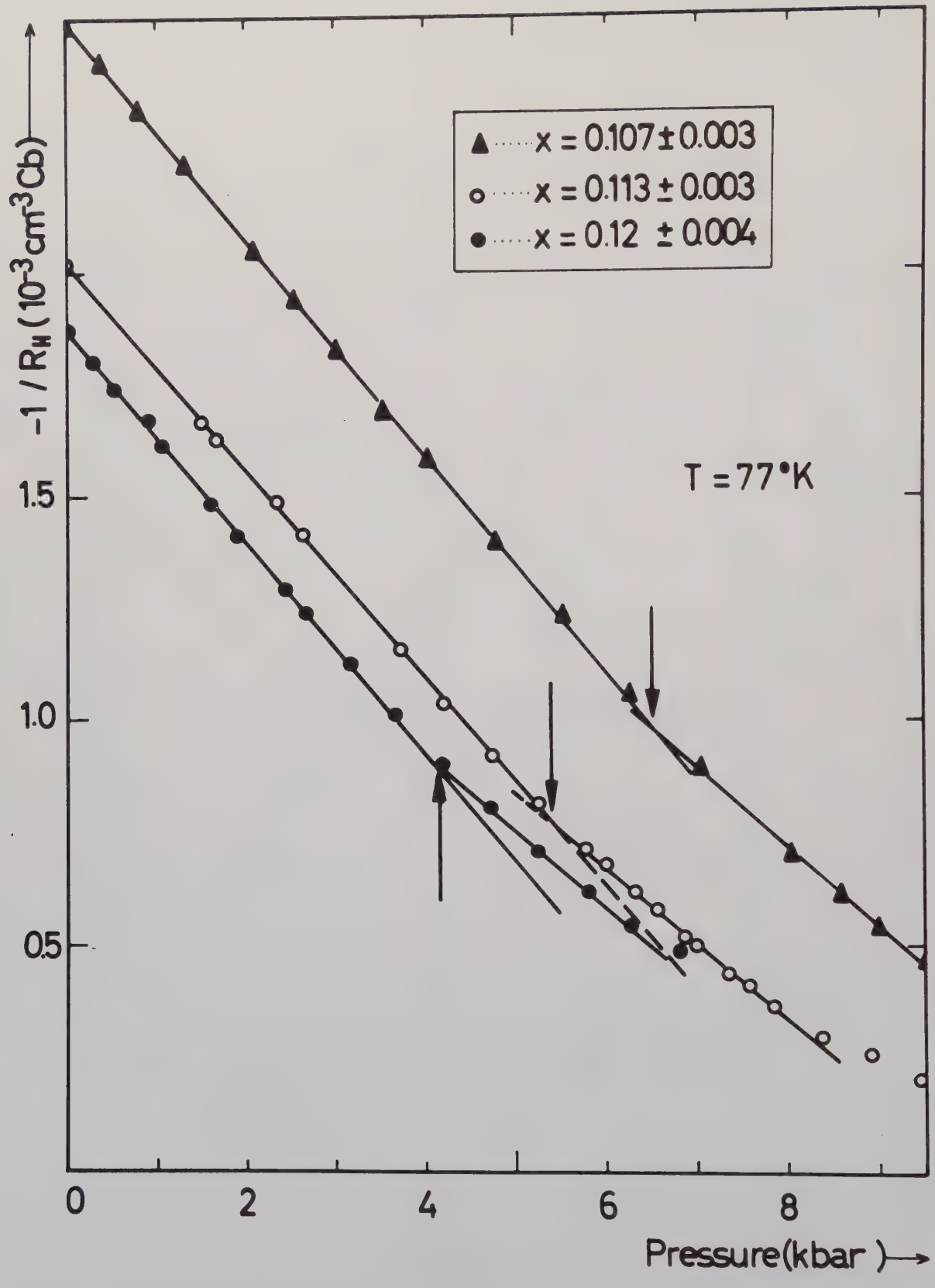
▲ ..... x = 0.107 ± 0.003
○ ..... x = 0.113 ± 0.003
● ..... x = 0.12 ± 0.004
T = 77°K
-1 / R_H (10^{-3} cm^{-3} Cb)
1.5
1.0
0.5
0
2
4
6
8
Pressure (kbar)

Fig. 16

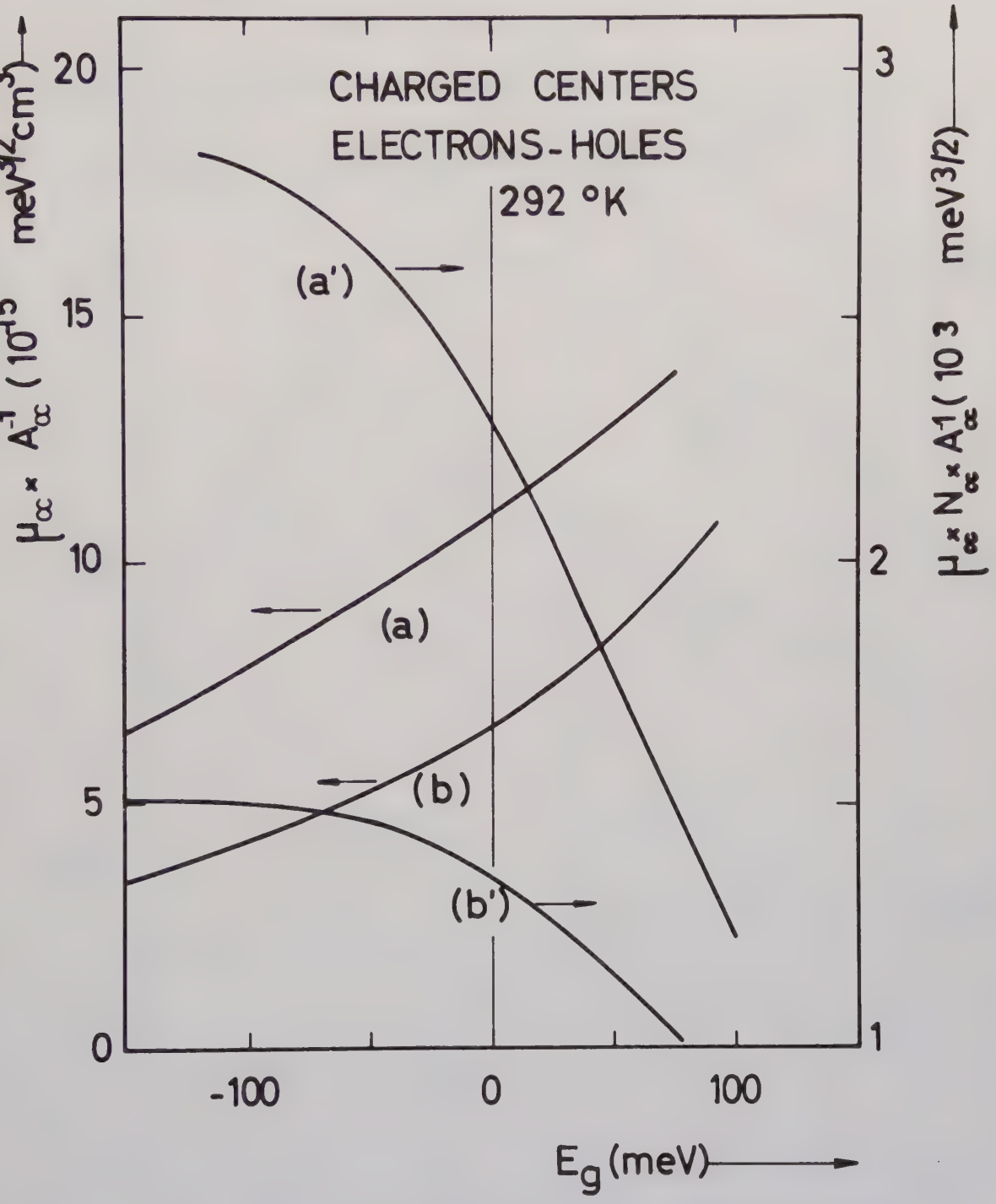
CHARGED CENTERS
ELECTRONS - HOLES
292 °K
(a')
(a)
(b)
(b')
20
15
10
5
0
3
2
1
-100
0
100
E_g (meV)
$\mu_{\alpha c} \times A_{\alpha c}^{-1}$ (10^{15} meV$^{3/2}$cm^{-3})
$\mu_{\alpha c} \times N_{\alpha c} \times A_{\alpha c}^{-1}$ (10^3 meV3/2)

Fig. 17

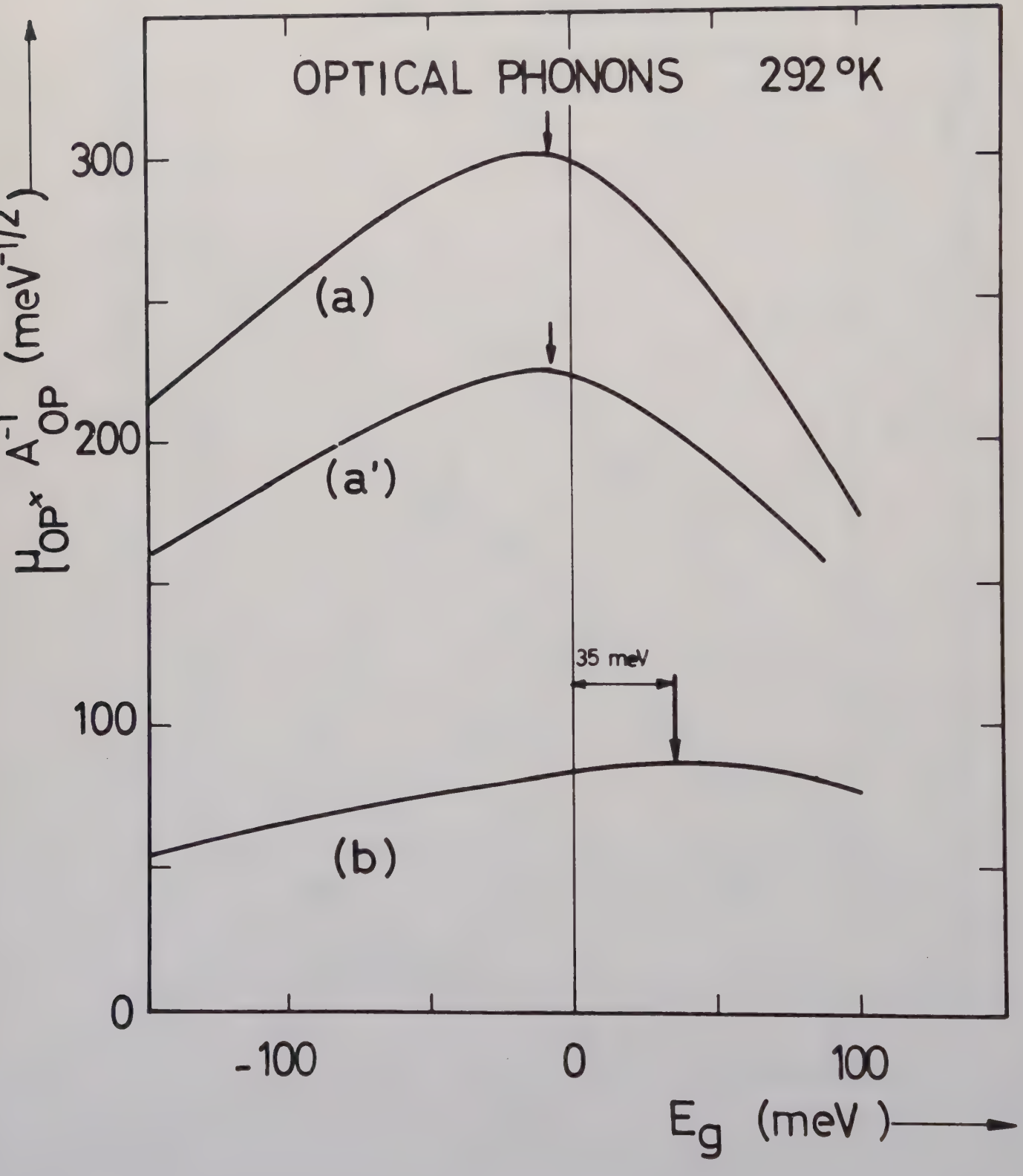
OPTICAL PHONONS 292 °K
300
200
100
0
(a)
(a')
(b)
35 meV
-100
0
100
E_g (meV)
$\mu_{OP}{}^{x}$ A_{OP}^{-1} (meV$^{-1/2}$)

Fig. 18

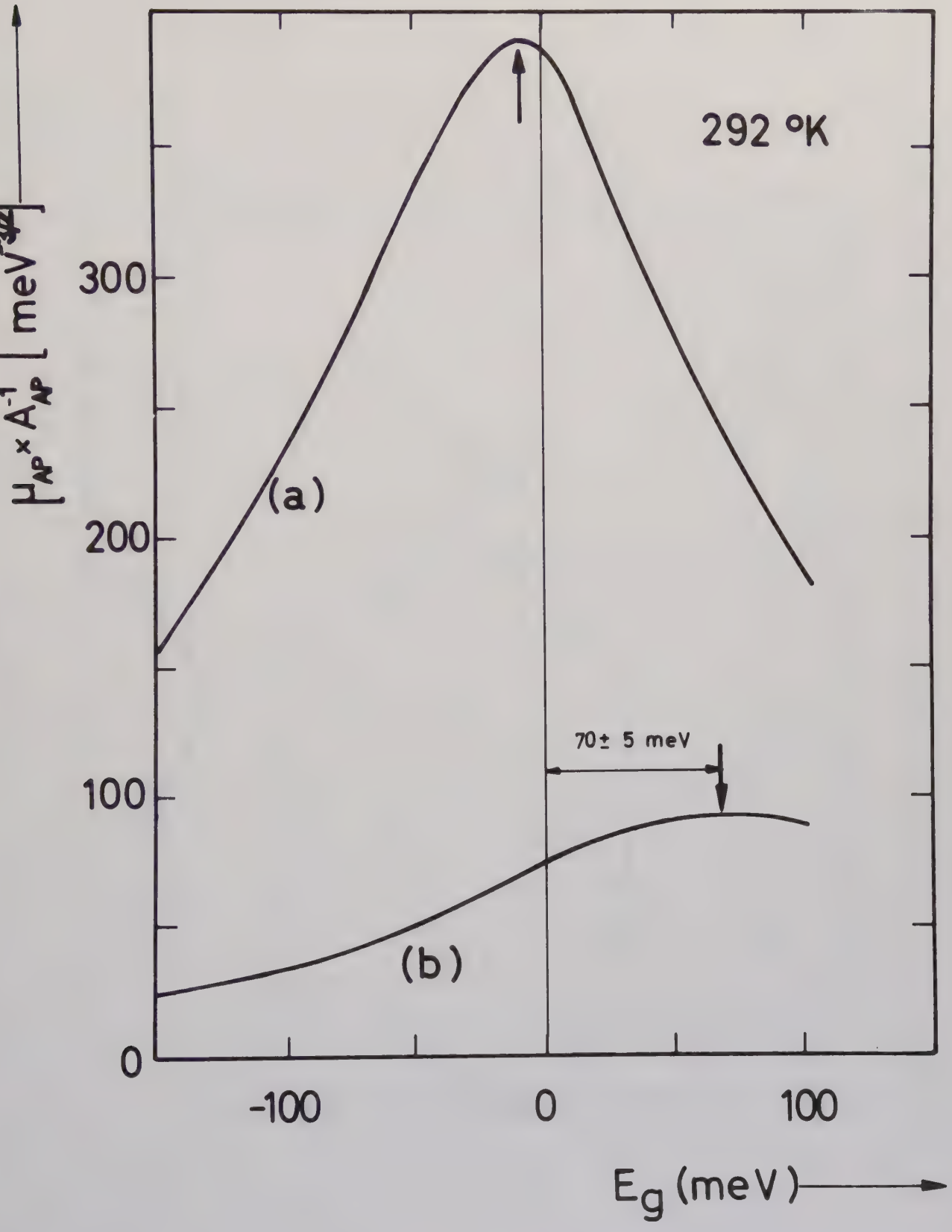

Fig. 19

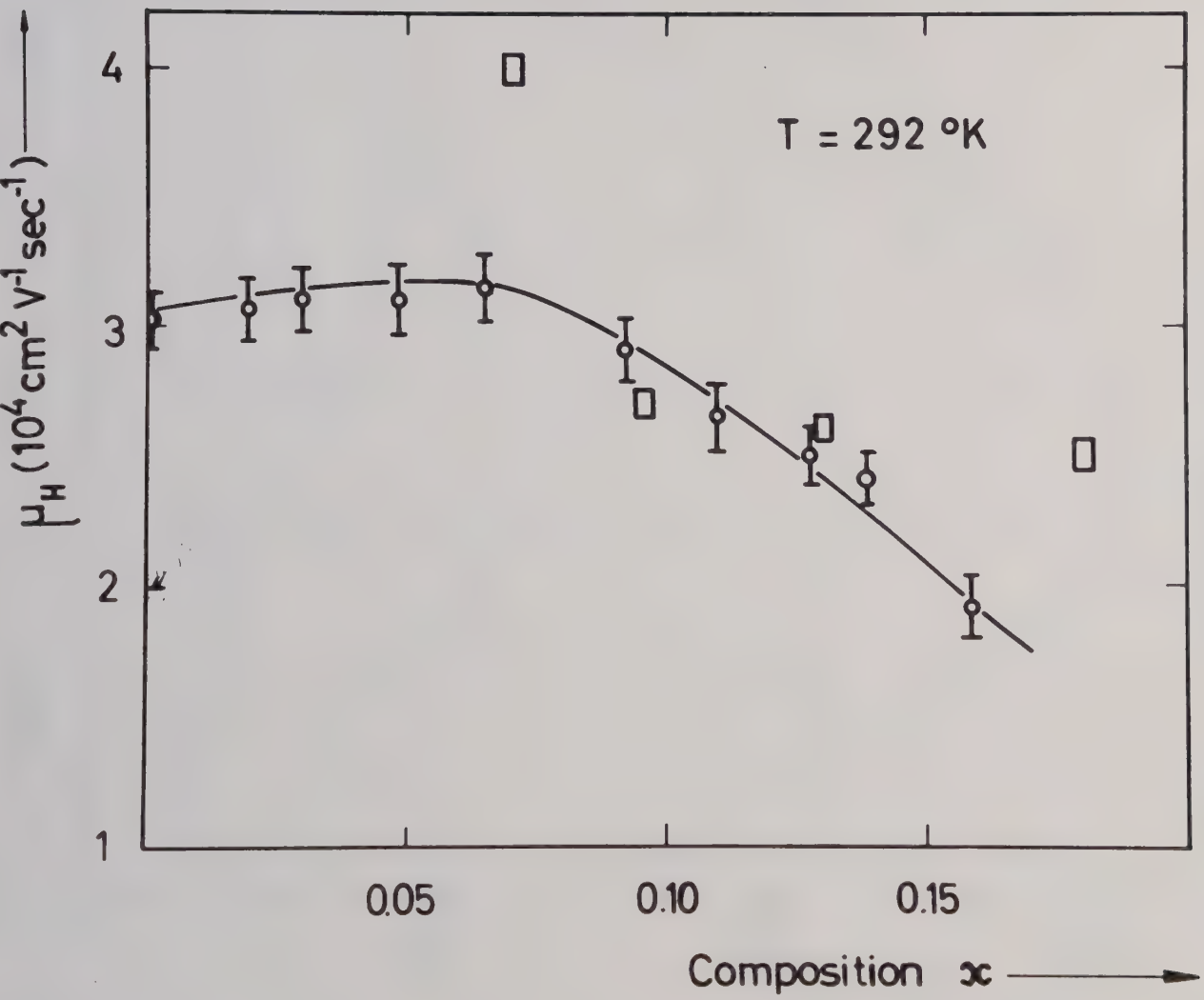

Fig. 20

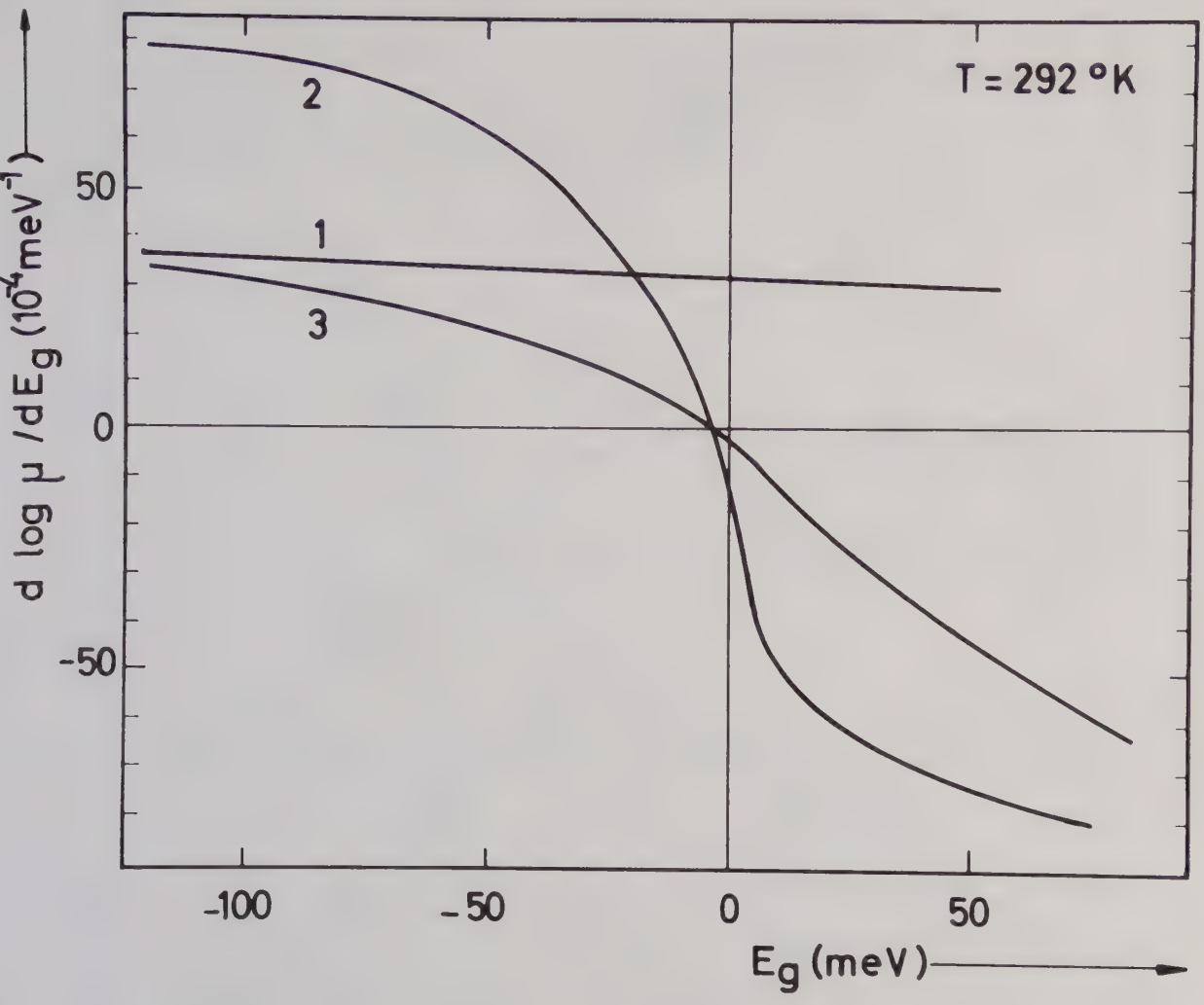

Fig. 21

Fig. 22

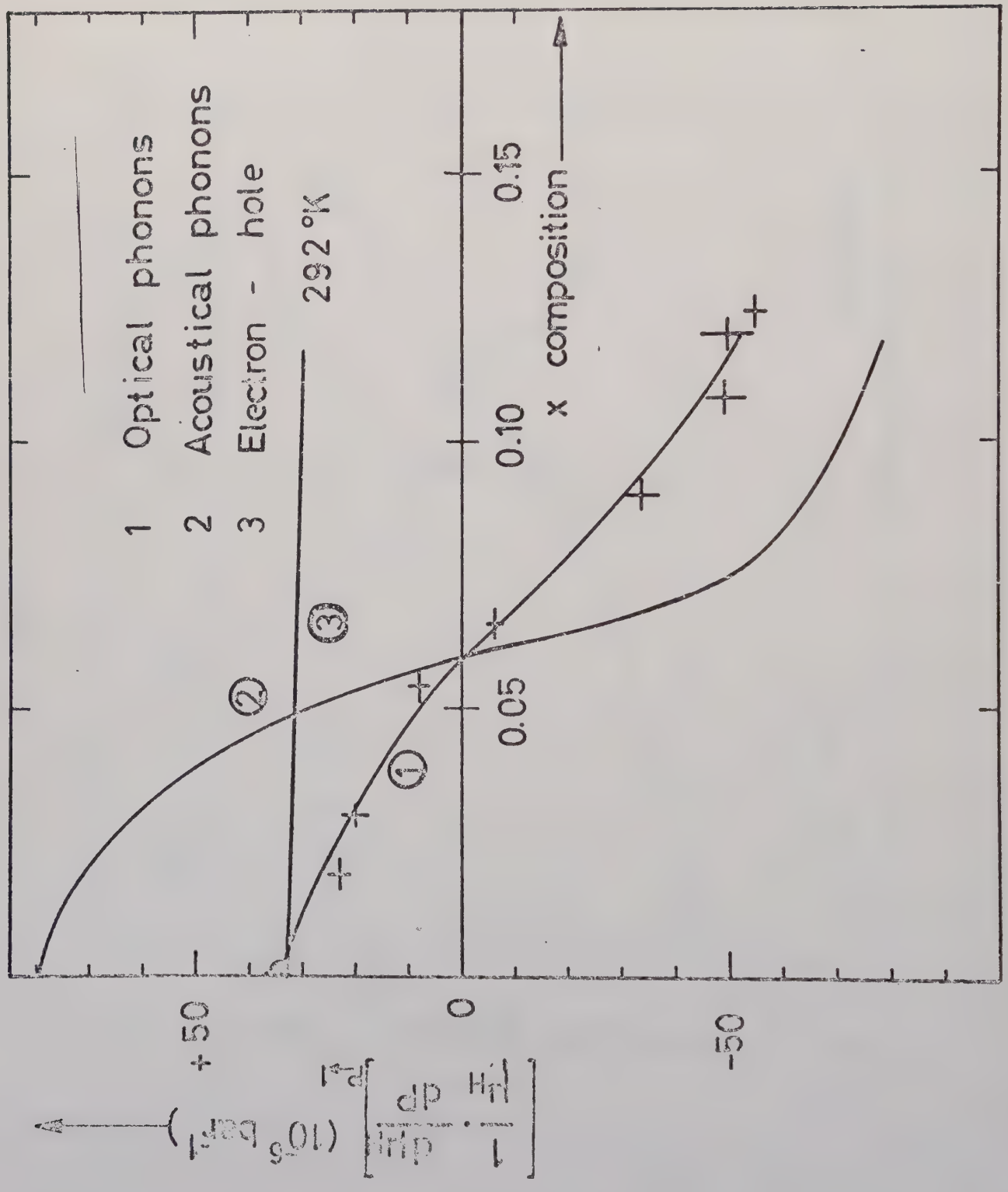
1 Optical phonons
2 Acoustical phonons
3 Electron - hole
292 °K
x composition
0.05
0.10
0.15
+50
0
-50
(10⁵ cm²/V sec)
$\frac{1}{\mu_H}\cdot\frac{H_H}{H_p}\left[\frac{d\rho}{dH}\right]_{H=0}$
①
②
③

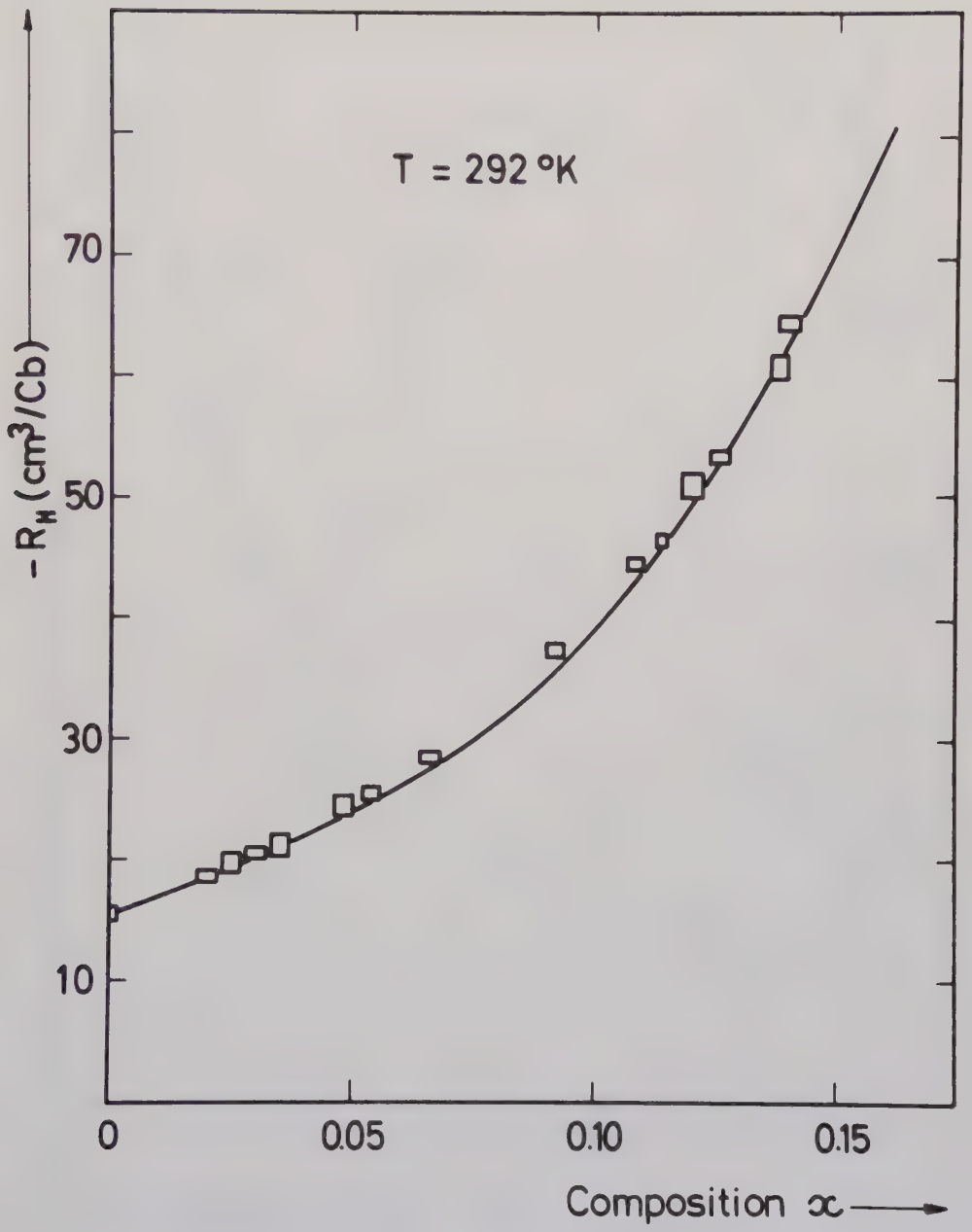

Fig. 23

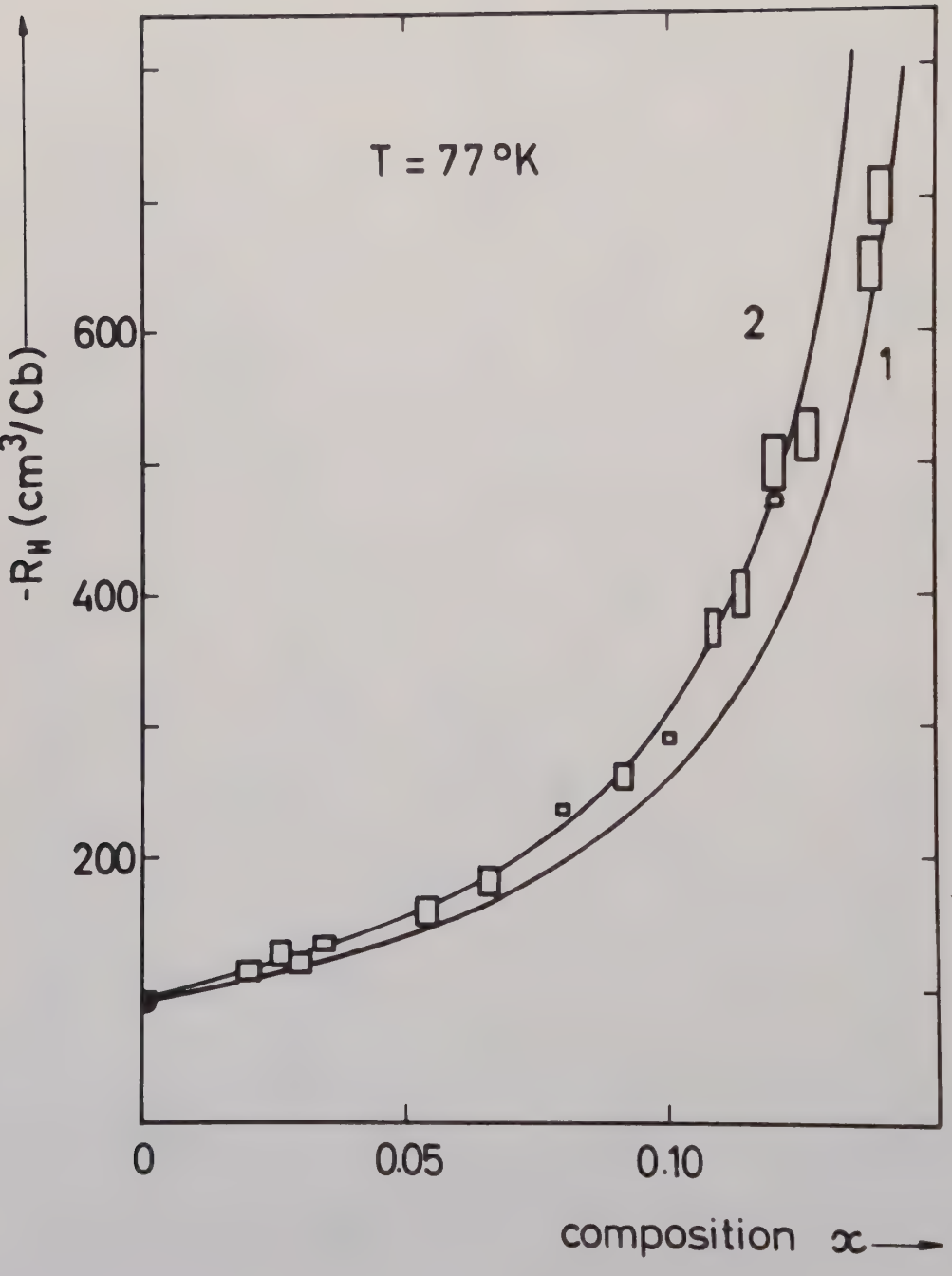

Fig. 24

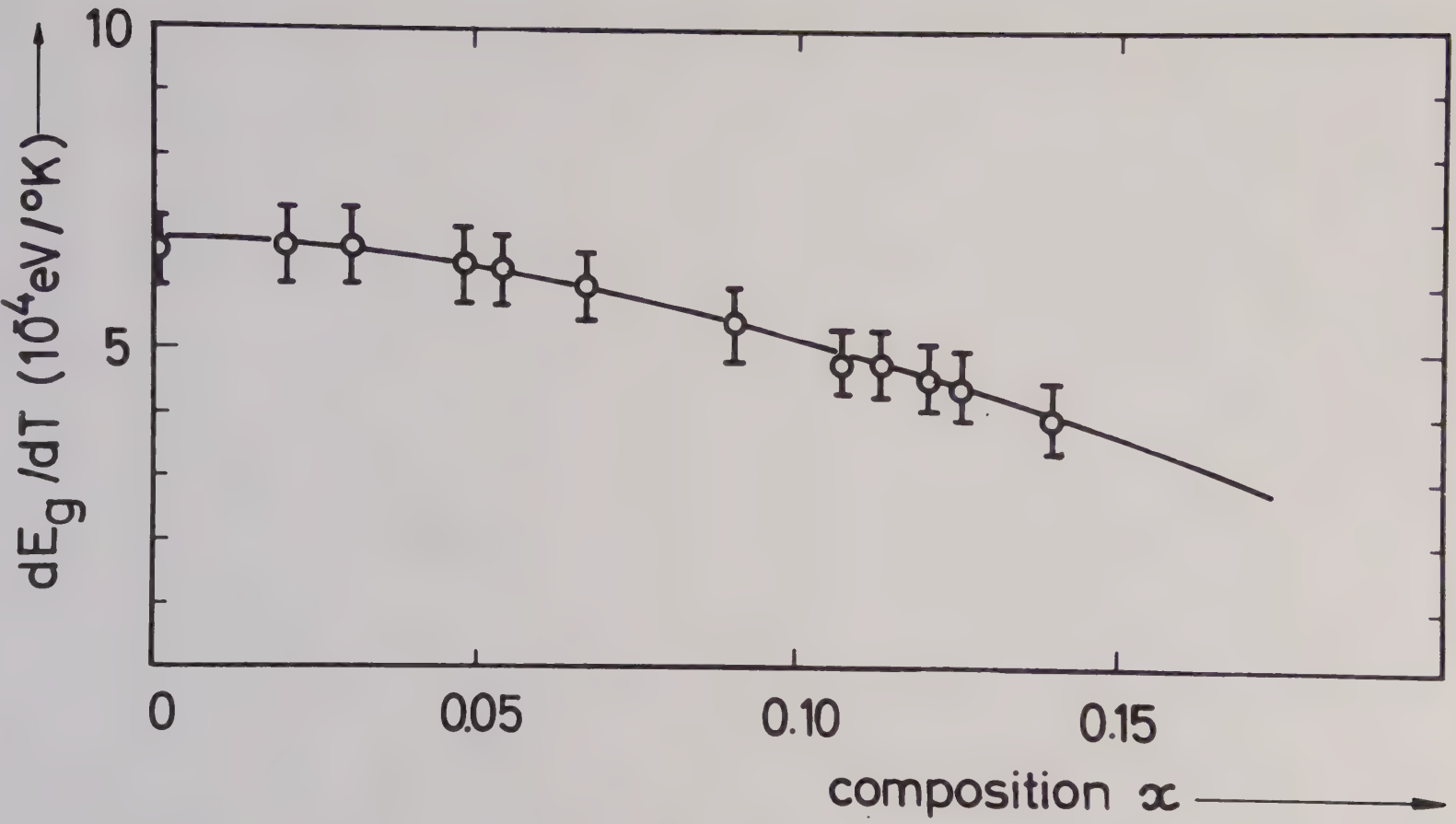

Fig. 25

ANNEXE II

ON THE PRESSURE-INDUCED SEMIMETAL-TO-SEMICONDUCTOR TRANSITION IN HgCdTe ALLOYS : II. EXTRINSIC EFFECTS.(+)(*)

S. OTMEZGUINE, A. MAUGER, M. MONCHANIN and C. VÉRIÉ
Laboratoire de Physique des Solides, CNRS-Bellevue,
1, Place A. Briand - 92190 Meudon (France)

(+) This paper is based on the second part of a thesis to be submitted by S. Otmezguine (Doctorat d'Etat, Université d'Orsay) and on the experimental part of a thesis submitted by A. Mauger (Doctorat de 3e Cycle, 17 April 1974, Université d'Orsay).

(*) Sponsored by the A.T.P. "Transition métal-isolant" of C.N.R.S. Part of this work has been presented by A. Mauger, S. Otmezguine and C. Vérié as a short communication to the International Conference on "Transition semiconducteur-semimétal" held at Nice, 10 - 12 September 1973.

ANNEXE II

ON THE PRESSURE-INDUCED SEMIMETAL-TO-SEMICONDUCTOR TRANSITION IN HgCdTe ALLOYS : II. EXTRINSIC EFFECTS.(+)(*)

S. OTMEZGUINE, A. MAUGER, M. MONCHANIN and C. VÉRIÉ
Laboratoire de Physique des Solides, CNRS-Bellevue,
1, Place A. Briand - 92190 Meudon (France)

(+) This paper is based on the second part of a thesis to be submitted by S. Otmezguine (Doctorat d'Etat, Université d'Orsay) and on the experimental part of a thesis submitted by A. Mauger (Doctorat de 3e Cycle, 17 April 1974, Université d'Orsay).

(*) Sponsored by the A.T.P. "Transition métal-isolant" of C.N.R.S. Part of this work has been presented by A. Mauger, S. Otmezguine and C. Vérié as a short communication to the International Conference on "Transition semiconducteur-semimétal" held at Nice, 10 - 12 September 1973.

ABSTRACT

The extrinsic properties of p-type HgTe and HgCdTe within the semimetal-to-semiconductor transition induced by hydrostatic pressure, are investigated. Using galvanomagnetic effects, both at low and high magnetic field, the experimental study indicated several pressure-induced effects on HgCdTe : the main results, illustrated in this paper on $Hg_{0.86}Cd_{0.14}Te$, show typical features exhibited by resonant acceptor states such as de-ionization, resonance scattering of conduction band electrons, strong shift of a virtual level A_1 attributed to Hg-vacancies. The combination pressure-quantizing magnetic field leads to an evidence of the crossover of the 0^- Landau level with A_1 in HgCdTe and to an accurate determination of the pressure coefficient of the Γ_6-Γ_8 energy interval in HgTe. The effects associated with substitutional impurity acceptor are investigated through a study on Cu-doped HgTe and HgCdTe. Transport coefficients measured as a function of magnetic field strenth indicate a conduction mechanism involving three sets of carriers. In addition to electrons and holes belonging to the extended states of conduction and valence bands, an evidence of "slow electrons" is attributed to electrons quasi-bounded to completely ionized resonant states. The differenct features exhibited by the virtual states A_1 and A_o are qualitatively discussed in terms of potential strengths.

I. INTRODUCTION

A continuous range of Mercury-Telluride-Cadmium Telluride alloys, (hereafter called $Hg_{1-x}Cd_xTe$), may be obtained with any value of x between

HgTe and CdTe. Strictly speaking, the concept of band fails to describe the electronic structure of an alloy, due to the lack of translation symmetry arising from a random substitution of Hg and Cd atoms in the lattice. Nevertheless most of the experimental results obtained till now lead to the description of the electronic structure of these alloys within the framework of a continuous variation of band parameters from the semimetal (SM) HgTe to the semiconductor (SC) CdTe ones. These well defined compounds have band structures similar to those of α - Sn[1] and InSb respectively. The main difference between α - Sn and InSb band structures lies in the ordering of the levels labelled Γ_6 and Γ_8 for such materials crystallizing in the zinc blende structure. Let the energy gap E_g be defined by $E_g = E(\Gamma_6) - E(\Gamma_8)$.

In the SM configuration $E_g < 0$. The conduction band and the heavy hole valence band both stem from the Γ_8 level, while the light hole valence band stems from the Γ_6 one.

In the SC configuration $E_g > 0$. The heavy and light hole valence bands are degenerate at Γ_8. The conduction band stems from Γ_6.

In both configurations, the band stemming from the spin split Γ_7 level is a far lying valence band. At low temperature, E_g changes its sign for some critical composition x_c around 0.165 and an alloying induced semimetal-semiconductor (SM - SC) transition occurs. The same transition can also be induced by pressure P and occurs at a critical pressure P_c for materials which are SM at zero pressure. All these features are illustrated in Fig. 1.

The pressure induced SM - SC transition is due to the moving up of the Γ_6 level (s type symmetry) with respect to the Γ_8 one (p type symmetry) when the lattice parameter is decreased, which involves that the pressure coefficient α of the Γ point energy gap (E_g) is positive. This experimental result has been observed for all known materials having either the zinc blende or the diamond-like structure, and may be understood by a description of the covalent bonds in a tight binding approximation[2] or by more elaborate band calculations like those performed by Harman et al for Ge[3].

This pressure induced SM - SC transition was studied for compositions ranging from $x = 0$ to $x = 0.15$, at room and liquid nitrogen temperatures by means of electrical measurements (Hall coefficient, resistivity and Hall mobility).

At such temperatures it was possible to explain these experimental results (briefly reported in Ref. 4, and detailed in Ref. 5) using the k.p description[6] of the electron states lying in the vicinity of Γ_6 and Γ_8. Such a description deals with the bands stemming from Γ_6 and Γ_8 levels together with that stemming from the Γ_7 level split from the Γ_8 by the spin orbit coupling energy Δ_o. In Ref. 5, a parabolic shape was chosen for the heavy hole valence band, with the following dispersion relation :

$$E_v(k) - E(\Gamma_8) = - \frac{\hbar^2 k^2}{2m_p} \qquad (1)$$

m_h was found to be equal to $(0.55 \pm 0.1)\ m_o$, where m_o is the free electron mass, and was assumed to be pressure independent. Such an assumption is based on the fact that the curvature of this band is due to an interaction with far lying ones[6].

This shape of the heavy hole valence band is oversimplified. The lack of inversion symmetry in zinc-blende structure, as discussed by Kane[6], leads to the existence of valence states in a small range of energies higher than $E(\Gamma_8)$, due to the linear k-terms occuring in the E(k) dispersion relation of this band in (111) and (110) directions. This band is thus no longer spherical. To analyse transport phenomena, a simplified picture may be used, according to which the non sphericity of the band is neglected. We shall only account for valence states above the Γ_8 point by a small shift ΔE of the effective top of the valence band E_v. Eq. 1 then becomes :

$$E_v(k) - E(\Gamma_8) = \Delta E - \frac{\hbar^2 k^2}{2m_p} \qquad (2)$$

The transposition of this model in terms of density of states g(E) is illustrated in Fig. 2. In the SM configuration (Fig. 2(a)), the densities of electron and heavy hole states overlap over a range ΔE. In the SC configuration (Fig. 2(b)), the effective thermal energy gap is $E_g - \Delta E$. A zero gap semiconductor is a zero overlap semimetal obtained in the SM configuration when ΔE is neglected.

Otherwise, in both SM and SC configurations, the strong interaction between the conduction and light hole valence bands through the k.p interaction induces the conduction band to be non parabolic, with a dispersion relation given by :

$$E(k) = \frac{-|E_g| + (E_g^2 + \frac{8}{3} k^2 P_K^2)^{1/2}}{2} \qquad (3)$$

This relation is valid under the following assumptions :

(i) the origin of energies is taken at the bottom of the conduction band.

(ii) The spin orbit splitting $\Delta_o = E(\Gamma_8) - E(\Gamma_7)$ is such that $\Delta_o \gg |E_g|$, $k P_K$ where P_K is the Kane matrix element.

Because of the non parabolicity of this band, the effective mass of the electrons depends upon their energy and is given by :

$$m^*(E) = m_n (1 + 2\gamma z) \qquad (4)$$

where $\gamma = k_o T/|E_g|$, $z = E/k_o T$, k_o is the Boltzmann constant, and m_n is the effective mass at the bottom of the conduction band. When $\Delta_o \gg |E_g|$,

$$m_n = \frac{3\hbar^2}{4P_k^2} |E_g| \qquad (5)$$

We can give a more convenient form to these relations by the use of a parameter $Q = (4 P_k^2 m_o)/3\hbar^3$ which has the dimension of energy. We can then write :

$$\frac{m^*(E)}{m_o} = \frac{(|E_g| + 2E)}{Q} \qquad (6)$$

$$\frac{m_n}{m_o} = \frac{|E_g|}{Q} \qquad (7)$$

The effect of the pressure P is assumed to make E_g vary linearly according to :

$$E_g(P) = E_g(o) + \alpha P \qquad (8)$$

$E_g(o)$ and α are respectively the zero pressure energy gap and its pressure coefficient at a given temperature. When the overlap ΔE is neglected, the pressure induced SM-SC transition occurs at such a critical pressure P_c that $E_g = 0$. It issues from Eq. 7 that m_n then vanishes, which should induce for example a strong singularity on the electron mobility when E_F is in the true vicinity of the bottom of the conduction band. Nevertheless, at 77°K, for

the samples studied under pressure in Ref. 5, the Fermi level was around 3 to 4 k_oT when $E_g = 0$, which removed such a singularity of the mobility, according to Eq. 6 and did not allow us to reach energies in the true vicinity of the Γ_6 and Γ_8 levels in this particular situation. It thus seemed necessary to lower the temperature in order to bring down the Fermi level.

In section II.A. we report measurements of the low field Hall coefficient, and of the electron mobility, versus pressure, performed at 4.2°K and 1.7°K for a sample of composition $x = 0.14$ (SM at zero pressure) already studied at 77°K in Ref. 5. These measurements illustrate a pressure induced SM-SC transition.

At each pressure, a study of the Hall coefficient versus magnetic field on this sample allowed a determination of the electron, hole, and ionized impurity concentrations (Sect. II.C.).

Such a simple band scheme as that illustrated in Fig. 2 could not account for the large number of electrons and holes for this sample. It was found necessary to assume the existence of a small density of valence states extending far away above the Γ_8 point. Such an extra density of states cannot be correlated to a symmetry induced overlap ΔE, and will be discussed in Section IV as an effect arising from local fluctuations of composition.

On the contrary, the same kind of analysis of the Hall coefficient versus magnetic field performed on an HgTe sample (hereafter $x = 0$ sample), which had a very low Fermi energy at 1.7°K, agrees quite well the description illustrated in Fig. 2(a) with $\Delta E < 1$ meV, as it will be shown in Section II.C..

Both samples were found to be p-type, with acceptor levels located in the conduction band. The theory of impurity states in gapless semiconductors has been recently given by Gel'mont and D'yakonov[7] who have shown the possible existence of quasi discrete acceptor levels interfering with the conduction band. Such a particular feature of the gapless semiconductors was put forward in order to explain some anomalies occuring in the transport properties of such materials[7 - 12] as well as the results of magnetooptical experiments on HgTe[13]. In Ref. 7 the perturbing potential is assumed to be Coulombian and the activation energy E_A of the acceptor level is not expected to vary significantly with E_g in the range of the investigated values of this band parameter. On the contrary, large

variations of E_A with $|E_g|$ may be expected when assuming a localized perturbing potential[14]. The former behaviour of E_A seems to have been observed for an acceptor level assigned to Cu impurities, evidenced in both x = 0 and x = 0.14 samples, while the latter behaviour has been indeed observed for another acceptor level in the x = 0.14 sample assigned to Hg vacancies. These results are presented in section II.C. and discussed in section IV.

For both samples quantum oscillations could be observed on the Hall coefficient and the magnetoresistivity because of the high electron mobility. The study of the shift of these oscillations versus pressure in the x = 0 sample allowed us to determine the pressure coefficient α at very low temperatures. These quantum effects are reported in Section II.B.

In Section III, we present an anlysis of the electron mobility. In particular, in x = 0.14 sample, a small dip clearly stands out from the background variations of the electron mobility, which are understood by taking into account all the particular features of such small gap materials. This dip is interpreted as a resonant effect on the electron mobility occuring when the Fermi and acceptor levels cross. This resonant effect led to an estimation of the width of the acceptor level. Some other effects which seem to be correlated to such resonance phenomena are reported along this paper.

II. EXPERIMENTAL RESULTS

According to the law E_g (x) leading to an overall understanding of the results obtained on samples with various compositions in Ref. 5 at 77°K, we found for x = 0.14 sample at this temperature : $E_g(o) \simeq -8$ meV at zero pressure. The variations of its low field Hall coefficient versus pressure fit a deformation of its band structure deduced from Eqs. 3 and 8, and showed the existence of a net concentration of acceptor type defects such that calling N_A and N_D the concentrations of acceptor and donor states we had $N_A - N_D \simeq 10^{16}$ cm^{-3}. Under the assumption that $m_p \gg m_n$ no sharp donor levels are possible in such materials[7, 10] so that donors should be ionized whatever be the temperature.

We report in Fig. 3 the results of Hall effect measurements versus magnetic field performed at 1.7°K and at various pressures, for x = 0.14 sample. The experimental set up allowed us to investigate a range of

pressures up to 7 kbars. The pressure transmitting medium was helium. The copper - beryllium experimental vessel was a cylinder with approximately 1.5 cm outer diameter, 0.4 cm inner diameter, and about 10 cm length[15]. The size of the pressure vessel enabled us to use a classical electromagnet which provides fields up to 10 kG.

The cryogenic set up[15] allowed us to perform measurements as a function of temperature and to obtain the freezing of helium under constant pressure conditions so that once the experimental vessel has frozen, a lowering of the temperature from the melting point was accompanied with a drop of pressure along an isochore. The pressure in the vessel was then determined at each temperature using the data of Spain and Segall[16].

Under such experimental conditions, any measurement versus temperature at constant pressure is not straightforward. In order to plot the variations of the low field Hall coefficient R_o (T) versus temperature (Fig. 4) we used a procedure depicted in Ref. 15.

The analysis of the experiments performed versus magnetic field will be divided in three subsections.

Section II.A. deals with measurements at low magnetic field, exhibiting the SM - SC transition, for x = 0.14 sample.

In Section II.B., we report and analyse quantum oscillations observed in both x = 0.14 and x = 0 samples.

Section II.C. consists of the Hall coefficient variations analysis as a two carrier type effect at such high magnetic fields that the 0^+ Landau level has already crossed the Fermi one.

II.A. SM - SC transition

The electron concentration n_1 and mobility μ_1 for x = 0.14 sample at 4.2°K and 1.7°K versus pressure are plotted in Figs. 5 and 6. The electron concentration is deduced from the Hall coefficient R(o) in the limit of vanishing magnetic fields by :

$$n_1 = - \frac{1}{eR(o)} \qquad (9)$$

where e is the absolute value of the electron charge. As we shall see later, the electron gas is highly degenerate so that we may assume the Hall factor

to be one. Under such conditions, μ_1 is given by :

$$\mu_1 = - R(o)\ \sigma\ (o) \qquad (10)$$

where σ (o) is the zero field conductivity.

The electron concentration plotted in Figs. 5 and 6 varies almost linearly in the range of pressures corresponding to the SM configuration. The slope changes quickly at some critical pressure P_c. This effect has been analized in Ref. 5 and interpreted as the crossover of the Γ_8 and Γ_6 levels induced by the pressure at the SM - SC transition.

A value of 5.4 ± 0.1 kbars is found for the crossover pressures P_c at both 4.2°K and 1.7°K.

The variations of μ_1 reported on the same figures exhibit a maximum in the vicinity of that pressure P_c, previously determined from the electron concentration variations. According to Eq. 7 a maximum of the electron mobility when E_g goes through zero may be qualitatively understood as the consequence of a minimum of the effective mass. But as discussed in Ref. 5, the study of the mobility is not a straightforward way of analysing the SM - SC transition. We must bear in mind that :

(i) the effective mass at the Fermi level m^* (E_F) is not the only parameter which determines the variations of μ_1.

(ii) m^* (E_F) is not necessarly minimum for $P = P_c$, due to the variations of E_F versus E_g.

All these topics will be further discussed in Section III.

II.B. Quantum domain analysis

Over the whole range of pressures, the electron mobility was higher than 10^5 cm^2 V^{-1} sec^{-1} for x = 0.14 sample at 4.2°K and 1.7°K, and equal to about 4.3×10^5 cm^2 V^{-1} sec^{-1} for the HgTe sample (x = 0) at 1.7°K. According to such high mobilities the condition $\mu_1 B > 1$ is fulfilled for magnetic fields as low as a few hundred gauss, so that it is easy to observe quantum oscillations once $\hbar\omega_c > k_o T$, ω_c being the cyclotron frequency.

x = 0.14 sample.

Each curve R (B) reported in Fig. 3 for x = 0.14 sample exhibits a plateau at a field which we shall call B_c. For each pressure, an arrow

indicates this critical field on the curve. The study of the transverse magnetoresistivity ρ (B) plotted in Fig. 7, for the same set of pressures, and the same temperature 1.7°K as in Fig. 3, shows that a bump occurs on the ρ (B) curves at these same fields Bc. The assignement of this bump to an usual Shubnikov - de Haas (S-d-H) effect requires the knowledge of the magnetic fields at which the quantum oscillations are expected to occur. Among the eigenvalues of the three bands k.p Hamiltonian in presence of a magnetic field, the ones assigned to the conduction band in both SM or SC narrow gap configurations are[17] :

$$E\ (N,\ k_z) = -\frac{|E_g|}{2} + \left(\frac{E_g^2}{2} + |E_g|\ D\ (N,\ k_z)\right)^{1/2}$$

$$D(N,\ k_z) = \hbar\ \omega_c\ (N + \tfrac{1}{2}) + \frac{\hbar^2\ k_z^2}{2m_n} \pm \frac{1}{2}\ \mu_B\ |g_o|\ B \qquad (11)$$

where $\omega_c = eB/m_n$ is the effective cyclotron frequency and $|g_o| = m_o/m_n$ is the absolute value of the g - factor at the bottom of the band, $\mu_B = e\hbar/2m_o$ is the Bohr magneton. m_n is given by Eq. 5. This dispersion relation is valid provided the energy E is quite small compared with the spin orbit coupling energy Δ_o. This condition was always fulfilled for both samples. The magnetic field B for which the N^{th} Landau level crosses the Fermi energy E_F at $k_z = 0$ is given by :

$$(N + \tfrac{1}{2} \pm \tfrac{1}{4})\ \frac{e\ \hbar\ B}{m_n} = E_F\ (1 + \frac{E_F}{E_g}) \qquad (12)$$

So far as the magnetic field is not so high that the last Landau level has crossed the Fermi one, we shall neglect the variations of E_F versus B. E_F will thus be taken equal to its numerical value at zero field. For a non parabolic band described by Eq. 3, E_F is related to n_1 by :

$$n_1 = \frac{8}{3\sqrt{\pi}} \left(\frac{2\pi\ m_n\ k_o T}{h^2}\right)^{3/2} \int_o^\infty \left(-\frac{\partial f_o}{\partial z}\right) z^{3/2}\ (1 + \gamma z)^{3/2} dz \qquad (13)$$

It will be shown in this section that $E_F/k_o T$ is always higher than 20. The electron gas is thus highly degenerate and Eq. 13 takes the simpler form :

$$n_1 = \frac{8}{3\pi}\left(\frac{2\pi m_n}{h^2}\right)^{3/2} E_F^{3/2}\left(1 + \frac{E_F}{|E_g|}\right)^{3/2} \qquad (14)$$

The Eq. 12 may then be written :

$$(N + \frac{1}{2} \pm \frac{1}{4})\ B = \frac{\hbar}{2e}\ (3\pi^2\ n_1)^{2/3} \qquad (15)$$

At T = 1.7°K, the plot of B_c versus $n_1^{2/3}$ reported in Fig. 8 fits quite well Eq. 15, and the identification of the experimental slope with the theoretical one leads to the following relation :

$$(N + \frac{1}{2} \pm \frac{1}{4}) = 0.74 \qquad (16)$$

This value is very close to 3/4 so that B_c is the magnetic field at which the last quantum oscillation occurs, when the down spin level of N = 0 labelled 0^+, crosses E_F. This suggests that the plateau and bumps, observed in Figs 3 and 7 respectively, are the 0^+ quantum oscillations on the R (B) and ρ (B) curves.

The study of the longitudinal magnetoresistivity ρ plotted versus B in Fig. 9 at 1.7°K and zero pressure, corroborates this conclusion. Three oscillations can be observed in this geometry. According to Eq. 15 the first two correspond to the quantum numbers N = 2 and N = 1, without spin splitting, which may arise from the fact that the width of the up and down spin levels of N = 1 and 2 is not small compared with their relative spacing $\hbar\omega_c/2$. In this geometry the 0^+ oscillation is missing, which is generally considered as a typical feature of this oscillation at very low temperatures[18, 19]. However as may be seen in this same Fig. 9, the 0^+ maximum is observed when the temperature is raised to 10°K.

We can notice that the effect on the Hall coefficient is most pronounced at 5.2 kbars, in the vicinity of the crossover pressure. The reason is that the high maximum of μ_1 at $P \simeq P_c$ exhibited in Fig. 6 leads to a maximum value of $\mu_1 B_c$ which emphasizes the observation of such quantum effects.

II.B.2. HgTe

Hall effect quantum oscillations were also observed for the HgTe sample at 1.7°K. In Fig. 10, we can see an oscillatory component of R (B) superimposed on a non oscillatory background marked out by a dashed line. From the extrapolated zero field Hall coefficient R (0), we can deduce an electron concentration $n_1 = 9 \times 10^{14}$ cm^{-3} at zero pressure. According to Eq. 15, the oscillations shown in Fig. 10 may be labelled N = 2, N = 1 and 0^+.

Once more, the spin splittings of both Landau levels N = 1 and 2 are missing. An analysis of the location of these oscillations versus B^{-1} gives approximately the same electron concentration as the one deduced from R (O). Nevertheless the Hall coefficient of this sample is so sensitive to field at low fields that it is difficult to determine R (O) with a good accuracy. Hereafter we shall deduce the electron concentration and the Fermi energy from the location of quantum oscillations rather than from R (O).

For HgTe, the values of m_n and E_g at these very low temperatures are given by[20] :

$$m_n = 0.031\ m_o$$
$$E_g\ (O) = -\ 302.5\ meV \qquad (17)$$

The Fermi energy calculated from Eqs. 14 and 17 at 1.7°K and zero pressure is $E_F = 1.04$ meV. In Eq. 12, we may neglect $E_F/|E_g|$ with respect to 1, so that the magnetic fields B_c at which the 0^+ oscillation occurs is given by the relation :

$$\frac{3}{4} B_c = \frac{1}{e\hbar}\ m_n\ E_F \qquad (18)$$

The oscillatory part of the Hall coefficient, ΔR, was also determined at P = 2 kbars and P = 4 kbars for this sample at T = 1.7°K. The pressure was found to induce a shift of the three oscillations. The plot of ΔR versus magnetic field is illustrated in Fig. 11 for the intermediate pressure P = 2 kbars. For the two others, we have only plotted the 0^+ oscillation, since its shift could be determined with the best accuracy. For P = 0, 2 and 4 kbars, the values of B_c are respectively 4.80, 4.56, and 4.32 kG, indicating that B_c varies linearly with P.

Considering Eq. 18, we may account for this linear variation when we assume :

(i) that the Fermi level does not significantly depend upon pressure. This assumption will be discussed in Section II.C., and allows us to write :

$$\frac{1}{B_c}\ \frac{dB_c}{dP} = \frac{1}{m_n}\ \frac{d\ m_n}{dP} = -\frac{1}{|E_g|}\ \frac{dE_g}{dP} \qquad (19)$$

(ii) That the effective mass varies linearly with the pressure through the energy gap E_g, according to Eqs. 5 and 8.

The knowledge of E_g and B_c at zero pressure, and that of dB_c/dP allows us to calculate $\alpha = dE_g/dP$ from Eq. 21. Taking all the experimental uncertainties into account, we find that the pressure coefficient of the energy gap E_g, at 1.7°K, is :

$$\frac{dE_g}{dP} = (8.5 \pm 0.5) \times 10^{-6} \text{ eV/bar} \qquad (22)$$

This value of α obtained for HgTe is very close to 8.2×10^{-6} eV/bar given for CdTe by Meltz and Ortenburger[22] at 77°K and 293°K.

We may then assume that the value of α does not depend strongly upon the composition at low temperature and is the same in HgTe and in the $x = 0.14$ sample, for which the energy gap at zero pressure, at 1.7 and 4.2°K, is then :

$$E_g (P = 0, x = 0.14) = - \alpha P_c = - 46 \pm 3 \text{ meV} \qquad (23)$$

For this sample with $x = 0.14$, the Eqs. 22 and 23 allowed us to calculate E_g at each pressure, but the determination of E_F still requires the knowledge of the matrix element P_K. The values of P_K reported in the litterature spread over a wide range.

The overall agreement between calculations and experiments performed in Ref. 5 was obtained for $P_K = (7.6 \pm 0.3) \times 10^{-8}$ eV cm, and in this paper, we have chosen $P_K = 7.6\ 10^{-8}$ eV cm for x = 0.14. The plot of its Fermi energy E_F versus pressure at 4.2°K, deduced from the Eqs. 5 and 14 is reported in Fig. 12. It must be noticed that in the whole range of pressures P < 6.5 kbars, $E_F > 8$ meV the electron gas would be completely degenerate, with $E_F/k_oT > 20$.

All through this Section, we have been mainly concerned with quantum effects on the Hall coefficient which, although observed since a long time, have been theoretically explained only recently, by Bastin et al[23]. We have been able to account for the positions and shifts of the oscillations for $B < B_c$, using the k.p method to describe the electron states in the conduction band of small gap SM or SC materials. The theoretical study of the Hall effect and magnetoresistivity at $B < B_c$, and in the so called ultra quantum limit, i.e. at $B > B_c$, also performed in Ref. 23 does not account for the strong variations of the non oscillatory background of the Hall coefficient,reported in Figs. 3 and 10, either for $B < B_c$ or for $B > B_c$. They will be analysed in the following Section as a two carrier type effect.

II.C. Two carrier type Hall effect

When two types of carriers are efficient in galvanomagnetic properties,an analysis[24] briefly summarized in Appendix A makes possible the determination of their respective concentrations (n_1, n_2) and mobilities (μ_1, μ_2). The (n, μ) set of parameters for both carrier types can be obtained for instance, by measurements of the Hall coefficient versus magnetic field R(B). The method then consists in plotting $A(B) = R(0)/[R(0) - R(B)]$ against B^{-2}. The low field limits of the Hall coefficient R(0), and of the conductivity $\sigma(0)$, together with A(B) are given by Eqs. A2, A3 and A4 respectively. They are functions of the Hall coefficients and conductivities of each carrier type ; (R_1, σ_1) and (R_2, σ_2). Under the assumption that R_1, σ_1, R_2, σ_2 are independent of the magnetic field, A(B) must present a linear dependance versus B^{-2} according to the law :

$$\frac{R(0)}{R(0) - R(B)} = a + s\ B^{-2} \qquad (24)$$

The slope s and intercept a are functions of R_1, σ_1, R_2, σ_2 (see Eqs. A4.2 and A4.3). According to Eq. A5, it is possible to determine both sets (R, σ) from the knowledge of R(0), $\sigma(0)$, a and s, whatever carrier types

we may have, electrons and electrons (e^-, e^-), or electrons and holes (e^-,h). In this latter case, the hole concentration will be called p instead of n_2. From now, the subscript 1 will index the electrons of the conduction band. In the limit of infinite magnetic field, the knowledge of $R(\infty)$ leads to a determination of p-n_1 (see Eq. A12.1) or $n_1 + n_2$ (see Eq. A12.2), according as the carrier types are (e^-, h) or (e^-,e^-). The intercept a in Eq. 24 is equal to $R(0)/\left[R(0) - R(\infty)\right]$ and gives a determination of $R(\infty)$.

II.C.1. HgTe at 1.7°K.

For this sample, the classical non oscillatory part of the Hall coefficient, $R_{NO}(B)$, distinctly present, was separated from the quantum oscillatory part (see Fig. 10). The plot of $R(0)/[R(0) - R_{NO}(B)]$ against B^{-2} in Fig. 13 is a straight line in the whole range of magnetic fields $B < 10$ kG. At zero pressure for instance, the complete solution of the set of Eqs. A5, deduced from R(0), $\sigma(0)$, a and s, shows the existence of two types of electrons, the concentration and mobility of which are respectively $n_1 = 8 \times 10^{14}$ cm^{-3}, $\mu_1 = 4.3 \times 10^5$ cm^{2}V^{-1}sec^{-1} and $n_2 = 7 \times 10^{14}$ cm^{-3}, $\mu_2 = 9 \times 10^3$cm^{2}V^{-1}sec^{-1}. The same analysis performed at the other investigated pressures did not give significant variations for the set of parameters n_2, μ_2 whereas μ_1 slowly increased and n_1 decreased, as in x = 0.14 sample, because of the deformation of the conduction band through E_g. Nevertheless, the relative variations of n_1, deduced from the shift of B_c in Fig. 11, and of μ_1, are much smaller than those observed in x = 0.14 sample within the range of available pressures, owing to the high value of $|E_g|$ in HgTe. If we may assign the first kind of electrons (i.e. those with a high mobility) to the Γ_8 conduction band, the presence of the second kind of electrons is more surprising when we consider the model of the band structure described in Section I. The presence of such slow electrons was already observed by Harman[25] who analysed magneto-Hall and magnetoresistivity measurements within the framework of a three carrier type model (two types of electrons, and one type of holes). He referred such an effect to the complex shape of the heavy hole valence band stemming from Γ_8. On n type HgTe samples, Yamamoto and Fukuroi[26] observed two sets of S-d-H oscillations with different periods, which they attributed to two kinds of electrons. They stressed the fact that the second kind of electrons should have a mobility $\mu_2 \simeq 10^4$cm^{2}V^{-1}sec^{-1} to fulfill the condition $\mu B \gg 1$ at magnetic fields as low as 9 kG.

According to more recent results concerning the electrical properties of HgTe and $Hg_{1-x}Cd_xTe$ alloys at low temperature, we may try to understand the existence of this second kind of electrons within the framework of these acceptor states located in the conduction band. As was already pointed out in

Ref. 7, such an acceptor level is broadened into a resonance, since it interferes with the conduction band continuum, so that the electrons located on these levels are expected to have a finite mobility, and may be efficient in transport phenomena. We shall then assume that these above evidenced electrons, with a mobility $\mu_2 = 9 \times 10^3 cm^2 V^{-1} sec^{-1}$ are coming from the N_A^- ionized acceptor states so that we may write :

$$N_A^- = n_2 = 7 \times 10^{14} cm^{-3} \qquad (25)$$

For quasi discrete levels, N_A^- is related to the concentration N_A of acceptor states, their energy E_A and the Fermi energy E_F (both measured from the Γ_8 level) by the expression[10] :

$$N_A^- = \frac{N_A}{1 + 4 \exp\left(\frac{E_A - E_F}{k_o T} \right)} \qquad (26)$$

Optical and electrical measurements in HgTe may be accounted for, assuming that an acceptor state is located at about 0.7 meV above the Γ_8 level[11, 13]. This level is probably due to the presence of Cu acceptor impurities[11]. In our sample, the Fermi energy determined in Section II.B. is $E_F = 1.04$ meV at zero pressure and $T = 1.7°K$ ($k_o T = 0.14$ meV), and for such an acceptor, Eq. 26 leads to $N_A^- \simeq 2 N_A/3$. Eq. 25 can thus be accounted for by the presence of a concentration $N_A \simeq 10^{15}$ cm^{-3} of Cu impurities.

The general equation for electrical neutrality is :

$$n_1 + N_A^- = p + N_D \qquad (27)$$

N_D is the concentration of donor states. Assuming the band scheme is the one depicted in Fig. 2, the hole concentration p is given by :

$$p = 2 \left(\frac{2\pi m_h k_o T}{h^2} \right)^{3/2} \mathcal{F}_{1/2} (-\eta') \qquad (28)$$

$$\mathcal{F}_{1/2}(\eta) = \frac{2}{\sqrt{\pi}} \int_0^\infty f_o(\eta) \, z^{1/2} \, dz \qquad (29)$$

$$\eta' = \frac{E_F + \varepsilon E_g - \Delta E}{k_o T} \qquad (30)$$

E_F is measured from the bottom of the conduction band as usual, while the reduced energy $z = E/k_oT$ is measured from the top of the valence band. When $E_g < 0$, $\varepsilon = 0$, and when $E_g > 0$, $\varepsilon = 1$, so that $E_F + \varepsilon E_g$ is the Fermi energy measured from Γ_8.

When $\eta' < 0$, we may use Boltzmann statistics to determine p :

$$p = 2\left(\frac{2\pi m_h k_o T}{h^2}\right)^{3/2} \exp\left(-\frac{E_F - \Delta E}{k_o T}\right) \qquad (31)$$

Assuming for the time being that $\Delta E = 0$, $E_F = 1.04$ meV and $m_p = 0.55\ m_o$, the hole concentration at 1.7°K should be $p \simeq 5.10^{12}$ cm^{-3}, which is quite negligible compared to $n_1 + N_A^- \simeq 1.5 \times 10^{15}$ cm^{-3}. So, the electrons in the conduction band and on the acceptor level must be supplied by donors, and Eq. 27 becomes : $n_1 + N_A^- = N_D$. Differentiating this equation with respect to the pressure, we obtain :

$$\frac{dn_1}{dP} = -\frac{dN_A^-}{dP} \qquad (32)$$

n_1 was found to decrease to an amount of $\Delta n_1 = 10^{14}$ cm^{-3} between 1 bar and 4 kbars. To account for an increase of N_A^- equal to $\Delta N_A^- = \Delta n_1$ according to Eq. 32, it would be necessary to increase E_F with pressure so much that taking this variation into account to differentiate Eq. 18, the calculation of α would lead to a pressure coefficient $\alpha \simeq 18 \times 10^{-6}$ eV bar^{-1}. Such a high value does not agree with those of the Γ point gap in zinc blende materials. Furthermore, as was said in this Section, such a variation of $n_2 = N_A^-$ was not experimentally observed. We are thus led to conclude that the electrons are supplied by valence band heavy holes rather than by donors, which is possible if we introduce an overlap ΔE as discussed in Section I. In order to fulfill the condition $n_1 + N_A^- = p$, with $p = 1.5 \times 10^{15}$ cm^{-3} at zero pressure, we must choose : $\Delta E < 1$ meV. The value of ΔE varies from 0.8 meV to 1 meV when m_h is varied from $0.55\ m_o$ to $0.3\ m_o$. Eq. 32 is then replaced by :

$$\frac{dn_1}{dP} - \frac{dp}{dP} = -\frac{dN_A^-}{dP} \qquad (33)$$

With such an overlap, only a very small shift of the Fermi level is required in order to make the variation of the hole concentration balance the electron one since :

(i) the density of states of the valence band is very high

(ii) the experimental dependence of p on E_F is exponential according to Eq. 31.

According to the smallness of the shift of E_F, we do not expect significant variations of N_A^- as experimentally observed. Consequently the variations of n_1, only induced by the deformation of the conduction band through the variations of E_g, are now balanced by the variations of p without any significant variation of E_F. The previous determination of α which assumed that $dE_F/dP \simeq 0$ is thus valid, and the value $\alpha = (8.5 \pm 0.5) \times 10^{-6}$ eV bar^{-1} is thus reliable.

We must notice that there are now three carrier types : electrons in the conduction band (n_1, μ_1), electrons on the acceptor level (n_2, μ_2), and holes (p, μ_p). The holes belong to the heavy hole valence band, and are expected to have a mobility $\mu_p \simeq 500$ cm^{2}V^{-1}sec^{-1} [9, 25, 27] so that $\mu_2 \gg \mu_p$. This may explain why in transport properties they were hidden by the electrons in the acceptor states, at least in the range of magnetic field we used.

II.C.2. $Hg_{0.86}Cd_{0.14}Te$ at 4.2°K.

For this sample, it was not possible to determine the non oscillatory part of the Hall coefficient $R_{NO}(B)$ hidden by quantum oscillations, in the range of magnetic fields $B < B_c$. The two carrier type analysis of $R_{NO}(B)$ was thus only possible in the range $B > B_c$ for which $R_{NO}(B) = R(B)$. Nevertheless, the plot of A(B) versus B^{-2} did not give a straight line. Such a plot is reported in Fig. 14 (a) (dashed line) as an example, at P = 4.1 kbars for $B_c < B < 10$ kG. However, at each pressure, it was possible to replace R(0) by such a parameter $R'(0)$ that the variations of $A'(B) = R'(0)/[R'(0) - R(B)]$ against B^{-2} were linear (see Fig. 14). Nevertheless, at P > 5.5 kbars, a departure from the straight line is observed at B > 7 kG (Fig. 14 (b). This effect will be discussed in Section IV. For the time being, we shall only notice that the range of magnetic fields $B_c < B < 7$ kG is wide enough to evidence a linear variation of $A'(B)$ versus B^{-2}, since $B_c < 2.4$ kG at such high pressures. The parameter $R'(0)$ was found lower than R(0) at all pressures, and can thus be written :

$$R'(0) = R(0)\,(1 - \lambda) \qquad (34)$$

Due to the high electron mobility in this sample $R(0) \simeq R_1$. So, the physical meaning of this equation is that there may be a relative variation λ of the electron Hall coefficient from its value R_1 in the low field limit to its value R'_1 in the ultraquantum limit. We may then write :

$$R'_1 = R_1 (1 - \lambda) \tag{35}$$

We found $\lambda < 0.1$ at $P < 3$ kbars, $\lambda = 0.2$ at $P = 4.1$ kbars and $\lambda < 0.05$ at $P > 5$ kbars. A possible explanation of Eq. 35 may be found from the analysis performed by Bastin et al[23] summarized in Appendix B. The linearity of the variations of $A'(B)$ versus B^{-2} leads us to expect that the variations of $R(B)$ versus B are induced by a two carrier type effect. Moreover such a behaviour of $A'(B)$ implies that the Hall coefficients and conductivities of the two carrier types do not significantly depend on the magnetic field (see Appendix A). In particular, this shows that σ_1, the only parameter for which a dependance on B is possible (see Appendix B), does not significantly vary in the range $B > B_c$ where the curves reported in Fig. 14 are straight lines. We shall then admit that its constant value is the one measured at zero magnetic field. The values of n_1 and μ_1 determined at each pressure by the solution of Eqs. A5 agree with those plotted in Fig. 5. The other carriers evidenced by this analysis are holes, with a concentration p, and a mobility $\mu_p = R_2\sigma_2$ plotted in Fig. 15.

We can notice two striking features of the hole mobility :

(i) its value is much higher than those determined for holes belonging either to the Γ_8 heavy hole valence band ($\mu_p \simeq 500$ $cm^2V^{-1}sec^{-1}$) or to impurity bands[9] ($\mu_p \ll 500$ $cm^2V^{-1}sec^{-1}$).

(ii) In the whole range of pressures, the hole concentration p was found higher than 10^{15} cm^{-3}. Since $(E_F + \epsilon E_g)/k_oT > 20$, Boltzmann statistics may be used to calculate p by the use of Eqs. 28 - 30 when we assume that the symmetry induced overlap can be neglected ($\Delta E = 0$). We then find $p < 10^5 cm^{-3}$, whatever may be the value of m_h in the range $0.3 < (m_h/m_o) < 0.7$, which is negligible with respect to the experimental value. We can thus admit that at such low temperatures the holes issue from valence states which have an higher energy than that of Γ_8. If we consider a finite value of ΔE in Eqs. 28 - 30, we can see that the agreement with the experimental hole concentration requires at each pressure $\Delta E \simeq E_F + \epsilon E_g$, which involves that ΔE is higher than 7 meV and varies with the pressure (see Fig. 12). Such values and

variations of ΔE are not consistent with the results obtained for HgTe, which leads us to think that the nature of the valence states extending above the Γ_8 point in this x = 0.14 sample is different from that of such states evidenced in the x = 0 sample. Otherwise, if we assume the existence of an overlap ΔE independent of P, with $\Delta E < E_F$ at any pressure whatever, the variations of E_F would induce exponential variations of p, since Boltzmann statistics might be used. This is not observed. We are thus led to assume that a density of valence states located above the Γ_8 point, $g_v(E)$, is superimposed on the density $g_v^o(E)$ of the heavy hole valence band states depicted in Fig. 2. $g_v(E)$ stretches to such high an energy E_R that degenerate statistics may be used to determine p.

For mathematical convenience, we shall describe the dependence of $g_v(E)$ upon E by an $E^{1/2}$ law as if we had a parabolic band (Fig. 16(a). The concentration of holes p is then given by :

$$p = \left(\frac{2m_v^*}{\hbar^2} \right)^{3/2} 3\pi^2 \, (E_R - E_F + \varepsilon E_g)^{3/2} \qquad (36)$$

where m_v^* is a density of states effective mass. In the SM configuration we have deduced from Figs 12 and 15, the variations of $p^{2/3}$ against E_F plotted in Fig. 17. This curve is approximately a straight line. In the rather small range of energies scanned by E_F, we thus find that the experimental curve may be fitted by Eq. 36. The intercept and the slope of the line determine the phenomenological parameters E_R and m_v^* :

$$E_R \simeq 17 \text{ meV}$$
$$m_v^* \simeq 2 \times 10^{-2} \, m_o \qquad (37)$$

According to the numerical values of m_h and m_v^* obtained within the above over-simplified description, the density of states $g_v^o(E)$ and $g_v(E)$ are in the same ratio as $(m_p/m_v^*)^{3/2} \simeq 150$, so that the density of valence states above Γ_8 is very small compared to the one below Γ_8.

A departure from the straight line reported in Fig. 17 was observed in the semiconductor configuration, but the model depicted by Eq. 36 does not have any physical significance. The physical result to be pointed out lies in the fact that $g_v(E)$ looks like a tail of density of valence states efficiently extending up to $E_R > 17$ meV beyond the Γ_8 point. This result

illustrated in Fig. 16 (b) will be discussed in Section IV but in any case this tail cannot be compared with the symmetry induced overlap ΔE evidenced in the HgTe sample.

From the knowledge of the number of holes, it is now possible to investigate the behaviour of the acceptor levels using the condition for electrical neutrality (Eq. 27). We show in Fig. 18 the variations of $p - n_1$ against pressure at 4.2°K. As already said in such small gap materials N_D is not expected to vary with pressure so that the decrease of $p - n_1$ observed in Fig. 18 in the SM configuration ($P < 5.5$ kbars) means that N_A^- decreases because of the deionization of an acceptor level. For $P > 5.5$ kbars, $p - n_1$ no longer varies. This overall behaviour of $p - n_1$ may be understood by assuming that two acceptor levels are present in this sample. Let N_{A1}, N_{A2} be their respective concentrations and E_{A1}, E_{A2} their respective energies measured from Γ_8 with $E_{A1} > E_{A2}$. We then have $N_A^- = N_{A1}^- + N_{A2}^-$. For $P < 5.5$ kbars, the E_{A1} level looses its electrons and N_A^- decreases because N_{A1}^- decreases. For $P > 5.5$ kbars this first level is almost empty and N_A^- is equal to the concentration N_{A2} of acceptor states in the second level, which are completely ionized ($N_{A2}^- = N_{A2}$) since N_A^- is constant in this range of pressures. For $P > 5.5$ kbars we then have $p - n_1 = N_{A2} - N_D$ with $N_{A2} - N_D \simeq 1.1 \times 10^{15}\,cm^{-3}$. For $P < 5.5$ kbars, by substracting this value of $N_{A2} - N_D$ from the value of $p - n_1$, we obtain the variations of N_{A1}^- against the pressure. N_{A1}, N_{A1}^-, E_{A1} and E_F are correlated by the relation :

$$N_{A1}^- = \frac{N_{A1}}{1 + 4 \exp \dfrac{E_{A1} - E_F - \varepsilon E_g}{k_o T}} \qquad (38)$$

As usual, $\varepsilon = 0$ for $E_g < 0$ and $\varepsilon = 1$ for $E_g > 0$. We shall see in Section III that $N_{A1} \simeq 8.5 \times 10^{15}\ cm^{-3}$. Using this result we have deduced from Eq. 38 the variations of $E_{A1} - E_F$ against pressure in the range $P < 5.4$ kbars in which this level is not completely empty (see Fig. 19). We can see on this figure that E_A always increases with respect to E_F in the SM configuration. At low pressures, the acceptor level is lower than the Fermi level, but crosses it at $P \simeq 3.7$ kbars.

In the following section, we are going to show how the large variations of N_A^- against pressure lead to the large enhancement of the electron mobility exhibited in Figs 5 and 6, and probably account for the variations of the hole mobility exhibited in Fig. 15.

III. MOBILITY AND RESONNANCES

The analysis of the electron mobility in small gap materials must take into account some of their particular features, mainly the symmetry of the elctron wave function in both SM and SC confgurations, and the problem of the static dielectric constant in the SM one. By the k.p method, we can deduce the wave function of an electron in an eigenstate belonging to the conduction band stemming either from Γ_8 or from Γ_6. In both cases, this wave function is a linear combination of one s-type and two p-type functions, respectively weighted by coefficients a, b and c which only depend on $E_F/|E_g|$ when $\Delta_o \gg |E_g|$. At Γ_6, $b = c = 0$ and $a = 1$ so that the wave function is s-type, while at Γ_8, $a = 0$ and it is p-type. At $k \neq 0$, the mixing is stronger as much as $E_F/|E_g|$ is greater than one, and is maximum when $E_g \simeq 0$. This problem was discussed in Ref. 5, when analysing the SM-SC transition at room and liquid nitrogen temperatures. Broermann[28] was the first to stress the importance of the p-type symmetry of the wave function to analyse the scattering by charged centers at low temperature in HgSe.

Otherwise, in such SM materials, the dielectric function $\varepsilon(q)$ diverges at zero momentum transfer at $T = 0°K$[29] in intrinsec regime, due to the symmetry induced degeneracy of the conduction and valence bands at Γ_8. This singularity is removed when carriers are present, but $\varepsilon(q)$ still depends on the carrier concentration n_1, according to the following expressions[30] :

$$\varepsilon(q) = \varepsilon_o + \varepsilon_1(q)$$
$$\varepsilon_1(q) = \frac{3e^2}{\Gamma\hbar}\left(\frac{2m_n}{E_F}\right)^{1/2} f(q) \qquad (39)$$

ε_1 is an interband part, calculated in the Random Phase Approximation (R.P.A.), which appears because the conduction and heavy hole valence bands are degenerate at Γ_8. ε_o is a background part due to all other bands. The interband part ε_1 depends on the momentum transfer through f(q) so that the screened coulombian potential due to an impurity is no longer of the Yukawa form.

These features were taken into account by Broerman[31] in a calculation of the ionized impurity limited mobility of HgTe and HgSe. It will be shown that the calculated and measured mobilities agree fairly well for our HgTe sample.

In Eq. 39, $f(q = 0) = 4/3$[30]. Neglecting the variations of the dielectric function with q, Gel'mont et al[32] used $\varepsilon(q = 0)$ to calculate μ_1 versus n_1 in HgTe at low temperature. In the whole range of concentrations, the agreement between the results of Gel'mont et al and those of Broerman was better than 10%, which justifies the approximation $\varepsilon(q) \simeq \varepsilon(q = 0)$.

In the above calculations, the non parabolicity of the conduction band was neglected. This effect has been discussed by Broerman[33] in α - Sn, for which is was found negligible owing to the high value of $|E_g|$. The same is not the case when $E_g \simeq 0$, and it was shown in Ref. 32 that the effect of the interband screening was negligible, owing to the decrease of the density of states in the conduction band, and the moving up of the Fermi level. The mobility in the x = 0.14 sample will be analysed by completely neglecting the interband part $\varepsilon_1(q = 0)$ in Eq. 39 but taking into account the true symmetry of the wave function. Under the assumption that $\Delta_o \gg |E_g|$, we shall use the following expression of μ_1[5] :

$$\mu_1 = A_{cc} \left(\frac{m_n}{m_o}\right) - 1/2 \frac{(k_o T)^{3/2}}{{}^{o}L_o^{3/2}} \int_o^\infty - \frac{\partial f_o}{\partial z} \frac{1}{F} \frac{z^3(1 + \gamma z)^3}{(1 + 2\gamma z)^2} dz \qquad (40)$$

$${}^{o}L_o^{3/2} = \int_o^\infty \left(- \frac{\partial f_o}{\partial z}\right) (z + \gamma z^2)^{3/2} dz$$

$$F = \text{Log}(1+\xi) - \frac{\xi}{1+\xi} - (4L - L^2)\left[1 + \frac{1}{1+\xi} - \frac{2}{\xi}\text{Log}(1+\xi)\right] + \frac{3}{2}L^2\left(1 - \frac{4}{\xi}\right) \qquad (41)$$

The L factor[34] measures the importance of the p component of the wave function. Its expression depends on the symmetry of the extremum Γ_8 or Γ_6 of the conduction band[5] :

$$L(\Gamma_8) = \frac{E_F + |E_g|}{|E_g| + 2E_F} \qquad L(\Gamma_6) = \frac{E_F}{E_F + 2|E_g|} \qquad (42)$$

$L(\Gamma_8)$ and $L(\Gamma_6)$ are respectively used when $E_g < 0$ and $E_g > 0$.

$\xi = 4k^2R^2$, k is the wave vector, and R is the scattering length in the Thomas-Fermi approximation :

$$R^{-2} = \frac{2}{\pi} \frac{e^2}{\varepsilon_o k_o T} \left(\frac{2m_n k_o T}{\hbar^2}\right)^{3/2} \int_o^\infty \left(- \frac{\partial f^o}{\partial z}\right) (z + \gamma z^2)^{1/2}(1 + 2\gamma z) dz \qquad (43)$$

When the mobility is expressed in $cm^2V^{-1}sec^{-1}$:

$$A_{cc} \simeq 3 \times 10^{16} \frac{\varepsilon_o^2}{N_{cc}} \qquad (44)$$

N_{cc} is the concentration of scattering charge centers expressed in cm^{-3}. When the scattering by the holes (considered as fixed charges) is taken into account :

$$N_{cc} = p + N_D + N_A^- = n_1 + 2N_A^- \qquad (45)$$

In Eqs. 40 and 43, m_n is given by Eq. 5.

Since the electron gas in x = 0.14 sample is degenerate, we shall assume that $-(\partial f_o/\partial z) = \delta (x - \eta)$, δ being the Dirac function and $\eta = E_F/k_oT$. Eq. 40 can then be written :

$$\mu_1 = C \frac{1}{N_{cc}} \frac{[E_F (E_F + |E_g|)]^{3/2}}{F [|E_g| + 2E_F]^2} \qquad (46)$$

C is a numerical constant since ε_o is a constant. μ_1 is thus the product of a term $1/N_{cc}$ accounting for the effect of the number of ionized scattering centers, by a term accounting for the effect of the pressure on the band structure through $|E_g|$. In order to illustrate only the second one, we have plotted in Fig. 20 the relative variations of the product $\mu_1 \times N_{cc}$ at 4.2°K. μ_1 has been deduced from the experimental results reported in Fig. 5. In the same figure, we have plotted the theoretical variations of $\mu_1 \times N_{cc}$ deduced from Eq. 46. We have used a matrix element $P_k = 7.6 \times 10^{-8}$ eV cm and a pressure coefficient $\alpha = 8.5 \times 10^{-6}$ eV bar^{-1}. The Fermi energy has been given in Fig. 12. The experimental curve obtained under the assumption $N_D = 0$ by the use of the values of $p - n = N_A^-$ given in Fig. 18 presents a significant departure from the theoretical curve. On the other hand, this latter curve fits quite well another experimental curve, obtained by assuming that $N_D = 4 \times 10^{14}$ cm^{-3} (in which case $N_A^- = (p - n_1) + N_D$), except in the vicinity of P = 3.7 kbars. The shape of the curves in Fig. 20 is very different from that of the curve $\mu_1(P)$ plotted in Fig. 5. The high maximum of μ_1 at $P \simeq 5.8$ kbars does not exist in Fig. 20, and is thus due to the variations of N_A^- rather than a zero gap effect on the band structure.

A similar analysis may be performed for the hole mobility μ_p reported in Fig. 15. Assuming that these holes are only scattered by fixed charges, we have plotted the product of the concentration N_{cc} of such scattering centers by μ_p against pressure at 4.2°K in Fig. 21 when we have

$N_{cc} = N_A^-$ with $N_A^- = p - n_1$ (Fig. 21 (a)) and $N_{cc} = N_A^- + N_D$ with $N_A^- + N_D = p - n_1 + 2N_D$ and $N_D = 4 \times 10^{14}$ cm^{-3} (Fig. 21 (b)). A dip is again evidenced in the range of pressures 2 kbars to 4 kbars.

According to the discussion performed in the previous Section II.C two kinds of acceptor levels contribute to N_A^- :

$$N_A^- = N_{A1}^- + N_{A2}^- \qquad (47)$$

From now, we shall take $N_D = 4 \times 10^{14}$ cm^{-3} since this donor concentration was required to fit the variations of μ_1 versus P at 4.2°K. The analysis of the low field Hall coefficient versus P at 77°K[5] led to : $N_A - N_D = 10^{16}$ cm^{-3}. For P > 5.5 kbars at 4.2°K, we have shown that $N_{A1}^- \simeq 0$, $N_{A2}^- \simeq N_{A2}$ and Eq. 47 can be written : $N_A^- \simeq N_{A2}$; we can then deduce from Fig. 17 and Eq. 27 : $N_{A2} \simeq 1.5 \times 10^{15}$ cm^{-3}, so that $N_{A1} \simeq 8.5 \times 10^{15}$ cm^{-3}. Such a value of N_{A1} was used in Section II.C. to determine $E_{A1} - E_F$ at 4.2°K plotted in Fig. 19. E_{A1} crosses E_F around P = 3.7 kbars, the same pressure as the one at which dips appear on the curves reported in Figs 20 and 21. To bring out the dip on the curve $\mu_1 N_{cc}$ versus pressure, we have reported in Fig. 22 the variations of $[(\mu_1 N_{cc})_{cal} - (\mu_1 N_{cc})_{exp}]/(\mu_1 N_{cc})_{cal}$ against pressure. The subscripts "cal" and "exp" denote respectively calculated and experimental values of $\mu_1 N_{cc}$. This curve is a bump with a resonant like shape, centered at P $\simeq$ 3.7 kbars. This accident on the curve $\mu_1 N_{cc}$ versus P is expected to occur on the curve $\mu_1(P)$ since $N_{cc} = n_1 + 2N_A^-$ decreases in a large but monotonous manner according to Figs 5 and 18. Nevertheless, such an effect could hardly be evidenced in Fig. 5 since it was hidden by the much more important variations of n_1 and N_A^-. It is only after the contribution of these variations has been suppressed by plotting $\mu_1 N_{cc}$ instead of μ_1 that we can observe this resonant effect. Within the framework of the relaxation time approximation, the mobility of a degenerate gas takes the form $\mu = e\,\tau(E)/m(E)$ with $\tau(E) = A(E)/N_{cc}$ so that the product $\mu_1 N_{cc}$ may be written :

$$\mu_1 N_{cc} = e \frac{A(E)}{m(E)} \qquad (48)$$

The singularities observed in Figs 21 and 22 around P = 3.7 kbars are then understood as a resonant effect induced by the acceptor level on A(E). The curve 1 in Fig. 21 also shows that, under the validity of this

analysis, the energy dependent part A(E) of the relaxation time of holes does not depend on pressure away from the resonance. This result is reliable according to the expected small effect of the pressure on the tail of density of Γ_8 heavy hole valence band states.

An increase of the temperature also produces a shift of E_F which crosses E_A at a temperature T_o defined by $E_F(T_o) = E_A$. At this temperature an accident occurs not only on the variations of the conductivity and mobility versus temperature but also on the variations of the low field Hall coefficient R(T) versus temperature[10,11]. This effect can be observed at $T_o \simeq 10°K$ on those of the R(T) curves plotted in Fig. 4 which were obtained at $P > 3.7$ kbars. Since an increase of the temperature induces an increase of E_F, the equation $E_F(T_o) = E_{A1}$ can be satisfied in the range of temperatures investigated $4.2 < T < 77°K$ only when $E_F\ (4.2°K) < E_A$. According to the curve plotted in Fig. 12, this condition is equivalent to $P > 3.7$ kbars and explains why the dip on these curves was not observed at lower pressures. Otherwise, these experimental results on the Hall coefficient evidence the fact that at $4.2°K, E_F \simeq E_{A1}$ when $P \simeq 3.7$ kbars. This allows us to rely upon the determination of N_{A1} versus pressure, from which this result was first deduced, and corroborates the assertion according to which N_D is small ($N_D \simeq 4 \times 10^{14}$ cm^{-3}).

After having discussed the resonant effects induced by variations of temperature or pressure, we shall now discuss similar effects observed by allowing the magnetic field to vary. According to the analysis summarized in Appendix B, (in our case $N_{cc} > n_1$), the magnitude of the parameter λ in Eq. 35 depends on the scattering amplitude f of the impurity potential according to Eq. B7. It is thus expected that the nearer the Fermi level will be from the acceptor one, the larger will be λ. This may be the reason why λ was found maximum around $P \simeq 4$ kbars ($\lambda = 0.2$), while it was only equal to 0.1 at $P < 3$ kbars and 0.05 in the SC configuration.

Otherwise, in the SC configuration, a departure from the straight line was noticed in Section II.C., when plotting A'(B) versus B^{-2}, for magnetic fields $B > B_o$, which defines B_o (Fig. 14(b)). On the curves R(B), this effect leads to a Hall coefficient vanishing, without becoming positive although this $x = 0.14$ sample is p - type. It can be noticed from Fig. 14 (b) that $B_o > 3B_c$. At such high magnetic fields, $B_o > B > 3B_c$, all the electrons in the conduction band condense on the 0^- Landau level, and the Fermi level then remains clamped to it, so that E_F is determined at each field by the use of Eq. 12 :

$$\frac{1}{4}\ \frac{e\hbar B}{m_n} = E_F\ (1 + \frac{E_F}{|E_g|}) \qquad (49)$$

The abnormal behaviour of R(B) at $B > B_o$ may then be tentatively attributed to the fact that the 0^- Landau level crosses the acceptor level A_1 at $B = B_o$. This also means that the acceptor level crosses the Fermi level : $E_F = E_{A1} - \epsilon E_g$ so that Eq. 49 can be written :

$$\frac{1}{4}\ \frac{e\hbar\ B_o}{m_n} = (E_{A1} - \epsilon E_g)\ (1 + \frac{E_{A1} - \epsilon E_g}{|E_g|}) \qquad (50)$$

Eqs 50 and 18 then show that in first approximation :

$$E_{A1} - \epsilon E_g \simeq \frac{B_o}{3B_c}\ E_F \qquad (51)$$

E_F has been plotted versus pressure in Fig. 12. For example, at P = 6.4 kbars, $B_o \simeq 6.3$ kG (See Fig. 14 (b)), $B_c \simeq 1.8$ kG (See Fig. 3 (b)), $E_F(0) \simeq 9$ meV, so that Eq. 51 leads to $E_A - \epsilon E_g - E_F = 0.16\ E_F = 1.5$ meV. This value was also reported in Fig. 19.

At $B > B_o$, the electrons on the 0^- level fall into the acceptor level. They are then in resonant states and have a much smaller mobility. We could have a low field Hall effect with holes, and slow electrons having a small mobility, described by Eq. A2. Such a picture is fit to account for the behaviour of R(B) at $B > B_o$. Since $B_o \simeq 3B_c$, and the maximum field we could obtain in the experimental set up was $B \simeq 9$ kG, we can reach B_o provided that $B_c < 3$ kG, which is fulfilled at P > 5.2 kbars. This explains why these effects could not be evidenced in the SM configuration.

For HgTe, the complete calculation of the mobility has been already performed by Broerman[31]. He gives the results of his calculation for a given number of donors (curve $N_A = 0$ in Fig. 2 of this reference). For the electron concentration $n_1 = 8 \times 10^{14}\ cm^{-3}$ determined in Section II, the electron mobility is $\mu_1 \simeq 1.2 \times 10^6\ cm^2V^{-1}sec^{-1}$, when only donors are present ($N_{cc} \simeq n_1 = 8 \times 10^{14} cm^{-3}$). In our case, $N_{cc} = n + 2N_A^- \simeq 2.2\ 10^{15} cm^{-3}$. Performing the correction due to the difference of the concentrations of scattering centers, we obtain a calculated value of the mobility of $\mu_1 = 4.4\ 10^5 cm^2V^{-1}sec^{-1}$, in close agreement with the experimental one ($\mu_1 \simeq 4.3 \times 10^5 cm^2V^{-1}sec^{-1}$).

In order to account for the absolute value of μ_1 obtained for $x = 0.14$ sample from Eqs 44 and 46, we must use a static dielectric constant $\varepsilon_o \simeq 11$, much lower than any linear interpolation between the well known value $\varepsilon_o \simeq 9.25$ in CdTe[35] and the published value $18 < \varepsilon\ (q = 0) < 20$ for HgTe[36]. Nevertheless, for HgTe, this value was determined at 77°K in intrinsec regime, when $E_F \simeq 30$ meV. Owing to the high value of m_n, the Eq. 39 leads to $\varepsilon_1 = 7$ to 8, so that the part of the dielectric constant induced by all the transitions except the interband $\Gamma_8 - \Gamma_8$ ones would be $\varepsilon_o \simeq 12$. The value of 11 thus obtained for the $x = 0.14$ sample would then not be so strange, due to the fact that any RPA correction disappears when $m_n \longrightarrow 0$.

IV. DISCUSSION

Two kinds of results are to be discussed in this section. The first one concerns the electronic band structure of the materials studied in this paper, and is discussed in Section A. The second one concerns the acceptor levels. Their location together with the mobilities and resonant effects are discussed in Section B.

A. Electronic structure

The analysis of the 0^+ quantum oscillation, and of its shift induced by pressure, as well as the analysis of the background of the curve $\mu_1 N_{cc}$ vs P for the $x = 0.14$ sample in Fig. 20, supported quite well the picture of the conduction band described by the k.p method.

Morever, the change of slope of the curve n_1 vs P in Figs 5 and 6 for the $x = 0.14$ sample was assigned to the crossover of the Γ_6 and Γ_8 levels. Such an interpretation accounted for the results obtained in Ref. 4 when analysing the low field Hall coefficient versus pressure in almost intrinsic materials at 77°K and 292°K. The change of slope was understood as due to the existence of the two competing effects of the opening of the gap and of the increase of the density of states of the conduction band. At such temperatures, $|dn_1/dP|_{SC} < |dn_1/dP|_{SM}$; at 4.2°K and 1.7°K, if we assume the band structure is the one depicted in Fig. 2, the opening of the gap should lead to a drastic decrease of n_1 which could not be balanced by the increase of density of states since the thermal activation energy is

quite small, and we should have $\left| dn_1/dP \right|_{SC} > \left| dn_1/dP \right|_{SM}$. On the contrary, the existence of the tail of the density of valence states (See Fig. 16) leads to a diminution of the effect of the crossover of the Γ_8 and Γ_6 levels since the electrons in the conduction band issue from valence states which are still located in the conduction band. We may thus have again $\left| dn_1/dP \right|_{SC} < \left| dn_1/dP \right|_{SM}$ as it is observed in Figs 5 and 6. For the same reason, it was not possible, even at such a low temperature as 1.7°K, to lower the Fermi energy E_F in the true vicinity of the Γ_8 level, whereas that was possible in the HgTe sample.

For this last sample, experimental results fitted the existence of an overlap ΔE of the valence and conduction bands induced by the lack of inversion symmetry. We found $\Delta E < 1$ meV, in agreement with the previous experimental determinations[37 - 39]. Theoretically, Overhof[40] has found $\Delta E \simeq 0.3$ meV.

On the contrary the results obtained on the $x = 0.14$ sample cannot be understood by taking into account such a symmetry induced overlap. It has been shown that, according to Eq. 38, the density of valence states extending beyond the Γ_8 point looks like a tail. Such an effect may be understood in the framework of alloy theories[41, 42] and is expected to be associated with "clustering", e.g. local departures from stoechiometry. In effect, the energy of the Γ_8 level, as well as E_g are expected to depend upon x. So intuitive arguments suggest that flcutuations Δx of x induce fluctuations of $E(\Gamma_8)$. Consequently some states of the valence band corresponding to a concentration $x - \Delta x < x' < x + \Delta x$ may exist at energies between $E(\Gamma_8)_{x - \Delta x}$ and $E(\Gamma_8)_{x + \Delta x}$, and so at energies $E > E(\Gamma_8)_x$. These states contribute a tail to the density of the valence band. Without giving a detailed shape, Eqs. 37 show that this tail should extend up to 17 meV from the Γ_8 point, and Eq. 38 gives an order of magnitude of the number of valence states displaced from the usual band into the tail. Nevertheless it should be noticed that the magnitude of this tail, according to its cause, widely depends on the technique used to induce the growth of the crystal. In particular this tail may be almost non-existent for materials suitable prepared. Both the existence of the tail and the values of the parameters ΔE and m_v^* are thus features particular to this sample and not a specific effect of these materials.

Likewise, another tail is expected to issue from the conduction band, stretching in the valence band for the whole range of pressures investigated. Nevertheless, the numbers of conduction and valence states

induced by the alloying effect away from the extrema of the conduction and valence bands are expected to be in the ratio of the respective effective masses of the state density of these two bands. Since $m_n \ll m_h$ we can thus neglect this other tail.

If the disorder effects on the valence band accounts quite well for the experimental results at 4.2°K, we must also ascertain that the same is the case at T > 77°K, when Kane's model remains valid to describe the electronic transport properties of the alloy. In fact it is well expected that it is so indeed, since a tail only effects states which are in the vicinity of the band edge Γ_8, and not those which are at a distance from this point larger than E_R. To corroborate this argument, numerical calculations were performed with the help of a computer to determine the concentration of electrons n_1, of holes p, and the Fermi energy E_F of this sample at 77°K. Those calculations were performed with and without a tail characterized by Eq. 37 superimposed on the Kane's valence band. The results are identical in both cases within 2 %. The physical reason is that, at T > 77°K, the thermal activation energy k_oT being high enough to generate holes from states below the Γ_8 point, the tail does not have any significant effect on the statistical equilibrium at these temperatures since $m^*_v \ll m_h$.

On the contrary, at 4.2°K, the tail not only allows us to understand why holes are in such high concentrations as those experimentally observed, but also acts as a reservoir of electrons. In effect, at each pressure, those of the electrons in the valence states of the tail which have an energy $E > E_{A1}$ flow into the conduction band states and fill this band up to the acceptor level, which explains why we found at each pressure $E_F \simeq E_A$ within less than 2 meV.

From the analysis of the shift of the 0^+ quantum oscillation induced by pressure in the HgTe sample , we found a pressure coefficient $dE_g/dP = (8.5 \pm 0.5) \times 10^{-6}$ eV bar^{-1} at 4.2°K and 1.7°K.

Otherwise, the theoretical law $E_g(x)$ at T = 0 and P = 1 bar given by Chadi and Cohen[43] for $Hg_{1-x}Cd_xTe$ alloys is $E_g(x) = -302.5 + 1830\,x$. According to this law, we should have, for the x = 0.14 sample $E_g^o \simeq 47$meV, which agrees with our result ($E_g^o \simeq 46 \pm 3$ meV). A detailed discussion about this numerical value of the pressure coefficient of the energy gap is reported in Ref. 5.

B. Location of the acceptor levels

According to the submillimeter and far infrared magnetoabsorption experiments on HgTe reported in Ref. 13, together with the discussion on the nature of these acceptor levels in HgTe and $Hg_{1-x}Cd_xTe$ alloys reported

in Ref. 11, the level located at 0.7 meV above the Γ_8 point in HgTe is expected to be induced by Cu impurities. The perturbing potential in such a case is Coulombian, so that this level will not significantly vary with a change of the density of conduction band states induced by the pressure as can be shown from the calculation by Gel'mont and D'yakonov. This is consistent with the analysis developped, in Section II.B., to determine the pressure coefficient in the HgTe sample. For the same reason, the activation energy of this acceptor state is not expected to depend on the variation of E_g induced by a variation of composition. We then should have for such a level an activation energy E_A close to 1 meV even in $x = 0.14$ sample. We may then assume that the completely ionized level observed for pressures $P > P_c$ in the SC configuration (Fig. 18) should be assigned to Cu impurities , with a concentration $N_{A2} = 1.5 \times 10^{15} cm^{-3}$.

For $x = 0.14$ sample, it was possible to show another acceptor level for which the activation energy, labelled E_{A1} in the previous sections, widely increased with pressure. We have plotted in Fig. 23 E_{A1} (measured from Γ_8) versus pressure. E_{A1} was deduced from the knowledge of $E_F + \epsilon E_g - E_{A1}$ and of E_F reported in Figs. 12 and 19. In the SM configuration, the increase of E_{A1} implies that the acceptor level moves up in the conduction band when P increases, i.e. when the density of states in this band decreases, according to Eqs. 3 and 22. Variations of E_g may also be induced by variations of the composition x, and the same behaviour of E_{A1} versus E_g in the SM configuration was reported in Ref. 11 from galvanomagnetic measurements performed on various compositions versus temperature at ambiant pressure. It is shown in this reference that the acceptor level A_1 observed in the $x = 0.14$ sample is also present in HgTe with an activation energy $E_{A1} = 2.25$ meV. Such large variations of E_{A1} either with pressure or composition are by no means consistent with a Coulombian potential, but can be accounted for when assuming that we have a localized potential[14], like those induced by crystalline defects involving for instance mercury vacancies. In the SC configuration, i.e. for pressures $P > 5.4$ kbars, the Fig. 23 shows that the acceptor level E_{A1} still rises with respect to the Γ_8 point, and has a pressure coefficient dE_{A1}/dP larger than in the SM configuration. The physical reason of such an effect is that the opening of the gap may be considered as a dramatic decrease of the density of conduction band states in the true vicinity of Γ_8, in the range of energies $E(\Gamma_8) < E < E(\Gamma_8) + E_g$. Nevertheless, the larger

the gap in this SC configuration, the nearer we approach the configuration in which only the valence band must be taken into account to determine E_{A1} which then no further moves. This effect, together with the increase of the density of conduction band states at energies $E > E(\Gamma_6)$ (far from the Γ_8 point) attenuate the increase of E_{A1} with E_g and allows us to understand why the acceptor level is found to move down in the conduction band, with respect to the Γ_6 point, or in order words why $dE_{A1}/dP < dE_g/dP$, as can be seen in Fig. 23. All these points will be further discussed theoretically in Ref. 14.

The presence of such acceptor levels leads us to take into account two scattering mechanismes. The first one is the scattering by the localized potential leading to the existence of a resonance, efficient only for electrons the energy of which lies in the range $[E_{A1} - \Delta E_{A1}/2, E_{A1} + \Delta E_{A1}/2]$ where ΔE_{A1} is the width of the resonance. The second one is induced by the fact that, as will be seen below, the resonance is narrow enough to be considered as a quasi discrete level. The electrons in resonant states then act as almost localized electrostatic charges, and thus give rise to a Coulombian potential. The other electrons in the conduction band with a high mobility screen this long range potential and are thus scattered by it. This scattering mechanism was found to account quite well for the values of $\mu_1 N_{cc}$ in the whole range of pressures for which the first mechanism can be neglected, as can be seen in Fig. 20. In the range of pressures $2.8 < P < 4.5$ kbars, $|E_{A1} - E_F| < k_oT$, and a part of the electrons efficient in transport phenomena, thus having an energy E in the range $[E_F - k_oT, E_F + k_oT]$, is scattered in a resonant manner by the localized potential. This additional screening leads to the dip in the curves in Fig. 20, or the bump of the curve in Fig. 22 which we shall now analyse.

For temperatures $k_oT \ll \Delta E_A$, when the condition $E_F = E_{A1}$ is fulfilled, all the electrons in the range k_oT around E_F would undergo a resonant scattering. By scanning E_F in a range ΔE_A around E_A, one should perform a spectroscopy of the resonance. The measured electron mobility should then be very smalll and should be that of the electrons resonantly scattered. The bump in Fig. 22 has an half width equal to about 1 kbar and is centered at $P \simeq 3.7$ kbars. According to the results plotted in Fig. 12, the shift of the Fermi energy in this range of pressures is around 0.3 meV. An estimation of the width of the acceptor level should then be $\Delta E_{A1} \simeq 0.3$ meV for an energy gap $E_g = -14$ meV, which is the value of E_g at 3.7 kbars for $x = 0.14$ sample at 4.2°K. Since $k_oT \simeq 0.36$ meV, $k_oT \simeq \Delta E_{A1}$ and the condition

$k_oT \ll \Delta E_{A1}$ is not fulfilled. It is thus possible that the value of ΔE_{A1} so determined is rather the width of the Fermi level, and not exactly the width of the acceptor level, for which 0.3 meV should be an upper limit. Since $k_oT > \Delta E_{A1}$, only a small amount of the electrons efficient in transport phenomena are concerned with the resonant scattering, even when the acceptor level is in the range k_oT around E_F, so that the transport properties are not fundamentally modified. This may explain why the resonance observed in Fig. 20 gives a quite small effect which does not exceed ten per cent of the background of the curve $\mu_1 N_{cc}$ versus P. Consequently, the experimental mobility measured for $P \simeq 3.7$ kbars on this sample cannot be correlated with the mobility μ_R of the electrons in the resonance.

As already shown in Section II, this mobility could be determined in the HgTe sample by the analysis of the two carrier types Hall effect. Using a similar procedure, Zakrzewski and Dziuba also determined such a mobility μ_R of electrons in HgTe, which they attributedto an impurity band[44]. For x = 0.14 sample, the determination of μ_R could not be performed at 4.2°K since the two carrier type analysis showed the presence of electrons in the conduction band states, and of holes. In order to understand why , in this sample, the holes prevail over the second kind of electrons in resonant states, we suppose that, at 4.2°K, $\mu_R < \mu_P$ or, according to the Fig. 16, $\mu_R < 2000$ $cm^2V^{-1}sec^{-1}$. However, at 90°K, the plot of $R(0)/[R(B) - R(0)]$ against B^{-2} illustrated in Fig. 24 at 4 kbars and 5 kbars gave a straight line in the whole range of magnetic fields $B < 9.5$ kG available in the experimental set up. The solution of Eqs A5 showed that, at this temperature, the two efficient carriers were two types of electrons, so that the situation was quite similar to that of the x = 0 sample at 1.7°K. The concentration of the second type of electrons was about 9×10^{15} cm^{-3} and shows that these electrons are in the N_{A1} completely ionized acceptor states. Their mobility was found to be $\mu_R \simeq 2000$ $cm^2V^{-1}sec^{-1}$, larger than the expected value at 4.2°K, and equal to the one recently found in $Hg_{1-x}Cd_xTe$ alloys for various compositions[45]. It should be noticed that this mobility is high enough so that these resonant electrons prevail over holes in transport phenomena. The reason is that at 90°K, most of the holes arise from the host valence band below the Γ_8 point and are thus classical ones with a mobility which is expected to be $\mu_P \simeq 500$ $cm^2V^{-1}sec^{-1}$ so that $\mu_P \ll \mu_R$. It is not surprising, under such conditions, not to observe holes at 90°K.

It has been shown otherwise that the mobility of electrons on Cu acceptor states in the x = 0 sample was $\mu_R \simeq 9000$ $cm^2V^{-1}sec^{-1}$.

Nevertheless, the large decrease of both m_n and the density of conduction band states, is expected to lower greatly this mobility in $x = 0.14$ sample[14]. As a matter of fact, such electrons could not be evidenced in this sample whatever were the temperature and pressure. This illustrates the fact that the characteristic features of the resonances, like their width or the mobility μ_R depend on the density of states in their vicinity or in other words depend on E_g. The results described in this paper are thus only partial and measurements of transport properties like those performed for this $x = 0.14$ sample at 4.2°K are needed to investigate the resonance parameters μ_R and E_A more systematically. Attention should then be drawn to the fact that the resonant effects cannot be exhibited at first sight from experiment, since it is necessary to take into account the variations of the concentration of scattering centers N_{cc} when E_F moves with respect to E_A. Such variations are important in the vicinity of $E_F \simeq E_A$ and widely affect the Hall coefficient and the mobility of the carriers in the vicinity of the resonance, as it is illustrated by the comparison of the curves in Figs. 5 and 15 with those in Figs. 20 and 21.

Otherwise, when ΔE_A and k_oT have the same order of magnitude, the investigation of ΔE_A and μ_R is difficult as was shown above. In this common case, the analysis of transport properties versus T performed in order to observe temperature induced resonances like those plotted in Fig. 4 are not a convenient means of determining ΔE_A, because of the enlargment of the spread out k_oT of the Fermi level . The width $\Delta E_A \simeq 0.3$ meV for $E_g \simeq -14$ meV determined from the pressure induced resonance is very small. The mobility $\mu_R \simeq 2000$ $cm^2V^{-1}sec^{-1}$ for $x = 0.14$ sample at 90°K was also quite small compared to that of the electrons in the conduction band states. Such values of ΔE_{A1} and μ_R corroborate with the fact that the level is quasi discrete and that the electrons in resonant states are almost localized.

Moreover, at 90°K, these acceptor states were found occupied, so that this level is expected to be still in the conduction band when the energy gap is $E_g \simeq +40$ meV at 5 kbars. The investigation of such levels in small gap semiconductors obtained for a concentration of Cd atoms $x > 16$ % should allow a determination of the value of E_g beyond which this level falls into the energy gap.

CONCLUSIONS

In this work, the transport properties at low temperature exhibited by $Hg_{0.86}Cd_{0.14}Te$ within the semimetal-to-semiconductor transition induced by hydrostatic pressure, give a strong experimental evidence of the resonant configuration of acceptor states occuring in vanishing bandgap HgCdTe - like materials. In particular, useful informations are obtained about the heights E_A and the resonance widths ΔE of the virtual states A_1 and A_o, corresponding to Hg - vacancies and substitutional Cu-impurities respectively. In the general context of virtual electronic states as widely observed in solid state physics, the HgCdTe system offers the interesting possibility of a unique tool to study the effect of changes of conduction band density of states n(E) upon E_A and ΔE_A. In the present work, these features are illustrated by a comparison of the results obtained on HgTe and $Hg_{0.86}Cd_{0.14}Te$ and by the pressure effects on the later material. Due to their different chemical nature, A_1 and A_o show different behaviours. Whereas we do not observe any significant change of the height of A_o by comparing the results on HgTe and HgCdTe, A_1 exhibit a drastic variation of E_A vs n(E). In particular, a salient feature is the observation of A_1 still interferring with the conduction band in $Hg_{0.86}Cd_{0.14}Te$ with a pressure-opened-gap value of 50 meV. Using a carefull study of the magnetic field dependance of the Hall constant at different pressures, together with electron mobility measurements, the strong upward shift of A_1 induced by pressure was observed through a de-ionization of this virtual level leading to a change of the carrier concentration p-n and to a variation of the charged center concentration affecting the strength of the ionized impurity scattering mechanism of the conduction band electrons. These two analysis were consistent. In the course of the scattering study, a pressure-induced resonance states of the conduction band is observed at the resonance condition $E_F = E_A$. This feature is characterized by a dip of the mobility experimental curve superimposed on the calculated curve using the appropriate theory of ionized impurity scattering.

The pressure-induced resonance effect appears to be a more convenient way than the temperature-induced one for a study of the resonance width of virtual states. This work, performed at 4.2°K, allows a substantial decrease of the distribution thermal spread-out and leads to ΔE_A 0.3 meV for A_1 in $Hg_{0.86}Cd_{0.14}Te$. In the case of A_o, no quantitative information could be obtained because of a complete ionization

When the mobility is expressed in $cm^2V^{-1}sec^{-1}$:

$$A_{cc} \simeq 3 \times 10^{16} \frac{\varepsilon_o^2}{N_{cc}} \qquad (44)$$

N_{cc} is the concentration of scattering charge centers expressed in cm^{-3}. When the scattering by the holes (considered as fixed charges) is taken into account :

$$N_{cc} = p + N_D + N_A^- = n_1 + 2N_A^- \qquad (45)$$

In Eqs. 40 and 43, m_n is given by Eq. 5.

Since the electron gas in x = 0.14 sample is degenerate, we shall assume that $-(\partial f_o/\partial z) = \delta (x - \eta)$, δ being the Dirac function and $\eta = E_F/k_oT$. Eq. 40 can then be written :

$$\mu_1 = C \frac{1}{N_{cc}} \frac{[E_F (E_F + |E_g|)]^{3/2}}{F [|E_g| + 2E_F]^2} \qquad (46)$$

C is a numerical constant since ε_o is a constant. μ_1 is thus the product of a term $1/N_{cc}$ accounting for the effect of the number of ionized scattering centers, by a term accounting for the effect of the pressure on the band structure through $|E_g|$. In order to illustrate only the second one, we have plotted in Fig. 20 the relative variations of the product $\mu_1 \times N_{cc}$ at 4.2°K. μ_1 has been deduced from the experimental results reported in Fig. 5. In the same figure, we have plotted the theoretical variations of $\mu_1 \times N_{cc}$ deduced from Eq. 46. We have used a matrix element $P_k = 7.6 \times 10^{-8}$ eV cm and a pressure coefficient $\alpha = 8.5 \times 10^{-6}$ eV bar^{-1}. The Fermi energy has been given in Fig. 12. The experimental curve obtained under the assumption $N_D = 0$ by the use of the values of $p - n = N_A^-$ given in Fig. 18 presents a significant departure from the theoretical curve. On the other hand, this latter curve fits quite well another experimental curve, obtained by assuming that $N_D = 4 \times 10^{14}$ cm^{-3} (in which case $N_A^- = (p - n_1) + N_D$), except in the vicinity of P = 3.7 kbars. The shape of the curves in Fig. 20 is very different from that of the curve $\mu_1(P)$ plotted in Fig. 5. The high maximum of μ_1 at $P \simeq 5.8$ kbars does not exist in Fig. 20, and is thus due to the variations of N_A^- rather than a zero gap effect on the band structure.

A similar analysis may be performed for the hole mobility μ_p reported in Fig. 15. Assuming that these holes are only scattered by fixed charges, we have plotted the product of the concentration N_{cc} of such scattering centers by μ_p against pressure at 4.2°K in Fig. 21 when we have

$N_{cc} = N_A^-$ with $N_A^- = p - n_1$ (Fig. 21 (a)) and $N_{cc} = N_A^- + N_D$ with $N_A^- + N_D = p - n_1 + 2N_D$ and $N_D = 4 \times 10^{14}$ cm^{-3} (Fig. 21 (b)). A dip is again evidenced in the range of pressures 2 kbars to 4 kbars.

According to the discussion performed in the previous Section II.C two kinds of acceptor levels contribute to N_A^- :

$$N_A^- = N_{A1}^- + N_{A2}^- \tag{47}$$

From now, we shall take $N_D = 4 \times 10^{14}$ cm^{-3} since this donor concentration was required to fit the variations of μ_1 versus P at 4.2°K. The analysis of the low field Hall coefficient versus P at 77°K[5] led to : $N_A - N_D = 10^{16}$ cm^{-3}. For $P > 5.5$ kbars at 4.2°K, we have shown that $N_{A1}^- \simeq 0$, $N_{A2}^- \simeq N_{A2}$ and Eq. 47 can be written : $N_A^- \simeq N_{A2}$; we can then deduce from Fig. 17 and Eq. 27 : $N_{A2} \simeq 1.5 \times 10^{15}$ cm^{-3}, so that $N_{A1} \simeq 8.5 \times 10^{15}$cm^{-3}. Such a value of N_{A1} was used in Section II.C. to determine $E_{A1} - E_F$ at 4.2°K plotted in Fig. 19. E_{A1} crosses E_F around P = 3.7 kbars, the same pressure as the one at which dips appear on the curves reported in Figs 20 and 21. To bring out the dip on the curve $\mu_1 \quad N_{cc}$ versus pressure, we have reported in Fig. 22 the variations of $[(\mu_1 \quad N_{cc})_{cal} - (\mu_1 \quad N_{cc})_{exp}]/(\mu_1 \quad N_{cc})_{cal}$ against pressure. The subscripts "cal" and "exp" denote respectively calculated and experimental values of $\mu_1 N_{cc}$. This curve is a bump with a resonant like shape, centered at $P \simeq 3.7$ kbars. This accident on the curve $\mu_1 N_{cc}$ versus P is expected to occur on the curve $\mu_1(P)$ since $N_{cc} = n_1 + 2N_A^-$ decreases in a large but monotonous manner according to Figs 5 and 18. Nevertheless, such an effect could hardly be evidenced in Fig. 5 since it was hidden by the much more important variations of n_1 and N_A^-. It is only after the contribution of these variations has been suppressed by plotting $\mu_1 N_{cc}$ instead of μ_1 that we can observe this resonant effect. Within the framework of the relaxation time approximation, the mobility of a degenerate gas takes the form $\mu = e\,\tau(E)/m(E)$ with $\tau(E) = A(E)/N_{cc}$ so that the product $\mu_1 \quad N_{cc}$ may be written :

$$\mu_1 \quad N_{cc} = e\,\frac{A(E)}{m(E)} \tag{48}$$

The singularities observed in Figs 21 and 22 around P = 3.7 kbars are then understood as a resonant effect induced by the acceptor level on A(E). The curve 1 in Fig. 21 also shows that, under the validity of this

analysis, the energy dependent part A(E) of the relaxation time of holes does not depend on pressure away from the resonance. This result is reliable according to the expected small effect of the pressure on the tail of density of Γ_8 heavy hole valence band states.

An increase of the temperature also produces a shift of E_F which crosses E_A at a temperature T_o defined by $E_F(T_o) = E_A$. At this temperature an accident occurs not only on the variations of the conductivity and mobility versus temperature but also on the variations of the low field Hall coefficient R(T) versus temperature[10,11]. This effect can be observed at $T_o \simeq 10°K$ on those of the R(T) curves plotted in Fig. 4 which were obtained at $P > 3.7$ kbars. Since an increase of the temperature induces an increase of E_F, the equation $E_F(T_o) = E_{A1}$ can be satisfied in the range of temperatures investigated $4.2 < T < 77°K$ only when E_F (4.2°K) $< E_A$. According to the curve plotted in Fig. 12, this condition is equivalent to $P > 3.7$ kbars and explains why the dip on these curves was not observed at lower pressures. Otherwise, these experimental results on the Hall coefficient evidence the fact that at $4.2°K, E_F \simeq E_{A1}$ when $P \simeq 3.7$ kbars. This allows us to rely upon the determination of N_{A1} versus pressure, from which this result was first deduced, and corroborates the assertion according to which N_D is small ($N_D \simeq 4 \times 10^{14}$ cm^{-3}).

After having discussed the resonant effects induced by variations of temperature or pressure, we shall now discuss similar effects observed by allowing the magnetic field to vary. According to the analysis summarized in Appendix B, (in our case $N_{cc} > n_1$), the magnitude of the parameter λ in Eq. 35 depends on the scattering amplitude f of the impurity potential according to Eq. B7. It is thus expected that the nearer the Fermi level will be from the acceptor one, the larger will be λ. This may be the reason why λ was found maximum around $P \simeq 4$ kbars ($\lambda = 0.2$), while it was only equal to 0.1 at $P < 3$ kbars and 0.05 in the SC configuration.

Otherwise, in the SC configuration, a departure from the straight line was noticed in Section II.C., when plotting A'(B) versus B^{-2}, for magnetic fields $B > B_o$, which defines B_o (Fig. 14(b)). On the curves R(B), this effect leads to a Hall coefficient vanishing, without becoming positive although this $x = 0.14$ sample is p - type. It can be noticed from Fig. 14 (b) that $B_o > 3B_c$. At such high magnetic fields, $B_o > B > 3B_c$, all the electrons in the conduction band condense on the 0^- Landau level, and the Fermi level then remains clamped to it, so that E_F is determined at each field by the use of Eq. 12 :

$$\frac{1}{4}\ \frac{e\hbar B}{m_n} = E_F\ (1 + \frac{E_F}{|E_g|}) \qquad (49)$$

The abnormal behaviour of R(B) at $B > B_o$ may then be tentatively attributed to the fact that the 0^- Landau level crosses the acceptor level A_1 at $B = B_o$. This also means that the acceptor level crosses the Fermi level : $E_F = E_{A1} - \varepsilon E_g$ so that Eq. 49 can be written :

$$\frac{1}{4}\ \frac{e\hbar\ B_o}{m_n} = (E_{A1} - \varepsilon E_g)\ (1 + \frac{E_{A1} - \varepsilon E_g}{|E_g|}) \qquad (50)$$

Eqs 50 and 18 then show that in first approximation :

$$E_{A1} - \varepsilon E_g \simeq \frac{B_o}{3B_c}\ E_F \qquad (51)$$

E_F has been plotted versus pressure in Fig. 12. For example, at P = 6.4 kbars, $B_o \simeq 6.3$ kG (See Fig. 14 (b)), $B_c \simeq 1.8$ kG (See Fig. 3 (b)), $E_F(0) \simeq 9$ meV, so that Eq. 51 leads to $E_A - \varepsilon E_g - E_F = 0.16\ E_F = 1.5$ meV. This value was also reported in Fig. 19.

At $B > B_o$, the electrons on the 0^- level fall into the acceptor level. They are then in resonant states and have a much smaller mobility. We could have a low field Hall effect with holes, and slow electrons having a small mobility, described by Eq. A2. Such a picture is fit to account for the behaviour of R(B) at $B > B_o$. Since $B_o \simeq 3B_c$, and the maximum field we could obtain in the experimental set up was $B \simeq 9$ kG, we can reach B_o provided that $B_c < 3$ kG, which is fulfilled at P > 5.2 kbars. This explains why these effects could not be evidenced in the SM configuration.

For HgTe, the complete calculation of the mobility has been already performed by Broerman[31]. He gives the results of his calculation for a given number of donors (curve $N_A = 0$ in Fig. 2 of this reference). For the electron concentration $n_1 = 8 \times 10^{14}\ cm^{-3}$ determined in Section II, the electron mobility is $\mu_1 \simeq 1.2 \times 10^6\ cm^2V^{-1}sec^{-1}$, when only donors are present ($N_{cc} \simeq n_1 = 8 \times 10^{14} cm^{-3}$). In our case, $N_{cc} = n + 2N_A^- \simeq 2.2\ 10^{15} cm^{-3}$. Performing the correction due to the difference of the concentrations of scattering centers, we obtain a calculated value of the mobility of $\mu_1 = 4.4\ 10^5 cm^2V^{-1}sec^{-1}$, in close agreement with the experimental one ($\mu_1 \simeq 4.3 \times 10^5 cm^2V^{-1}sec^{-1}$).

In order to account for the absolute value of μ_1 obtained for $x = 0.14$ sample from Eqs 44 and 46, we must use a static dielectric constant $\varepsilon_o \simeq 11$, much lower than any linear interpolation between the well known value $\varepsilon_o \simeq 9.25$ in CdTe[35] and the published value $18 < \varepsilon\ (q = 0) < 20$ for HgTe[36]. Nevertheless, for HgTe, this value was determined at 77°K in intrinsec regime, when $E_F \simeq 30$ meV. Owing to the high value of m_n, the Eq. 39 leads to $\varepsilon_1 = 7$ to 8, so that the part of the dielectric constant induced by all the transitions except the interband $\Gamma_8 - \Gamma_8$ ones would be $\varepsilon_o \simeq 12$. The value of 11 thus obtained for the $x = 0.14$ sample would then not be so strange, due to the fact that any RPA correction disappears when $m_n \longrightarrow 0$.

IV. DISCUSSION

Two kinds of results are to be discussed in this section. The first one concerns the electronic band structure of the materials studied in this paper, and is discussed in Section A. The second one concerns the acceptor levels, Their location together with the mobilities and resonant effects are discussed in Section B.

A. Electronic structure

The analysis of the 0^+ quantum oscillation, and of its shift induced by pressure, as well as the analysis of the background of the curve $\mu_1 N_{cc}$ vs P for the $x = 0.14$ sample in Fig. 20, supported quite well the picture of the conduction band described by the k.p method.

Morever, the change of slope of the curve n_1 vs P in Figs 5 and 6 for the $x = 0.14$ sample was assigned to the crossover of the Γ_6 and Γ_8 levels. Such an interpretation accounted for the results obtained in Ref. 4 when analysing the low field Hall coefficient versus pressure in almost intrinsic materials at 77°K and 292°K. The change of slope was understood as due to the existence of the two competing effects of the opening of the gap and of the increase of the density of states of the conduction band. At such temperatures, $|dn_1/dP|_{SC} < |dn_1/dP|_{SM}$; at 4.2°K and 1.7°K, if we assume the band structure is the one depicted in Fig. 2, the opening of the gap should lead to a drastic decrease of n_1 which could not be balanced by the increase of density of states since the thermal activation energy is

quite small, and we should have $| dn_1/dP |_{SC} > | dn_1/dP |_{SM}$. On the contrary, the existence of the tail of the density of valence states (See Fig. 16) leads to a diminution of the effect of the crossover of the Γ_8 and Γ_6 levels since the electrons in the conduction band issue from valence states which are still located in the conduction band. We may thus have again $| dn_1/dP |_{SC} < | dn_1/dP |_{SM}$ as it is observed in Figs 5 and 6. For the same reason, it was not possible, even at such a low temperature as 1.7°K, to lower the Fermi energy E_F in the true vicinity of the Γ_8 level, whereas that was possible in the HgTe sample.

For this last sample, experimental results fitted the existence of an overlap ΔE of the valence and conduction bands induced by the lack of inversion symmetry. We found $\Delta E < 1$ meV, in agreement with the previous experimental determinations[37 - 39]. Theoretically, Overhof[40] has found $\Delta E \simeq 0.3$ meV.

On the contrary the results obtained on the $x = 0.14$ sample cannot be understood by taking into account such a symmetry induced overlap. It has been shown that, according to Eq. 38, the density of valence states extending beyond the Γ_8 point looks like a tail. Such an effect may be understood in the framework of alloy theories[41, 42] and is expected to be associated with "clustering", e.g. local departures from stoechiometry. In effect, the energy of the Γ_8 level, as well as E_g are expected to depend upon x. So intuitive arguments suggest that flcutuations Δx of x induce fluctuations of $E(\Gamma_8)$. Consequently some states of the valence band corresponding to a concentration $x - \Delta x < x' < x + \Delta x$ may exist at energies between $E(\Gamma_8)_{x - \Delta x}$ and $E(\Gamma_8)_{x + \Delta x}$, and so at energies $E > E(\Gamma_8)_x$. These states contribute a tail to the density of the valence band. Without giving a detailed shape, Eqs. 37 show that this tail should extend up to 17 meV from the Γ_8 point, and Eq. 38 gives an order of magnitude of the number of valence states displaced from the usual band into the tail. Nevertheless it should be noticed that the magnitude of this tail, according to its cause, widely depends on the technique used to induce the growth of the crystal. In particular this tail may be almost non-existent for materials suitable prepared. Both the existence of the tail and the values of the parameters ΔE and m_v^* are thus features particular to this sample and not a specific effect of these materials.

Likewise, another tail is expected to issue from the conduction band, stretching in the valence band for the whole range of pressures investigated. Nevertheless, the numbers of conduction and valence states

induced by the alloying effect away from the extrema of the conduction and valence bands are expected to be in the ratio of the respective effective masses of the state density of these two bands. Since $m_n \ll m_h$ we can thus neglect this other tail.

If the disorder effects on the valence band accounts quite well for the experimental results at 4.2°K, we must also ascertain that the same is the case at T > 77°K, when Kane's model remains valid to describe the electronic transport properties of the alloy. In fact it is well expected that it is so indeed, since a tail only effects states which are in the vicinity of the band edge Γ_8, and not those which are at a distance from this point larger than E_R. To corroborate this argument, numerical calculations were performed with the help of a computer to determine the concentration of electrons n_1, of holes p, and the Fermi energy E_F of this sample at 77°K. Those calculations were performed with and without a tail characterized by Eq. 37 superimposed on the Kane's valence band. The results are identical in both cases within 2 %. The physical reason is that, at T > 77°K, the thermal activation energy k_oT being high enough to generate holes from states below the Γ_8 point, the tail does not have any significant effect on the statistical equilibrium at these temperatures since $m^*_v \ll m_h$.

On the contrary, at 4.2°K, the tail not only allows us to understand why holes are in such high concentrations as those experimentally observed, but also acts as a reservoir of electrons. In effect, at each pressure, those of the electrons in the valence states of the tail which have an energy $E > E_{A1}$ flow into the conduction band states and fill this band up to the acceptor level, which explains why we found at each pressure $E_F \simeq E_A$ within less than 2 meV.

From the analysis of the shift of the 0^+ quantum oscillation induced by pressure in the HgTe sample , we found a pressure coefficient $dE_g/dP = (8.5 \pm 0.5) \times 10^{-6}$ eV bar^{-1} at 4.2°K and 1.7°K.

Otherwise, the theoretical law $E_g(x)$ at T = 0 and P = 1 bar given by Chadi and Cohen[43] for $Hg_{1-x}Cd_xTe$ alloys is $E_g(x) = -302.5 + 1830\,x$. According to this law, we should have, for the x = 0.14 sample $E_g^o \simeq 47$meV, which agrees with our result ($E_g^o \simeq 46 \pm 3$ meV). A detailed discussion about this numerical value of the pressure coefficient of the energy gap is reported in Ref. 5.

B. Location of the acceptor levels

According to the submillimeter and far infrared magnetoabsorption experiments on HgTe reported in Ref. 13, together with the discussion on the nature of these acceptor levels in HgTe and $Hg_{1-x}Cd_xTe$ alloys reported

in Ref. 11, the level located at 0.7 meV above the Γ_8 point in HgTe is expected to be induced by Cu impurities. The perturbing potential in such a case is Coulombian, so that this level will not significantly vary with a change of the density of conduction band states induced by the pressure as can be shown from the calculation by Gel'mont and D'yakonov. This is consistent with the analysis developped, in Section II.B., to determine the pressure coefficient in the HgTe sample. For the same reason, the activation energy of this acceptor state is not expected to depend on the variation of E_g induced by a variation of composition. We then should have for such a level an activation energy E_A close to 1 meV even in $x = 0.14$ sample. We may then assume that the completely ionized level observed for pressures $P > P_c$ in the SC configuration (Fig. 18) should be assigned to Cu impurities , with a concentration $N_{A2} = 1.5 \times 10^{15} cm^{-3}$.

For $x = 0.14$ sample, it was possible to show another acceptor level for which the activation energy, labelled E_{A1} in the previous sections, widely increased with pressure. We have plotted in Fig. 23 E_{A1} (measured from Γ_8) versus pressure. E_{A1} was deduced from the knowledge of $E_F + \epsilon E_g - E_{A1}$ and of E_F reported in Figs. 12 and 19. In the SM configuration, the increase of E_{A1} implies that the acceptor level moves up in the conduction band when P increases, i.e. when the density of states in this band decreases, according to Eqs. 3 and 22. Variations of E_g may also be induced by variations of the composition x, and the same behaviour of E_{A1} versus E_g in the SM configuration was reported in Ref. 11 from galvanomagnetic measurements performed on various compositions versus temperature at ambiant pressure. It is shown in this reference that the acceptor level A_1 observed in the $x = 0.14$ sample is also present in HgTe with an activation energy $E_{A1} = 2.25$ meV. Such large variations of E_{A1} either with pressure or composition are by no means consistent with a Coulombian potential, but can be accounted for when assuming that we have a localized potential[14], like those induced by crystalline defects involving for instance mercury vacancies. In the SC configuration, i.e. for pressures $P > 5.4$ kbars, the Fig. 23 shows that the acceptor level E_{A1} still rises with respect to the Γ_8 point, and has a pressure coefficient dE_{A1}/dP larger than in the SM configuration. The physical reason of such an effect is that the opening of the gap may be considered as a dramatic decrease of the density of conduction band states in the true vicinity of Γ_8, in the range of energies $E(\Gamma_8) < E < E(\Gamma_8) + E_g$. Nevertheless, the larger

the gap in this SC configuration, the nearer we approach the configuration in which only the valence band must be taken into account to determine E_{A1} which then no further moves. This effect, together with the increase of the density of conduction band states at energies $E > E(\Gamma_6)$ (far from the Γ_8 point) attenuate the increase of E_{A1} with E_g and allows us to understand why the acceptor level is found to move down in the conduction band, with respect to the Γ_6 point, or in order words why $dE_{A1}/dP < dE_g/dP$, as can be seen in Fig. 23. All these points will be further discussed theoretically in Ref. 14.

The presence of such acceptor levels leads us to take into account two scattering mechanismes. The first one is the scattering by the localized potential leading to the existence of a resonance, efficient only for electrons the energy of which lies in the range $[E_{A1} - \Delta E_{A1}/2, E_{A1} + \Delta E_{A1}/2]$ where ΔE_{A1} is the width of the resonance. The second one is induced by the fact that, as will be seen below, the resonance is narrow enough to be considered as a quasi discrete level. The electrons in resonant states then act as almost localized electrostatic charges, and thus give rise to a Coulombian potential. The other electrons in the conduction band with a high mobility screen this long range potential and are thus scattered by it. This scattering mechanism was found to account quite well for the values of $\mu_1 N_{cc}$ in the whole range of pressures for which the first mechanism can be neglected, as can be seen in Fig. 20. In the range of pressures $2.8 < P < 4.5$ kbars, $|E_{A1} - E_F| < k_oT$, and a part of the electrons efficient in transport phenomena, thus having an energy E in the range $[E_F - k_oT, E_F + k_oT]$, is scattered in a resonant manner by the localized potential. This additional screening leads to the dip in the curves in Fig. 20, or the bump of the curve in Fig. 22 which we shall now analyse.

For temperatures $k_oT \ll \Delta E_A$, when the condition $E_F = E_{A1}$ is fulfilled, all the electrons in the range k_oT around E_F would undergo a resonant scattering. By scanning E_F in a range ΔE_A around E_A, one should perform a spectroscopy of the resonance. The measured electron mobility should then be very smalll and should be that of the electrons resonantly scattered. The bump in Fig. 22 has an half width equal to about 1 kbar and is centered at $P \simeq 3.7$ kbars. According to the results plotted in Fig. 12, the shift of the Fermi energy in this range of pressures is around 0.3 meV. An estimation of the width of the acceptor level should then be $\Delta E_{A1} \simeq 0.3$ meV for an energy gap $E_g = -14$ meV, which is the value of E_g at 3.7 kbars for $x = 0.14$ sample at 4.2°K. Since $k_oT \simeq 0.36$ meV, $k_oT \simeq \Delta E_{A1}$ and the condition

$k_oT \ll \Delta E_{A1}$ is not fulfilled. It is thus possible that the value of ΔE_{A1} so determined is rather the width of the Fermi level, and not exactly the width of the acceptor level, for which 0.3 meV should be an upper limit. Since $k_oT > \Delta E_{A1}$, only a small amount of the electrons efficient in transport phenomena are concerned with the resonant scattering, even when the acceptor level is in the range k_oT around E_F, so that the transport properties are not fundamentally modified. This may explain why the resonance observed in Fig. 20 gives a quite small effect which does not exceed ten per cent of the background of the curve $\mu_1 N_{cc}$ versus P. Consequently, the experimental mobility measured for $P \simeq 3.7$ kbars on this sample cannot be correlated with the mobility μ_R of the electrons in the resonance.

As already shown in Section II, this mobility could be determined in the HgTe sample by the analysis of the two carrier types Hall effect. Using a similar procedure, Zakrzewski and Dziuba also determined such a mobility μ_R of electrons in HgTe, which they attributedto an impurity band[44]. For x = 0.14 sample, the determination of μ_R could not be performed at 4.2°K since the two carrier type analysis showed the presence of electrons in the conduction band states, and of holes. In order to understand why , in this sample, the holes prevail over the second kind of electrons in resonant states, we suppose that, at 4.2°K, $\mu_R < \mu_P$ or, according to the Fig. 16, $\mu_R < 2000$ $cm^2V^{-1}sec^{-1}$. However, at 90°K, the plot of $R(O)/[R(B) - R(O)]$ against B^{-2} illustrated in Fig. 24 at 4 kbars and 5 kbars gave a straight line in the whole range of magnetic fields $B < 9.5$ kG available in the experimental set up. The solution of Eqs A5 showed that, at this temperature, the two efficient carriers were two types of electrons, so that the situation was quite similar to that of the x = 0 sample at 1.7°K. The concentration of the second type of electrons was about 9×10^{15} cm^{-3} and shows that these electrons are in the N_{A1} completely ionized acceptor states. Their mobility was found to be $\mu_R \simeq 2000$ $cm^2V^{-1}sec^{-1}$, larger than the expected value at 4.2°K, and equal to the one recently found in $Hg_{1-x}Cd_xTe$ alloys for various compositions[45]. It should be noticed that this mobility is high enough so that these resonant electrons prevail over holes in transport phenomena. The reason is that at 90°K, most of the holes arise from the host valence band below the Γ_8 point and are thus classical ones with a mobility which is expected to be $\mu_P \simeq 500$ $cm^2V^{-1}sec^{-1}$ so that $\mu_P \ll \mu_R$. It is not surprising, under such conditions, not to observe holes at 90°K.

It has been shown otherwise that the mobility of electrons on Cu acceptor states in the x = 0 sample was $\mu_R \simeq 9000$ $cm^2V^{-1}sec^{-1}$.

Nevertheless, the large decrease of both m_n and the density of conduction band states, is expected to lower greatly this mobility in $x = 0.14$ sample[14]. As a matter of fact, such electrons could not be evidenced in this sample whatever were the temperature and pressure. This illustrates the fact that the characteristic features of the resonances, like their width or the mobility μ_R depend on the density of states in their vicinity or in other words depend on E_g. The results described in this paper are thus only partial and measurements of transport properties like those performed for this $x = 0.14$ sample at 4.2°K are needed to investigate the resonance parameters μ_R and E_A more systematically. Attention should then be drawn to the fact that the resonant effects cannot be exhibited at first sight from experiment, since it is necessary to take into account the variations of the concentration of scattering centers N_{cc} when E_F moves with respect to E_A. Such variations are important in the vicinity of $E_F \simeq E_A$ and widely affect the Hall coefficient and the mobility of the carriers in the vicinity of the resonance, as it is illustrated by the comparison of the curves in Figs. 5 and 15 with those in Figs. 20 and 21.

Otherwise, when ΔE_A and k_oT have the same order of magnitude, the investigation of ΔE_A and μ_R is difficult as was shown above. In this common case, the analysis of transport properties versus T performed in order to observe temperature induced resonances like those plotted in Fig. 4 are not a convenient means of determining ΔE_A, because of the enlargment of the spread out k_oT of the Fermi level . The width $\Delta E_A \simeq 0.3$ meV for $E_g \simeq -14$ meV determined from the pressure induced resonance is very small. The mobility $\mu_R \simeq 2000$ $cm^2V^{-1}sec^{-1}$ for $x = 0.14$ sample at 90°K was also quite small compared to that of the electrons in the conduction band states. Such values of ΔE_{A1} and μ_R corroborate with the fact that the level is quasi discrete and that the electrons in resonant states are almost localized.

Moreover, at 90°K, these acceptor states were found occupied, so that this level is expected to be still in the conduction band when the energy gap is $E_g \simeq +40$ meV at 5 kbars. The investigation of such levels in small gap semiconductors obtained for a concentration of Cd atoms $x > 16$ % should allow a determination of the value of E_g beyond which this level falls into the energy gap.

CONCLUSIONS

In this work, the transport properties at low temperature exhibited by $Hg_{0.86}Cd_{0.14}Te$ within the semimetal-to-semiconductor transition induced by hydrostatic pressure, give a strong experimental evidence of the resonant configuration of acceptor states occuring in vanishing bandgap HgCdTe - like materials. In particular, useful informations are obtained about the heights E_A and the resonance widths ΔE of the virtual states A_1 and A_o, corresponding to Hg - vacancies and substitutional Cu-impurities respectively. In the general context of virtual electronic states as widely observed in solid state physics, the HgCdTe system offers the interesting possibility of a unique tool to study the effect of changes of conduction band density of states n(E) upon E_A and ΔE_A. In the present work, these features are illustrated by a comparison of the results obtained on HgTe and $Hg_{0.86}Cd_{0.14}Te$ and by the pressure effects on the later material. Due to their different chemical nature, A_1 and A_o show different behaviours. Whereas we do not observe any significant change of the height of A_o by comparing the results on HgTe and HgCdTe, A_1 exhibit a drastic variation of E_A vs n(E). In particular, a salient feature is the observation of A_1 still interferring with the conduction band in $Hg_{0.86}Cd_{0.14}Te$ with a pressure-opened-gap value of 50 meV. Using a carefull study of the magnetic field dependance of the Hall constant at different pressures, together with electron mobility measurements, the strong upward shift of A_1 induced by pressure was observed through a de-ionization of this virtual level leading to a change of the carrier concentration p-n and to a variation of the charged center concentration affecting the strength of the ionized impurity scattering mechanism of the conduction band electrons. These two analysis were consistent. In the course of the scattering study, a pressure-induced resonance states of the conduction band is observed at the resonance condition $E_F = E_A$. This feature is characterized by a dip of the mobility experimental curve superimposed on the calculated curve using the appropriate theory of ionized impurity scattering.

The pressure-induced resonance effect appears to be a more convenient way than the temperature-induced one for a study of the resonance width of virtual states. This work, performed at 4.2°K, allows a substantial decrease of the distribution thermal spread-out and leads to ΔE_A 0.3 meV for A_1 in $Hg_{0.86}Cd_{0.14}Te$. In the case of A_o, no quantitative information could be obtained because of a complete ionization

of A_o in our samples at all pressures. This work is under study at the present time at higher pressures and with higher Cd-contents in the alloys. Nevertheless, indirect informations appear through the characteristics of the additional concentration of carriers, i.e. "slow electrons" observed in HgTe and $Hg_{0.86}Cd_{0.14}Te$. In the past, observations of such carriers have been repported. In the present work, we have attributed this phenomenon to the complete ionization of acceptors inducing a concentration of electrons quasi bounded these resonant states. In HgTe, where the density of the conduction band continum interfering with the virtual state is large, the broadening of a resonance is stronger than in $Hg_{0.86}Cd_{0.14}Te$. This is consistent with the observed mobility values of the "slow electrons" which appear significantly higher in HgTe than in HgCdTe.

Finally, another evidence of the resonant configuration of acceptor states is shown through transport studies combining pressure and quantizing magnetic field. An illustration is provided by the observation, in the quantum limit, of an anomalous behaviour of the magnetic field dependance of the Hall coefficient, attributed to a complete resonance of the condensated electron population occuring at the crossover of the O^- Landau and virtual levels.

An interesting aspect of these quantum transport studies is related to the existence of strong oscillations of the Hall coefficient, with amplitudes much larger than expected from the theoretical work of Bastin et al. A rough analysis neglecting Luttinger effects, yields apparently a reliable determination of the location of the O and O^+ levels. On p-type HgTe, the pressure-induced shift of the Hall coefficient quantum oscillations corresponding to the conduction electrons leads to a determination of $dE_g/dP = 8 \pm 0.5$ meV/Kbar at 1.7°K. Qualitatively, other features such as absence of spin-splitting in HgTe, observation of the O^+ oscillation on the magnetoresistance at 10°K of $Hg_{0.86}Cd_{0.14}Te$, magnetoresistance extra oscillation observed in the ultra-quantum limit on HgTe and apprently due to a crossover of the fundamental Landau level with a virtual acceptor state, indicate interesting possibilities for future.

ACKNOWLEDGMENTS

We are indebted to Professor J. Friedel for many enlightening discussions on the virtual acceptor state problem. We wish to thank Professor P. Nozières for stimulating interest and A.T.P. sponsorship. We are pleased to acknowledge helpful discussions with O. Betbeder-Matibet, P. Leroux-Hugon and C. Lewiner. In the course of experiments, help and suggestions of G. Weill have been greatly appreciated. We are indebted to M. Escorne for technical assistance and to C. Finck for the crystal growing.

Appendix A

Two carrier types analysis of the Hall coefficient

When two types of carriers are present, the Hall effect against magnetic field may be expressed as[24] :

$$R(B) = \frac{(R_1\sigma_1^2 + R_2\sigma_2^2) + R_1R_2\sigma_1^2\sigma_2^2 (R_1 + R_2) B^2}{(\sigma_1 + \sigma_2)^2 + \sigma_1^2\sigma_2^2 (R_1 + R_2)^2 B^2} \qquad (A1)$$

R_1 and R_2 are the Hall coefficients which would be obtained if only the first type of carriers or only the second one were present, and σ_1, σ_2 are the transverse magnetoconductivities of the first and second carrier types respectively. Of course, these four quantities may depend on the magnetic field B in the most general case, but we shall restrict the following analysis to the case of a complete independence of R_1, R_2, σ_1 and σ_2 upon B in the range of fields considered.

At zero field, Eq. A1 becomes :

$$R(0) = \frac{R_1\sigma_1^2 + R_2\sigma_2^2}{(\sigma_1 + \sigma_2)^2} \qquad (A2)$$

while the conductivity is :

$$\sigma(0) = \sigma_1 + \sigma_2 \qquad (A3)$$

Using Eqs. A2 and A3, Eq. A1 can be written :

$$\frac{R(0)}{R(0) - R(B)} = a + s\, B^{-2} \qquad (A4.1)$$

with :

$$s = \frac{R(0)\sigma(0) [\sigma(0) - \sigma_1]^2}{\sigma_1^2 [R_1\sigma(0) + R(0)\sigma(0) - 2R_1\sigma_1] [R_1\sigma_1 - R(0)\sigma(0)]^2} \qquad (A4.2)$$

and :

$$a = \frac{R(0)\sigma(0) [R_1\sigma(0) + R(0)\sigma(0) - 2R_1\sigma_1]}{(R(0)\sigma(0) - R_1\sigma_1)^2} \qquad (A4.3)$$

Eq. A4.1 shows that it is convenient to plot the quantity $R(0)/[R(0) - R(B)]$ versus B^{-2}, since a straight line must be obtained, provided that R_1, R_2, σ_1 and σ_2 are independent of B. The slope s and the intercept a are then given by experiment, as well as R(0) and $\sigma(0)$. We thus have a system of four equations A2, A3, A4.2 and A4.3 with four unknown quantities R_1, R_2, σ_1 and σ_2. Under the condition $R_1 + R_2 < 0$, the solution of the system is :

$$\sigma_1 = \frac{\sigma(0)}{2}\left[1 + \left(\frac{\alpha}{4+\alpha}\right)^{1/2}\right] \qquad (A5.1)$$

$$\sigma_2 = \frac{\sigma(0)}{2}\left[1 - \left(\frac{\alpha}{4+\alpha}\right)^{1/2}\right] \qquad (A5.2)$$

with α given by :

$$\alpha = \frac{(a\,s)^{1/2}}{[R(0)\sigma(0)]}\left[R(0)\sigma(0) + \left(\frac{a}{s}\right)^{1/2}{}^{2}\right] \qquad (A5.3)$$

and :

$$R_1 = \frac{1}{2\sigma_1 - \sigma(0)}\left[R(0)\sigma(0) + \frac{\sigma_1}{\sigma_2}\left(\frac{a}{s}\right)^{1/2}\right] \qquad (A5.4)$$

$$R_2 = \frac{1}{2\sigma_2 - \sigma(0)}\left[R(0)\sigma(0) + \frac{\sigma_1}{\sigma_2}\left(\frac{a}{s}\right)^{1/2}\right] \qquad (A5.5)$$

We are now to discuss the condition of validity of Eqs. A5 :

$$R_1 + R_2 < 0 \qquad (A6)$$

In our samples, one type of carriers (hereafter the first one) is constituded by the electrons in the conduction band, with the concentration n_1 given by :

$$n_1 = -\frac{1}{eR_1} \qquad (A7)$$

- If the other carriers are also electrons, with a concentration n_2 :

$$n_2 = -\frac{1}{eR_2} \qquad (A8)$$

the condition A6 is fulfilled since R_1 and R_2 are both negative quantities.

- If the other carriers are holes, with a concentration p :

$$p = + \frac{1}{eR_2} \tag{A9}$$

the condition A6 can ben weitten :

$$p - n_1 > 0 \tag{A10}$$

This second case will be shown to occur at 4.2°K, for the x = 0.14 sample only. The condition A10 is thus fulfilled at all pressures according to Eq. 27 and Fig. 17.

It should be noticed that, according to Eq. A1 :

$$R(\infty) = \frac{R_1 R_2}{R_1 + R_2} \tag{A11}$$

so that, when we have electrons and holes, Eqs. A7 and A9 lead to :

$$\frac{1}{eR(\infty)} = p - n_1 \tag{A12.1}$$

and when we have two types of electrons, Eqs. A7 and A8 lead to :

$$- \frac{1}{e\ R(\infty)} = n_1 + n_2 \tag{A12.2}$$

$R(\infty)$ may be obtained from a and R(0) (Eq. A4.1).

Eqs. 12 are useful to determine the concentration of the second type carriers, p or n_2. In effect, so far as we do not require any determination of σ_2 nor the Hall mobility μ_2, Eq. A5 can be reduced to simpler expressions, since it is well known that in our materials $\mu_2 \ll \mu_1$, so that :

$$\sigma_2 \ll \sigma_1 \tag{A13}$$

According to Eq. A13, Eqs A2 and A3 can be simplified as follows :

$$R(0) \simeq R_1 \tag{A14}$$

$$\sigma(0) \simeq \sigma_1 \qquad \text{(A15)}$$

Eqs. A14, A7 and A12 then give the concentrations of each type of carriers.

Appendix B

Study of the Hall effect in the ultraquantum limit for electrons

In this Appendix, by the use of the results of an analysis performed by Bastin and Al[23], and briefly summarized hereunder, we shall study the Hall effect and magnetoresistivity when the electrons are scattered by impurities in presence of such high magnetic fields that the ultra quantum limit (as defined in Section II) is reached.

It is assumed in Ref. 23 that the random perturbing potential V can be decomposed into a sum of contributions of single scatterers associated with each site i :

$$V = \sum_{i=1}^{N_{cc}} v(r - r_i) \qquad (B1)$$

N_{cc} is the number of scattering centers in our sample. The potential v associated with a single scatterer is supposed localized for mathematical convenience. (This approximation is justified hereafter). The two characteristic lengths in the problem are the scattering amplitude f of the localized potential v defined by :

$$v(r) = \frac{2\pi \hbar^2 f}{m^*} \delta(r) \qquad (B2)$$

and the radius of the cyclotron orbit l, defined by :

$$l = \left(\frac{\hbar}{m^* \omega_c} \right)^{1/2} \qquad (B3)$$

when ω_c is the cyclotron frequency, m^* is the effective mass of the electrons in a parabolic conduction band. A calculation of the electron conductivity tensor in the ultraquantum limit using a Green's function method allowed Bastin and al to find tractable expressions in two cases :

a) In the case of a strong potential ($f \gg 1$) :

$$\sigma_{xx} = \frac{2}{\pi} \frac{N_{cc} e^2}{m^* \omega_c} \qquad (B4)$$

$$\sigma_{xy} = - \frac{n_1 e^2}{m^* \omega_c} \left[1 + \frac{N_{cc}}{n_1} \right] \qquad \text{(B5)}$$

b) In the case of a weak potential ($f \ll 1$), the results can be written :

$$\sigma_{xx} = \frac{n_1 e^2}{m^* \omega_c} \frac{2}{\pi} \frac{N_{cc}}{n_1} \left\{ \frac{3f}{1} \left(\frac{\hbar \omega_c}{2E_F^o} \right)^{3/2} \right\}^2 \qquad \text{(B6)}$$

$$\sigma_{xy} = - \frac{n_1 e^2}{m^* \omega_c} \left[1 + \frac{4}{3\pi} \frac{N_{cc}}{n} \left\{ \frac{3f}{1} \left(\frac{\hbar \omega_c}{2E_F^o} \right)^{3/2} \right\}^3 \right] \qquad \text{(B7)}$$

In all these expressions n_1 is the electron concentration, and E_F^o the Fermi energy at zero magnetic field.

It is important to determine the conditions of validity of the foregoing formula. In the particular case $N_{cc} = 0$, Eqs. B4 - B7 are reduced to the trivial expressions :

$$\begin{cases} \sigma_{xx} = 0 \\ \sigma_{xy} = - \dfrac{n_1 e^2}{m^* \omega_c} \end{cases} \qquad \text{(B8)}$$

The expressions of σ_{xx} or σ_{xy} in Eqs. B4 - B7 only involve the first term of a series determined in the framework of a first order calculation, when scatterers are present in the material. It follows that such expressions are only valid provided that the corrective terms with respect to Eq. B8 are small, for the truncation of the series to their first term to be legitimate. According to Eqs. B4 and B5, the condition of validity in the strong potential case is :

$$\frac{N_{cc}}{n_1} \ll 1 \qquad \text{(B9)}$$

while, according to Eqs B6 and B7, we may have in the weak potential case :

$$\frac{N_{cc}}{n_1} \gg 1 \qquad \text{(B10)}$$

Since the single condition is :

$$\frac{N_{cc}}{n_1}\left\{\frac{3f}{l}\left(\frac{\hbar\omega_c}{2E_F^o}\right)^{3/2}\right\}^3 \ll 1 \qquad \text{(B11)}$$

We can notice that in both cases, Eqs. B9 and B11 imply :

$$\frac{\sigma_{xx}}{\sigma_{xy}} \ll 1 \qquad \text{(B12)}$$

It remains to determine R_1 and σ_1, which are the Hall coefficient and the magnetoconductivity which would be observed if the electrons of the conduction band were the single type of carriers present in the material. They are given by :

$$\sigma_1(B) = \frac{\sigma_{xx}^2 + \sigma_{xy}^2}{\sigma_{xx}} \qquad \text{(B14)}$$

$$R_1(B) = \frac{1}{B}\,\frac{\sigma_{xx}}{\sigma_{xx}^2 + \sigma_{xy}^2} \qquad \text{(B15)}$$

In both weak and strong potential cases, Eq. B12 leads to further simplifications ; if we neglect the second order terms in σ_{xx}/σ_{xy}, Eqs B14 and B15 can be written :

$$\sigma_1(B) = \frac{\sigma_{xy}^2}{\sigma_{xx}} \qquad \text{(B16)}$$

$$R_1(B) = \frac{1}{B\,\sigma_{xy}} \qquad \text{(B17)}$$

According to Eqs. B5 and B7, we obtain :

$$R_1(B) = -\frac{1}{e\,n_1}(1 - \lambda) \qquad \text{(B18)}$$

In the case of a strong potential λ is given by $\lambda = N_{cc}/n_1$.

In the case of a weak potnetial λ is given by :

$$\lambda = \frac{4}{3\pi} \frac{N_{cc}}{n_1} \left\{ \frac{3f}{l} \left(\frac{\hbar \omega_c}{2E_F^o} \right)^{3/2} \right\}^3$$

Using Eq. A7 we obtain :

$$R_1(B) = R_1(0) \quad (1 - \lambda) \tag{B19}$$

Since the dependence of R_1 upon the magnetic field is entirely contained in the small quantity λ, we can neglect it, and write, according to Eq. A14 :

$$R_1 \simeq R'(0) = R(0) \ (1 - \lambda) \tag{B20}$$

This formula being valid as well in the case of a strong potential as in the case of a weak potential, we shall interpolate this result for an arbitrary strength of scattering and for an arbitrary concentration of scatterers according to Eqs. B9 and B10. We can then conclude, that the observed experimental variations of the Hall coefficient R(B) in the ultraquantum domain cannot be explained within the framework of this quantum theory, so that we are led to attribute them to the presence of two types of carriers. R(B) is then given by Eq. A1 with $R'(0)$ in place of R(O).

As to the approximation lying in choosing a δ-like potential in Eq. B2, we can hope that this is of no moment. The main reason is that R_1 is only sensitive to the shape of the potential through the dependence of λ upon B, which anyhow can be neglected, because $\lambda \ll 1$. In other words, R_1 does not depend to the first order on the relaxation time which contains the features of the scattering potential.

The same is not the case about the conductivity according to Eq. B16. As a matter of fact, the dependence of σ_1 upon B is quite sensitive to the choice of the potential. For example, $\sigma_1 \propto B^{-1}$ according to Eqs B4 and B5, $\sigma_1 \propto B^{-5}$ according to Eqs B6 and B7, while $\sigma_1 \propto B^{5}$ for a screened Coulombian potential [46], so that any attempt to foresee the variations of σ_1 is quite difficult.

However, owing to the fact that the quantity $R'(0)/[R'(0) - R(B)]$ has a linear dependence upon B^{-2} (section II.C.) we can infer, according to Appendix A, that in our case, σ_1 does not significantly vary with magnetic field in the range $B > B_c$.

REFERENCES

[1] S.H. Groves and W. Paul, in Proceedings of the International Conference on Semiconductor Physics (Dunod, Paris, 1964), p. 41.

[2] G. Leman and J. Friedel, J. Appl. Phys. Supplément 33, 281 (1962).

[3] F. Herman, C.D. Kuglin, K.F. Kuff and R.L. Kortum, in Quantum Theory of Atoms, Molecular and the Solid State, edited by P.O. Lowdin (Academic Press New York, 1966) p. 381.

[4] S. Otmezguine, F. Raymond, G. Weill and C. Vérié, in Proceedings of the Tenth International Conference on the Physics of Semiconductors, edited by S.P. Keller, J.C. Hensel and F. Stern (U.S. Atomic Energy Commission, Cambridge, Mass., 1970), p. 536.

[5] S. Otmezguine, G. Weill, C. Vérié, Annexe I.

[6] E.O. Kane, in Semiconductors and Semimetals, edited bu R.K. Willardson and A.C. Beer (Academic, New York, 1966), Vol. 1, p. 75 ; J. Phys. Chem. Sol., 1, 249 (1957).

[7] B.L. Gel'mont, M.I. Dyakonov, Zh. Ekop. Teor. Fiz. 62, 713 (1972) [Sov. Phys. JETP 35, 377 (1972)]

[8] C. Vérié, in New Developments in Semiconductors, edited by P.R. Wallace, R. Harris, M.J. Zuckermann (Noordhoff International Publishing, Leyden, 1973), p. 511.

[9] C.T. Elliott, John Melngailis, T.C. Harman, J.A. Kafalas, W.C. Kernan , Phys. Rev. B 5, 2985 (1972).

[10] B.L. Gel'mont et al., in Proceedings of the 11th International Conference on the Physics of Semiconductors, edited by PWN - Polish Scientific Publishers (Warsaw, Poland, 1972), Vol. 2, p. 938.

[11] C. Finck, S. Otmezguine, G. Weill, C. Vérié, ibid., p. 944.

12 V.I. Ivanov-Omskii, Colloque CNRS n° 228, Nice, 1973.

13 J. Tuchendler, M. Grynberg, Y. Couder, H. Thomé, in Proceedings of the 11th International Conference on the Physics of Semiconductors, edited by PWN - Polish Scientific Publishers (Warsaw, Poland, 1972), Vol. 1, p. 346.
J. Tuchendler, M. Grynberg, Y. Couder, H. Thomé, R. Le Toullec, Phys. Rev. B 8, 3884 (1973).

14 A. Mauger and J. Friedel, to be published.

15 M. Monchanin, G. Weill, S. Otmezguine, to be published.

16 I.L. Spain and S. Segall, Cryogenics 11, 26 (1971).

17 P. Kachan and W. Zawadzki, Phys. Stat. Sol. (b) 47, 629 (1971).

18 S. Askenazy, in New Developments in Semiconductors, edited by P.R. Wallace, R. Harris and M.J. Zuckermann (Noordhoff International Publishing, Leyden, 1973), p. 331.

19 A.L. Efros, Fiz. Tved. Tela 7, 1501 (1965) [Sov. Phys. Sol. Stat. 7, 1206 (1965)].

20 Y. Guldner, C. Rigaux, A. Mycielski, M. Grynberg, in Proceedings of the 11th International Conference on the Physics of Semiconductors, edited by PWN - Polish Scientific Publishers (Warsaw, Poland, 1972), Vol. 1, p. 351.

21 W.J. Scouler and G.B. Wright, Phys. Rev., 133, A 736 (1964).

22 P.J. Melz and I.B. Ortenburger, Phys. Rev. B 3, 3257 (1971).

23 A. Bastin, C. Lewiner, B. Betbeder Matibet, P. Nozières, J. Phys. Chem. Sol. 32, 1811 (1971).

24 C.C.Y. Kwan, J. Basinski, J.C. Woolley, Phys. Stat. Sol. (b) 48, 699 (1971).

25 T.C. Harman, in Proceedings of the International Conference on II-VI Semiconducting Compounds, edited by D.G. Thomas (W.A. Benjamin, New York, 1967) p. 982.

26 M. Yamamoto and T. Fukuroi, J. Phys. Soc. Japan 21, 2428 (1966).

27 M. Royer, Thèse de 3ème Cycle, Paris (1973).

28 J.G. Brcerman, Phys. Rev. 183, 754 (1969).

29 L. Liu and D. Brust, Phys. Rev. 173, 777 (1968).

30 L. Liu and E. Tosatti, Phys. Rev. B 2, 1926 (1970).

31 J.G. Broerman, Phys. Rev. B 2, 1818 (1970).

32 B.L. Gel'mont, V.I. Ivanov-Omskii, B.T. Kolomiets, V.K. Ogorodnikov, K.P. Smekalova, Fiz. Tekh. Polupov. 5, 266 (1971) [Sov. Phys. Semicond. 5, 228 (1971)].

33 J.G. Broerman, Phys. Rev. B 1, 4568 (1970).

34 W. Zawadzki and W. Szymanska, Phys. Stat. Sol. (b) 45, 415 (1971).

35 M. Balkanski, in Proceedings of the Interntional Conference on II-VI Semiconductiong Compounds, edited by D.G. Thomas (W.A. Benjamin, New York, 1967) p. 1007.

36 V.I. Ivanov-Omski, B.T. Kolomiets, A.A. Mal'kova, Yu. F. Markov, A. Sh. Mekhtiev, Fiz. Tekh. Poluprov. 4, 417 (1970) [Sov. Phys. Semicond. 4, 352 (1970)].

37 C. Vérié, Phys. Stat. Sol. 17, 889 (1966).

38 R.R. Galazka, Phys. Rev. Lett. 32 A, 101 (1970).

[39] V.I. Ivanov-Omskii, Colloque CNRS n° 228, Nice, 1973.

[40] H. Overhof, Phys. Stat. Sol. 43, 221 (1971).

[41] I.M. Lifshitz, Usp. Fiz. Nauk 83, 617 (1964) [Sov. Phys. Usp. 7, 549 (1965).

[42] S. Kirpatrick, B. Velicky, and H. Ehrenreich, Phys. Rev. B 1, 3250 (1970).

[43] D.J. Chadi and M. L. Cohen, Phys. Rev. B 7, 692 (1973).

[44] T. Zakrzewski and F.Z. Dziuba, Phys. Stat. Sol. (b) 52, 665 (1972).

[45] O. Ohtsuki, R. Ueda, K. Shinohara, Y. Ueda and S. Narita, Colloque CNRS, n° 228, Nice, 1973.

[46] S. Askenazy, in New Developments in Semiconductors, edited by P.R. Wallace, R. Harris, M.J. Zuckermann (Noordhoff International Publishing, Leyden, the Netherlands, 1973), p. 333, and references therein

FIGURE CAPTIONS

Fig. 1. Simplified band structure of $Hg_{1-x}Cd_xTe$ alloys at the zone center versus composition x or pressure P, (a) in the semimetallic configuration, (b) at the semimetal-semiconductor transition, (c) in the semiconductor configuration.

Fig. 2. (a) Simplified picture of the density of states g(E) vs energy in the vicinity of the Γ_6 and Γ_8 levels for zinc blende materials, owing to the lack of inversion symmetry which may induce a small overlap ΔE of the electron and heavy hole states in the SM configuration. (b) Corresponding scheme in the SC configuration.

Fig. 3. (a) and (b) Variations of the Hall coefficient R(B) in arbitrary units vs magnetic field B at T = 1.7°K and at various pressures for the $Hg_{0.86}Cd_{0.14}Te$ sample. Data points are not reported to improve clarity. Arrows indicate the "plateaux" on the curves.

Fig. 4. Variations of the low field Hall coefficient R(O) vs temperature at various pressures for $Hg_{0.86}Cd_{0.14}Te$ sample. Dashed lines indicate the hollows on the curves. Such an accident only appear for P > 3 kbars.

Fig. 5. Electron concentration n_1 and electron mobility μ_1 at 4.2°K as a function of pressure P for the $Hg_{0.86}Cd_{0.14}Te$ sample.

Fig. 6. Electron concentration n_1 and electron mobility μ_1 at 1.7°K as a function of pressure P for the $Hg_{0.86}Cd_{0.14}Te$ sample.

Fig. 7. Transverse magnetoresistivity ρ_1 of the $Hg_{0.86}Cd_{0.14}Te$ sample at 1.7°K in arbitrary units as a function of magnetic field. The arrows indicate the quantum oscillations. The dashed lines illustrate the non oscillatory background.

Fig. 8. Dependance of the magnetic field B_c at which the quantum oscillations occur, on the 2/3 power of the electron concentration for the $Hg_{0.86}Cd_{0.14}Te$ sample at 1.7°K.

Fig. 9. Relative variations of the longitudinal magnetoresistivity $\rho_{//}$ of the $Hg_{0.86}Cd_{0.14}Te$ sample at zero pressure as a function of magnetic field at T = 1.7°K (left scale) and T = 10°K (right scale). On both curves, the arrows indicate the quantum oscillations corresponding to Landau levels labelled N = 1 and 2. The 0^+ oscillation clearly appears at 10°K but is not observed at 1.7°K.

Fig. 10. Hall coefficient R(B) of the HgTe sample at 1.7°K as a function of magnetic field (solid curve) at zero pressure. Three oscillation peaks corresponding to quantum numbers N = 2, N = 1 and N = 0 are superimposed on the background variations (dashed curve).

Fig. 11. Oscillatory component of the Hall coefficient ΔR for the HgTe sample at 1.7°K as a function of magnetic field at P = 2 kbars (solid curve). The oscillations correspond to N = 2, 1 and 0. The last oscillation is also shown at P = 0 (dotted line) and P = 4 kbars (dashed line).

Fig. 12. Calculated values of the Fermi energy E_F measured from the bottom of the conduction band as a function of pressure at 4.2°K for the $Hg_{0.86}Cd_{0.14}Te$ sample. P_c is the crossover pressure.

Fig. 13. Analysis of the two carrier type Hall effect for the HgTe sample at zero pressure and at T = 1.7°K. R(0) is the low field Hall coefficient, and R_{NO} (B) is the non oscillatory component of R(B) deduced from Fig. 10.

Fig. 14. Analysis of the two carrier type Hall effect in the ultraquantum domain at 4.2°K for the $Hg_{0.86}Cd_{0.14}Te$ sample at various pressures, (a) in the SM configuration, and (b) in the SC configuration. R'(0) is the low field Hall coefficient and R(0) is the experimental one. Datum points at high magnetic field are not reported to improve clarity. We have plotted at P = 4.1 kbars $R(0)/[R(0) - R(B)]$ vs B^{-2} (dashed line).

Fig. 15. Hole concentration p (left scale) and hole mobility μ_p (right scale) as a function of pressure at 4.2°K for the $Hg_{0.86}Cd_{0.14}Te$ sample.

Fig. 16. Density of valence states in the vicinity of the Γ_8 point as a function of energy, for the $Hg_{0.86}Cd_{0.14}Te$ sample. $g_v^o(E)$ is the density of states of the heavy hole valence band described by the Kane's model. $g_v(E)$ is the extra density of valence states beyond the Γ_8 point. We have assumed for mathematical convenience that $g_v(E)$ is an $E^{1/2}$ law (a) while a more realistic model might be an exponential law (b).

Fig. 17. Plot of the 2/3 power of the hole concentration as a function of the Fermi energy E_F in the semimetallic configuration for the $Hg_{0.86}Cd_{0.14}Te$ sample at 4.2°K.

Fig. 18. Difference between hole and electron concentrations as a function of P pressure in the $Hg_{0.86}Cd_{0.14}Te$ sample at 4.2°K P_c is the crossover pressure.

Fig. 19. Variations of $E_F + \epsilon E_g - E_{A1}$ vs pressure for the $Hg_{0.86}Cd_{0.14}Te$ sample at 4.2°K. E_F is the Fermi energy, and $E_{A1} - \epsilon E_g$ is the energy of the acceptor level A_1, when the origin of energies is taken at the bottom of the conduction band. The datum points have been deduced from measurements of the concentration of ionized acceptors, except the point at 6.4 kbars which has been deduced from the determination of the field at which the last Landau level 0^- crosses the acceptor level A_1.

Fig. 20. Plot of $\mu_1 \times N_{cc}$ vs pressure for the $Hg_{0.86}Cd_{0.14}Te$ sample at 4.2°K. μ_1 is the electron mobility, N_{cc} is the concentration of the charged centers scattering the electrons. The solid curve (1) and the triangles are obtained for a donor concentration $N_D = 0$. Assuming that $N_D = 4 \times 10^{14} cm^{-3}$, the experimental points (full circles) are located on the theoretical (curve 2, dashed line) except in the range $2.7 < P < 4.7$ kbars, where a dip can be observed.

Fig. 21. Variations of $\mu_P \times N_{cc}$ against pressure in the $Hg_{0.86}Cd_{0.14}Te$ sample at 4.2°K. μ_P is the hole mobility and N_{cc} the concentration of the charged centers scattering the holes, for donor concentrations $N_D = 4 \times 10^{14}$ cm^{-3} (curve 1, full circles), and $N_D = 0$ (curve 2, triangles).

Fig. 22. Relative difference between the theoretical and the experimental values of $\mu_1 \times N_{cc}$ deduced from the curve (2) in Fig. 20 for the $Hg_{0.86}Cd_{0.14}Te$ sample at 4.2°K. μ_1 is the electron mobility and N_{cc} the concentration of scattering centers. This curve indicates that a resonance is located at P = 3.7 kbars and is 2 kbars wide.

Fig. 23. Variation of the energy E_{A1}, at which the resonance is located in the $Hg_{0.86}Cd_{0.14}Te$ sample, against pressure at 4.2°K. The origin of energies is taken at Γ_8 . P_c is the crossover pressure.

Fig. 24. Analysis of the two carrier type Hall effect for the $Hg_{0.86}Cd_{0.14}Te$ sample at T 90°K for P = 4 kbar and P = 5 kbar.

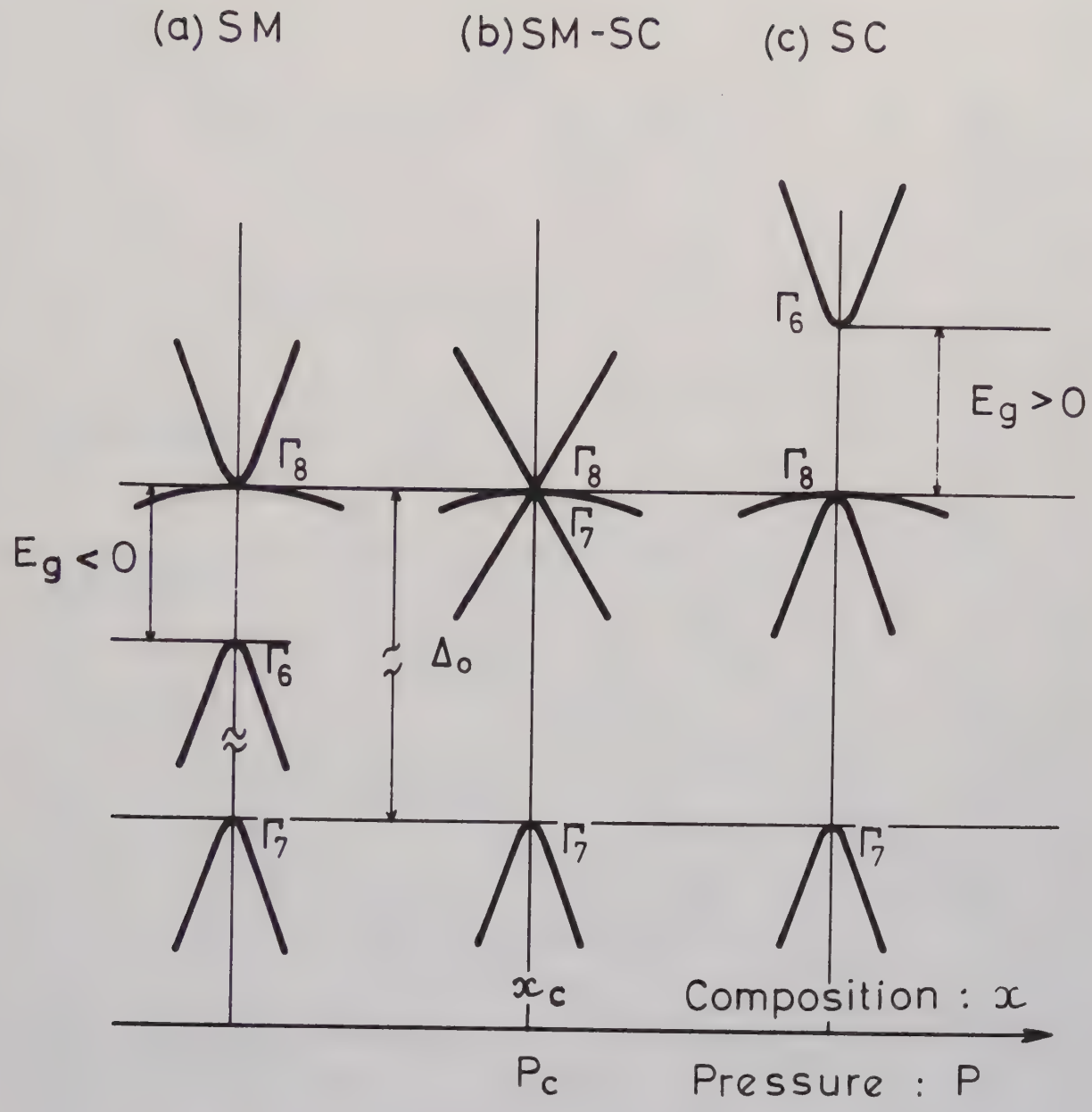
(a) SM
(b) SM-SC
(c) SC
Γ6
Eg > 0
Γ8
Γ8
Γ8
Γ7
Eg < 0
Δo
Γ6
Γ7
Γ7
Γ7
xc
Composition : x
Pc
Pressure : P

Fig. 1

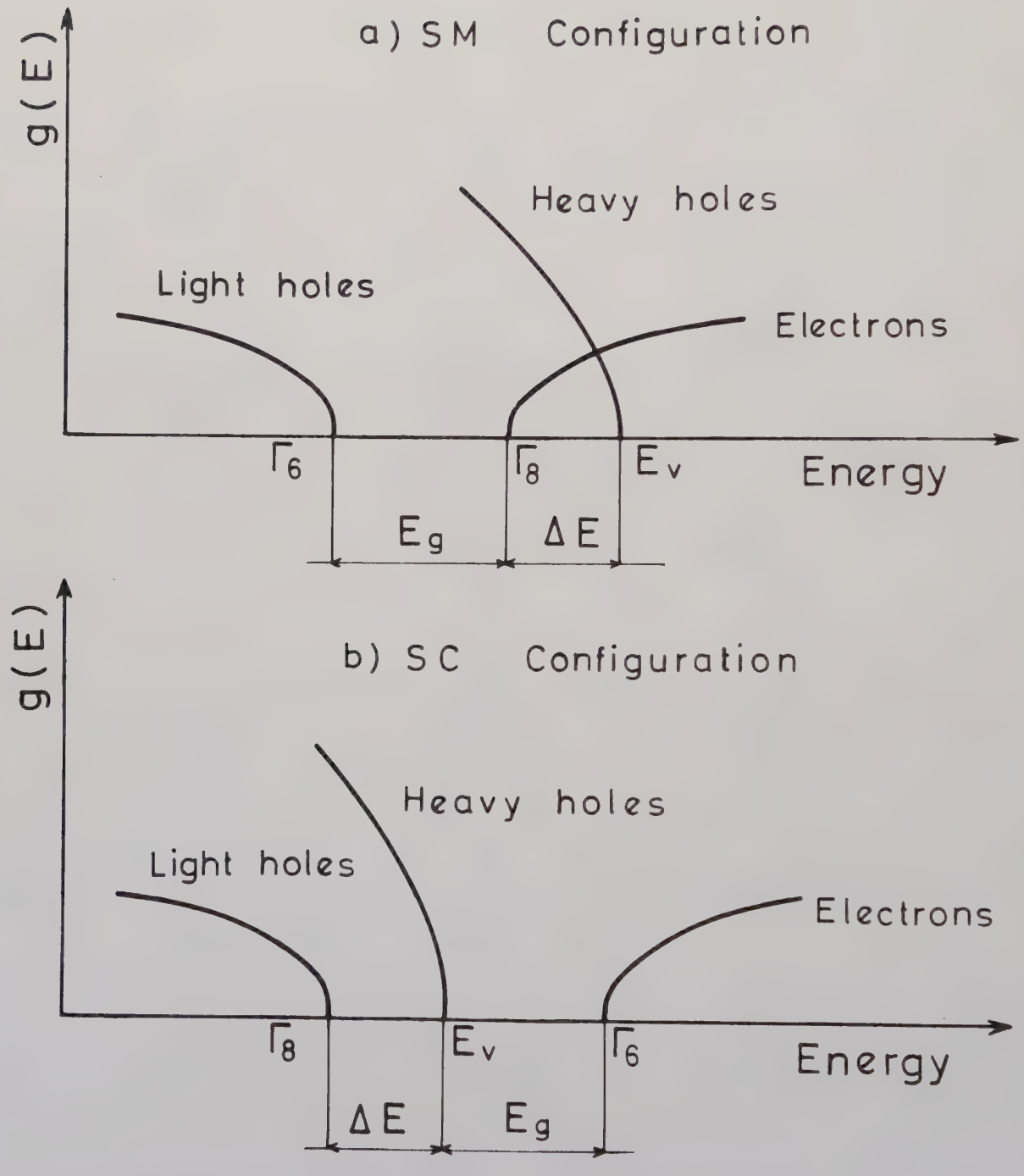
a) SM Configuration
g(E)
Heavy holes
Light holes
Electrons
Γ6
Γ8
Ev
Energy
Eg
ΔE
b) SC Configuration
g(E)
Heavy holes
Light holes
Electrons
Γ8
Ev
Γ6
Energy
ΔE
Eg

Fig. 2

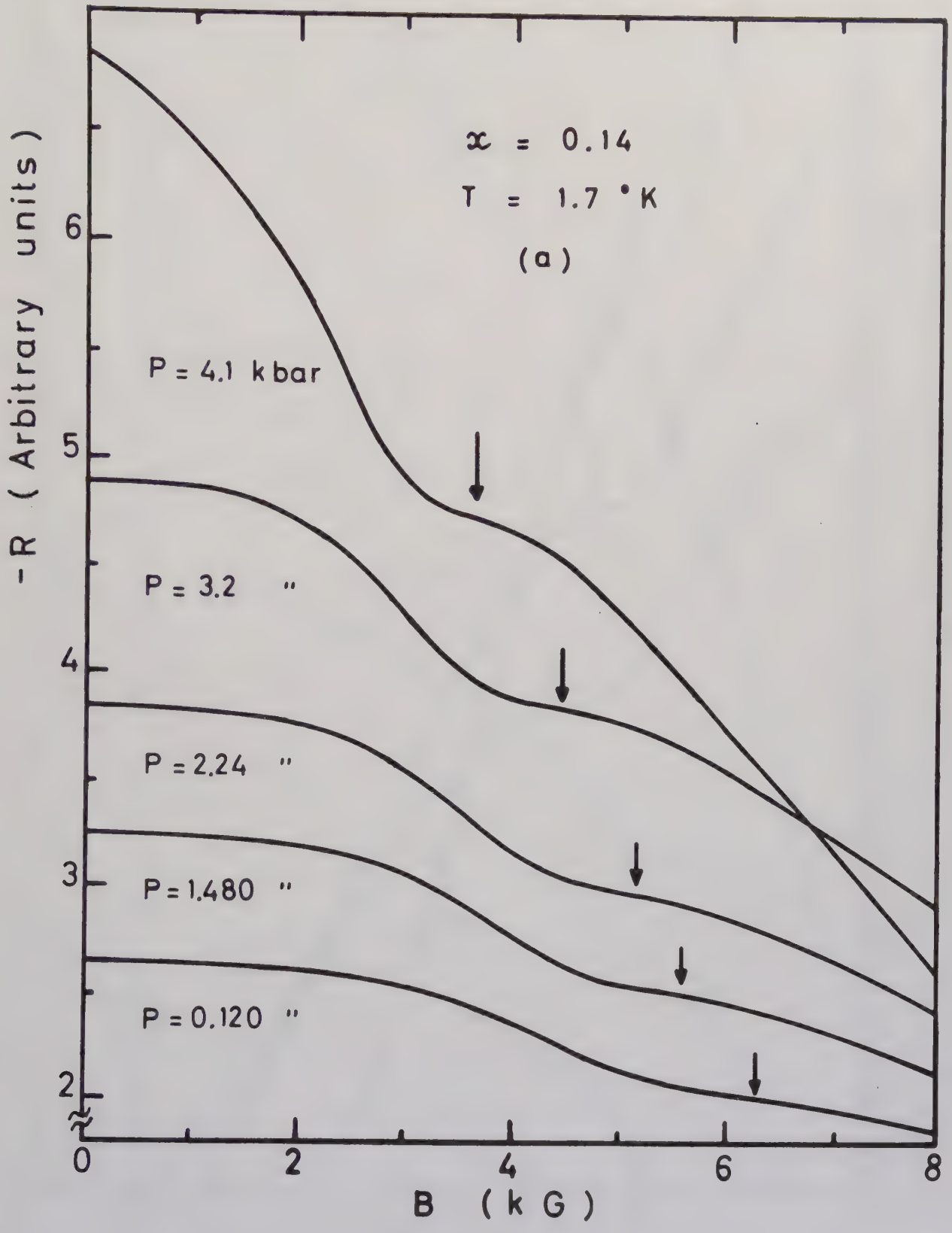
x = 0.14
T = 1.7 °K
(a)
P = 4.1 k bar
P = 3.2 "
P = 2.24 "
P = 1.480 "
P = 0.120 "
-R (Arbitrary units)
B (k G)
0
2
4
6
8
2
3
4
5
6

Fig.3a

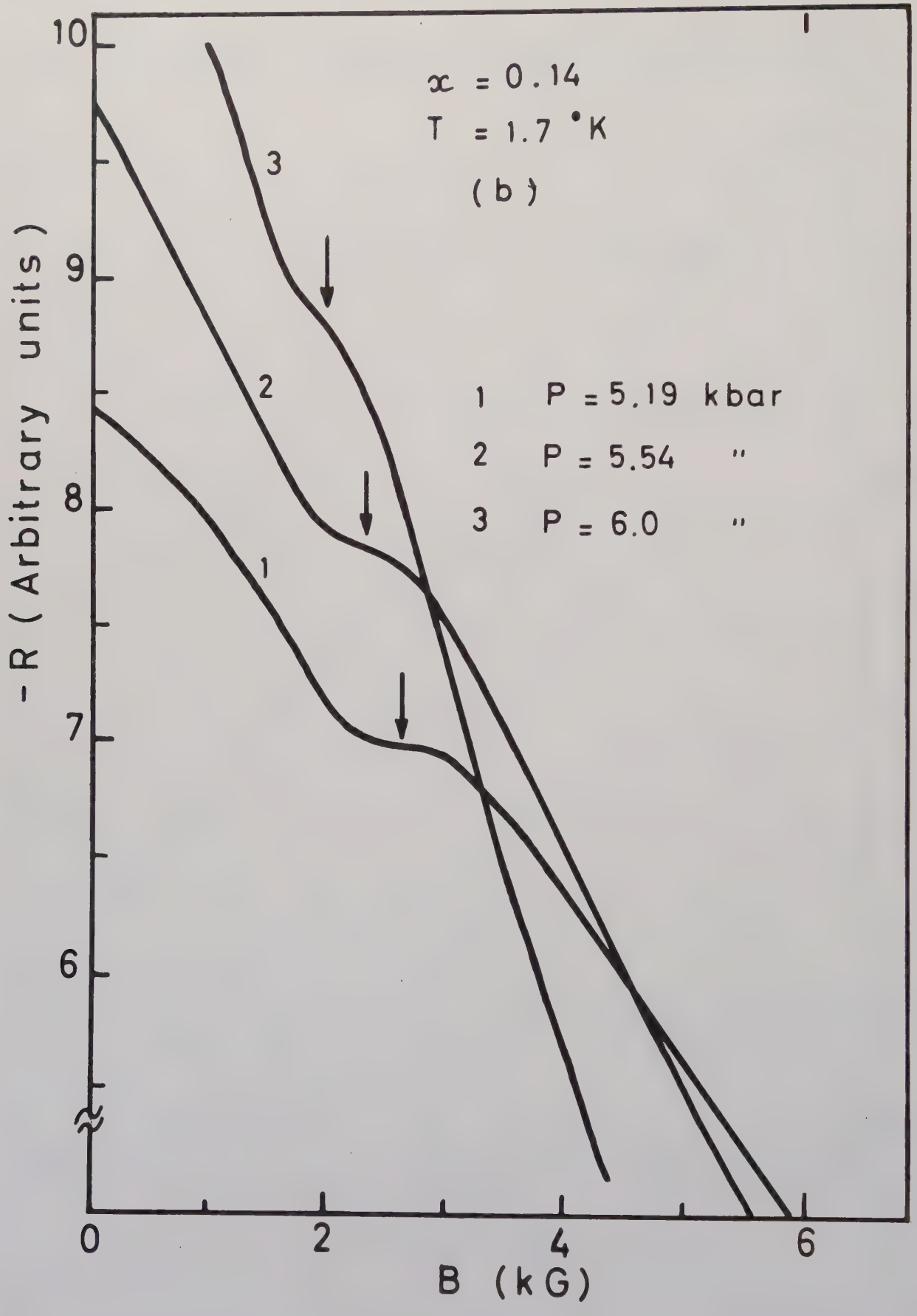
x = 0.14
T = 1.7 °K
(b)
1 P = 5.19 kbar
2 P = 5.54 "
3 P = 6.0 "
-R (Arbitrary units)
B (kG)
10
9
8
7
6
0
2
4
6
1
2
3

Fig.3 b

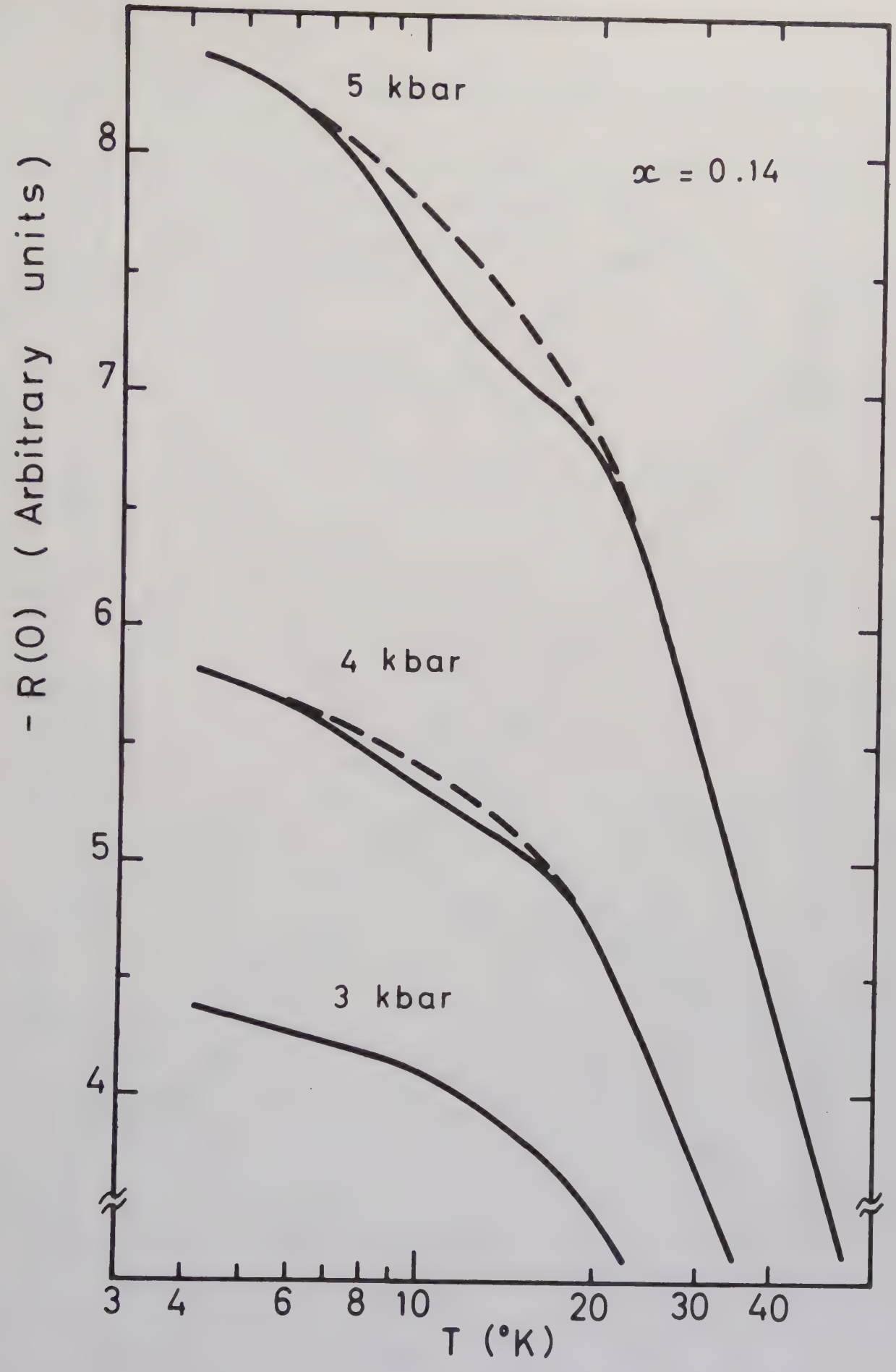
5 kbar
x = 0.14
4 kbar
3 kbar
- R(O) (Arbitrary units)
8
7
6
5
4
3
4
6
8
10
20
30
40
T (°K)

Fig. 4

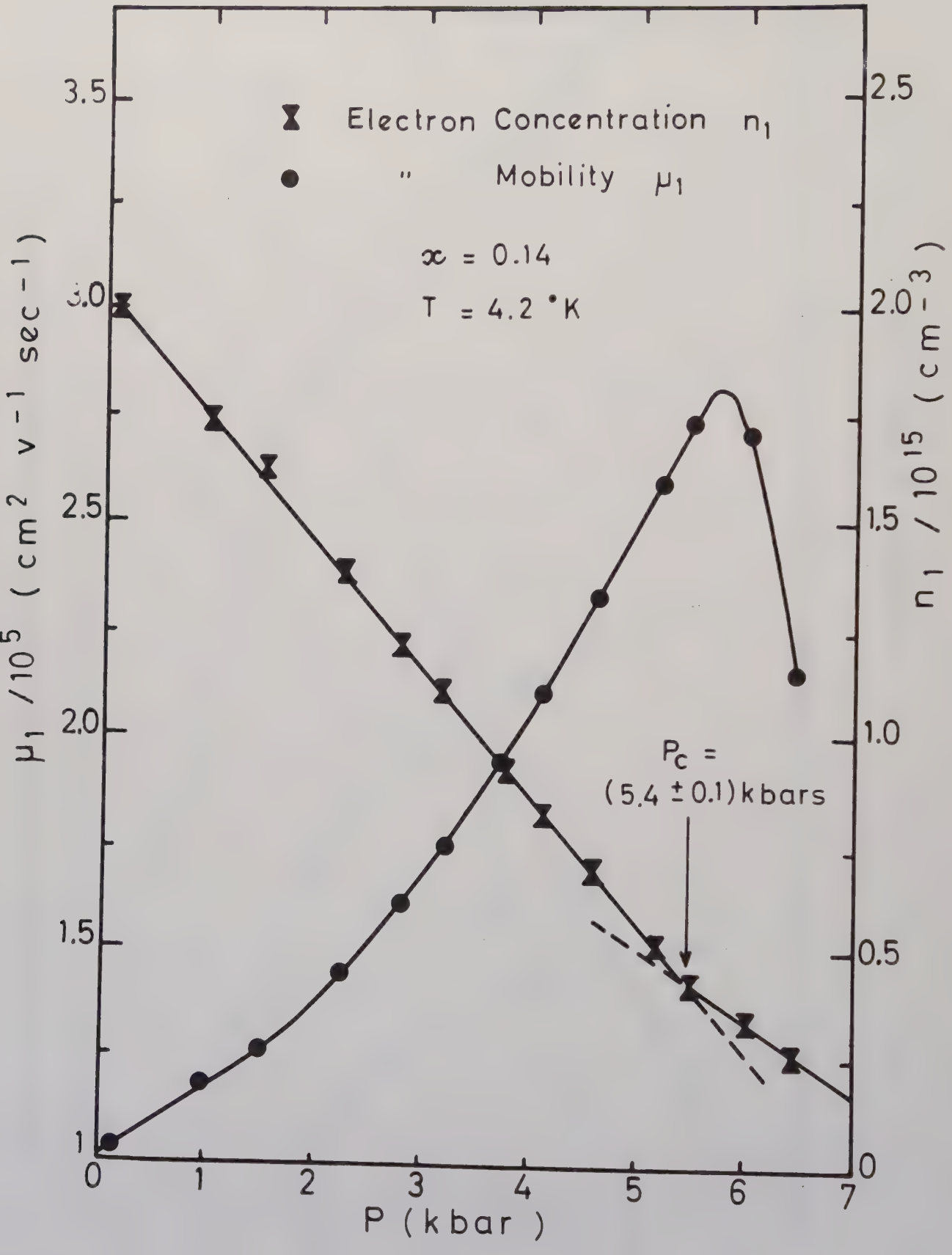
Electron Concentration n_1
" Mobility μ_1
$x = 0.14$
$T = 4.2\ ^\circ K$
$P_c =$
(5.4 ± 0.1) kbars
$\mu_1 / 10^5$ ($cm^2\ v^{-1}\ sec^{-1}$)
$n_1 / 10^{15}$ (cm^{-3})
P (kbar)
3.5
3.0
2.5
2.0
1.5
1
2.5
2.0
1.5
1.0
0.5
0
0
1
2
3
4
5
6
7

Fig. 5

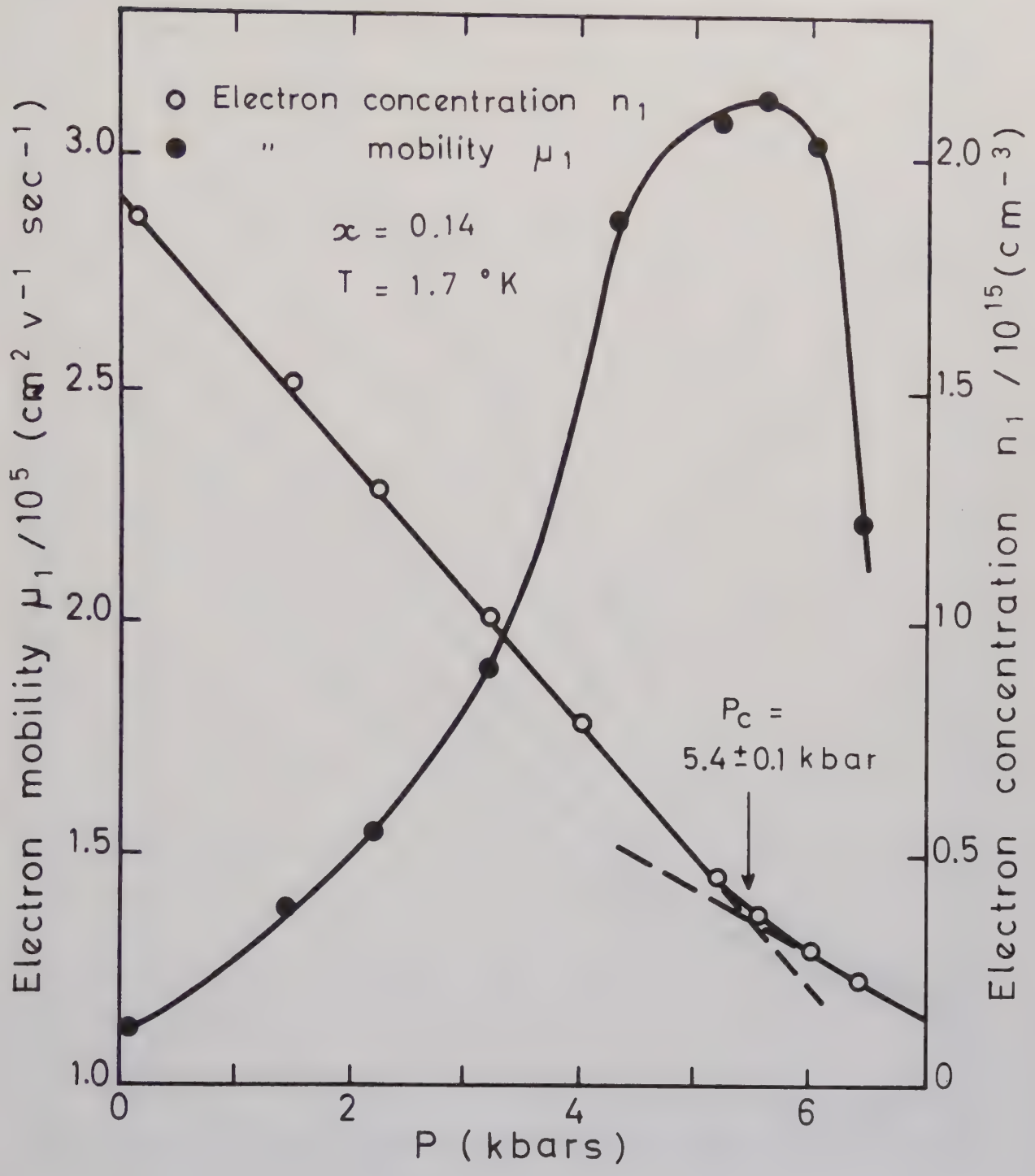
Electron concentration n_1
" mobility μ_1
$x = 0.14$
$T = 1.7\ ^\circ K$
$P_c =$
5.4 ± 0.1 kbar
Electron mobility $\mu_1 / 10^5$ ($cm^2\ v^{-1}\ sec^{-1}$)
Electron concentration $n_1 / 10^{15} (cm^{-3})$
P (kbars)
3.0
2.5
2.0
1.5
1.0
2.0
1.5
1.0
0.5
0
0
2
4
6

Fig. 6

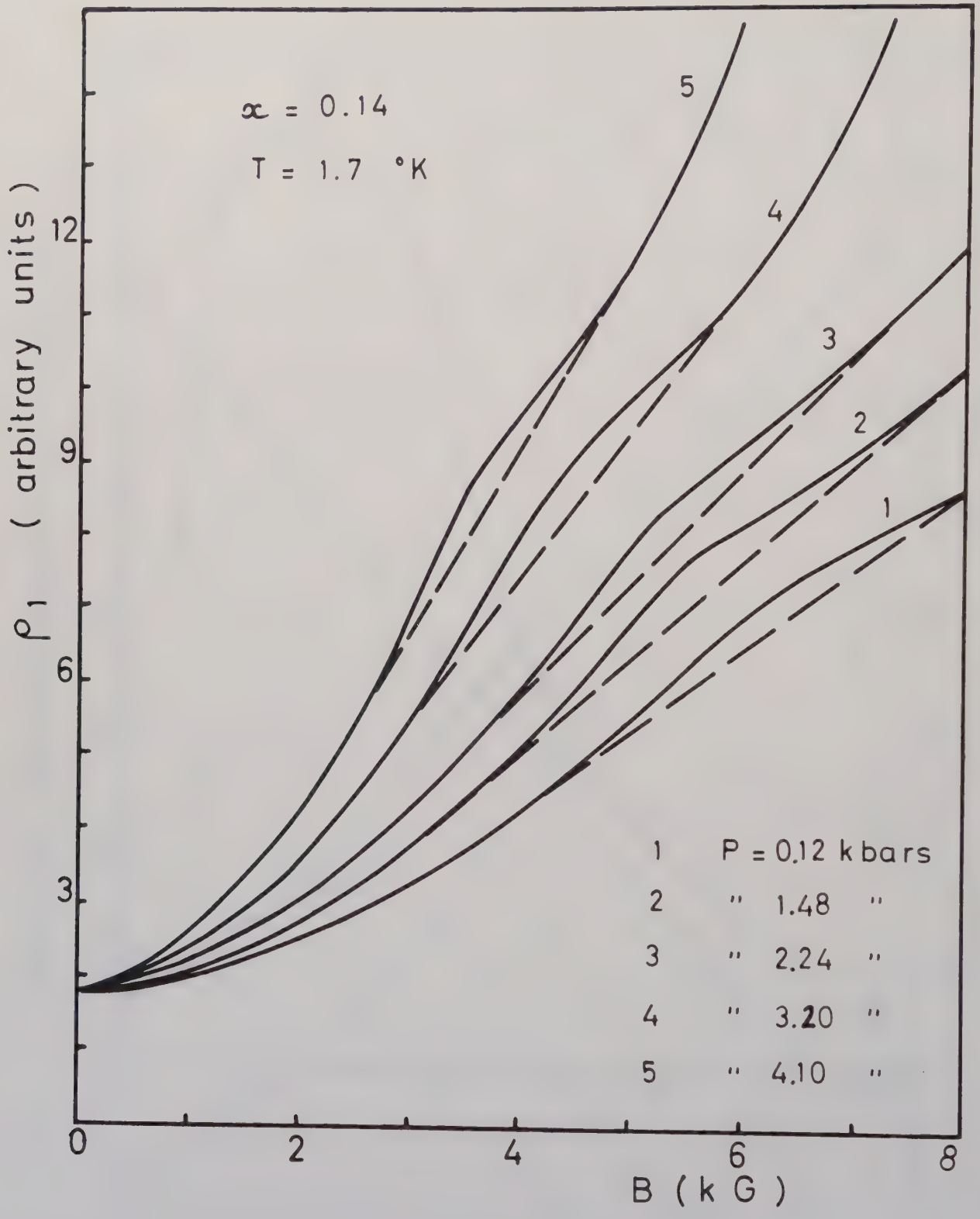
x = 0.14
T = 1.7 °K
5
4
3
2
1
ρ1 (arbitrary units)
12
9
6
3
0
2
4
6
8
B (k G)
1 P = 0.12 k bars
2 " 1.48 "
3 " 2.24 "
4 " 3.20 "
5 " 4.10 "

Fig. 7

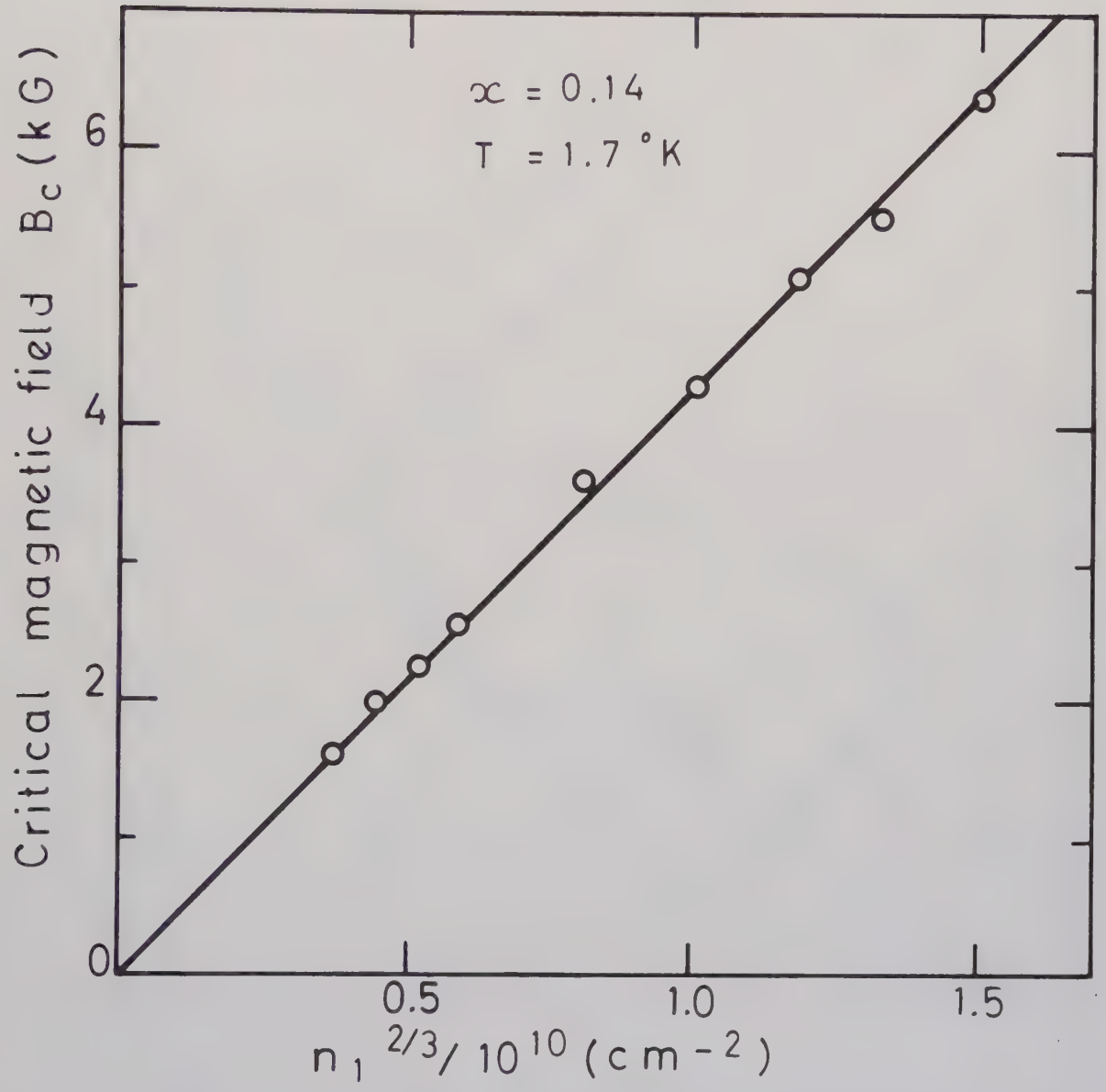
x = 0.14
T = 1.7 °K
Critical magnetic field Bc (kG)
0
2
4
6
0.5
1.0
1.5
n1 2/3 / 10 10 (cm-2)

Fig. 8

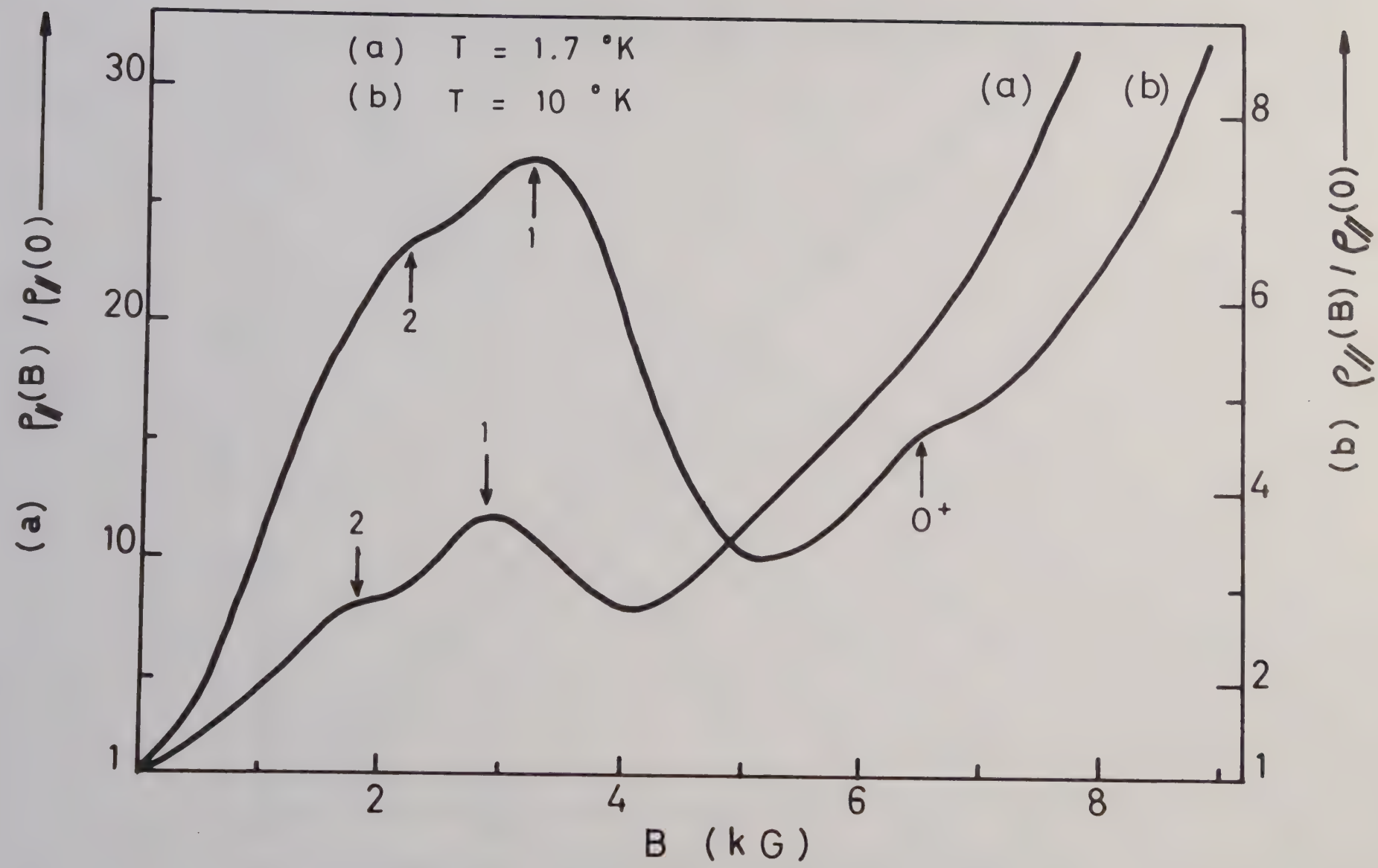

Fig. 9

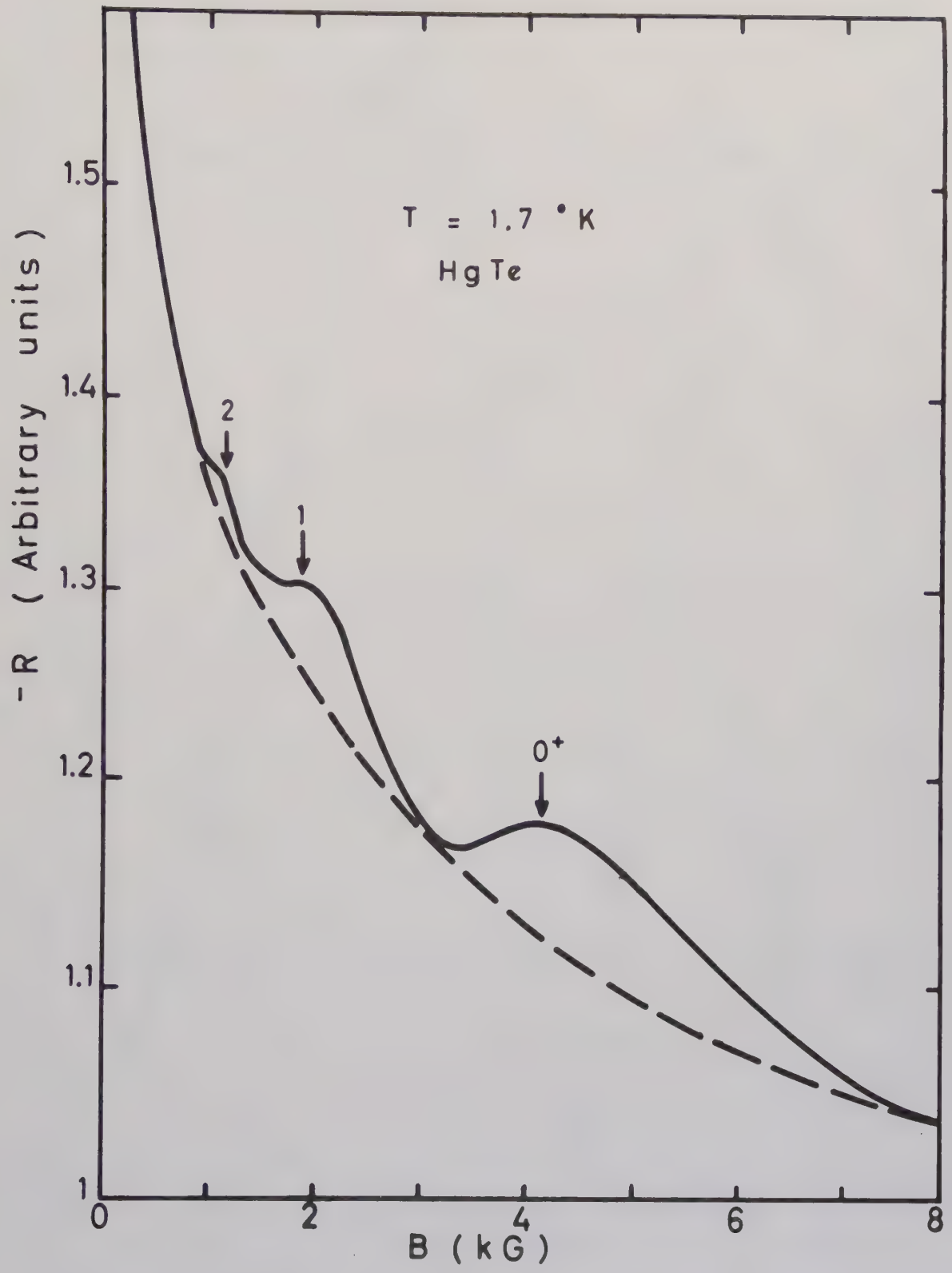

Fig. 10

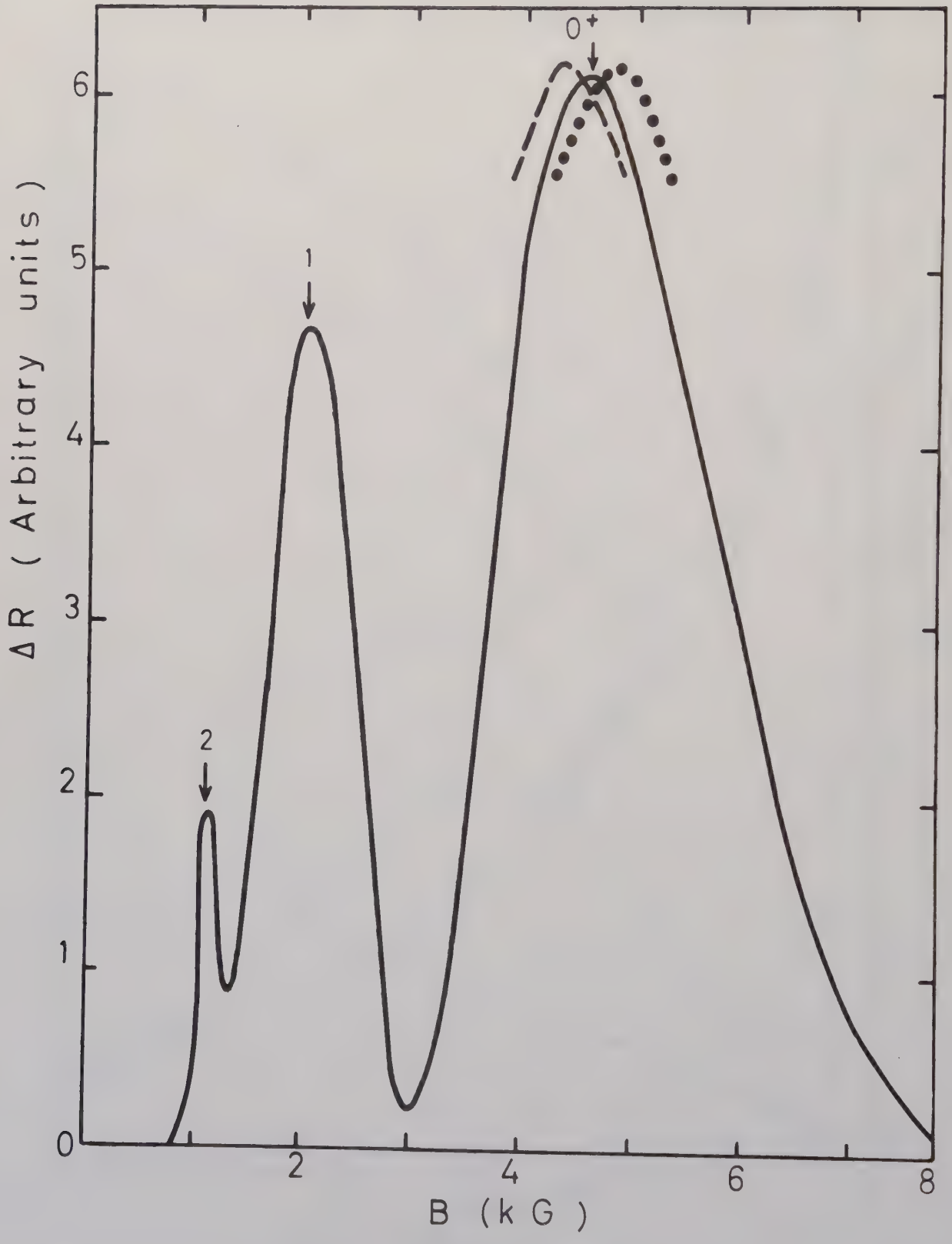

Fig. 11

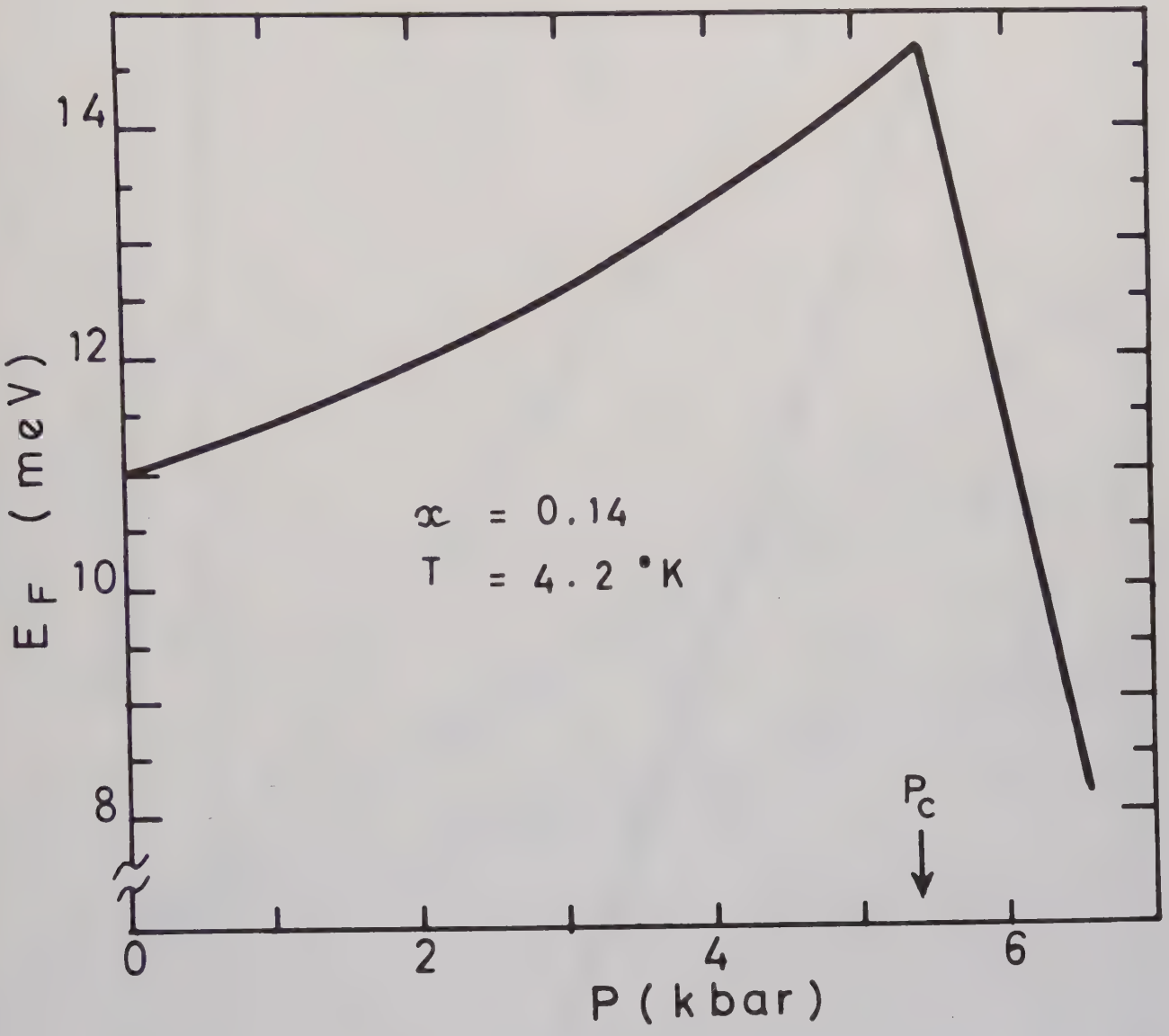

Fig. 12

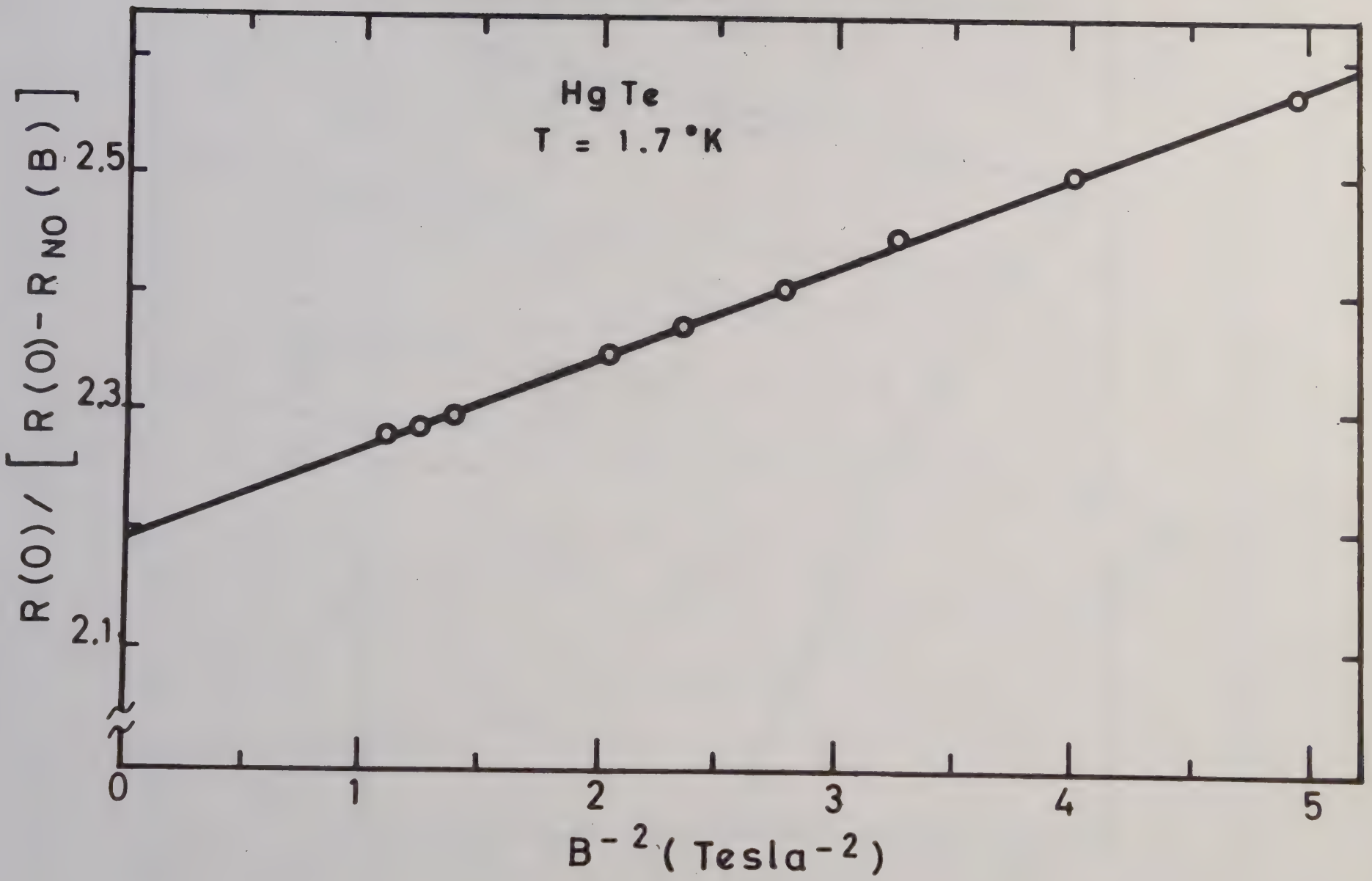

Fig.13

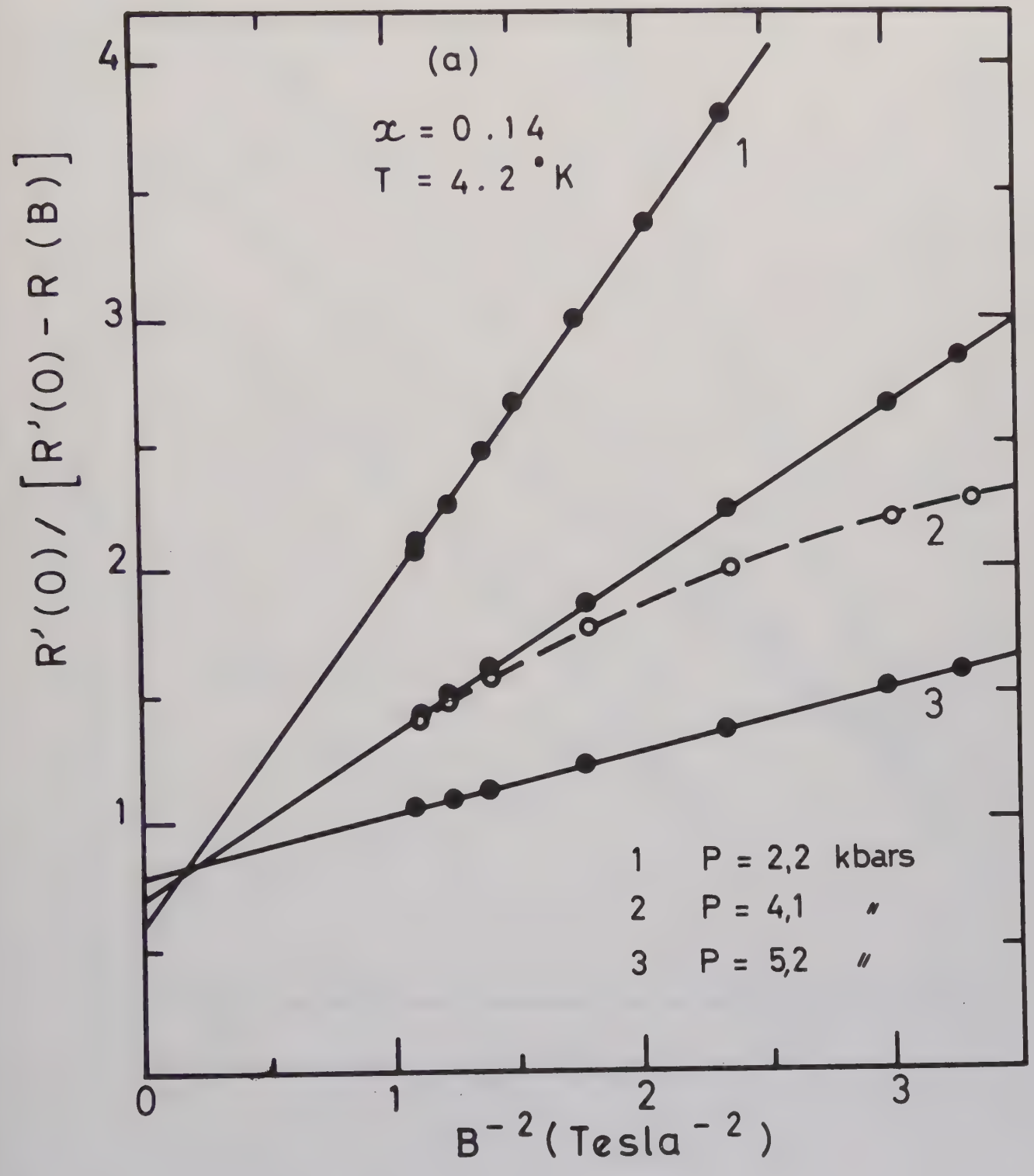

Fig. 14a

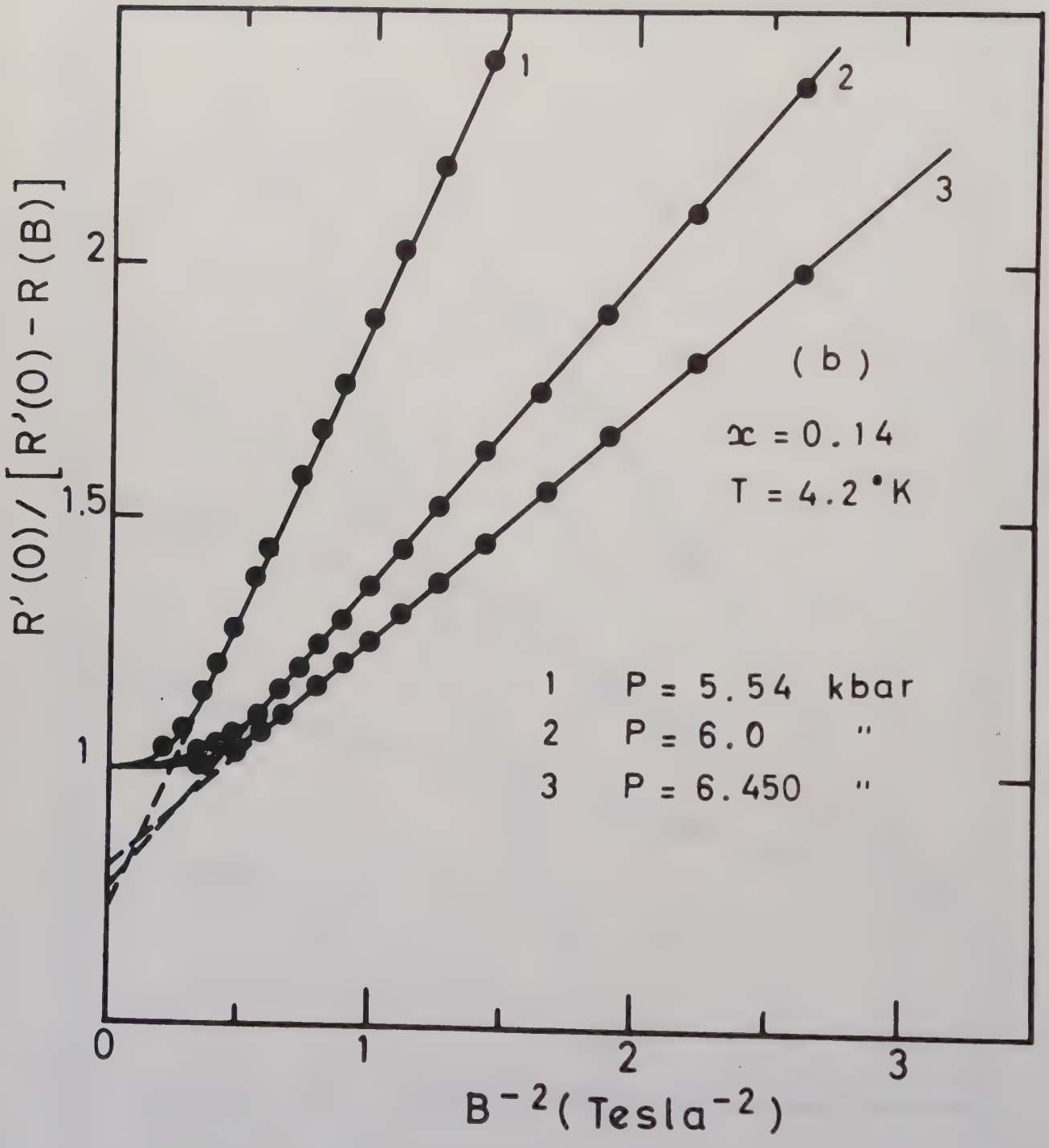
R'(O) / [R'(O) - R(B)]
2
1.5
1
0
1
2
3
B⁻²(Tesla⁻²)
1
2
3
(b)
x = 0.14
T = 4.2 °K
1 P = 5.54 kbar
2 P = 6.0 "
3 P = 6.450 "

Fig. 14 b

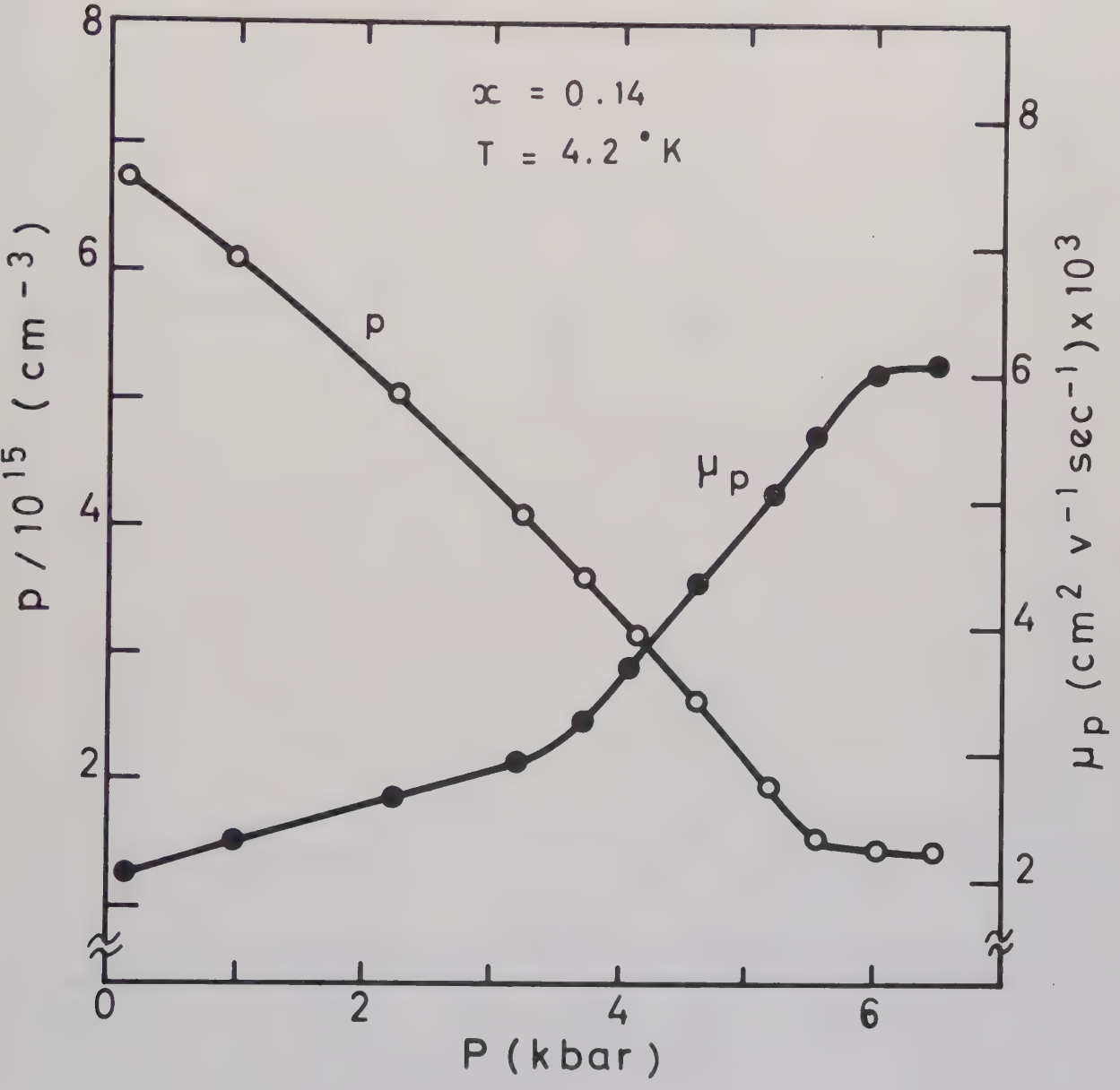

Fig. 15

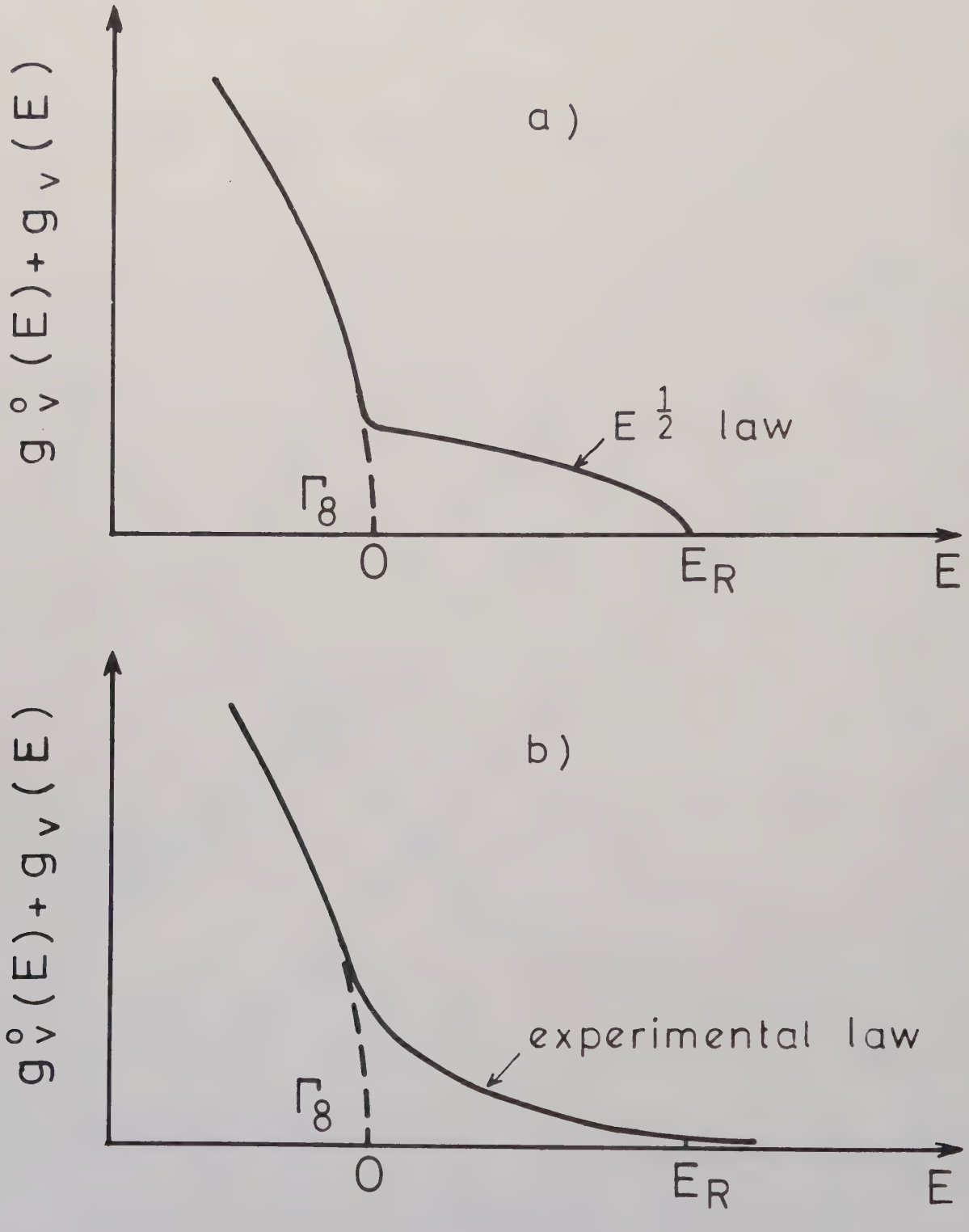
a)
$g^{\circ}_{v}(E)+g_{v}(E)$
$E^{\frac{1}{2}}$ law
Γ_8
0
E_R
E
b)
$g^{\circ}_{v}(E)+g_{v}(E)$
experimental law
Γ_8
0
E_R
E

Fig. 16

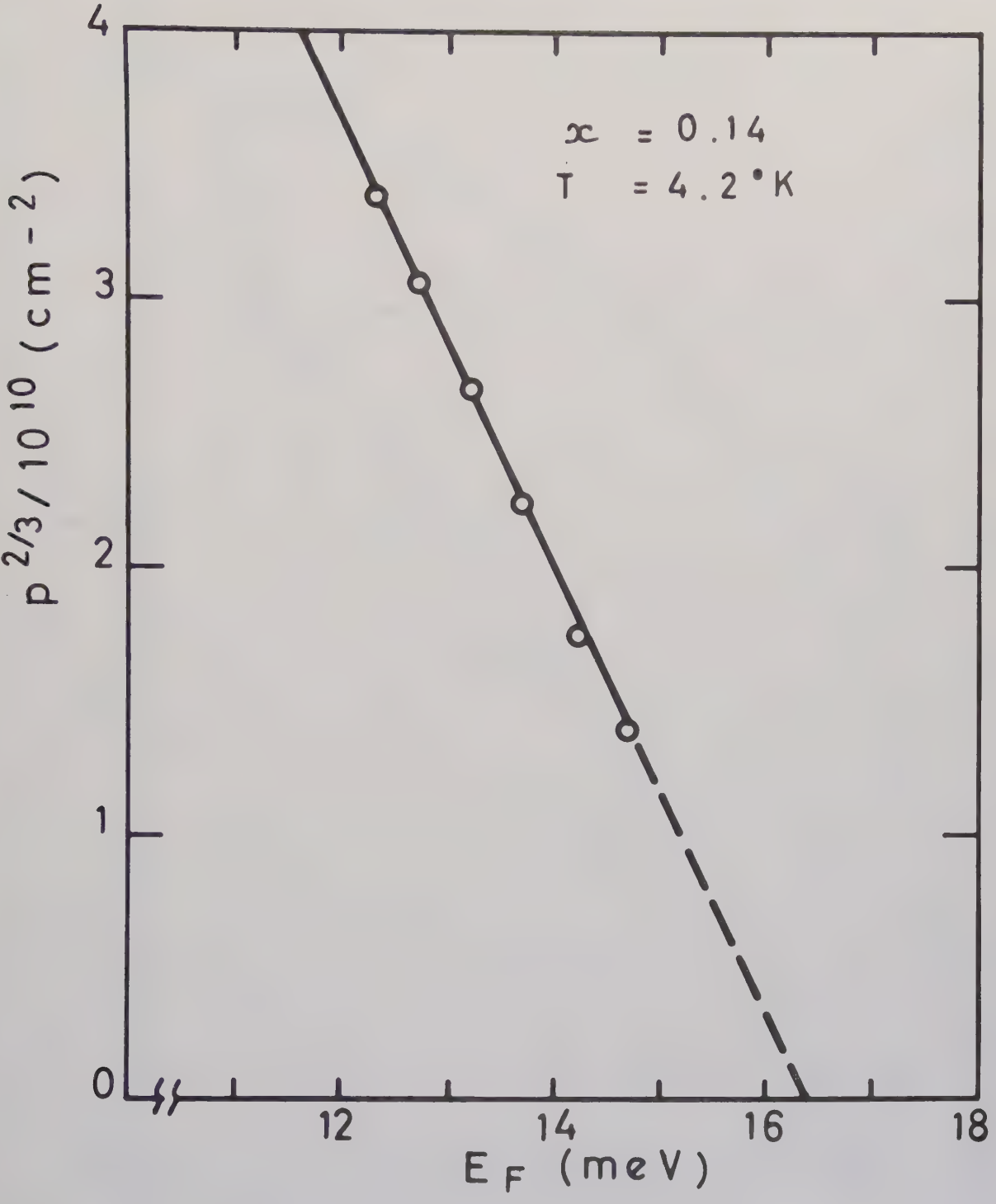

Fig. 17

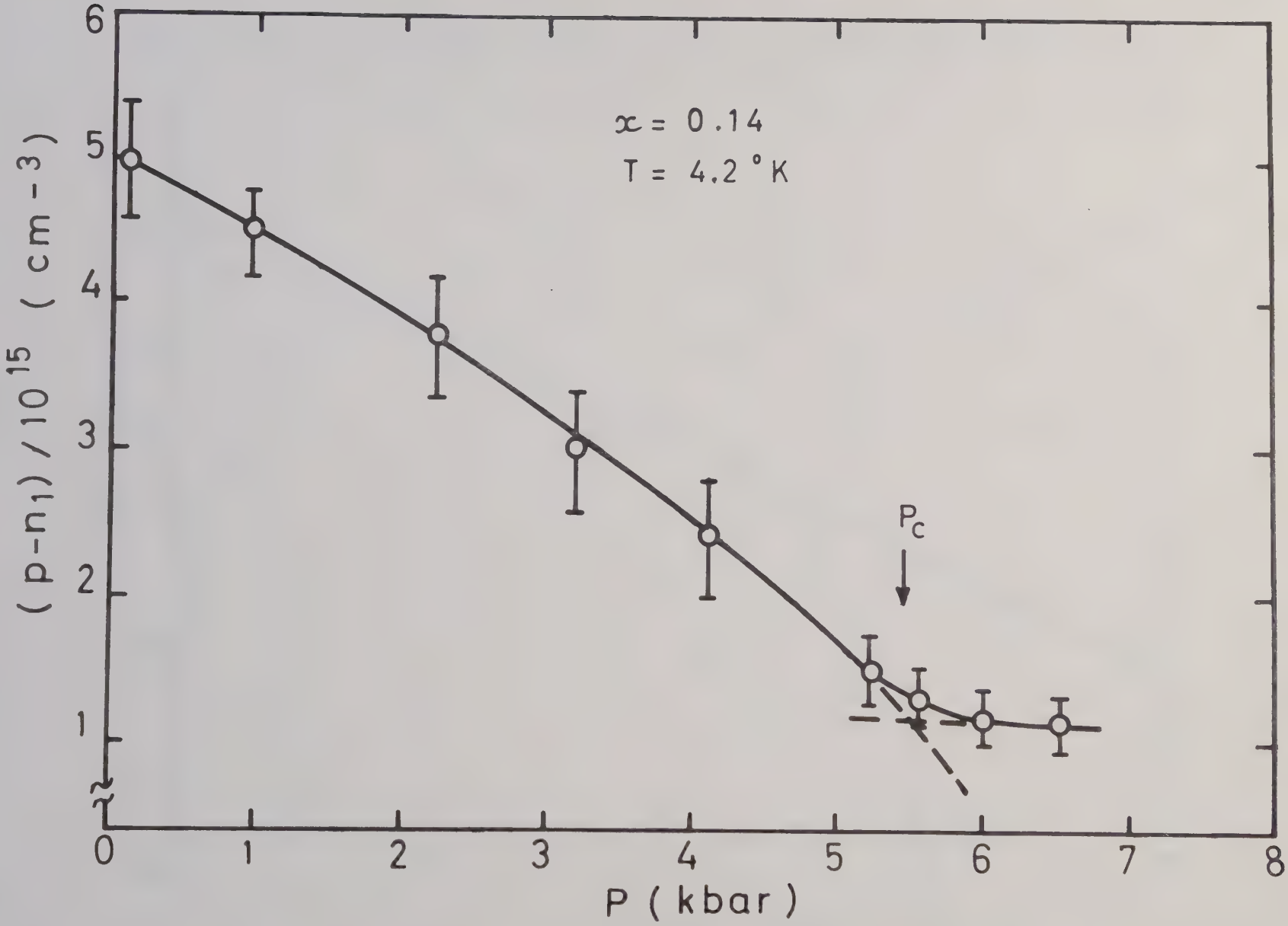

Fig. 18

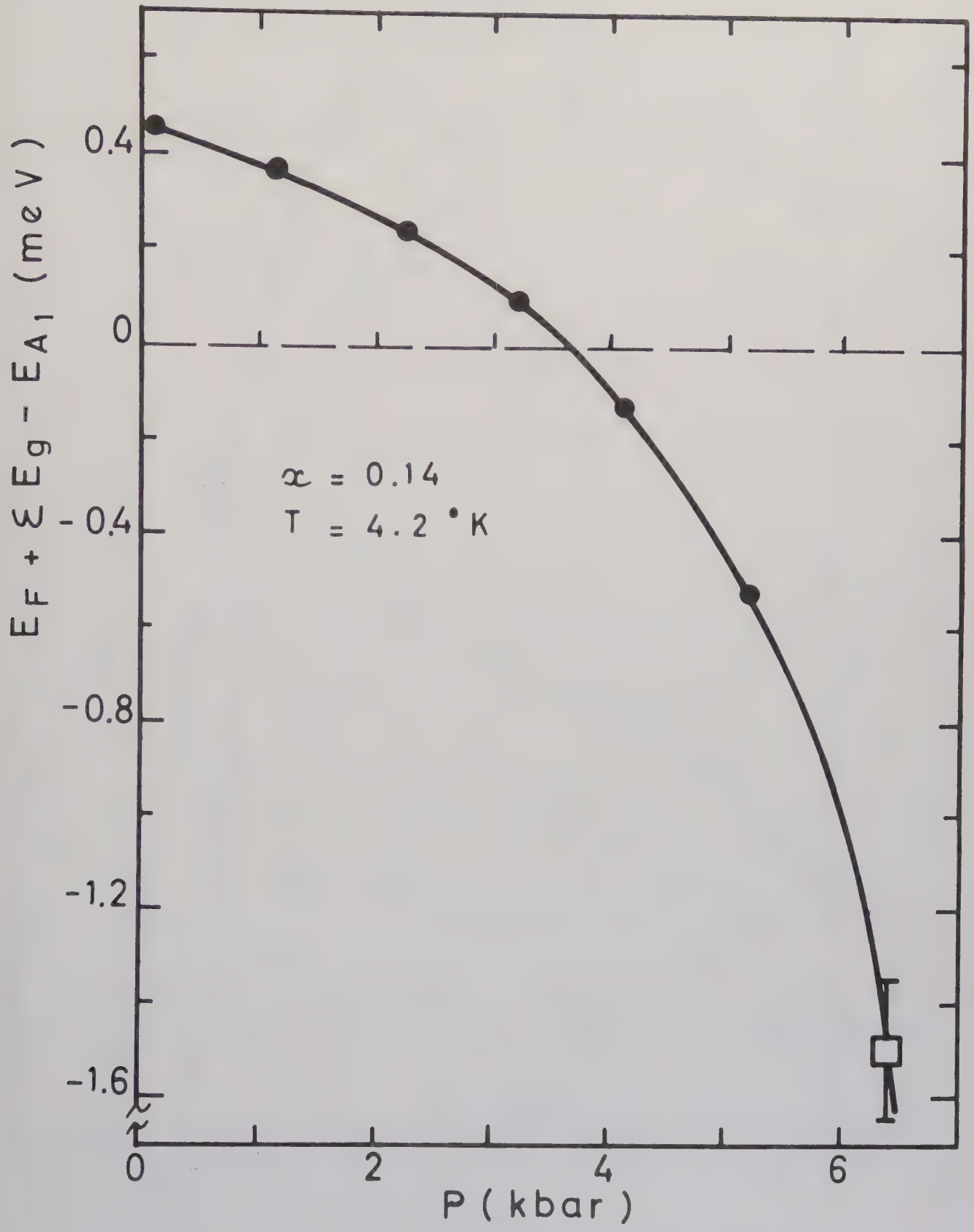

Fig. 19

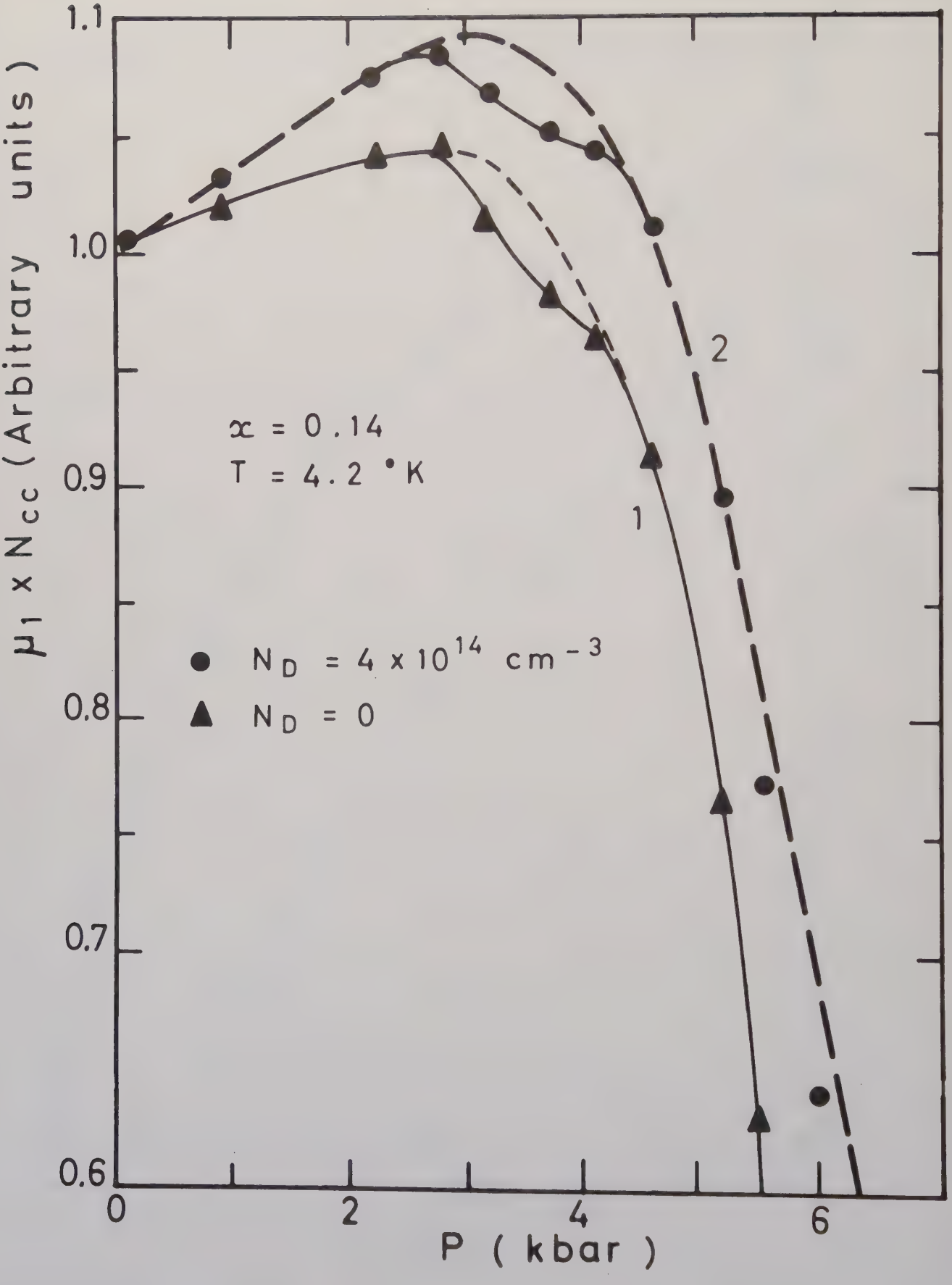
1.1
1.0
0.9
0.8
0.7
0.6
$\mu_1 \times N_{cc}$ (Arbitrary units)
x = 0.14
T = 4.2 °K
$N_D = 4 \times 10^{14}$ cm^{-3}
$N_D = 0$
1
2
0
2
4
6
P (kbar)

Fig. 20

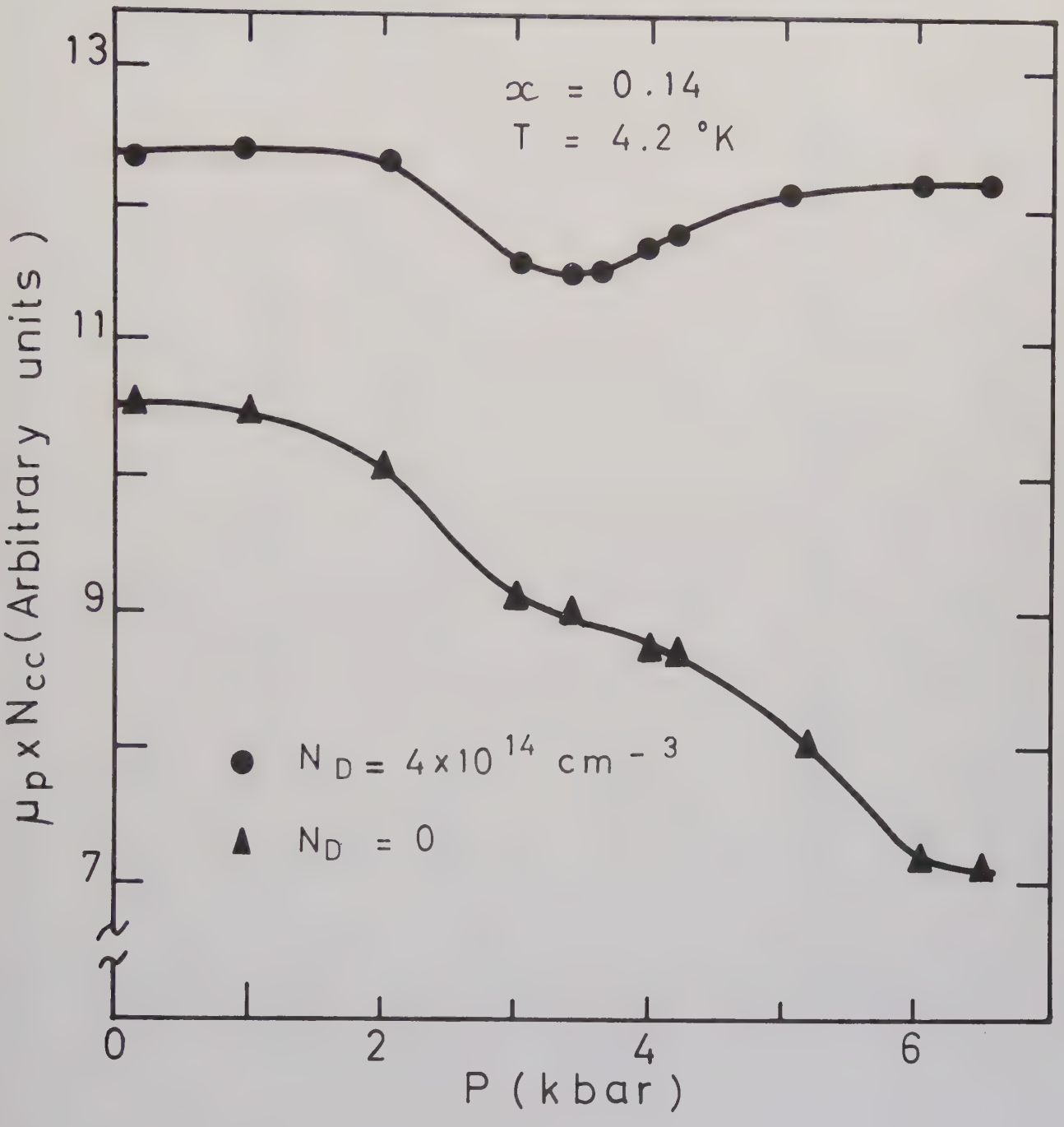
13
11
9
7
0
2
4
6
x = 0.14
T = 4.2 °K
$N_D = 4 \times 10^{14}$ cm^{-3}
$N_D = 0$
$\mu_p \times N_{cc}$ (Arbitrary units)
P (kbar)

Fig. 21

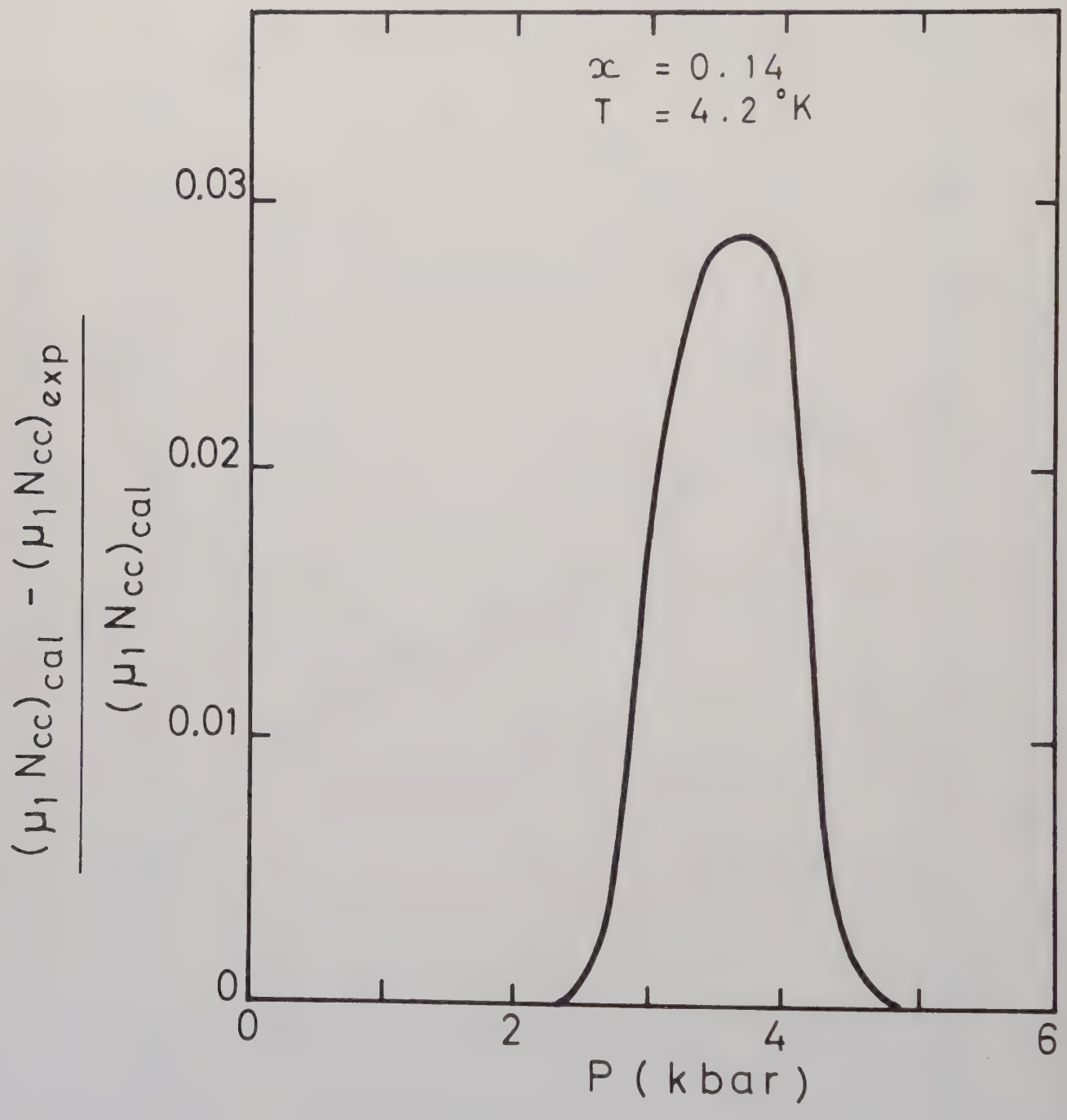
x = 0.14
T = 4.2 °K
0.03
0.02
0.01
0
0
2
4
6
P (kbar)
$\frac{(\mu_1 N_{cc})_{cal} - (\mu_1 N_{cc})_{exp}}{(\mu_1 N_{cc})_{cal}}$

Fig. 22

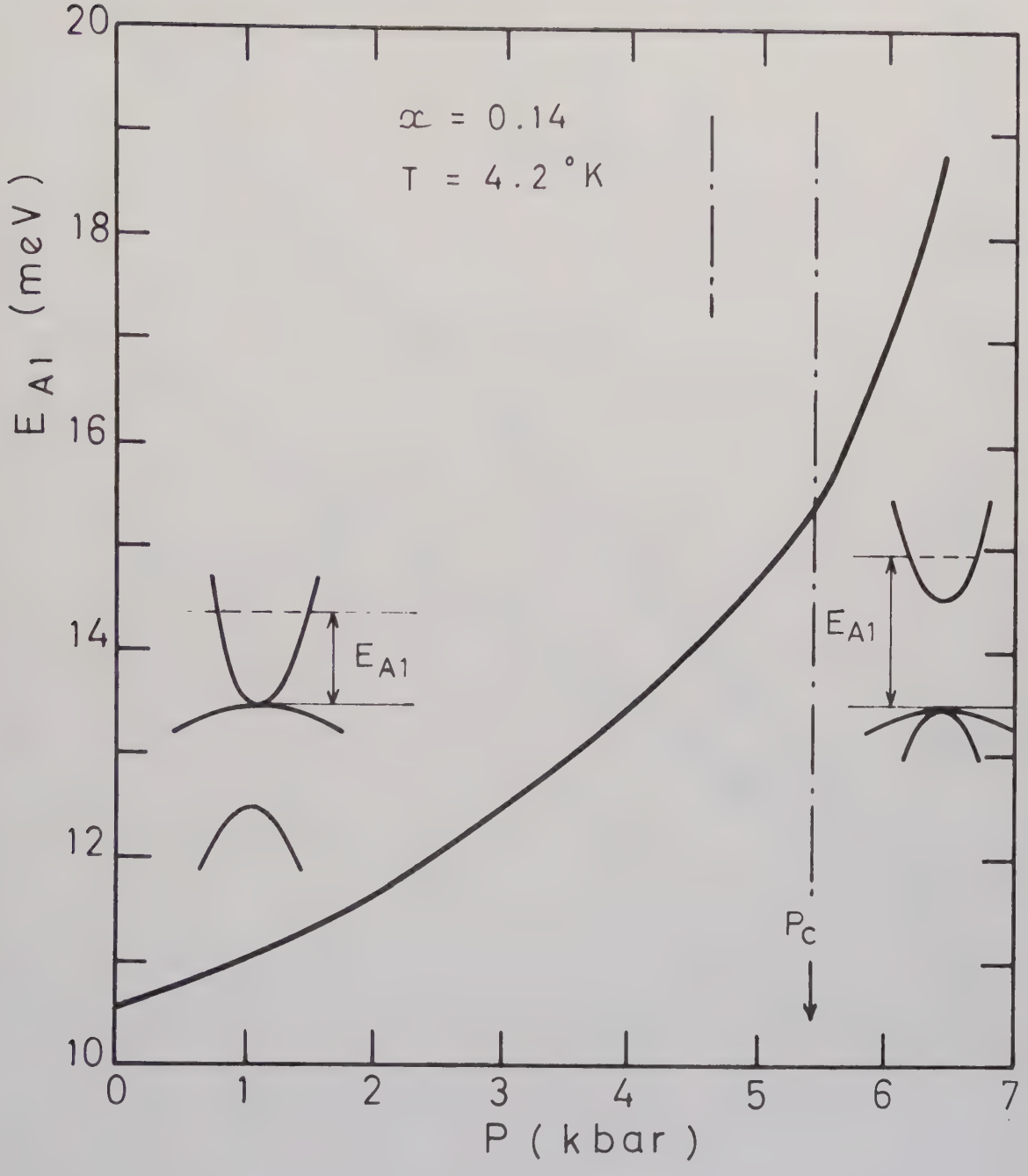

Fig. 23

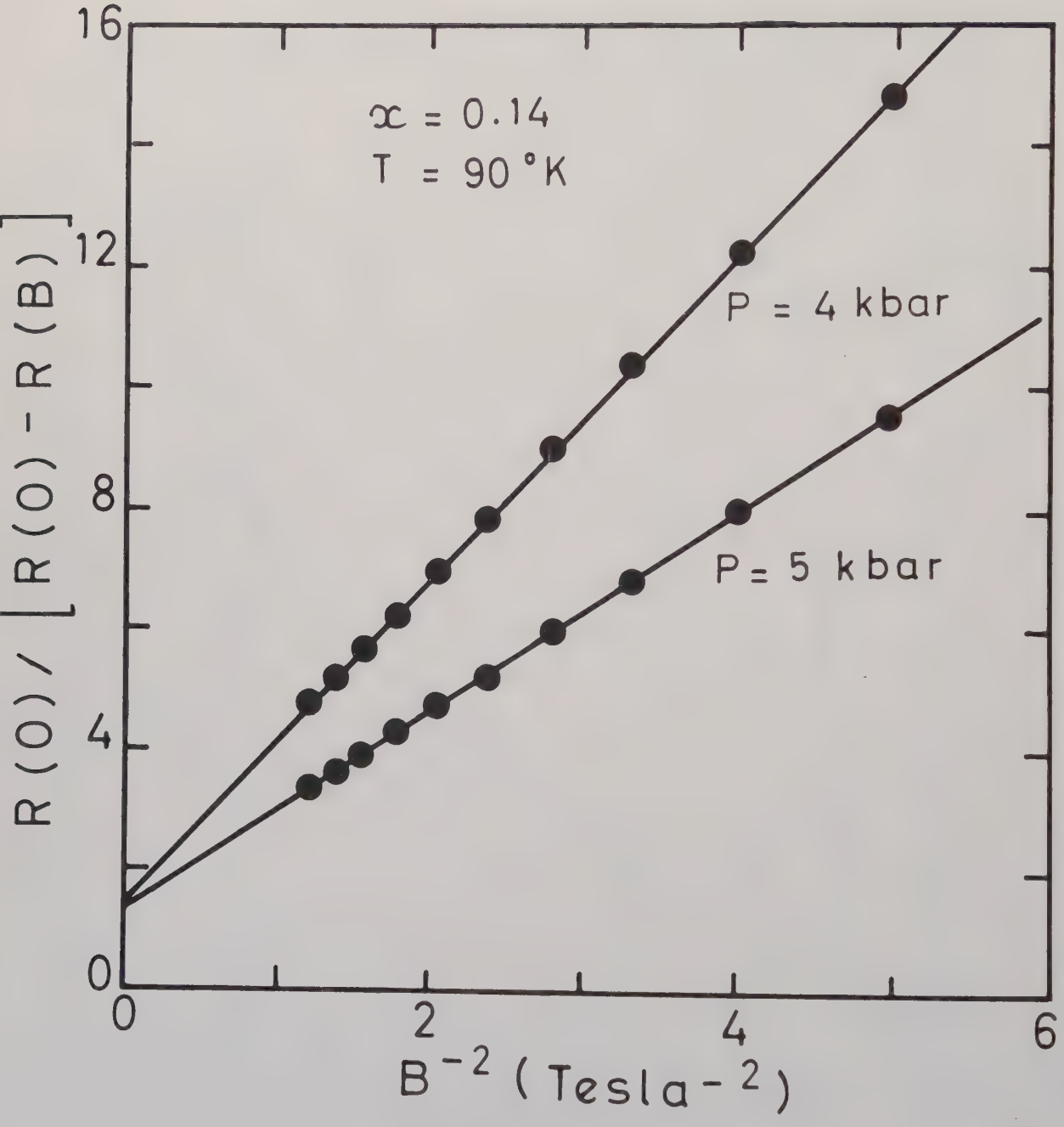

Fig. 24